Performance of Receiver Autonomous Integrity Monitoring (RAIM) for Vertically Guided Approaches

Anaïs Martineau

THÈSE

En vue de l'obtention du

DOCTORAT DE L'UNIVERSITÉ DE TOULOUSE

Délivré par *l'Institut National Polytechnique de Toulouse*
Discipline ou spécialité : *Signal, Image, Acoustique*

Présentée et soutenue par *Anaïs Martineau*
Le *14 Novembre 2008*

Titre :

Etude de la Performance du Contrôle Autonome d'Intégrité pour les Approches à Guidage Vertical

Performance of Receiver Autonomous Integrity Monitoring (RAIM) for Vertically Guided Approaches

---

JURY

Professeur Francis Castanié
Professeur Penina Axelrad
Professeur Igor Nikiforov
Docteur Todd Walter
Docteur Audrey Giremus
Docteur Christophe Macabiau

Ecole doctorale : *Mathématiques, Informatique et Télécommunications de Toulouse*
Unité de recherche : *Laboratoire de Traitement du Signal et des Télécommunications de l'Ecole Nationale de l'Aviation Civile*
Directeur(s) de Thèse : *Christophe Macabiau et Igor Nikiforov*
Rapporteurs : *Penina Axelrad, Todd Walter et Audrey Giremus*

THESE

en vue
de l'obtention du

DOCTORAT DE L'UNIVERSITE DE TOULOUSE

délivré par
l'Institut National Polytechnique de Toulouse

Ecole Doctorale Mathématique Informatique et Télécommunication

Spécialité Signal, Image et Acoustique

par

Anaïs Martineau

Etude de la Performance du Contrôle Autonome d'Intégrité
pour les Approches à Guidage Vertical

Performance of Receiver Autonomous Integrity Monitoring (RAIM)
for Vertically Guided Approaches

Soutenue le 14 Novembre 2008 à l'Ecole Nationale de l'Aviation Civile (ENAC) devant le jury composé de :

Prof. Dr Francis Castanié	Président
Prof. Dr Penina Axelrad	Rapporteur
Dr Todd Walter	Rapporteur
Dr Audrey Giremus	Rapporteur
Dr Christophe Macabiau	Directeur de thèse
Prof Dr Igor Nikiforov	Directeur de thèse

Thèse préparée au Laboratoire de Traitement du Signal et des Télécommunications
de l'Ecole Nationale de l'Aviation Civile

Abstract

The International Civil Aviation Organization (ICAO) has recognized the Global Navigation Satellite System (GNSS) as a key element of the Communications, Navigation, and Surveillance / Air Traffic Management (CNS/ATM) systems as well as a foundation upon which States can deliver improved aeronautical navigation services. But civil aviation requirements can be very stringent and up to now, the bare systems cannot alone be used as a means of navigation. Therefore, in order to ensure the levels required in terms of accuracy, integrity, continuity of service and availability, ICAO standards define different architectures to augment the basic constellations. Some of them use control stations to monitor satellite signals and provide corrections, others only use measurement redundancy. This study focuses on this last type of augmentation system and more particularly on Receiver Autonomous Integrity Monitoring (RAIM) techniques and performance.

RAIM is currently a simple and efficient solution to check the integrity of GNSS down to Non Precision Approaches. But the future introduction of new satellite constellations such as the European satellite navigation system Galileo or modernized Global Positioning System (GPS) will imply great improvements in the number as well as the quality of available measurements. Thus, more demanding phases of flight such as APproaches with Vertical guidance could be targeted using RAIM to provide integrity monitoring. This would result in some interesting safety, operational and environmental benefits. This Ph.D. evaluates the potential capacity of RAIM algorithms to support approach and landing phases of flight with vertical guidance.

A thorough bibliographic study of civil aviation requirements is first presented; some candidate LPV200 signal in space performance requirements not yet included in the ICAO standards are also provided.

To evaluate GNSS positioning performance, pseudorange measurements have to be modeled as precisely as possible and especially the different errors that affect them. The main sources of error are signal propagation delays caused by the ionosphere and the troposphere, space vehicle clock error, satellite position estimation error, multipath, receiver errors which main source is code tracking loop noise. Thus, these errors can be due to the space segment, the control segment or the user segment. Systematic errors are gathered in the fault free case measurement model; unusual errors, that may cause a dangerous positioning failure and that may have to be detected, are gathered in the faulty case measurement model. Finally, a complete model of pseudo range measurements, including interference effects and satellite failures, is given. A special attention is put on the User Equivalent Range Error (UERE) variance computation. Indeed, among all input parameters of RAIM availability simulator, UERE has, by far, the most significant impact on the estimated availability.

Three distinct classes of RAIM algorithms are studied in this thesis. The Least Square Residual method in which the sum of the squares of the pseudorange residuals plays the role of the basic observable is first recalled. The Maximum Solution Separation method which is

based on the observation of the separation between the position estimate generated by a full-set filter (using all the satellite measurements) and the position estimate generated by each one of the subset filters (each using all but one of the satellite measurements) is then discussed and an improved way of computing the associated protection level is proposed. Finally, a new promising method based on the Generalized Likelihood Ratio test is presented and several implementations are described.

The way these different methods are implemented to take into account both civil aviation requirements and threat model is then detailed. In particular some methods to obtain the inner probability values that RAIM algorithms need to use are presented. Indeed, high level requirements interpretation for RAIM design is not clearly standardized.

Finally simulations results are presented. They permit to evaluate RAIM ability to provide integrity monitoring for approaches with vertical guidance operations considering various scenarios.

The main contributions of this thesis are a detailed computation of user equivalent range error variance, an analysis of the effect of interferences on pseudorange measurement, an adaptation of LSR RAIM algorithm to nominal biases, an improvement of MSS protection levels computation, the implementation of GLR algorithm as a RAIM including the computation of an analytical expression of the threshold that satisfies the false alarm probability and the prediction of the probability of missed detection, design of a sequential GLR algorithm to detect step plus ramp failure and an analysis of the amplitude of smallest single biases that lead to a positioning failure.

Least Squared Residual, Maximum Solution Separation and constrained Generalized Likelihood Ratio RAIM availabilities have been computed for APVI and LPV200 approaches using both GPS L1/L5 and Galileo E1/E5b pseudorange measurements. It appears that both APV I and LPV200 (VAL=35m) operations are available using GPS/Galileo + RAIM to provide integrity as an availability of 100 % has been obtained for the detection function of the three studied algorithms. An availability of 100 % has also been obtained for the LSR exclusion function. On the contrary, LSR RAIM FDE availabilities seem not sufficient to have Galileo + RAIM or GPS +RAIM as a sole means of navigation for vertically guided approaches.

Résumé

L'Organisation de l'Aviation Civile Internationale (OACI) a reconnu la navigation par satellite, Global Navigation Satellite System (GNSS), comme un élément clé des systèmes CNS/ATM (Communications, Navigation, and Surveillance / Air Traffic Management) et comme une base sur laquelle les Etats peuvent s'appuyer afin de délivrer des services de navigation aérienne performants.

Mais l'utilisation des systèmes de navigation par satellites pour des applications de type aviation civile ne va pas sans répondre à des exigences en terme de précision, de continuité, d'intégrité et de disponibilité. Ces exigences opérationnelles liées aux différentes phases de vol requièrent pour les systèmes GNSS l'appui de moyens d'augmentation tels ceux utilisant des stations de surveillance sol pour vérifier la validité des signaux satellitaires et calculer des corrections ou ceux fonctionnant de manière autonome, tel le RAIM (Receiver Autonomous Integrity Monitoring).

Ce dernier moyen est particulièrement intéressant car il engendre des coûts de mise en œuvre réduits et il constitue à l'heure actuelle un moyen simple et efficace d'effectuer des approches de non précision. La prochaine mise en place du système de navigation européen Galileo ainsi que la modernisation du système historique américain GPS vont entrainer une nette amélioration, à la fois en terme de nombre et de qualité, des mesures satellitaires disponibles, laissant entrevoir la possible utilisation du RAIM pour des approches à guidage vertical, très intéressantes du point de vue opérationnel.

Les différentes notions liées aux exigences de l'aviation civile sont définies dans le chapitre 2, notamment les différents critères de performance. Chaque phase de vol, et plus particulièrement chaque catégorie d'approche, y est également décrite ainsi que les niveaux de performance associés.

Plusieurs types d'erreurs sont susceptibles d'affecter les mesures GNSS. Parmi elles il convient de distinguer les erreurs systématiques ou nominales des perturbations liées à une défaillance du système de navigation. Ces dernières peuvent être dues soit à un problème matériel survenant au niveau d'un des satellites ou du récepteur, soit d'une perturbation de l'environnement de propagation des signaux GNSS. Ces aspects sont adressés dans le chapitre 3 à l'issu duquel un modèle complet de mesure de pseudo distance GNSS est proposé.

Les algorithmes de contrôle d'intégrité ont été développés pour détecter ces anomalies et exclure les mesures erronées de la solution de navigation. Il s'agit de méthodes uniquement basées sur la redondance des mesures satellite, éventuellement enrichies de celles d'autres capteurs, devant déterminer si les conditions sont réunies pour occasionner une erreur de position dépassant une limite spécifiée. Devant répondre à des exigences relatives aux performances décrites dans le chapitre 2, le choix du type d'algorithme de contrôle d'intégrité est laissé à l'utilisateur. Le chapitre 4 étudie plusieurs de ces méthodes et propose des innovations.

Les chapitres 5 et 6 adressent l'implémentation puis l'évaluation des performances des différents algorithmes pour les approches à guidage vertical.

Les principales contributions de cette thèse sont le calcul détaillé de la variance de l'erreur equivalente utilisateur de mesure de pseudodistance, une adaptation de l'algorithme LSR à la présence de biais nominaux, une amélioration du calcul des niveaux de protection de l'algorithme MSS, l'implémentation de la technique GLR en tant qu'algorithme RAIM à part entière (calcul analytique du seuil de détection satisfaisant à la probabilité de fausse alarme, prédiction de la probabilité de détection manquée), la conception d'un algorithme séquentiel GLR destiné à detecter les pannes de type échelon – rampe ainsi qu'une analyse de l'amplitude des plus petits biais pouvant conduire à une erreur de positionnement.

Les disponibilités des algorithmes RAIM LSR, MSR et GLR contraint ont été évaluées pour les approches APVI et LPV 200 en utilisant à la fois les mesures de pseudodistance GPS L1/L5 et Galileo E1/E5b. Une disponibilté de 100% a été obtenue pour la fonction de detection des ces trois algorithmes pour ces deux types d'approche. Une disponibilté de 100% a également été obtenue pour la fonction d'exclusion du RAIM LSR. Par contre, les disponibilités prédites de cette fonction d'exclusion ne semblent pas suffisament élévées pour considérer Galileo + RAIM ou GPS +RAIM comme un moyen primaire de navigation pour les approches à guidage vertical.

Acknowledgements

Je tiens en premier lieu à remercier mon directeur de thèse Christophe Macabiau pour sa disponibilité, sa gentillesse, sa simplicité ainsi que pour avoir supporté mon caractère de cochon au cours de ces trois dernières années. L'étendue de ses connaissances et son grand sens pédagogique m'impressionneront toujours.

Je remercie la Direction Générale de l'Aviation Civile ainsi que la direction de l'Ecole Nationale de l'Aviation Civile pour m'avoir permis d'être affectée au Laboratoire de Traitement du Signal et des Télécommunications en premier poste et d'ainsi avoir pu effectuer cette thèse.

I gratefully acknowledge Penina Axelrad and Todd Walter for accepting to review this thesis.

J'adresse un grand merci à Audrey Giremus pour avoir être accepté d'être rapporteur de ma thèse.

Je remercie également Igor Nikiforov, Benoit Roturier, Anne-Laure Vogel et Mikaël Mabilleau pour l'aide qu'ils m'ont apportée lors de ces travaux de thèse ainsi que tous les membres du LTST.

Je n'oublie pas mon co-bureau Olivier Julien qui a su par de brillantes analyses me faire prendre conscience de ce que signifiait réellement le contrôle d'intégrité. J'espère à l'avenir pouvoir calculer des sorties de corrélateurs aussi bien que lui.

Mes pensées vont également vers Emilie, Mathieu et Xavier dont la présence le jour de ma soutenance m'a beaucoup touchée.

Je remercie mon mari, Romain, pour sa lecture minutieuse de mon manuscrit ainsi que pour la patience dont il fait preuve au jour le jour à mon égard.

Table of Contents

List of Figures

List of Tables

Chapître 1

Introduction

Alors que les systèmes et les procédures de navigation aérienne de l'époque semblaient atteindre leurs limites (coût élevé des équipements, manque de cohérence des méthodes de gestion du trafic au niveau mondial) et ne pas permettre le développement du trafic aérien au rythme prévu, l'Organisation de l'Aviation Civile Internationale (OACI) créa en 1983 le comité sur les Futurs Systèmes de la Navigation Aérienne (FANS). Sa tâche était d'étudier les questions techniques, opérationnelles, institutionnelles et économiques relatives aux potentiels futurs systèmes aériens de navigation, d'identifier et d'évaluer de nouveaux concepts et de nouvelles technologies ainsi que de faire des recommandations. En 1991 la dixième conférence de l'OACI sur la navigation aérienne, approuvant les conclusions de FANS, adopta le concept CNS/ATM, (Communication, Navigation and Surveillance/Air Traffic Management) et en particulier le concept de navigation par satellite Global Navigation Satellite System (GNSS) [ICAO, 1991].

Mais l'utilisation de la navigation par satellite pour l'aviation civile fut rendue possible par la décision du gouvernement américain d'offrir le service de positionnement GPS sans percevoir de charges directes. Cela conduisit l'OACI à engager les travaux de standardisation du GNSS, avec pour objectif de définir des systèmes utilisables durant toutes les phases de vol, de la navigation océanique aux atterrissages de précision de Catégorie III. Les travaux du groupe d'expert GNSS Panel permirrent à l'OACI, en Novembre 2002, de publier dans l'Annexe 10 à la Convention de Chicago, une première version des standards GNSS couvrant l'ensemble des phases de vol jusqu'aux approches de Catégorie I [Roturier, 2004].

Cependant les exigences aviation civile peuvent être très strictes, en particulier celle liées au contrôle d'intégrité et même si des procedures de qualité ont été implémentées en termes de surveillance d'erreur, le segment de contrôle du système GPS ne peut pas corriger des pannes satellitaires ou prévenir l'utilisateur en l'espace des quelques secondes exigées par l'OACI. Ainsi, jusqu'à présent, les systèmes de navigation par satellites seuls ne peuvent pas être utilisés comme un moyen unique de navigation. Afin d'assurer les niveaux requis en matière de précision, d'intégrité, de continuité de service et de disponibilité pour les différentes phases de vol, les normes GNSS OACI définissent différentes architectures de venant compléter les constellations de base:

- Ground Based Augmentation Systems (GBAS)
- Satellite Based Augmentation Systems (SBAS)
- Airborne Based Augmentation Systems (ABAS)

Un système GBAS consiste en une station de referénce qui émet dans la zone de service de l'aéroport des corrections de mesure de pseudo-distance, des informations d'intégrité ainsi que des données concernant le segment d'approche final par un lien VHF. Actuellement, GPS

L1 C/A et un système GBAS permettent d'atteindre toutes les phases de vol jusqu'à la CAT I incluse avec pour objectif futur les approches de précision de catégorie III.

Un système SBAS consiste en un réseau de stations de référence qui surveillent les signaux des satellites de la constellation de base et qui transmettent les informations pertinentes (corrections, message d'intégrité) aux utilisateurs au moyen de satellites géostationnaires. Selon l'architecture du système et le niveau de performance attendu, 20 à 35 stations peuvent être nécessaire pour couvrir la zone de service qui est typiquement de la taille d'un un continent. Au vu des couts de mise en œuvre des stations de surveillance sol, le meilleur niveau de performance pouvant actuellement être atteint par les systèmes SBAS correspond aux approches APV.

Finalement, les systèmes ABAS fournissent un contrôle d'intégrité du calcul de position en utilisant la redondance des mesures fournies par les constellations GNSS. À la différence d'autres systèmes d'augmentations du type de GBAS ou SBAS, ce moyen d'augmentation n'améliore pas la précision du positionement. On parle de contrôle autonome d'intégrité (en anglais Receiver Autonomous Integrity Monitoring, RAIM) lorsqu'on utilise exclusivement les mesures GNSS (mesures de distances) et d'AAIM (de l'anglais Aircraft Autonomous Integrity Monitoring) lorsque des informations issues d'autres capteurs embarquées tels que altimètres barométriques, horloge ou systèmes de navigation inertielle sont utilisés.

Cette étude se concentrera sur ce dernier type de système d'augmentation et plus particulièrement sur les techniques RAIM et leurs performances.

Les techniques RAIM sont largement utilisées aujourd'hui pour fournir le contrôle d'intégrité jusqu'aux approches de non précision (en anglais, Non Precision Approaches NPA) en utilisant la constellation GPS et les mesures disponibles sur la fréquence L1. Il s'agit en effet d'un moyen simple et efficace de controler l'intégrité pour les applications aviation civile. Cependant ses performances sont limitées jusqu'à présent aux approches de non précision.

D'autre part, l'OACI et l'industrie aéronautique reconnaissent depuis longtemps que les approches aux instruments à guidage vertical présentent un apport significatif en termes de sécurité ainsi que de réels avantages opérationnels et environnementaux par rapport aux approches de non précision pourtant largement pratiquées.

Avec la future introduction de nouvelles constellations satellitaires, comme Galileo et GPS modernisé, de grandes améliorations pourraient être attendues quant à la performance des algorithmes RAIM. Tout d'abord grace à la qualité des mesures disponibles. GPS et Galileo transmettront des signaux réservés à l'usage aéronautique sur deux fréquences distinctes ce qui permettra l'utilisation de mesures exemptes d'erreur ionosphérique. De plus les futurs signaux offriront de meilleures performances de poursuite. Ces futurs systèmes fourniront aussi des informations d'horloge et d'ephemeride plus précises. Ces facteurs contribueront donc de manière significative à réduire les erreurs de mesures de pseudodistances. D'autre part, le nombre de mesures disponibles augmentera considérablement, ce qui réduira l'impact d'une panne satellite sur l'erreur globale d'estimation de position. Pourtant, ce potentiel bénéfice en terme de contrôle d'intégrité doit être précisement évalué. En effet un plus grand nombre de mesures disponibles implique également un plus grand nombre de mesures défectueuses potentielles au niveau du récepteur. De plus, les phases de vol visées sont caractérisées par des erreurs de position tolérables plus petites comparées à NPA. Donc les erreurs sur les mesures pseudodistance dite « dangereuses » devant être détectées par

l'algorithme de surveillance doivent être réexaminées. En effet, elles pourraient avoir une plus petite amplitude et des taux d'occurrence qui ne sont pas clairement définie pour le moment.

C'est dans ce contexte que la Direction Générale de l'Aviation Civile a initié cette thèse dont l'objectif est d'évaluer le potentiel des algorithmes RAIM pour les approches à guidage vertical. On tachera de savoir dans quelle mesure l'augmentation du nombre de satellites et de l'amélioration de qualité de mesures de pseudodistance pourraient elles permettre l'utilisation de RAIM les approches à guidage vertical.

Cette thèse est organisée de la manière suivante. Tout d'abord, le chapitre 2 présente les exigences de l'aviation civile quant à l'utilisation du GNSS. Cette section inclut une description des différentes phases de vol et plus particulièrement des phases d'approche. Elle introduit les concepts RNAV et RNP et définit également les critères de performance requis par l'OACI pour chaque les phases de vol. Finalement, les termes de détectionet d'exclusion de faute, plus spécifiques au contrôle autonome d'intégrité, sont définis. Le chapitre 3 a pour objectif de donner un modèle complet des mesures GNSS en adressant aussi bien le mode nominal et le mode défectueux, en tenant compte des pannes satellite et de l'effet des interférences. Le chapitre 4 a pour but d'étudier differents algorithmes RAIM mais certains aspects généraux comme l'estimation de la position d'utilisateur ou le calcul du plus petit biais sur une mesure de pseudo distance entrainant une erreur de positionnement sont d'abord présentés. La manière dont les exigences aviation civile et le modèle d'erreur sont interprétés afin de constituer les paramètres d'entrée des algorithmes RAIM est discutée au chapitre 5. Le chapitre 6 présente des résultats des simulations qui ont été effectuées pour évaluer la performance RAIM pour les approches à guidage vertical. Cette évaluation a été réalisée grâce à des simulations Matlab. Finalement, le chapitre 7 résume les principaux résultats de ce travail de doctorat et propose quelques pistes de reflexion quant à de futurs travaux.

Chapter 1

Introduction

1-1 Motivation

As it was recognized that the ever-increasing demand for air transportation services, the high cost of equipment and the need for increased efficiency while maintaining safety were beginning to stress the existing global air navigation system to its limits, the International Civil Aviation Organization (ICAO) established the Future Air Navigation Systems (FANS) committee in 1983. Its task was to study technical, operational, institutional and economic questions relative to future potential air navigation systems, to identify and assess new concepts and new technology and to make recommendations for the coordinated evolutionary development of air navigation. The ICAO's Tenth Air Navigation Conference in 1991, approving the FANS conclusions, agreed to endorse the satellite-based Communications, Navigation and Surveillance (CNS) and Air Traffic Management (ATM) system for the use of international civil aviation well into the 21st century [ICAO, 1991]. But the use of satellite navigation for civil aviation has been made possible by the United States government decision to offer the Global Positioning System (GPS) for civilian use without collecting direct costs. This has lead ICAO to undertake standardization work for Global Navigation Satellite System (GNSS), with the objective of defining GNSS systems that could be used during all phases of flight, ranging from ocean navigation to Category III precision landings. The work done by the GNSS Panel expert group enabled ICAO, in November 2002, to publish a first version of GNSS standards covering all phases of flight up to Category I approaches in Annex 10 of the Chicago Convention [Roturier, 2004].

But civil aviation requirements can be very stringent, in particular integrity monitoring ones. For instance, even if quality failure monitoring processes have been implemented, GPS Control Segment cannot correct satellite anomalies or warn the user within the few seconds required by ICAO and, up to now, satellite systems alone cannot be used as a means of navigation. Therefore, in order to ensure the levels required in terms of precision, integrity, continuity of service and availability of GNSS for various phases of flight, the ICAO GNSS standards define different architectures to augment the basic constellations:

- Ground Based Augmentation Systems (GBAS)
- Satellite Based Augmentation Systems (SBAS)

- Airborne Based Augmentation Systems (ABAS)

GBAS uses a technique known as local area differential corrections. A control station at an airport for example, precisely measures errors and relays them to a user so that he can eliminate them from his own measurement. This technique uses a data link in the VHF frequency band of ILS - VOR systems (108 - 118 MHz). The other elements transmitted through this VHF link are integrity data of various satellites in view, as well as the database used for the final approach segment. For a GBAS station, the coverage is about thirty kilometers and the objective of GBAS systems is to carry out Category I precision approaches. GBAS is also foreseen to support Category II and Category III operations.

SBAS transmits differential corrections and integrity messages for navigation satellites that are within sight of a network of stations, typically deployed for an entire continent. Depending on the architecture of the system and the required performance level, 20 to 35 stations may be required to cover a continent. There are four important differences compared to GBAS. First of all, the frequency band of the data link is identical to that of the GPS signals. Next, the use of geostationary satellites enables messages to be broadcast over very wide areas. These geostationary satellites can also transmit ranging measurements, as if they were GPS satellites. Finally, SBAS provides vectorial corrections (clock, ionosphere, ephemeris corrections) while GBAS transmits scalar ones (pseudorange corrections). Considering the limitation of the number of ground-based control stations to control deployment and operation costs, it is thought that the best performance level that can currently be attained by the SBAS corresponds to APV I or II performance approaches. Today, various SBAS are implemented:

- the Wide Area Augmentation System (WAAS), operated by the United States Federal Aviation Administration (FAA).
- the European Geostationary Navigation Overlay Service (EGNOS), today operated by the European Space Agency (ESA) and then operated by the ESSP (European Satellite Service Provider) from the beginning of the year 2009.
- the Multi-functional Satellite Augmentation System (MSAS) system, operated by Japanese Civil Aviation Bureau (JCAB).

Finally, **ABAS** provides integrity monitoring for the position solution using redundant information that is within the GNSS constellation. Unlike other types of augmentations of the GBAS and SBAS type, ABAS augmentation does not improve positioning accuracy. ABAS are referred as Receiver Autonomous Integrity Monitoring (RAIM) when GNSS information (range measurements) is exclusively used and as Aircraft Autonomous Integrity Monitoring (AAIM) when information from additional on-board sensors (e.g. barometric altimeter, clock and Inertial Navigation System, INS) is also used.

This study will focus on this last type of augmentation system and more particularly on RAIM techniques and performance.

RAIM is worldwide used today to provide integrity monitoring up to Non Precision Approach (NPA) operations using the GPS constellation with single frequency L1 measurements. Indeed, it is a simple and efficient solution to check the integrity of GNSS in civil aviation applications. But its performance is limited at best to NPA up to now. Indeed current nominal errors on GPS L1 C/A pseudorange measurements and current constellation geometry do not allow GPS L1 C/A+RAIM to fulfil stringent vertical requirement on positioning error.

On the other hand, ICAO and the international aviation industry have long recognized that instrument approaches that give pilots vertical guidance provide significant safety, operational and environmental benefits over the now widely used non precision approaches. Specific advantages of approaches with vertical guidance include safer approach path guidance, simpler approach procedures and lower minimum descent altitudes in adverse weather.

In the context of the introduction of future satellite constellations, such as Galileo and modernized Global Positioning System GPS, great improvements could be expected from RAIM performance.

First concerning the quality of the available measurements. Both GPS and Galileo will broadcast signal for aeronautic use on two distinct frequencies that will allow the use of iono-free measurements. Moreover future signals will offer improved tracking accuracy. Future systems will also provide better clock and ephemeris information. These factors will contribute to significantly reduce the nominal error on pseudo range measurements.

Secondly, the number of available measurements will considerably increase. That will reduce the impact of a single satellite failure on the position estimation error and significantly improve RAIM capability to monitor integrity during more stringent operations.

Thus, approaches with vertical guidance such as APV or LPV 200 operations could reasonably be targeted using RAIM to provide integrity monitoring.

However, the benefit for position integrity needs to be evaluated, as a larger number of available measurements also implies a larger number of potential faulty measurements for the receiver. Moreover, the targeted phases of flight are characterized by smaller horizontal and vertical tolerable position errors compared to NPA, and by lower acceptable probabilities for the corresponding alert limits to be exceeded. Therefore, the threatening range errors that need to be detected by the fault detection algorithm have to be reconsidered, since they could have smaller amplitude, and a probability of occurrence that is not clearly defined currently. This is why these improvements need to be precisely quantified.

It is within this context that the French Civil Aviation has sponsored this Ph.D. which objective is to evaluate the potential capacity of RAIM algorithms to support approach and landing phases of flight with vertical guidance. The extent to which the augmentation of the number of satellites and the improvement of pseudorange measurements quality could enable the use of RAIM for both horizontal and vertical guidance is investigated.

Currently, several studies deal with these aspects and address common issues. Among these projects we can mention:

The GNSS Evolutionary Architecture Study GEAS panel which is an expert panel established by the FAA GNSS Program Office in order to develop candidates for an integrity architecture for modernized GNSS that would satisfy en route, terminal and precision approach operation and be capable to provide LPV 200 performance worldwide [GEAS, 2008].

The Galileo Supervising Authority GSA project GIRASOLE (Galileo Integrity Receiver for Advanced Safety Of Life Equipment) which scope includes the definition of the three types of receivers (aviation, maritime and rail), core technologies investigation and implementation

with main focus on integrity concepts, breadboards development and finally the development of testing tools. The objective of the project is that, at the end, receiver manufacturers will have available basic building blocks to continue the development of the Galileo SoL receiver of their own application domain [GSA, 2008]

The European Organization for the Safety of Air Navigation, EUROCONTROL, study which analyzes the RAIM capabilities in a multi-constellation and multi-frequency GNSS environment in order to evaluate the actual need for the Galileo Safety-of-Life Service.

The European Commission Framework Programme (FP6) ANASTASIA (Airborne New Advanced Satellite Techniques and Technologies in A System Integrated Approach) whose scientific and technical objectives are to provide on-board Communication, Navigation and Surveillance (CNS) solutions to cope with the foreseen doubling of air traffic by 2020. In particular, ANASTASIA project carries out research of future technology and system architectures for navigation, resulting in the development of a new generation of airborne GNSS receivers for all phases of flight. This program started in April 2005 and is expected to continue until early 2009 [Anastasia, 2008].

1-2 Original contributions

The main contributions of this thesis are enumerated below and are detailed all along this dissertation. We indicate the section number where contributions can be found knowing that contributions from other authors are also presented in each of these sections:

- Detailed computation of user equivalent range error variance (3.2)
- Analysis of the effect of interferences on pseudorange measurement (3.3)
- Adaptation of LSR RAIM algorithm to nominal biases (appendix B)
- Improvement of Maximum Solution Separation protection levels computation (4.3)
- Implementation of GLR algorithm as a RAIM: analytical expression of the threshold that satisfies the false alarm probability, prediction of the probability of missed detection (4.4)
- Design of a sequential GLR algorithm to detect step plus ramp failure (4.4)
- Analysis of the amplitude of smallest single biases that lead to a positioning failure (5.6)

Details on the specific contributions compared to background information are provided in each section.

1-3 Dissertation organization

This dissertation is structured as follows.

First of all, chapter 2 presents the civil aviation requirements relative to GNSS use. This section includes a description of the different phases of flight and especially approaches operations. It provides an introduction to the area navigation and to the required navigation performance concepts. It also defines each ICAO performance navigation criteria and Signal in Space Requirement for each phases of flight is then given. Finally, fault

detection/exclusion terms which are more specific to autonomous integrity monitoring are defined.

Chapter 3 intends to give a complete model of GNSS measurement addressing the fault free and the faulty case, taking into account satellite failure and interference effects.

Chapter 4 addresses the study that has been made concerning RAIM techniques. Some general aspects like the user position estimation or the computation of the smallest single pseudorange bias that leads to a positioning failure are first presented. The most classical RAIM technique that is to say the least square residual method is then recalled. The Maximum Solution Separation method is also studied and new ways of computing horizontal protection level are presented. The use of generalized likelihood ratio test as a RAIM technique is then considered for snapshot and sequential implementation.

The way both civil aviation requirements and threat model are interpreted to constitute an input to RAIM algorithms is discussed in chapter 5.

Chapter 6 presents results of the simulations that have been conducted to measure RAIM performance for vertically guided approaches. This evaluation has been realized thanks to Matlab simulations.

Finally, chapter 7 summarizes the main results of this Ph.D. work and concludes on the obtained results. Some outstanding issues are introduced as opening and propositions for future work.

Chapître 2

Exigences Aviation Civile

L'Organisation de l'Aviation Civile Internationale (OACI), en anglais International Civil Aviation Organization (ICAO), est une organisation internationale qui dépend des Nations Unies. Son rôle est de participer à l'élaboration des normes qui permettent la standardisation du transport aéronautique international ainsi que d'assurer un développement sûr, sécuritaire et durable de l'aviation civile. Le conseil de l'OACI adopte les normes et recommandations règlementant la navigation (en anglais : SARP, Standards and Recommended Practices), le partage des fréquences radio, les brevets du personnel d'aviation, la circulation aérienne, etc. Il définit aussi les protocoles à suivre lors des enquêtes sur les accidents aériens, protocoles qui sont respectés par les pays signataires de la Convention de l'Aviation Civile Internationale, communément appelée Convention de Chicago [ICAO, 2008].

En particulier, l'OACI établit les standards concernant les moyens de radionavigation, dont ceux concernant la navigation par satellite. Ils sont principalement recensés dans l'annexe 10 de Convention de l'Aviation Civile Internationale.

L'objectif de ce chapitre est de rappeler les principales définitions et les principales exigences relatives aux approches à guidage vertical anisi qu'au contrôle d'intégrité.

Les principales phases de vol ainsi que les classes d'appoches sont tout d'abord présentées dans la section 2.1.

La section 2.2 présente le concept de navigation fondée sur les performances (en anglais Performance Based Navigation concept, PBN), qui s'appuit notamment sur les concepts RNAV et RNP et au sein duquel la navigation par satellite aura un role prépondérant. Ainsi la navigation de surface (RNAV) est une méthode de navigation de plus en plus répandue, permettant le vol sur n'importe quelle trajectoire voulue, utilisant une position absolue de l'aéronef indépendante de l'emplacement des infrastructures sol. Le concept RNP (Required Navigation Performance) est défini par l'OACI comme l'indication de la précision de navigation nécessaire pour évoluer à l'intérieur d'un espace aérien défini.

La section 2.3 présente les critères de performance de navigation que doivent remplir les signaux GNSS.

Ainsi la précision est le degré de conformité entre la position ou la vitesse mesurée ou estimée à un instant donné et la position ou la vitesse réelle. La précision de position est généralement présentéecomme la borne de l'intervalle de confiance à 95% de l'erreur de position.

La disponibilité du service est la probabilité que le service soit rendu au début de chaque cycle d'utilisation (par exemple pour une approche).

La continuité de service est la probabilité que les performances seront atteintes pendant toute la durée d'un cycle d'opération (par exemple pendant une approche), à condition que les performances soient atteintes au début de l'opération.

L'intégrité représente la confiance qui peut être accordée à la validité des informations fournies par le système. Elle inclut la capacité du système à fournir des alertes à l'utilisateur dans le temps imparti lorsque le système ne peut plus être utilisé.

Les valeurs assignées à ces paramètres dependent de l'application ou de l'opération envisagée Elles sont fixées par l'OACI et sont détaillées dans la section 2.4

Des définitions plus spécifiques au contrôle autonome d'intégrité sont ensuite présentées dans la section 2.5.

Chapter 2

Civil Aviation Requirements

2-1 Phases of flight
2-2 Performance based navigation Concept
2-3 Performance Navigation Criteria
2-4 Signals in Space Performance Requirements
2-5 Fault Detection, Fault Exclusion
2-6 Synthesis

The International Civil Aviation Organization (ICAO) is the agency of the United Nations, which codifies the principles and techniques of international air navigation and fosters the planning and development of international air transport to ensure safe and orderly growth. The ICAO Council adopts standards and recommended practices concerning air navigation, prevention of unlawful interference, and facilitation of border-crossing procedures for international civil aviation. In addition, the ICAO defines the protocols for air accident investigation followed by transport safety authorities in countries signatory to the Convention on International Civil Aviation, commonly known as the Chicago Convention [ICAO, 2008].

In particular, the International Civil Aviation Organization (ICAO) is responsible for establishing the standards for radio navigation aids, including the ones concerning GNSS. They are mainly defined in the Annex 10 to the Convention on International Civil Aviation.

The objective of this chapter is to recall the main definitions and the main requirements related to approaches with vertical guidance operations and especially integrity monitoring.

2-1 Phases of flight

A flight of an aircraft consists of six major phases [CICTT, 2006]:

- **Take-Off**: “From the application of takeoff power, through rotation and to an altitude of 35 feet above runway elevation or until gear-up selection, whichever comes first”.

- **Departure**: “From the end of the Takeoff sub-phase to the first prescribed power reduction, or until reaching 1000 feet above runway elevation or the VFR pattern (Visual Flight Rules), whichever comes first”

- **Cruise**: “Any level flight segment after arrival at initial cruise altitude until the start of descent to the destination.”

- **Descent**:
    - Instrument Flight Rules (IFR): Descent from cruise to either Initial Approach Fix (IAF) or VFR pattern entry).
    - Visual Flight Rules (VFR): Descent from cruise to the VFR pattern entry or 1000 feet above the runway elevation, whichever comes first.

- **Final Approach**: "From the FAF (Final Approach Fix) to the beginning of the landing flare."

- **Landing**: "Transition from nose-low to nose-up attitude just before landing until touchdown."

Three classes of approaches and landing operation have been defined by the ICAO in the Annex 6 [ICAO, 2001] and are classified as follow:

- **Non precision Approaches** and landing operations: an instrument approach and landing which utilizes lateral guidance but does not utilize vertical guidance

- **Approaches** and landing operations **with vertical guidance**: an instrument approach and landing which utilizes lateral and vertical guidance but does not meet the requirements established for precision approach and landing operation.

- **Precision Approaches** and landing operation: an instrument approach and landing using precision lateral and vertical guidance with minima as determined by the category of operation.

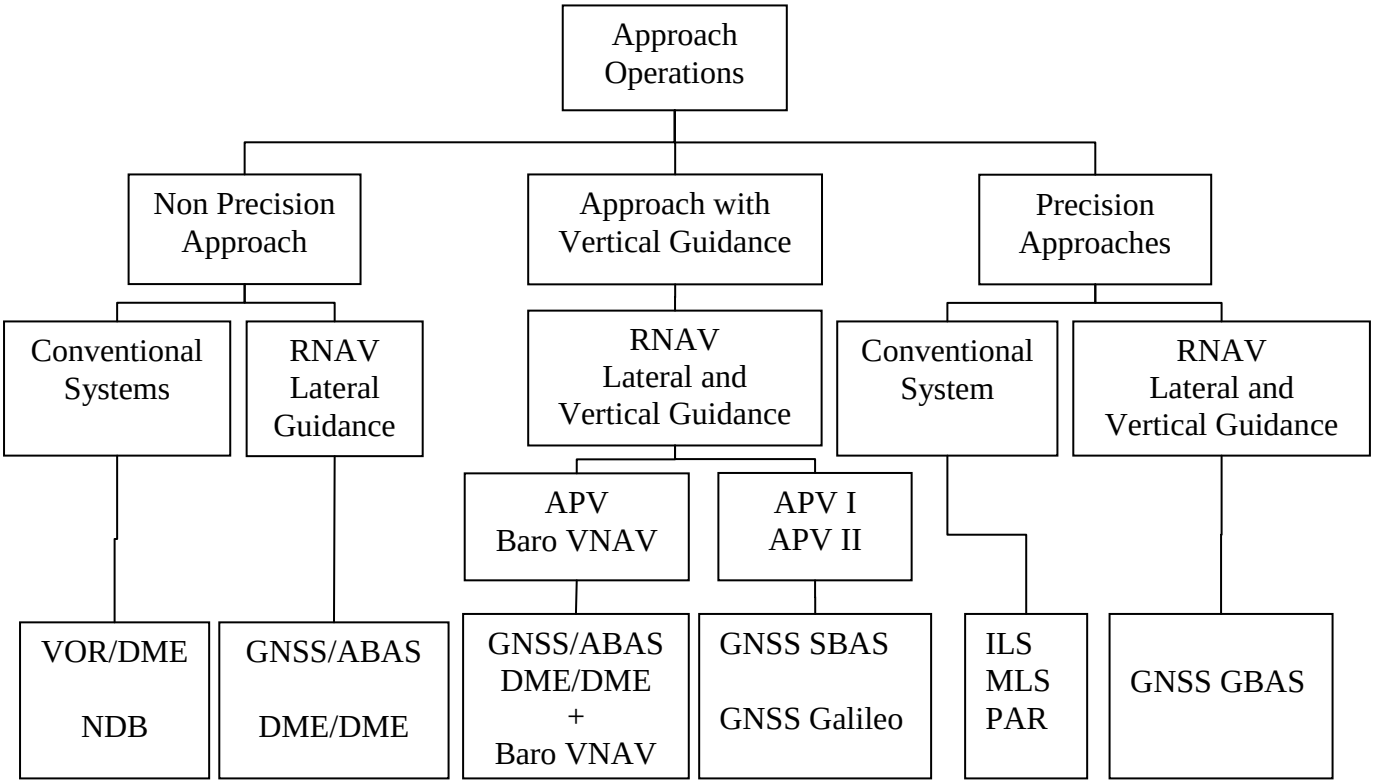

Figure 1 - ICAO classification of approaches [Roturier, 2004]

where PAR stand for Precision Approach Radar, DME for Distance Measuring Equipment, NDB for Non Directional Beacon, MLS for Microwave Landing System, ILS for Instrument Landing System, VOR for Very High Frequency Omni directional Range, RNAV for Area Navigation and VNAV for Vertical Navigation

Categories of aircraft approaches are defined according to the level of confidence that can be placed by the pilot into the system he is using to help him land the plane safely. Approaches are divided in two main segments: the aircraft first follows the indication provided by the landing system, then the pilot takes over in the final part and controls the aircraft using visual outside information. As the reliability of the aircraft, of the crew and of the landing system increases, the height of the aircraft over the ground at the end of the interval of use of the information provided by the system can be decreased [Macabiau, 1997].

The **Decision Height** (DH) is specified as the critical point in the approach path which is the minimum height above the runway threshold at which a missed approach procedure must be executed if the minimum visual reference is not established.

The **Visibility** is the greatest distance determined by atmospheric conditions and expressed in unit of length at which it is possible with the unaided eye to see and identify, in daylight a prominent dark object and at night a remarkable light source [ICAO, 2005]

The **Runway Visual Range (**RVR) is the maximum distance in the landing direction at which the pilot on the center line can see the runway surface markings or the runway lights, as measured at different point along the runway and in particular in the touchdown area [OFCM, 2005].

Approaches can be defined by their decision height, the visibility or runway visual range:

Approaches		Decision Height	Visual Requirement
NPA		$DH \geq 350\ ft$	Depending on the airport equipment
APV		$DH \geq 250\ ft$	
LPV 200		$DH \geq 60\ m\ (200\ ft)$	
CAT I		$DH \geq 60\ m\ (200\ ft)$	Visibility $\geq 800m$ $RVR \geq 550$ m
CAT II		$(100\ ft)$ 30 m $\leq DH \leq 60$ m	$RVR \geq 350$ m
CAT III	A	0 m $\leq DH \leq 30$ m	$RVR \geq 200$ m
	B	0 m $\leq DH \leq 15$ m	50 m $\leq RVR \leq 200$ m
	C	$DH = 0$ m	$RVR = 0\ m$

Table 1 - Decision heights and Visual requirements [ICAO, 2006]

2-2 Performance based Navigation Concept

The Performance Based Navigation (PBN) concept specifies aircraft RNAV system performance requirements in terms of accuracy, integrity, availability, continuity and functionality needed for the proposed operations in the context of a particular airspace concept. It represents a shift from sensor-based to performance-based navigation.

Performance requirements are identified in navigation specifications, which also identify the choice of navigation sensors and equipment that may be used to meet the performance requirements. This concept relies on the area navigation method and is implemented through the required navigation performance procedures [ICAO, 2008].

2-2-1 Area Navigation (RNAV)

Area Navigation (RNAV) is a method of navigation which permits aircraft operation on any desired flight path within the coverage of station-referenced navigation aids or within the limits of the capability of self-contained navigation aids, or a combination of these [RTCA, 2003].

This navigation method allows designing more routes and most of all shorter routes, permits noise reduction and offers greater flexibility in the use of the airspace resources. It allows aircraft to fly user-preferred routes from waypoint to waypoint, where waypoints do not depend on ground infrastructure.

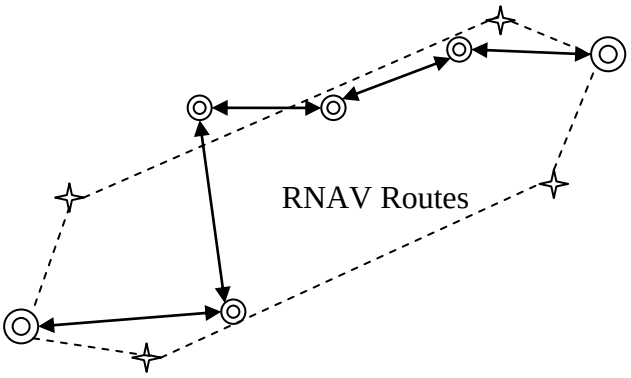

Figure 2 - RNAV principle

The trend toward an Area Navigation concept means a greater role for GNSS, especially in areas that lack suitable ground based navigation aids or surveillance equipment.

As the future CNS/ATM operations are expected to be based on navigation defined by geographic fixes and not to be restricted to the location of ground-based navigation aids, this concept of RNAV has been developed. But an element that has been missing is the level of confidence of navigation accuracy. This is provides by the Required Navigation Performance (RNP) concept.

2-2-2 Required Navigation Performance (RNP)

Required Navigation Performance (RNP) is defined by ICAO as a statement of the navigation performance necessary for operation within a defined airspace.

Part of the broader concept PBN, RNP is a method of implementing routes and flight paths that differs from previous methods in that not only does it have an associated performance specification that an aircraft must meet before the path can be flown but must also monitors the achieved performance and provide an alert in the event that this fails to meet the specification. It is the monitoring and alerting facility that distinguishes RNP from RNAV from which it is developed. RNP equipped aircrafts can safely operate routes with less separation than previously required which is significant because it increases the number of

aircraft that can safely use a particular airspace and therefore accommodate the increasing demand for air traffic capacity. GNSS is the primary navigation system to support currently defined RNP standards.

Under RNP, the nature of the navigational aids is not specified, rather the volume of airspace around the aircraft is, and this volume may be smaller (in some cases much smaller) than the one of conventional navigation.

The performance required to fly an RNP route is generally specified in nautical miles, for example, RNP 4. This RNP type is a statement of the navigation performance accuracy to be achieved within the corresponding airspace by the population of aircraft operating within the airspace. The RNP specification also requires that if the error exceeds or is likely to exceed twice the specified value (i.e. 8NM for RNP 4) then an alert must be generated (containment region). As route spacing must be sufficient to ensure that two aircraft deviating to the alert level toward one another will remain safely separated, it is typically set to 5 or 6 times the RNP value [ICAO, 1999]. Thus RNP types can be used by airspace planners to determine airspace utilization potential and as an input in defining route widths and traffic separation requirements, although RNP by itself is not sufficient basis for setting a separation standard.

To evaluate RNP RNAV compliance, several errors are to be taken into account. According to [RTCA, 2003], the required navigation performance is defined by the Total System Error (TSE), which represents:

- **PDE** (Path Definition Error): difference between the desired path (the path that the crew and air traffic control can expect the aircraft to fly) and the path defined by the Flight Management System (FMS).
- **FTE** (Flight Technical Error): difference between the estimated position of the aircraft and the path defined by the FMS. This error is due to the way the aircraft is controlled and it is also called XTK (Cross Track Error)
- **NSE** (Navigation System Error): difference between the estimated position and the true position of the aircraft.

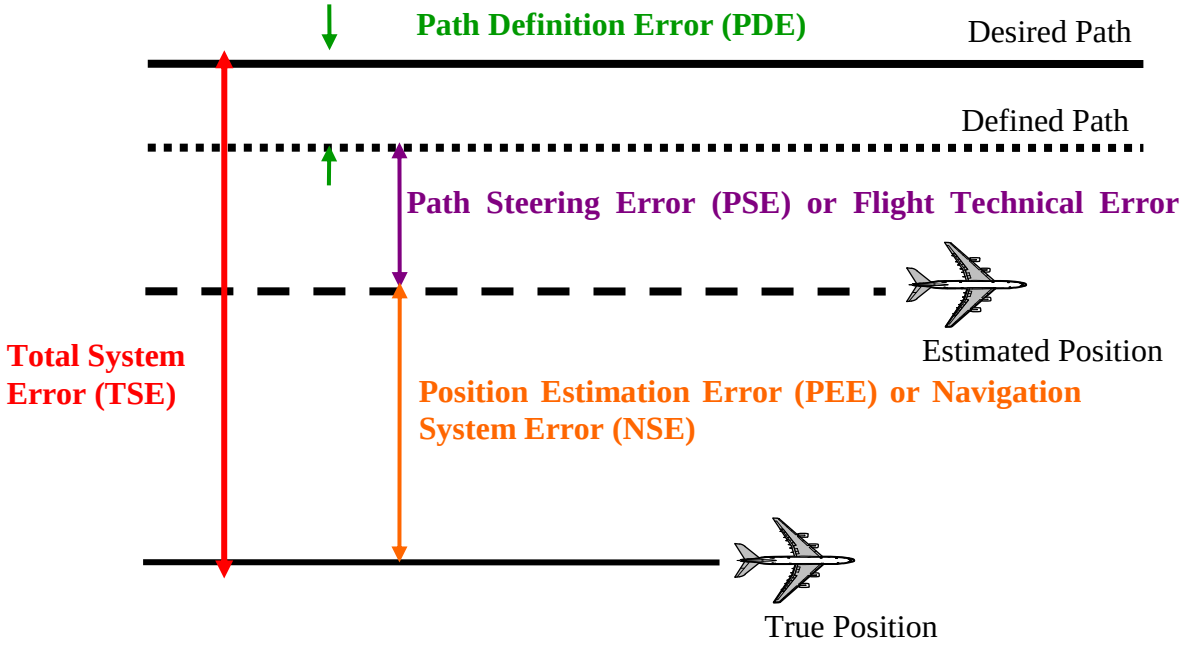

Figure 3 - Total System Error

2-3 Performance Navigation Criteria

Navigation system performance requirements are defined in the Manual on Required Navigation Performance [ICAO, 1999] for a single aircraft and for the total system which includes the signal-in-space, the airborne equipment and the ability of the aircraft to fly the desired trajectory. These total system requirements were used as a starting point to derive GNSS signal-in-space performance requirements which criteria definitions are given in this section [ICAO, 2006].

2-3-1 Accuracy

GNSS position error is the difference between the estimated position and the actual position. For an estimated position at a specific location, the probability that the position error is within the accuracy requirement should be at least 95 per cent.

2-3-2 Availability

The availability of a navigation system is the ability of the system to provide the required function and performance at the initiation of the intended operation.

The availability of GNSS is characterized by the portion of time the system is to be used for navigation during which reliable navigation information is presented to the crew, autopilot, or other system managing the flight of the aircraft.

2-3-3 Continuity

The continuity of a system is the ability of the total system to perform its function without unscheduled interruption during the intended operation.

More specifically, continuity is the probability that the specified system performance will be maintained for the duration of a phase operation, presuming that the system was available at the beginning of that phase operation and was predicted to operate throughout the operation.

2-3-4 Integrity

Integrity is a measure of trust that can be placed in the correctness of the information supplied by the total system. Integrity includes the ability of a system to provide timely and valid warning to the user (alerts) when the system must not be used for the intended operation (or phase of flight).

Integrity requirements are defined thanks to three parameters:
- the integrity risk
- the alert limit
- the time to alert

Integrity risk is the probability of providing a signal that is out of tolerance without warning the user in a given period of time.

To assure that the position error is acceptable, an **alert limits** is defined that represents the largest position error allowable for safe operation:

- The Horizontal Alert Limit (HAL) is the radius of a circle in the horizontal plane (the local plane tangent to the WGS-84 ellipsoid), with its center being at the true position, that describes the region that is required to contain the indicated horizontal position with the required probability for a particular navigation mode

- The Vertical Alert Limit (VAL) is half the length of a segment on the vertical axis (perpendicular to the horizontal plane of WGS-84 ellipsoid)), with its center being at the true position, that describes the region that is required to contain the indicated vertical position with the required probability for a particular navigation mode

Time to alert is the maximum allowable elapsed time from the onset of a positioning failure until the equipment annunciates the alert.

The probability of non-integrity detection quantifies the integrity risk. It represents the probability that an error exceeds the alert limit without the user being informed within the time to alert.

The values assigned to these three parameters depend on the specific application and intended operation, and are determined by the International Civil Aviation Organization.

2-4 Signal in Space Performance Requirements

2-4-1 Annex 10 Signal in Space Performance Requirements

According to [ICAO, 2006] the combination of GNSS elements and a fault-free GNSS user receiver shall meet the signal-in-space requirements defined in the table next page.

The concept of a fault-free user receiver is applied only as a means of defining the performance of combinations of different GNSS elements. The fault-free receiver is assumed to be a receiver with nominal accuracy and time-to-alert performance. Such a receiver is assumed to have no failures that affect the integrity, availability and continuity performance.

Ranges of values are given for the continuity requirement for en-route, terminal, initial approach, NPA and departure operations, as this requirement is dependent upon several factors including the intended operation, traffic density, complexity of airspace and availability of alternative navigation aids. The lower value given is the minimum requirement for areas with low traffic density and airspace complexity. The higher value given is appropriate for areas with high traffic density and airspace complexity.

A range of values is also given for the availability requirements as these requirements are dependent upon the operational need which is based upon several factors including the frequency of operations, weather environments, the size and duration of the outages, availability of alternate navigation aids, radar coverage, traffic density and reversionary operational procedures.

Typical Operation	Accuracy Horizontal 95%	Accuracy Vertical 95%	Integrity risk	Time To Alert	Horizontal Alert limit	Vertical Alert limit	Continuity	Availability
En-route	3.7 km (2.0 NM)	N/A	$1-1\times10^{-7}$/h	5 min	7.4 km	N/A	$1-1\times10^{-4}$/h to $1-1\times10^{-8}$/h	0.99 to 0.99999
En-route, Terminal	0.74 km (0.4 NM)	N/A	$1-1\times10^{-7}$/h	15 s	3.7 km	N/A	$1-1\times10^{-4}$/h to $1-1\times10^{-8}$/h	0.99 to 0.99999
Initial approach, Intermediate approach, Non precision approach, Departure	220 m (720 ft)	N/A	$1-1\times10^{-7}$/h	10 s	556 m	N/A	$1-1\times10^{-4}$/h to $1-1\times10^{-8}$/h	0.99 to 0.99999
Approach Operations with vertical Guidance APV I	16 m (52 ft)	20 m (66 ft)	$1-2\times10^{-7}$ per approach	10 s	40 m	50 m	$1-8\times10^{-6}$/h in any 15 s	0.99 to 0.99999
Approach Operations with vertical Guidance APV II	16 m (52 ft)	8 m (26 ft)	$1-2\times10^{-7}$ per approach	6 s	40 m	20 m	$1-8\times10^{-6}$/h in any 15 s	0.99 to 0.99999
Category I precision approach	16 m (52 ft)	6 m to 4m (20 ft to 13ft)	$1-2\times10^{-7}$ per approach	6 s	40 m	15.0 m to 10 m	$1-8\times10^{-6}$/h in any 15 s	0.99 to 0.99999

Table 2 - Signal in Space Performance [ICAO, 2006]

2-4-2 LPV 200 Signal in Space Performance

Whereas Localizer Performance with Vertical guidance (LPV) approaches is a category of approaches with vertical guidance that include APV I and APV II operations, LPV 200 is a new concept of aircraft instrument approach procedure in which guidance is provided down to a minimum decision altitude as low as 200 feet height above touchdown.

LPV 200 approaches are published by the FAA and built to exploit the high accuracy of the American satellite-based augmentation system WAAS. This operation allows a lateral guidance with the accuracy of the typical ILS and would provide a significant operational benefit compared to the existing APV operations [Cabler and DeCleene, 2002].

This category of approach is not included yet in the Annex 10 but some proposed requirements to support this new operation can be presented [DeCleene, 2007]:

Accuracy Horizontal 95%	Accuracy Vertical 95%	Integrity risk	Time To Alert	Horizontal Alert limit	Vertical Alert limit	Continuity	Availability
16 m	4 m	$1 - 2 \times 10^{-7}$/h	6 s	40 m	35 m	$1 - 1 \times 10^{-4}$/h to $1 - 1 \times 10^{-8}$/h	0.99 to 0.99999

Table 3 - LPV 200 Signal in Space Performance

The accuracy requirement is equivalent to ILS. The accuracy has a significant effect on obstacle clearance criteria and on the probability of a successful landing after transitioning to the visual segment. The continuity and availability are also equivalent to ILS and are already harmonized across precision approach, APV II and APV I.

The integrity risk requirement is equivalent to ILS and is already harmonized across precision approach, APV II and APV I. The time-to-alert is equivalent to ILS. This time-to-alert for APV II and precision approach is based on the requirement for ILS glideslope, which is 6 seconds. The HAL is equivalent to ILS, and is already harmonized across precision approach, APV II and APV I. The VAL was derived by assuming a bias error equal to the VAL and evaluating the conditional risk of going outside the obstacle clearance area. The 35 m VAL was initially derived using a simplified analysis technique, which has since been validated through more rigorous analysis including consideration of the impact to the missed approach surface.

LPV200 operations would then fall between APV II and Category I approaches.

It is to be noticed that the 35 m VAL satisfies obstacle clearance requirement but does not necessarily set up the aircraft to land safely on the runway. Studies conducted by the FAA and NavCanada show that more than a positive 10 m bias in positioning causes pilots to overcompensate and descent too rapidly in a way that would cause significant damage to the aircraft. This is why a system that is intended to provide LPV 200 must also have a very low probability of 10 meter positioning errors. Unfortunately this requirement is not yet well documented [Walter, 2008].

2-5 Fault Detection, Fault Exclusion

The aim of this section is to recall Minimal Operational Performance Standard (MOPS) definitions relative to integrity monitoring functions [RTCA, 2006].

2-5-1 Introduction

Fault Detection and Exclusion (FDE) is a receiver processing scheme that autonomously provides integrity monitoring for the position solution, using redundant range measurements.

The FDE consists of two distinct parts:

- The fault detection part detects the presence of an unacceptably large position error for a given mode of flight.
- Upon the detection, the fault exclusion follows and excludes the source of the unacceptably large position error, thereby allowing navigation to return to normal performance without an interruption of service.

The fault detection aspects of FDE are referred to as Receiver Autonomous Integrity Monitoring.

2-5-2 FDE algorithms events

If the equipment is aware of the navigation mode, a **Positioning Failure** is defined to occur whenever the difference between the true position and the indicated position exceeds the applicable alert limit. If the equipment is not aware of the navigation mode/alert limit, a positioning failure is defined to occur whenever the difference between the true position and the indicated position exceeds the applicable protection level.

A **Missed Detection** is defined to occur when a positioning failure is not detected.

A **Failed Exclusion** is defined to occur when a true position failure is detected and the detection condition is not eliminated within the time to alert (from the onset of the positioning failure). A failed exclusion would cause a navigation alert.

A **Wrong Exclusion** is defined to occur when a detection occurs, and a positioning failure exists but is undetected after exclusion.

Positioning failures that are not annunciated as an alert within the time-to-alert are defined to be **Missed Alerts**. Both missed detection and wrong exclusion can cause missed alerts after the time-to-alert expires.

A **False Detection** is defined as the detection of a positioning failure when a positioning failure has not occurred.

A **False Aler**t is defined as the indication of a positioning failure when a positioning failure has not occurred (a result of false detection). A false alert would cause a navigation alert.

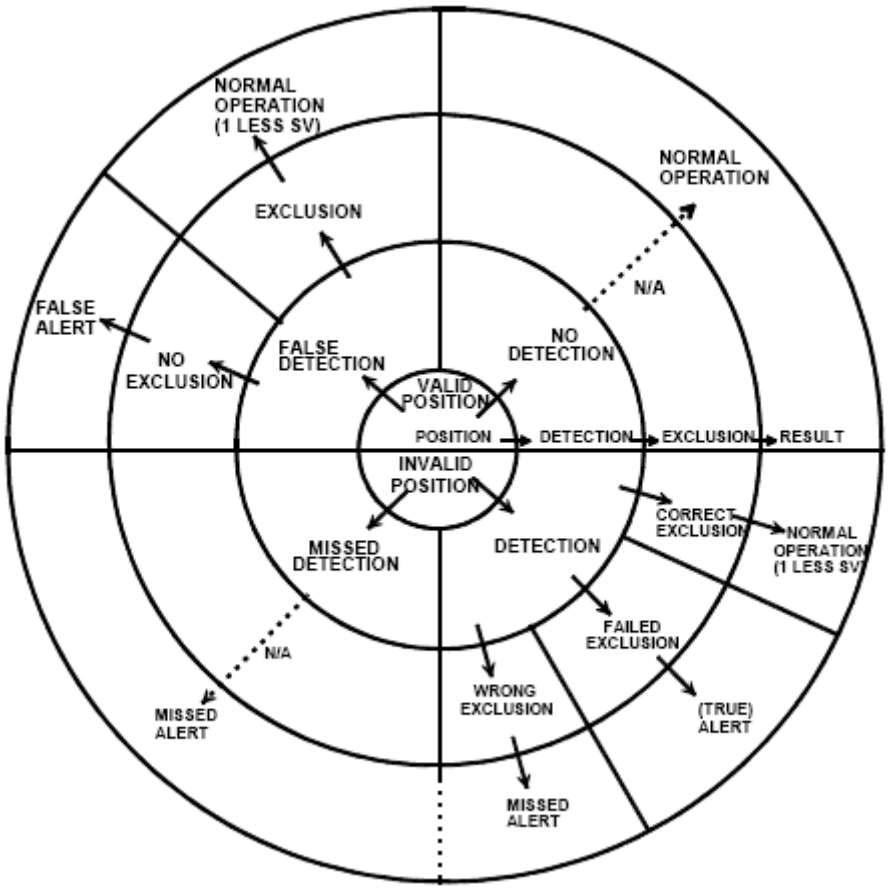

Figure 4 - Diagram of FDE Conditions [RTCA, 2006]

2-5-3 Protection Levels

As the position error remains unknown for the user, statistic tools have to be used to check requirements compliance.

The **Horizontal Protection Level** (HPL) is the radius of a circle in the horizontal plane (the local plane tangent to the WGS-84 ellipsoid), with its center being at the true position, that describes the region assured to contain the indicated horizontal position. It is an horizontal region where the missed alert and false alert requirement are met for the chosen set of satellites when autonomous fault detection is used.

The **Vertical Protection Level** (VPL) is half the length of a segment on the vertical axis (perpendicular to the horizontal plane of WGS-84 ellipsoid), with its center being at the true position, that describes the region assured to contain the indicated vertical position. It defines the vertical region where the missed alert and false alert requirement are met for the chosen set of satellites when autonomous fault detection is used.

Protection Levels are functions of the satellites and user geometry and the expected error characteristics: they are not affected by actual measurements. Their value is predictable given reasonable assumptions regarding the expected error characteristics.

2-6 Synthesis

Major aircraft phases of flight and especially approaches operation have been described. The Area Navigation method and the Required Navigation Performance concept have been briefly introduced. A review of Signal In Space performance requirements as defined by ICAO and the associated criteria definitions have been then presented. In particular, autonomous integrity monitoring function specifications have been recalled.

More internal parameters such as the allowed probability of missed detection (Pmd) or the required probability of false alert will be discussed in chapter 5.

These requirements and terms definitions constitute a major input to RAIM algorithms design as well as the measurement model which is addressed in the next chapter.

Chapître 3

Modèle de Mesure

La mesure fondamentale en navigation par satellite est la mesure de pseudodistance. L'utilisateur reçoit un signal de navigation et en particulier un code pseudo aléatoire de la part d'un satellite. Le satellite est identifié par le recepteur qui génére une réplique locale du code. La durée dont laquelle la replique doit être décalée pour maintenir le maximum de correlation avec le signal en provenance du satellite, multipliée par la vitessse de la lumière correspond approximativement à la distance entre le satellite et l'utilisateur. On parle de pseudo distance en raison de la présence de l'erreur de l'horloge utilisateur considérée comme une quatrième inconnue au même titre que les trois inconnues de position.

Les principales différences entre la pseudodistance réelle et la pseudodistance mesurée sont dues à plusieurs sources d'erreur :

- les retards de propagation du signal causés par l'ionosphère et la troposphère
- erreur d'horloge du satellite
- erreur équivalente d'estimation de la position satellite
- les phénomènes de multitrajet
- le bruit recepteur

Ces erreurs peuvent être dues au segment spatial, au segment de controle et au segment utilisateur.

Afin d'évaluer précisement les performances de positionement GNSS, toutes ces sources d'erreur doivent être prises en compte et les erreurs de mesures correspondantes doivent être modélisées aussi précisement que possible. Les erreurs systèmatiques seront adressées dans le modèle dit « sans panne » (en anglais, fault free case) et les erreurs inhabituelles pouvant causer une erreur de positionnement dangereuse et devant peutêtre être détectées seront traitées dans le modèle dit « avec panne » (en anglais, faulty case).

La section 3.1 présente les signaux GNSS destinés à un usage aéronautique et plus précisément les signaux GPS et Galiléo situés dans les bandes L1/E1 et L5/E5. Les densités spectrales de puissance de ces différents signaux sont données. Elles servent de base au calcul du bruit de poursuite au niveau du recepteur.

La section 3.2 décrit le modèle « sans panne » (fault free case). La plupart de ces modèles suppose que les composantes de l'erreur de mesure de pseudodistance suivent une loi nomale centrée dont la variance est supposée connue. L'erreur résultante a pour distribution $N(0, \sigma^2)$ où la variance σ^2 est égale à la somme des variances de chacune de ses composantes. Cependant, certaines composantes d'erreur ne sont pas rigoureusement modélisables par une distribution centrée ainsi on peut trouver des biais nominaux dans le cas « fault free ». Ceci est adressé dans la section 3-2-2. La section 3 2 1 traite du calcul de la variance de l'erreur

globale de pseudo distance au niveau uilisateur (en anglais User Equivalent Range Error, UERE). C'est pourquoi les effets sur les mesures de pseudodistances des principales source d'erreur sont modélisées.

La section 3.3 adresse le modèle de mesure avec « panne ». On parle de panne lorsqu'une erreur significativement grande apparait sur une mesure de pseudodistance (que cette erreur soit due au dysfonctionnement du satellite lui-même ou à des pertubations locales du signal comme des multitrajets ou des interferences) pouvant causer une perte d'intégrité. Afin de concevoir des systèmes de controle d'intégrité adaptés dont on puisse correctement évaluer les performances, il est nécessaire d'etudier ces modes de défaillance ainsi que leur probablité d'occurrence. C'est l'objet de cette section qui traite en premier lieu des pannes satellitaires (section 3.3.1) puis de l'effet des interferences sur les mesures de pseudo distance (section 3.3.2).

La question de l'autocorrélation temporelle des mesures, devant notamment être prise en compte par algorithmes de contrôle d'intégrité sequentiels mais également dans la spécification du taux de fausse alarme, est abordée dans la section 3.4.

Un modèle de mesure complet est ensuite proposé en section 3.5.

Chapter 3

Measurement Model

3-1 GNSS signals for Civil Aviation
3-2 Fault free case measurement model
3-3 Faulty case measurement model
3-4 Temporal Aspects
3-5 Synthesis

The fundamental measurement in satellite navigation is pseudorange. The user equipment receives the navigation signal, and in particular the pseudo random noise code, from a satellite and, generates code replicas in order to identify the satellite. The phase by which the code replica must be shifted in the receiver to maintain maximum correlation with the satellite code, multiplied by the speed of light, is approximately equal to the satellite to receiver range. It is called the pseudorange because of the presence of the user's receiver clock error which is considered as a fourth unknown in addition to the three position unknowns.

The true pseudorange model can be expressed as follow:

$$\rho_i = \sqrt{(x_0 - x_i)^2 + (y_0 - y_i)^2 + (z_0 - z_i)^2} + c\,\Delta t \qquad (3\text{-}1)$$

where x_0, y_0, z_0 design the user position
Δt is the offset between the receiver clock and GNSS system time
x_i, y_i, z_i design the ith satellite position

The main differences between the true pseudorange and the measured pseudorange are due to several sources of error from the space segment, the control segment or the user segment:

- signal propagation delays caused by the ionosphere and the troposphere
- space vehicle clock error
- satellite position estimation error
- multipath
- receiver errors which main source is code tracking loop noise

Some satellite payload hardware propagation delays could also exist. In this study, we will assume that they are corrected by the Timing Group Delay (TGD).

To evaluate GNSS positioning performance, error sources have to be taken into account and corresponding measurement errors have to be modeled as precisely as possible. Systematic errors will be gathered in the fault free case, and unusual errors that may cause a dangerous positioning failure and that may have to be detected are addressed in the faulty case.

3-1 GNSS signals for Civil Aviation

The aim of this part is to briefly present the different signals that will be available for a civil aviation use in the future for both GPS and Galileo systems. Because of their influence on acquisition and tracking performances, each available signal structure will be described. In particular, the power spectrum density of each these signal will be used to determine the standard deviation of the tracking error due to noise using [Betz and Kolodziejski, 2000] formulas and to analyse the impact of interferences.

The available GNSS signals for Civil Aviation (frequency occupation, structure) are summarized in the following table [Macabiau and Julien, 2006]:

	Signal	Code Length	Chip Rate (Mcps)	Modulation	Navigation Data (sps)	Secondary code
Galileo	E5b-I	10230	10.23	$QPSK(10)$	Yes (250)	Yes
	E5b-Q	10230	10.23		Pilot	Yes
	E1B	4092	1.023	$CBOC(6,1,1/11)$	Yes (250)	No
	E1C	8184 (on GIOVEA)	1.023		Pilot	Yes
GPS	L5-I	10230	10.23	$QPSK(10)$	Yes (1000)	Yes
	L5-Q	10230	10.23		Pilot	Yes
	L1 C/A	1023	1.023	$BPSK(1)$	Yes (50)	No
	L1 C-I	10230	1.023	$TMBOC(6,1,1/11)$	Yes (100)	No
	L1 C-Q	10230	1.023		Pilot	Yes

Table 4 - GNSS Signals for Civil Aviation

3-1-1 GNSS signals for civil aviation use in L1 band

L1 is an Aeronautical Radio Navigation Service (ARNS) band dedicated to Radio Navigation Satellite Service (RNSS) where both GPS and Galileo propose restricted and open signal.

The Galileo E1 OS and GPSIII L1C signals are still under a definition phase but the desire of interoperability of both signals has led to a common US/EU agreement that defines a common normalized power spectral density for both civil signals referred to as Multiplexed Binary Offset Carrier (MBOC).

The $MBOC$ power spectral density is defined as a weighted linear combination of the $BOC(1,1)$ and $BOC(6,1)$ normalized power spectral densities and includes the whole GPS III L1C or Galileo E1 OS civil signals, which means both their data and pilot components. Its expression is given as follows [Julien et al., 2007]:

$$G_{MBOC}(f) = \frac{10}{11} G_{BOC(1,1)}(f) + \frac{1}{11} G_{BOC(6,1)}(f) \qquad (3\text{-}2)$$

The use of $MBOC$ modulation will allow better mitigation of thermal noise, multipath and narrow-band interference compared to the current GPS legacy signal.

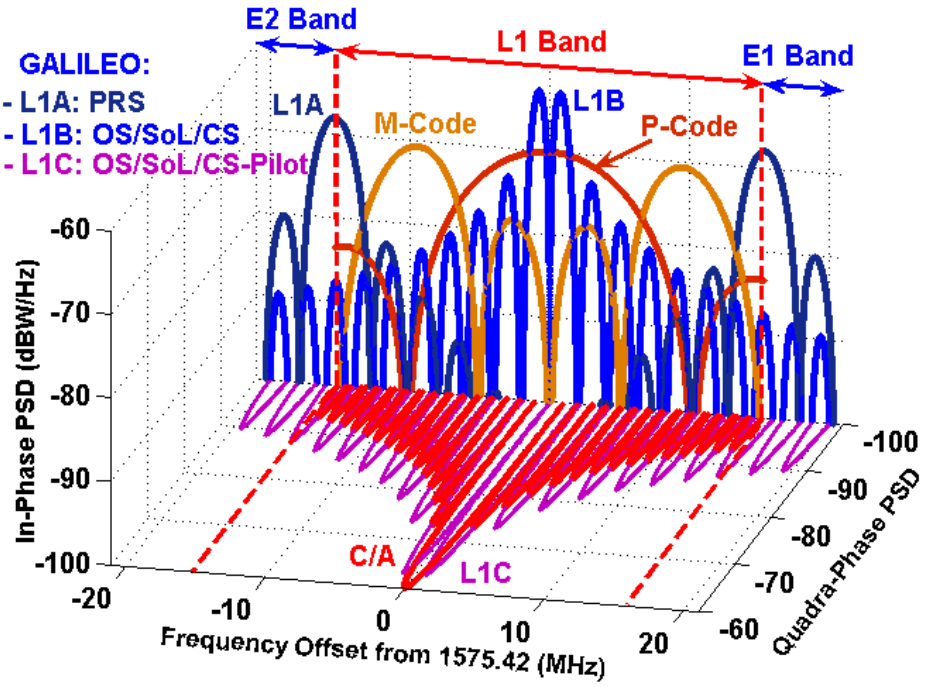

Figure 5 - Frequency plan for L1 for GPS (red colours) and Galileo (blue colours)

Since the $MBOC$ is defined only in the frequency domain, different compliant temporal signals can be used. In the literature, two different modulations were proposed to implement the $MBOC$:

- the Time-Multiplexed BOC (TMBOC) modulation, that multiplexes in the time domain BOC(1,1) and BOC(6,1) sub-carriers

- the Composite BOC (CBOC) modulation, that linearly combines the BOC(1,1) and BOC(6,1) sub-carriers (both components being present at all times).

The CBOC modulation is the candidate for Galileo E1 OS signal whereas TMBOC modulation will be used for GPS L1C.

This Ph.D. study assumes that receivers for civil aviation will be designed to only track BOC(1,1) modulation.

3-1-2 GNSS signals for civil aviation use in L5 band

L5 is an Aeronautical Radio Navigation Service (ARNS) band where GPS proposes one signal L5 and Galileo two signals. This is meant to have a third Galileo signal in ARNS band.

The Galileo signals broadcast on E5a and E5b originate from the same modulation known as ALTBOC modulation. It offers the possibility of coherently tracking the whole signal (E5a+E5b) or non-coherently E5a and E5b signals separately. The former configuration allows for extremely high code tracking accuracy, but with the constraint of using an extra-wide front-end filter (minimum of 50 MHz).

Both GPS and Galileo broadcast wide-band signals in this frequency band (resulting in excellent tracking accuracy).

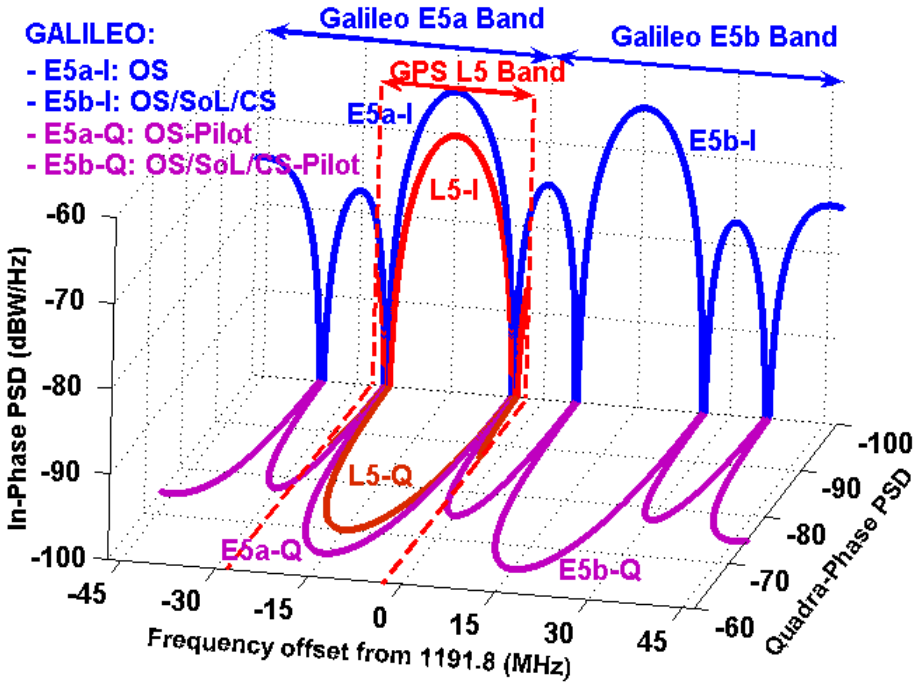

Figure 6 - Frequency plan for L5(E5a)/E5b for GPS (red col.) and Galileo (blue col.)

3-1-3 Structure of the broadcasted signals

3-1-3-1 BPSK signal definition and power spectrum density expression

The expression of the broadcasted signal is:

$$s_{BPSK}(t) = Ad(t)c(t)\cos(2\pi f_0 t)$$

with

$$d(t) = \left[\sum_{k=-\infty}^{\infty} d_k \delta(t - kT_D)\right] * rect\left(\frac{t - \frac{T_D}{2}}{T_D}\right)$$

$$c(t) = \sum_{k=-\infty}^{\infty} c_k m(t - kT_C)$$

where $d_k = \pm 1$ contains the information, T_D is d_k bit length,

$c_k = \pm 1$ is the spreading code, T_C is c_k bit length

$m(t)$ is the code materialization such as:

$$m(t) = rect\left(\frac{t - \frac{T_C}{2}}{T_C}\right)$$

Assuming the complete binary sequence $d_k \times c_k$ is random (without considering the temporal repetition period of the Pseudo Random Noise sequence), the normalized power spectrum density expression of the signal is:

$$G_{BPSK}(f) = \frac{1}{T_C}|M(f)|^2 = T_C\left(\frac{\sin(\pi f T_C)}{\pi f T_C}\right)^2 \quad (3\text{-}3)$$

3-1-3-2 BOC signal definition and power spectrum density expression

The BOC signal is defined as the product of a materialized code with a sub - carrier which is equal to the sign of a sine or a cosine waveform. If $c(t)$ is the code sequence waveform and f_s the sub - carrier frequency, the expression of the sine - phased BOC signal is:

$$x(t) = c(t)\ \text{sign}(\sin 2\pi f_S\, t)$$

with

$$c(t) = \sum_{k=-\infty}^{\infty} c_k m(t - kT_C)$$

$m(t)$ is the NRZ code materialization equal to 1 over $[0, T_C]$ and 0 everywhere else.

BOC signals are commonly referred to $BOC(p,q)$. The first parameter p defines the sub-carrier rate and the second q defines the spreading code rate:

$$f_S = p \times 1.023\ MHz$$
$$f_C = q \times 1.023\ MHz$$

The ratio $n = 2\frac{f_S}{f_C} = 2\frac{p}{q}$ is the number of half periods of the sub carrier during one code chip. It can be odd or even.

If the BOC signal is sine-phase and n is even, the normalized power spectrum densities are equal to:

$$G_{BOC}(f) = \frac{1}{T_C}\left(\frac{\sin\left(\frac{\pi f T_C}{n}\right)\sin(\pi f T_C)}{\pi f\ \cos\left(\frac{\pi f T_C}{n}\right)}\right)^2 \quad (3\text{-}4)$$

In particular,

$$G_{BOC(1,1)}(f) = \frac{1}{T_C}\left(\frac{1 - \cos(\pi f T_C)}{\pi f}\right)^2 = T_C\left(\frac{1 - \cos(\pi f T_C)}{\pi f T_C}\right)^2 \quad (3\text{-}5)$$

3-1-3-3 ALTBOC signal definition and power spectrum density definition

The ALTBOC signal is defined as the product of a PRN code sequence with a complex sub carrier and can be composed of two or four codes.

If there are two codes, there is no pilot component and the expression of the signal is:

$$x_{ALTBOC}(t) = c_U(t).\mathrm{er}(t) + c_L(t).\mathrm{er}^*(t)$$

If there is a pilot channel, four codes are needed and the expression becomes:

$$x_{ALTBOC}(t) = \left(c_U(t) + jc_U{}'(t)\right).\mathrm{er}(t) + \left(c_L(t) + jc_L{}'(t)\right).\mathrm{er}^*(t)$$

with $\mathrm{er}(t) = sign[\cos(2\pi f_S t)] + j\ sign[\sin(2\pi f_S t)] = c_r(t) + j\ s_r(t)$
c_U the data upper code
$c_U{}'$ the pilot upper code
c_L the data lower code
$c_L{}'$ the pilot lower code

In order to have a constant envelope and avoid distortions in the satellite payload due to nonlinear amplification, a new signal has been created and called constant envelope ALTBOC. Its expression is [Rebeyrol and Macabiau, 2005]:

$$x_{ALTBOC}(t) = \begin{cases} \left(c_L(t) + jc_L{}'(t)\right).\left[\mathrm{sc_{as}}(\mathrm{t}) - \mathrm{j}\ \mathrm{sc_{as}}\left(\mathrm{t} - \frac{\mathrm{T_S}}{4}\right)\right] + \\ \left(c_U(t) + jc_U{}'(t)\right).\left[\mathrm{sc_{as}}(\mathrm{t}) + \mathrm{j}\ \mathrm{sc_{as}}\left(\mathrm{t} - \frac{\mathrm{T_S}}{4}\right)\right] + \\ \left(\overline{c_L(t)} + j\overline{c_L{}'(t)}\right).\left[\mathrm{sc_{ap}}(\mathrm{t}) - \mathrm{j}\ \mathrm{sc_{ap}}\left(\mathrm{t} - \frac{\mathrm{T_S}}{4}\right)\right] + \\ \left(\overline{c_U(t)} + j\overline{c_U{}'(t)}\right).\left[\mathrm{sc_{ap}}(\mathrm{t}) + \mathrm{j}\ \mathrm{sc_{ap}}\left(\mathrm{t} - \frac{\mathrm{T_S}}{4}\right)\right] \end{cases}$$

with $\overline{c_L} = c_U c_U{}' c_L{}'$, $\overline{c_L{}'} = c_U c_U{}' c_L$, $\overline{c_U} = c_L c_U{}' c_L{}'$ and $\overline{c_U{}'} = c_L c_L{}' c_U$

$$\mathrm{sc_{as}}(\mathrm{t}) = \frac{\sqrt{2}}{4} sign\left[\cos\left(2\pi f_S t - \frac{\pi}{4}\right)\right] + \frac{1}{2}\ sign[\cos(2\pi f_S t)] + \frac{\sqrt{2}}{4} sign\left[\cos\left(2\pi f_S t + \frac{\pi}{4}\right)\right]$$

$$\mathrm{sc_{ap}}(\mathrm{t}) = -\frac{\sqrt{2}}{4} sign\left[\cos\left(2\pi f_S t - \frac{\pi}{4}\right)\right] + \frac{1}{2}\ sign[\cos(2\pi f_S t)] - \frac{\sqrt{2}}{4} sign\left[\cos\left(2\pi f_S t + \frac{\pi}{4}\right)\right]$$

The normalized power spectrum density of the constant envelope ALTBOC signal for n odd is:

$$G_{ALTBOC}(f) = \frac{4}{\pi^2 f^2 T_C} \frac{\cos^2(\pi f T_C)}{\cos^2\left(\pi f \frac{T_C}{n}\right)} \times \left[\cos^2\left(\pi f \frac{T_S}{2}\right) - \cos\left(\pi f \frac{T_S}{2}\right) - 2\cos\left(\pi f \frac{T_S}{2}\right)\cos\left(\pi f \frac{T_S}{4}\right) + 2\right] \quad (3\text{-}6)$$

In fact, receivers for civil aviation will be designed to track separately E5a and E5b signals as two QPSK.

3-2 Fault free case measurement model

Most of the fault free case models assume that the pseudorange error components have a normal distribution with a known variance and a zero mean and that the pseudorange error components are combined by convolving their error distributions. The resulting pseudorange error distribution is set as $N(0, \sigma^2)$ where the variance is defined by the root-sum-square of the component variances. But some error components are not well characterized by a normal distribution, this aspect is addressed in part 3-2-2. In the next part of the study all errors are assumed to be zero mean and Gaussian and the global pseudorange error variance computation is detailed.

3-2-1 Pseudo range measurement error variance

The pseudo range measurement error variances from different sources are gathered in the User Equivalent Range Error UERE. The main contributions that have to be considered are: orbit determination and synchronization equivalent error, troposphere residual error, ionosphere residual error, multipath residual error and receiver noise residual error.

3-2-1-1 Receiver noise residual error

3-2-1-1-1 Introduction

Let‘s consider the way a GNSS receiver works. The goal is to line up a locally generated replica of the received PRN code with the received signal in order to determine its frequency and its propagation delay. The synchronisation is first roughly made through the acquisition step. A more precise estimation of signal parameters is then conducted thanks to two different cooperating tracking loops:

- the “Carrier-loop”, also called “Phase Lock Loop” (PLL) or “Frequency lock Loop” (FLL), whether it is the phase or the frequency that is being tracked. Its objective is to continuously generate a local carrier with the same phase or frequency that the incoming signal.
- the “Code-loop”, also called “Delay Lock Loop” (DLL), whose purpose is to continuously follow (“track”) the succession of code sequences (internal structure and coding depending on the GNSS system and frequency band), hence providing the receiver navigation computing unit with pseudo range measurements between the GNSS satellites and the receiver.

That constitutes the tracking program which is processed as long as the estimation error is lower than a given threshold. In the contrary case, a re-acquisition step is necessary. This mainly depends on the signal to noise ratio:

- If $C/N_0 \geq [C/N_0]_{\text{threshold}}$: the tracking loops are working
- If $C/N_0 < [C/N_0]_{\text{threshold}}$: a loss of lock of the tracking loops is possible and it is necessary to initiate a re-acquisition or to re-conduct a signal acquisition, and a bias can appear

The threshold $[C/N_0]_{\text{threshold}}$ is usually set such that the tracking loop does not provide abnormal measurements.

3-2-1-1-2 Code delay tracking: Error variance of a code-tracking loop

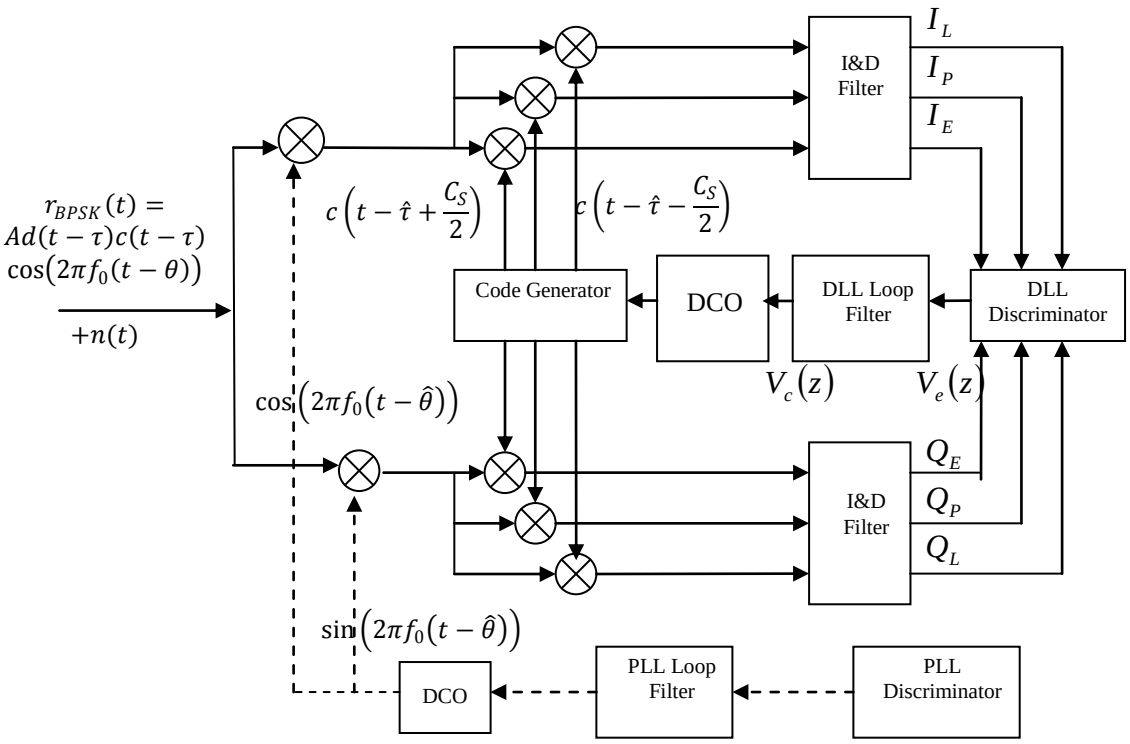

Figure 7 - Code delay tracking scheme

After the carrier wipe-offstage, the resulting in-phase and quadrature phase component are multiplied by three delayed spreading sequence replicas: Early, Prompt and Late that are given by:

$$E(t) = c\left(t-\hat{\tau}+\frac{C_S}{2}\right)$$
$$P(t) = c(t-\hat{\tau})$$
$$L(t) = c\left(t-\hat{\tau}-\frac{C_S}{2}\right)$$

with c the spreading sequence and C_S the chip spacing

The result of the multiplication of the in-phase and quadra-phase component with different delayed spreading sequences is followed by the I&D filtering that provide six correlation values:

$$I_L(n) = \frac{A}{2}\, d(n)K\left(\varepsilon_\tau - \frac{C_S}{2}\right)\cos(\varepsilon_\theta) + n_{IL}(n)$$
$$I_E(n) = \frac{A}{2}\, d(n)K\left(\varepsilon_\tau + \frac{C_S}{2}\right)\cos(\varepsilon_\theta) + n_{IE}(n)$$
$$I_P(n) = \frac{A}{2}\, d(n)K(\varepsilon_\tau)\cos(\varepsilon_\theta) + n_{IP}(n)$$

$$Q_L(n) = \frac{A}{2}\, d(n)K\left(\varepsilon_\tau - \frac{C_S}{2}\right)\sin(\varepsilon_\theta) + n_{QL}(n)$$

$$Q_E(n) = \frac{A}{2}\, d(n) K\left(\varepsilon_\tau + \frac{C_S}{2}\right)\sin(\varepsilon_\theta) + n_{QE}(n)$$

$$Q_P(n) = \frac{A}{2}\, d(n) K(\varepsilon_\tau)\sin(\varepsilon_\theta) + n_{QP}(n)$$

where

A the signal amplitude
d the information signal
K the code autocorrelation
ε_τ the code delay error
ε_θ the phase delay error
n_I the in-phase correlation noise
n_Q the quadra-phase correlation noise

These correlation values are then fed into a code delay discriminator that will use them to estimate the code delay tracking error ε_τ.

Two types of discriminator are widely used in GNSS receivers: the Early –Minus Late Power (EMLP) and the Dot –Product (DP). They are given by [Julien, 2005]:

$$D_{EMLP} = (I_E^2 + Q_E^2) - (I_L^2 + Q_L^2) \tag{3-7}$$

$$D_{DP} = (I_E - I_L)I_P + (Q_E - Q_L)Q_P \tag{3-8}$$

The error variance of the code-tracking loop will depend on the choice of the discriminator [Betz and Kolodziejski, 2000]:

$$\sigma_{EMLP}^2 = \frac{B_L(1 - 0.5B_L T)\int_{-B/2}^{B/2} G(f)\sin^2(\pi f C_S)\, df}{\frac{C}{N_0}\left(2\pi\int_{-B/2}^{B/2} f G(f)\sin(\pi f C_S)\, df\right)^2}\left(1 + \frac{\int_{-B/2}^{B/2} G(f)\cos^2(\pi f C_S)\, df}{\frac{C}{N_0}T\int_{-B/2}^{B/2} G(f)\cos(\pi f C_S)\, df}\right) \tag{3-9}$$

$$\sigma_{DP}^2 = \frac{B_L(1 - 0.5B_L T)\int_{-B/2}^{B/2} G(f)\sin^2(\pi f C_S)\, df}{\frac{C}{N_0}\left(2\pi\int_{-B/2}^{B/2} f G(f)\sin(\pi f C_S)\, df\right)^2}\left(1 + \frac{1}{\frac{C}{N_0}T\int_{-B/2}^{B/2} G(f)\cos(\pi f C_S)\, df}\right) \tag{3-10}$$

where

$B_L(H_z)$ the one sided bandwidth of the equivalent loop filter
T the data period
G the power spectrum density of the signal
C/N_0 the signal to noise ratio
C_S the chip spacing
B the two sided bandwidth of the front end filter

Note that this model is adequate when the loops implemented were derived from an analog loop model using an approximate analog to discrete transform. When the loops are directly designed in the digital domain using [Stephens and Thomas, 1995], the factor $(1 - 0.5B_L T)$ can be removed.

Without considering the temporal repetition period of the PN sequence, the power spectrum density expression of the BPSK signal is:

$$G_{BPSK}(f) = T_c \left(\frac{\sin \pi f T_C}{\pi f T_C} \right)^2$$

with T_C the code period.

This expression is used for GPS L1, GPS L5 and GALILEO E5b code tracking loop error variance. For Galileo E1, the normalized power spectrum density of the BOC(1,1) is equal to:

$$G_{BOC(1,1)}(f) = T_c \left(\frac{1 - \cos \pi f T_C}{\pi f T_C} \right)^2$$

The error variance of the code tracking loop, error due to noise, can be thus computed for different kind of signals, using for example the following values:

	GPS L1 C/A	GPS L5	Galileo E1	Galileo E5b
C_S	0.25	0.25	0.25	0.25
B_L	1	1	1	1
B	16×10^6Hz	20×10^6Hz	20×10^6Hz	14×10^6Hz
C/N_0	35 dBHz	29 dBHz	36.5 dBHz	29.7 dBHz
T	0.02 s	0.02 s	0.1 s	0.1 s
T_C	1/1.023 MHz	1/1.023 MHz	1/1.023 MHz	1/10.23 MHz

Table 5 - Values for code delay tracking error variance computation

Note that worst case C/N_0 are given here and not typical values [Eurocae, 2006]. This drop of the equivalent C/N_0 down to tracking threshold allows to take into account some level of interference in our fault free case model.

The obtained error variance of the code-tracking loop values are gathered in the following table:

	GPS L1 C/A	GPS L5	Galileo E1	Galileo E5b
σ_{EMLP} (m)	2.00	0.53	0.86	0.59
σ_{DP} (m)	2.00	0.53	0.86	0.59

Table 6 - Code-tracking loop error variance

3-2-1-1-3 Iono free measurements

In nominal mode, the pseudorange measurements that will be available to the aircraft receiver are the GPS L1, GPS L5, GALILEO E1, GALILEO E5b code and phase measurements. But for future civil aviation GNSS receivers complying with EUROCAE requirements, dual frequency measurements will be combined into a single composite measurement called the iono-free measurement, corrected for ionospheric error (see section 3-2-1-3).

Thus, from GPS L1 – L5, and from GALILEO E1 – E5b, two distinct iono-free measurements are built.

Denoting $P(k)$ the code measurement at the instant k and $\varphi(k)$ the phase measurement:

$$P_{\mathrm{L1-L5}}(k) = \frac{f_{\mathrm{L1}}^2}{f_{\mathrm{L1}}^2 - f_{\mathrm{L5}}^2} P_{\mathrm{L1}}(k) + \frac{f_{\mathrm{L5}}^2}{f_{\mathrm{L5}}^2 - f_{\mathrm{L1}}^2} P_{\mathrm{L5}}(k) \tag{3-11}$$

$$P_{\mathrm{E1-E5b}}(k) = \frac{f_{\mathrm{E1}}^2}{f_{\mathrm{E1}}^2 - f_{\mathrm{E5b}}^2} P_{\mathrm{E1}}(k) + \frac{f_{\mathrm{E5b}}^2}{f_{\mathrm{E5b}}^2 - f_{\mathrm{E1}}^2} P_{\mathrm{E5b}}(k) \tag{3-12}$$

$$\varphi_{\mathrm{L1-L5}}(k) = \frac{f_{\mathrm{L1}}^2}{f_{\mathrm{L1}}^2 - f_{\mathrm{L5}}^2} \varphi_{\mathrm{L1}}(k) + \frac{f_{\mathrm{L5}}^2}{f_{\mathrm{L5}}^2 - f_{\mathrm{L1}}^2} \varphi_{\mathrm{L5}}(k) \tag{3-13}$$

$$\varphi_{\mathrm{E1-E5b}}(k) = \frac{f_{\mathrm{E1}}^2}{f_{\mathrm{E1}}^2 - f_{\mathrm{E5b}}^2} \varphi_{\mathrm{E1}}(k) + \frac{f_{\mathrm{E5b}}^2}{f_{\mathrm{E5b}}^2 - f_{\mathrm{E1}}^2} \varphi_{\mathrm{E5b}}(k) \tag{3-14}$$

with

$$\frac{f_{\mathrm{L1}}^2}{f_{\mathrm{L1}}^2 - f_{\mathrm{L5}}^2} \approx 2.261\,, \frac{f_{\mathrm{E1}}^2}{f_{\mathrm{E1}}^2 - f_{\mathrm{E5b}}^2} \approx 2.422\,, \qquad \frac{f_{\mathrm{L5}}^2}{f_{\mathrm{L5}}^2 - f_{\mathrm{L1}}^2} \approx -1.261\,, \frac{f_{\mathrm{E5b}}^2}{f_{\mathrm{E5b}}^2 - f_{\mathrm{E1}}^2} \approx -1.422$$

No significant correlation factor can be expected for the noise and multipath error affecting the different measurements made on the four carrier frequencies. This is why the standard deviation of the error affecting the iono-free measurement is modeled as:

$$\sigma_{L1-L5} = \sqrt{2.261^2 \sigma_{L1}^2 + 1.261^2 \sigma_{L5}^2} \tag{3-15}$$

$$\sigma_{E1-E5b} = \sqrt{2.422^2 \sigma_{L1}^2 + 1.422^2 \sigma_{L5}^2} \tag{3-16}$$

Thus,

$$\sigma_{\mathrm{code}\,,L1-L5} = \sqrt{2.261^2 \sigma_{\mathrm{code}\,,L1}^2 + 1.261^2 \sigma_{\mathrm{code}\,,L5}^2} \tag{3-17}$$

$$\sigma_{\mathrm{code}\,,E1-E5b} = \sqrt{2.422^2 \sigma_{\mathrm{code}\,,E1}^2 + 1.422^2 \sigma_{\mathrm{code}\,,E5\mathrm{b}}^2} \tag{3-18}$$

3-2-1-1-4 Smoothing

Once elaborated, these two GPS and GALILEO iono-free measurements are then smoothed to reduce the influence of noise and multipath [Hegarty, 1996]:

$$\sigma_{\tilde{P}}{}^2 \approx \frac{\sigma_P^2}{2T_{\text{smooth}}} \tag{3-19}$$

where T_{smooth} is the time smoothing constant in seconds
σ_P^2 is the raw code pseudorange measurement error variance
$\sigma_{\tilde{P}}{}^2$ is the smoothed code pseudorange measurement error variance

3-2-1-1-5 Conclusion

Finally, the receiver noise residual error variance $\sigma_{noise}{}^2$ of smoothed iono free measurements is obtained. It corresponds to the receiver noise, thermal noise, inter channel bias and processing error.

	GPS L1/L5	Galileo E1/ E5b
$\sigma_{noise\,,EMLP}\ (m)$	0.32	0.16

Table 7 - Receiver noise residual error variance

3-2-1-2 Multipath error

This section addresses the multipath phenomenon during aircraft approaches. The sum of direct and reflected signal induces a biased measurement. Even if the resulting error may not be very large, it needs to be appropriately taken into account into the error budget.

This work has been tackled by RTCA for GPS L1/CA code users and the final result was a standard curve adopted in the ICAO SARPs stating the standard deviation of the error due to multipath as a function of the GPS satellite elevation angle [Booth, 2000].

This model was validated and adopted for GPS L1 C/A thanks to efforts made by the FAA, Boeing and Honeywell, mainly using data collected during normal production flight testing [Murphy and Booth, 2000], [Liu, 1998]. Their studies have shown that even if the distribution of airframe multipath errors does depend on the specific airframe, these distributions are similar enough that a single model may adequately cover all airframe.

The smoothed multipath error for the airborne equipment is described by [RTCA, 2006]:

$$\sigma_{\text{multipath}} = 0.13 + 0.53\, exp\left({}^{-\theta}/_{10\text{deg}}\right) \tag{3-20}$$

where θ is the elevation angle in degrees of the considered satellite.

The characteristics of the error induced by multipath need to be determined for an aircraft using new GNSS signals transmitted by future GPS and Galileo constellations. Preliminary studies have shown that smaller error can be anticipated for GPS L5, Galileo E1 and E5b since a flat sigma curve referring to a constant deviation of 7 cm for any elevation is proposed [Macabiau et al., 2006].

Nevertheless, to be conservative and before further validation, the L1 C/A SARPs [ICAO, 2006] error curve will be used in the following calculation for the other GNSS signals.

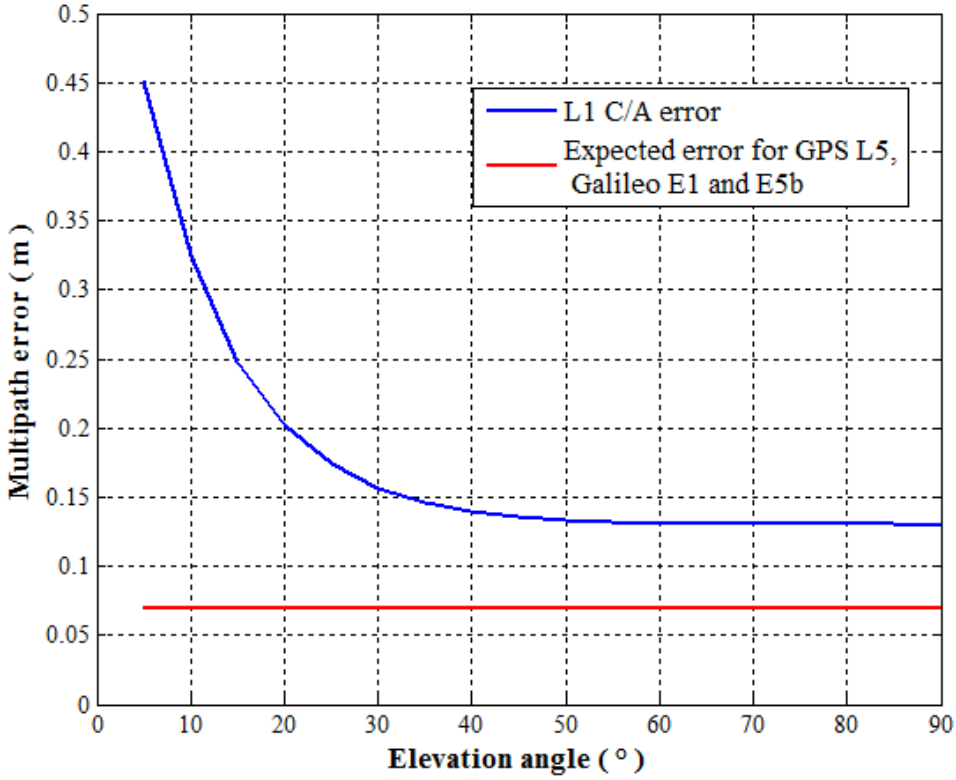

Figure 8 - Multipath error curve [Macabiau et al., 2006]

As for the error variance of the code-tracking loop, the smoothed multipath errors of each available signal are affected by the iono free combination:

$$\sigma_{\text{multipa th } L1-L5} = \sqrt{2.261^2 \sigma^2_{\text{multipath } L1} + 1.261^2 \sigma^2_{\text{multipath } L5}} \qquad (3\text{-}21)$$

$$\sigma_{\text{multipath } E1-E5b} = \sqrt{2.422^2 \sigma^2_{\text{multipath } E1} + 1.422^2 \sigma^2_{\text{multipath } E5\text{b}}} \qquad (3\text{-}22)$$

The resulting values of multipath error variance are represented on the following figure for GPS L1/L5 and Galileo E1/E5b.

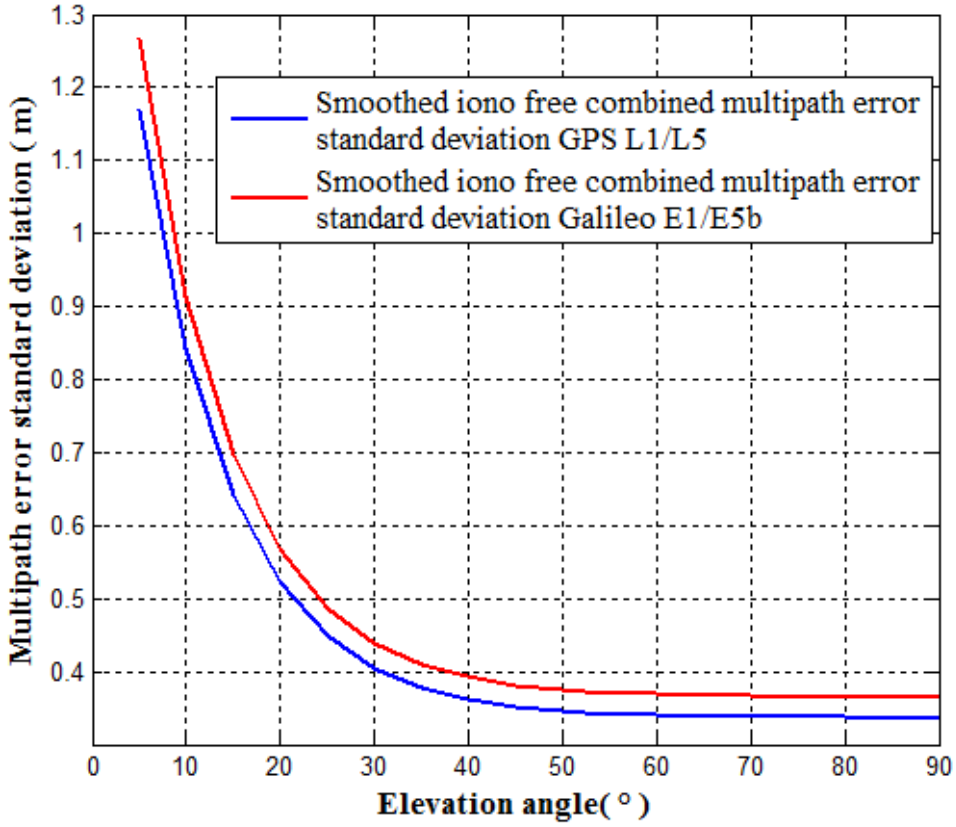

Figure 9 - Multipath error curve

3-2-1-3 Ionospheric residual error

The ionosphere is a dispersive medium which is located between 60 km and 1000 km above the earth's surface, in the atmosphere. In this area, ultraviolet rays coming from the sun ionize a portion of gas molecules and thus, it releases free electrons. These electrons influence the propagation of the electromagnetic waves and thus, the GNSS signals [Chibout, 2005].

The main problem to model the ionosphere is its very important versatility, both geographically and temporally speaking. Indeed, the electron density is very different from places to places in the world. Moreover, the ionosphere content changes a lot within the day duration (difference between night and day) and also during larger time scale.

Fortunately the ionospheric delay on GNSS signals is frequency-dependent and hence impacts on the L1 and L5 signals by a different amount. A linear combination of pseudo-range or carrier phase observations on the L1 and L5 carrier waves can be created to almost entirely eliminate this delay. The resulting observable is known as the ionosphere-free carrier phase (or pseudo-range).

Future civil aviation GNSS receivers will use dual frequency measurements and will combine them into this single composite measurement called the ionospheric-free measurement, corrected for ionospheric error. By this way the ionospheric residual error is not considered as significant anymore:

$$\sigma_{\text{iono}} = 0 \qquad (3\text{-}23)$$

3-2-1-4 Tropospheric residual error

The troposphere is the lowest portion of Earth's atmosphere which contains approximately 90% of its mass and almost all of its water vapor and aerosols. The average depth of the troposphere is about 11 km in the middle latitudes. It is deeper in the tropical regions (up to 20 km) and shallower near the poles (about 7 km) [Météo France, 2008].

Whereas the ionosphere correction is obtained either by measurement of dispersion using two frequencies or by calculation from a mathematical model, the tropospheric delay must be calculated since the troposphere is nondispersive. The model for the residual error for the tropospheric delay estimate is [RTCA, 2006]:

$$\sigma_{\text{tropo}} = \frac{1.001}{\sqrt{0.002001 + \sin^2 El}} \times 0.12\ m \qquad (3\text{-}24)$$

where El is the elevation angle

This model was adopted for GPS L1 C/A and is assumed for GPS L5 and Galileo E1 and E5b.

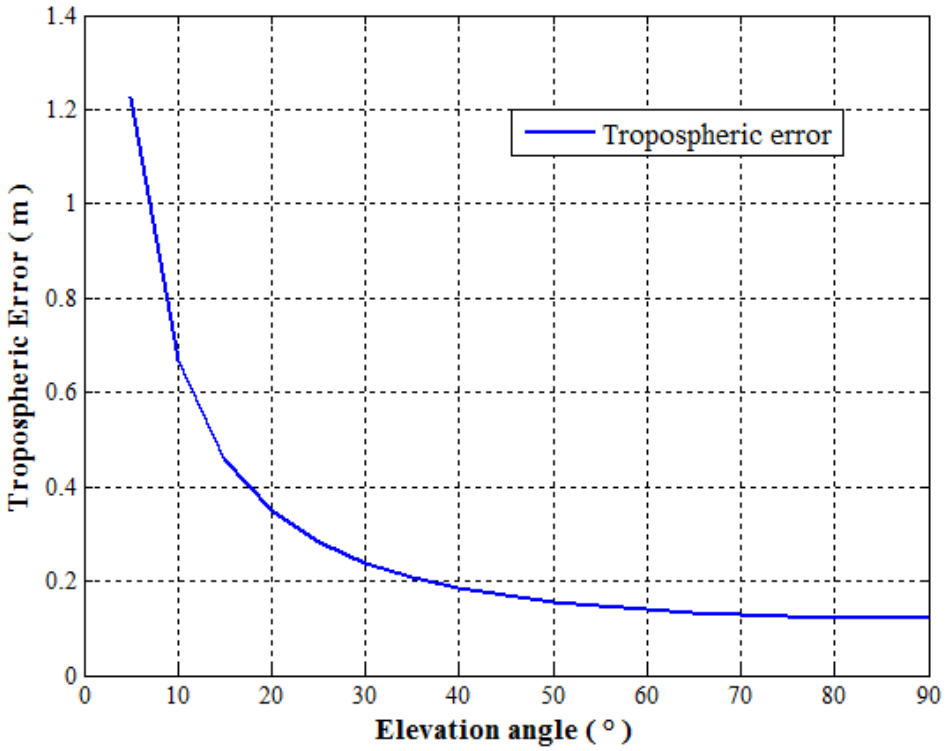

Figure 10 - Tropospheric residual error curve

3-2-1-5 Satellite clock and ephemeris error

Satellite clock and ephemeris error components will depend on the considered system and for GPS it has to be computed depending on the modernization step.

User Range Accuracy (URA) is the standard deviation of the range component of clock ephemeris error. Indeed, ephemeris errors result from a mismatch between the actual location of the satellite and the predicted satellite position as broadcast in the navigation message. Clock errors are due to satellite clock offset with regard to GPS time. For GPS, the distribution of every satellite's range error is over bounded by a zero mean Gaussian

distribution with standard deviation equal to URA [Have, 2003] and [Lee and McLaughlin, 2007].

For Galileo, the signal in space error (not necessarily Gaussian) of each satellite will be over-bounded by a nonbiased Gaussian distribution with the minimum standard deviation called Signal In Space Accuracy (SISA). The integrity performance requirement specifies a SISA value for both nominal and degraded mode [ESA, 2005]. This parameter will correspond to the GPS URA.

	GPS current	GPS II	GPS III	Galileo
σ_{URA} (m)	3.9	1.5	0.35 to 1	0.85

Table 8 - User Range Accuracy values [ESA, 2005], [Have, 2003] and [Lee and McLaughlin, 2007]

3-2-1-6 User equivalent range error

The User Equivalent Range Error is the value reflecting the error budget and it is based on the computation of the following contributions: orbit determination and synchronization equivalent error, troposphere residual error, ionosphere residual error, multipath residual error and receiver noise residual error.

$$\sigma^2_{UERE} = \sigma^2_{URA} + \sigma^2_{\text{iono}} + \sigma^2_{\text{noise}} + \sigma^2_{\text{multipath}} + \sigma^2_{\text{tropo}} \qquad (3\text{-}25)$$

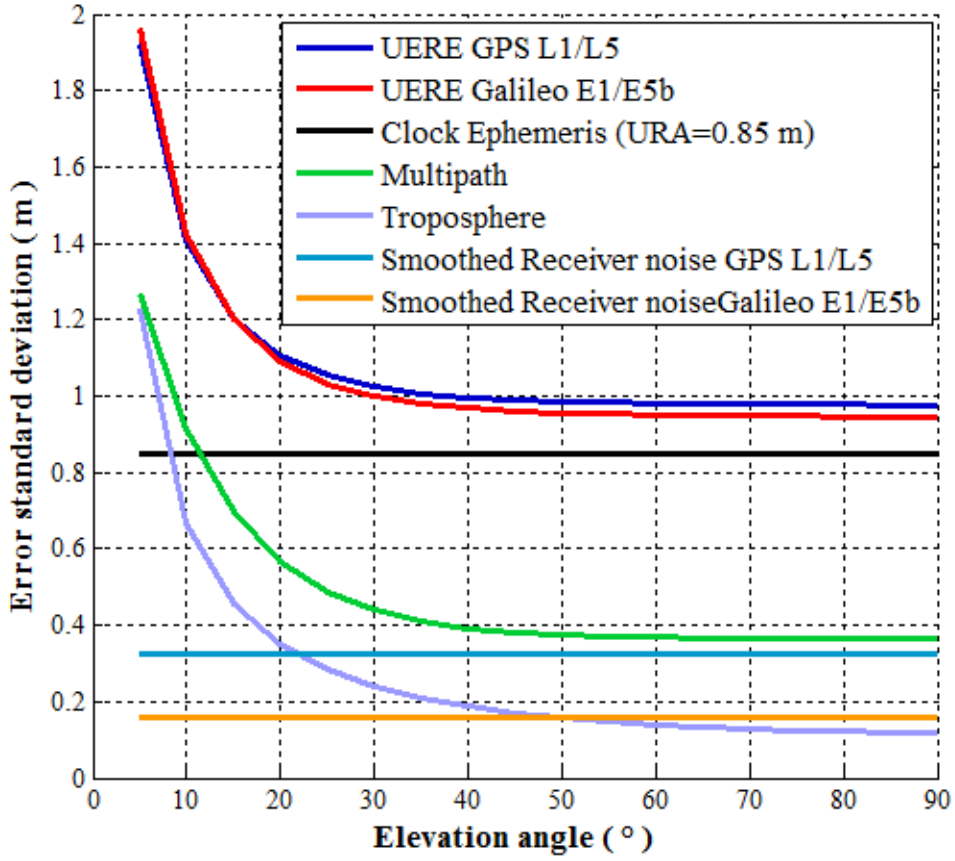

Figure 11 – User equivalent range error components

The effects of the interference is taken into account in this total standard deviation as the sigma noise is computed at the lowest $^{C}/_{N_0}$ possible for nominal conditions.

The following figure represents the obtained Galileo smoothed iono - free UERE for different elevation angles.

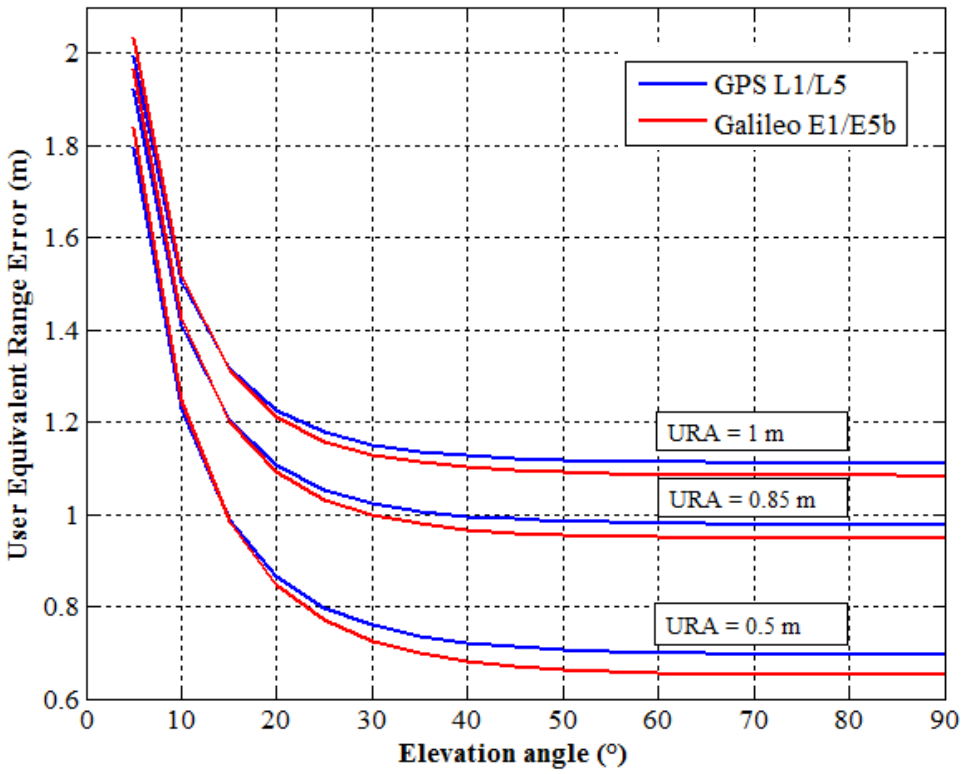

Figure 12 - GPS L1/L5 and Galileo E1/E5b smoothed iono-free UERE

Those values are gathered in the following table for $URA = 1\ m$:

UERE (m)	Elevation angle (°)								
	5	10	15	20	30	40	50	60	90
GPS III L1/L5	1.993	1. 504	1.314	1.224	1.151	1.127	1.117	1.113	1.110
Galileo E1/E5b	2.034	1.519	1.312	1.211	1.129	1.102	1.091	1.086	1.083

Table 9 - L1/L5 and Galileo E1/E5b smoothed iono-free UERE values

For $URA = 0.85\ m$:

UERE (m)	Elevation angle (°)								
	5	10	15	20	30	40	50	60	90
GPS III L1/L5	1.923	1.408	1.204	1.105	1.024	0.996	0.985	0.981	0.977
Galileo E1/E5b	1.964	1.425	1.201	1.091	0.999	0.968	0.956	0.950	0.946

Table 10 - L1/L5 and Galileo E1/E5b smoothed iono-free UERE values

3-2-2 Nominal biases

Most of the models assume that the pseudorange error components have a normal distribution with a known variance and zero mean. This is realistic thanks to overbounding techniques. Some of these methods require that the mean of the component distribution is exactly zero but several approaches address the effect of this mean by only requiring symmetry and unimodality [DeCleene, 2000].

Indeed, small nominal biases could exist even in fault free conditions. The error components that could create a mean are listed below:

- Mis-calibration of antenna phase center.

In fact GNSS receiver determines the coordinates of the antenna's electrical phase center. The phase center is defined as being the point where the satellite signal is collected. The offset between the mean phase center and the geometric center of an antenna can range from a few millimeters to several centimeters [Akrour et al, 2005]. As it can change as a function of elevation angle, the phase center of the antenna has to be carefully calibrated [DeCleene, 2000]. According to [Murphy et al, 2007], GPS antenna group delay variation can induce pseudorange measurement errors of the order of 1 meter.

- Multipath

In this study, it is considered that multipath is completely taken into account by the model presented in section 3.2.1.2.

- Nominal signal deformation, imperfection in the modulation of signals with PRN code

Therefore, in order to be more realistic, pseudorange measurement models can take into account a bias that bounds errors that may appear random but that affect user in the same way repeatedly [Walter et al., 2008].

For example, the study panel initiated by the FAA called the GPS Evolutionary Architectural Study (GEAS) has agreed to consider explicitly the presence of biases in range measurement under non faulted conditions and has assumed a level of bias magnitude under fault - free condition called maximum bias magnitude such as [Lee and McLaughlin, 2007]:

$$50\ cm \leq B_{max} \leq 2\ m \tag{3-26}$$

3-3 Faulty case measurement model

A fault is said to occur when a significantly large error in the range measurement (whether that error is due to an anomaly of the satellite itself or to environmental effects on the satellite ranging signal such as multipath or interference) may potentially cause an integrity failure [Lee, 2004].

In order to properly design GNSS integrity monitoring systems and to properly evaluate their performance, it is necessary to study failures mode as well as their probability of occurrence. This is the objective of this section.

3-3-1 Satellite failure

A satellite integrity fault can be defined as an error inconsistent with the fault free error distribution due to a fault condition when the satellite is marked "healthy" and which can lead to a position error larger than the maximum tolerable error for a given flight operation.

3-3-1-1 Major satellite failures

The GPS Standard Positioning Service (SPS) Performance Standard specifies two parameters regarding the satellite integrity: the definition of a major service failure and the specification of the maximum rate of such a satellite fault.

A **major service failure** is defined to be a condition over a time interval during which a healthy GPS satellite's ranging signal error (excluding atmospheric and receiver error) exceeds the range error limit [GPS SPS, 2001]. The range error limit is the larger of:

- 30 m
- 4.42 times the URA

The probability of occurrence of such an event is 3 per year for a 24 GPS satellites constellation.

3-3-1-2 Smaller satellite failures

However, for navigation with much tighter position protection limits, even small errors would be considered significant.

Several analyses have been made concerning the use of GPS associated with WAAS for En route to LPV flight operations or associated with LAAS for Cat I approaches.

GPS integrity related assumptions supporting the use of WAAS information are as follow [Van Dyke et al., 2003]:

- **Signal deformation and distortions** ("Evil Waveforms")
  The probability of signal deformation is assumed to be less than 10^{-4} per hour per satellite
- **Code Carrier divergence**
  The probability of code carrier divergence (code minus carrier phase at the output of the SV antenna) greater than $6.1\,m$ is assumed to be less than 10^{-4} per hour per satellite
- **Ephemeris error**
  The onset of erroneous GPS ephemeris data is assumed to occur with a probability of 10^{-4} per hour per satellite
- **Signal fault causing step errors, ramps errors or accelerations errors**
  The probability of GPS signal fault causing of any one of the following is assumed to be less than 10^{-4} per hour per satellite for
  - A step (discrete jump) error larger than 3.6 m
  - A range acceleration error larger than $0.019\ m/s^2$

3-3-1-3 Multiple satellite failure

Multiple satellite failure can be caused by the simultaneous occurrence of independent failure modes or by a common mode of failure.
According to [Van Dyke et al., 2003], it is assumed in WAAS assumptions that there is no common mode failure that causes more than one of the following signal faults: signal deformation, code /carrier divergence or step ramp error in the pseudorange residual.

More generally, [Lee and McLaughlin, 2007] refers to a rate of common mode faults causing multiple integrity failure of 1.3×10^{-8}/approaches.

3-3-2 Interference

Interference can be generally defined as any undesired signal that interferes with the reception of radio waves. Low power levels used in GNSS leave aircraft susceptible to unintentional interference in their frequency bands. Even if a large number of mitigation techniques have been investigated to improve the performance of the GNSS receivers, civil aviation system may remain vulnerable.

The main interference sources to be accounted for in the ARNS are, for unintentional interferences:

- CW interferences on all bands
- Wideband interferences on all bands
- Pulsed Interferences (DME/TACAN on L5, Radars on E5b, UWB)

In this study, the effect of interference has been modelled in the fault free case as a drop of the equivalent C/N_0 down to tracking threshold for all satellite. This section focuses on interference model on L1 as it is the most vulnerable band (narrower signal bandwidth). Pulsed interferences are not considered.

Wideband and CW interference effects models are investigated in this section. The potential impact of a worst case interference i.e. a CW heating the high PRN code spectrum line will be analysed in chapter 6.

Concerning intentional interference, one can refer to the study initiated by the FAA and conducted by the Johns Hopkins University Applied Physics Laboratory (JHU/APL) in order to quantify the ability of GPS, GPS/WAAS, and GPS/LAAS to satisfy required navigation performance [Corrigan et al., 1999]. The study concludes that there is no credible spoofing threat and that, although real, jamming threats can be managed.

Several models were already proposed to analyse the effect of interference on GNSS signal processing. Most of them model the effect of interference at correlator output as the effect of equivalent additional white noise at the receiver input.

3-3-2-1 Wideband interferences

Wideband interferences are commonly supposed to be white noise with limited bandwidth. The code tracking error variance for large and narrow band interference is given in [Betz and Kolodziejski, 2001]:

$$\sigma^2_{EMLP} = B_L(1 - 0.5B_L T) \times \left[\frac{\int_{-B/2}^{B/2} G(f) G_w(f) \sin^2(\pi f C_S)\, df}{C\left(\int_{-B/2}^{B/2} fG(f) \sin(\pi f C_S)\, df\right)^2} + \frac{\left(\int_{-B/2}^{B/2} G(f) G_w(f)\, df\right)^2 - \left|\int_{-B/2}^{B/2} G(f) G_w(f)\, e^{i2\pi f C_S} df\right|^2}{C^2 T\left(\int_{-B/2}^{B/2} fG(f) \sin(\pi f C_S)\, df \int_{-B/2}^{B/2} G(f) \cos(\pi f C_S)\, df\right)} \right] \quad (3\text{-}27)$$

where

$B_L(H_z)$ the one sided bandwidth of the equivalent loop filter
T the data period
G the power spectrum density of the signal
C/N_0 the signal to noise ratio
C_S the chip spacing
B the two sided bandwidth of the front end filter
G_w is the power spectrum density of the interference

3-3-2-2 CW interferences

A Carrier Wave interference is a sinusoidal waveform that can be continuous or pulsed. If this narrowband interference has a high power, it can be disastrous for the receiver, especially if it is centred in the GNSS frequency band.

The general model of a CW interference is given by:

$$J = A_J \cos\left(2\pi\left(f_I + \Delta f_J\right)t - \theta_J\right) \quad (3\text{-}28)$$

where

A_J is the amplitude of the CW,

Δf_J is the frequency offset of the jammer with respect to the considered GNSS signal's carrier frequency,

θ_J is the phase of the jammer.

$f_I + \Delta f_J$ is the central frequency

The power spectrum density of the noise and the interference will be:

$$G_w(f) = \frac{N_0}{2} + \frac{{A_J}^2}{4}\, \delta\left(f - \left(f_I + \Delta f_J\right)\right) \quad (3\text{-}29)$$

As pointed out by many authors, the tracking error induced by the presence of interference cannot be always be modelled as the tracking error induced by an equivalent increased white noise. A distinction must be made depending on the bandwidth of the incoming interference. In fact these models are valid as long as the bandwidth of the interference is quite large compared to the inverse duration of the integration. Thus it is desired to complete these models for narrowband interference and in particular for the case where the receiver is affected by CW interference.

By analyzing the correlator output components, an expression of the code tracking error envelope in presence of CW interference is proposed [Martineau et al., 2007]:

$$M = \left| \frac{A_J}{\alpha A} C_C(k_0) \frac{\sin(\pi\ \delta f\ T_D)}{\pi\ \delta f\ T_D} \sin(\pi k_0 f_R\ C_S) \right| \quad (3\text{-}30)$$

where

- M is the absolute value of the maximum code tracking error induced by the CW in chip
- C_S is the Early-Late chip spacing in seconds
- $\frac{A_J}{A}$ is the relative amplitude of the CW compared to the useful GNSS signal
- $C_C(k_0)$ is the relative amplitude of the PRN code ray which is the closest to the interference
- δf, the difference between the CW frequency and the closest signal peak
- α is the slope of the spreading waveform autocorrelation function in $C_S/2$

The code tracking error oscillates within this envelope.

Assuming that the code tracking error is uniformly distributed on$[-M, M]$, its variance will be:

$$\sigma^2 = M^2/3 \quad (3\text{-}31)$$

Assuming that the code tracking error can be written $\varepsilon = M \sin\theta$ with θ uniformly distributed on$[0,2\pi]$, its variance will be:

$$\sigma^2 = M^2/2 \quad (3\text{-}32)$$

This last assumption is more realistic and is chosen.

To predict this error variance, the Doppler shift has to be computed for each satellite-user couple in order to precisely know the difference between the CW frequency and the closest signal peak of the considered PRN. By this way the receiver error component due to CW interference is obtained and is to be added to the one due to noise obtained by usual formula.

3-3-2-3 Conclusion

When some interfering signal is superimposed to the received useful signal, this may have the following three impacts on the pseudo range measurements:

- the measurements are affected by some additional noise
- one or several measurements are affected by a bias (divergence of measurement)
- some or all of the measurements are no longer available (loss of tracking)

An RFI mask was adopted to define the RF environment for which the receiver must have compliant performance, but in any case, even with large power interference above the mask, the integrity performance of the receiver must be compliant with the specifications. This is why it is needed to take into account every interference effect in this model that will feed RAIM algorithms.

3-4 Temporal Aspects

Actually, the pseudo range errors are strongly auto correlated and this aspect has especially to be taken account in any sequential pseudorange model. The way this temporal correlation is taken into account is addressed in this section.

3-4-1 First order Markov process

A first order Markov process is defined by:

$$\dot{x}(t) = -\frac{1}{T}x(t) + w(t) \tag{3-33}$$

where w (the innovation) is a white random process

x is a system output whose transfer function is given by

$$H(f) = \frac{1}{\frac{1}{T} + i2\pi f} \tag{3-34}$$

Applying the Wiener-Lee relation, we get:

$$S_X(f) = |H(f)|^2 S_W(f)$$

with $S_W(f) = \frac{N_0}{2}$

Therefore,

$$S_X(f) = \frac{N_0/2}{(2\pi f)^2 + \frac{1}{T^2}} \tag{3-35}$$

and by computing the inverse Fourier transform we get the autocorrelation function:

$$R_X(\tau) = \frac{N_0 T}{4} e^{-\frac{|\tau|}{T}} \tag{3-36}$$

$$R_X(\tau) = R_X(0) e^{-\frac{|\tau|}{T}}$$

The correlation time T_C is defined such as:

$$R_X(T_C) = \frac{1}{e} R_X(0) \tag{3-37}$$

Thus it can be seen that $T_C = T$

The equivalent discreet first order Markov is such as [Fossard, 1983]:

$$x(k+1) = mx(k) + T(1-\alpha)w(k) \tag{3-38}$$

where $m = e^{-T_e/T}$ and $n = \int_0^{T_e} e^{-v/T}\,\mathrm{d}v = T\left(1 - e^{-T_e/T}\right)$

The following approximation is often used:

$$e^{-T_e/T} = 1 - \frac{T_e}{T} + \frac{1}{2!}\left(\frac{T_e}{T}\right)^2 + \cdots + \frac{1}{n!}\left(-\frac{T_e}{T}\right)^n$$

In the case where the correlation time is much greater than the sample period, the following approximation can be made:

$$x(n+1) = \left(1 - \frac{T_e}{T}\right)x(n) + T_e w(n) \tag{3-39}$$

If $T_e = 1\ s$,

$$x(n+1) = \left(1 - \frac{1}{T}\right)x(n) + w(n) \tag{3-40}$$

3-4-2 Fault free case error measurement model

The following simple autoregressive model can be proposed as a preliminary approximation for these correlated noises:

$$\xi(k+1) = a\,\xi(k) + \sqrt{1 - a^2}\,w(k) \tag{3-41}$$

with for $k \in \mathbb{N}$, $w_k \sim N(0, \Sigma)$ and $\xi_1 \sim N(0, \Sigma)$

$$\Sigma = \begin{bmatrix} \sigma_1^2 & \cdots & 0 \\ \vdots & \ddots & \vdots \\ 0 & \cdots & \sigma_N^2 \end{bmatrix}$$

a is the autoregressive coefficient such as

$$a = 1 - \frac{1}{T_C} \tag{3-42}$$

The term $\sqrt{1 - a^2}$ is a normalization coefficient that allows the process ξ to have the covariance matrix Σ. It does not influence the correlation time computation.

The correlation time will depend on the source of the measurement error:

- Receiver and multipath will be driven by the smoothing time constant of the receiver noise which is assumed to be on the order of two minutes.
- Tropospheric error will be modelled using this first order Gauss Markov process with a 30 minutes correlation time [RTCA, 2006].
- [RTCA, 2006] states that the satellite clock and ephemeris error shall be modelled using a first-order Gauss Markov process with a 2 hour correlation time. But a correlation time of approximately one hour, based on the average period of time satellites are visible to the user will be used.

The pseudorange measurement error can then be represented as the sum of several first order Markov processes with error variances the same as the ones described in 3-2-1.

$$E(k) = \xi_{\text{tropo}}(k) + \xi_{\text{noise /multipath}}(k) + \xi_{\text{clock /eph}}(k) \tag{3-43}$$

3-4-3 Faulty case error measurement model

A sudden frequency shift in the satellite clock will lead to a ramp in the pseudorange. Errors in the satellite clock correction parameters in the navigation message will have a similar impact.

This is why a combined step ramp error that could include nominal bias, satellite failure and interference effect, will be used for the faulty case model.

"Error couples" will be denoted $(b, \dot{b})$ with b and $\dot{b}$ constant such as the pseudorange additional error will be:

$$D(k) = b + \dot{b}\,\Delta t \tag{3-44}$$

where Δt is the elapsed time since the onset of the failure

In [RTCA, 2006], in the section addressing FDE off line test procedure, it is indicated that a GPS satellite malfunction shall be simulated as a ramp error in measured pseudorange with a slope of 5m/s.

3-5 Synthesis

The objective of this section is to give a complete model of pseudo range measurements, including interference effects and satellites failures.

3-5-1 General model

A general model of smoothed pseudorange measurement can be proposed such as:

$$Y(k) = h\big(X(k)\big) + E(k) \tag{3-45}$$

where $E(k)$ error measurement

$E(k)$ can be view as the sum several components:

- the ionosphere, the troposphere, the ephemeris, the clock errors
- the receiver noise and the multipath error with a correlation time corresponding to the receiver smoothing time
- a nominal additional bias
- a possible additional error measurement due to the tracking of mixed useful signal and interference or due to a satellite failure which is supposed to be a combined step ramp error

Nevertheless, a distinction has to be made between the fault free case and the faulty case. The model will also differ if it is an input for a sequential or a snapshot integrity monitoring algorithms.

3-5-2 Snapshot model

The fault free case represents the nominal situation. In this case, the pseudorange error measurement uses to be represented as:

$$E \sim N\left(\begin{bmatrix}0\\ \vdots \\ 0\end{bmatrix}, \begin{bmatrix}\sigma_1^2 & \cdots & 0\\ \vdots & \ddots & \vdots \\ 0 & \cdots & \sigma_N^2\end{bmatrix}\right) \quad (3\text{-}46)$$

where $\sigma_1^2, \ldots, \sigma_N^2$ are nominal error variances corresponding to UERE computation described in section 3-2-1

A nominal bias on each measurement can be considered. In this case, the pseudorange error measurement is represented as:

$$E \sim N\left(\begin{bmatrix}a_1\\ \vdots \\ a_N\end{bmatrix}, \begin{bmatrix}\sigma_1^2 & \cdots & 0\\ \vdots & \ddots & \vdots \\ 0 & \cdots & \sigma_N^2\end{bmatrix}\right) \quad (3\text{-}47)$$

with the same nominal error variance computation

This model has also to consider the faulty case, that is to say the potential case where one or several pseudo range measurement are simultaneously affected by errors from different sources that can be a satellite failure or an interference effect.

Since the temporal aspects are not taken into account here, any additional fault is modeled as a bias. In presence of interference, the measurements can be affected by some additional noise which is represented by inflated error variance:

$$E \sim N\left(\begin{bmatrix}b_1\\ \vdots \\ b_N\end{bmatrix}, \begin{bmatrix}\sigma_1^2 & \cdots & 0\\ \vdots & \ddots & \vdots \\ 0 & \cdots & \sigma_N^2\end{bmatrix}\right) \quad (3\text{-}48)$$

In the absence of interference, the standard deviation $\sigma_1, \ldots, \sigma_N$ of the corresponding unsmoothed error will be taken as in section 3-2-1-1. In presence of wideband or narrowband interference, the standard deviation of the corresponding unsmoothed error will be taken as in section 3-3-2-2-1. In presence of CW interference, the corresponding unsmoothed error will be taken as a random variable with envelope as expressed in 3-3-2-2-1.

3-5-3 Sequential Model

The pseudorange measurement error can then be represented as the sum of several first order Markov processes and of a combined step ramp error that could include nominal bias, satellite failure and interference effect, such as:

$$E(k) = \xi_{\text{tropo}}(k) + \xi_{\text{noise /multipath}}(k) + \xi_{\text{clock /eph}}(k) + D(k) \quad (3\text{-}49)$$

Chapître 4

Techniques RAIM

Le contrôle autonome d'integrité fait réference à des méthodes uniquement basées sur la redondance des mesures satellitaires, éventuellement enrichies de celles d'autres capteurs embarqués, devant déterminer si les conditions sont réunies pour occasionner une erreur de position dépassant une limite spécifiée.

Cette technique repose en général en general sur deux fonctions : la fonction de détection dont le but est de détecter la présence d'une erreur de position inacceptable et la fonction d'exclusion dont le but est de déterminer et d'exclure la source de cette erreur permettant ainsi à la navigation de se poursuivre sans interruption.

Il existe deux grandes classes d'algorithmes de contrôle autonome de l'intégrité: les algorihtmes RAIM (Receiver Autonomous Integrity Monitoring) qui utilise exclusivement les informations GNSS et les algorihtms AAIM (Aircraft Autonomous Integrity Monitoring) qui utilise également des informations en provenance d'autres capteurs embarqués Cette étude traite uniquement des techniques RAIM.

La section 4.1 introduit quelques principes généraux. La section 4.1.1 traite du calcul de la position utilisateur au moyen de la methode des moindre-carrés. Le but de la section 4.1.2 est d'identifier les biais sur les measures de pseudodistance conduisant à une erreur de position dangereuse. Cela consiste à calculer pour chaque mesure de pseudo distance disponible le plus petit biais qui conduira à dépasser la limite d'alerte dans le domaine des positions. Ces plus petit biais correspondent aux pires situations de detection/exclusion et peuvent être utilisé dans la conception et l'évaluation des algorithmes RAIM.

La section 4.2 traite de la methode la plus classique c'est-à-dire celle des moindre carrées. Le RAIM moindre carrés est basé sur la comparaison entre un test statistique dépendant du vecteur de prediction d'erreur et d'un seuil donné. La somme des carrés des residus des mesures de pseudo distance forme ce test statitique. Le seuil est lui fixé en considérant le comportement statistique du test dans le cas « fault free ». Les niveaux de protection découlent du plus petit biais que l'algorihtme est capable de détecter en satisfaisant les probabilities de fausse alarmes et de detection manqué exigées. Leur calcul s'effectue en considérant le comportement statistique du test dans le cas « faulty »

La section 4.3 traite de la méthode de séparation des solutions. Elle est basées sur la comparaison de l'estimée de position qui utilise toutes les mesure satellitaires disponibles (filtre principal) et celles générées par chacun des sous-filtres utilisant toute les mesures à l'exception d'une seule. La separation entre chaque paire d'estimées (l'estimée du filtre principal et celle de chaque sous filtre) forme un test statistique et chaque test statistique est comparé à son seuil de detection respectif qui est fixé de telle manière à respecter la

probabilité de fausse alarme requise. La manière dont les niveaux de protection associés sont obtenus est explicitée et une nouvelle methode est proposée.

La section 4.4 est consacrée à la méthode du rapport de vraisemblance généralisée et plus particulièrement à la methode rapport de vraisemblance généralisée contraint. Il s'agit d'une méthode interessante car elle prend en compte directement le plus petit biais à detecter ainsi que le plus grand biais nominal sur chaque pseudo distance. Cependant cet algorithme nécessite differents paramètres d'entrée en vue d'être implémenté et utilisé comme un RAIM : un seuil auquel sera comparé le test statistique et qui doit être en accord avec le taux de fausse alerte requis. On doit également être capable de prédire ces performances au regard de la probabilté de détection manquée exigée. Ces différents aspects ont été adressés durant ce travail de doctorat et sont traités dans cette section. L'implémentation séquentielle de cette méthode est également présentée ainsi que l'adaptation qui en a été faite pour la détection de pannes de type échelon plus rampe.

Chapter 4

RAIM Techniques

4-1 General principles

4-1-1 Introduction

Autonomous integrity monitoring refers to a situation where a receiver uses the redundancy of satellite measurements, possibly augmented by other sensors, to determine whether a fault condition exists that would cause it to have an unacceptable probability to experience a position error outside a specified bound.

There are two general classes of integrity monitoring:

- Receiver Autonomous Integrity Monitoring (RAIM) which uses GNSS information exclusively. It refers to integrity monitoring using only satellite signals tracked by the receiver.

- Aircraft Autonomous Integrity Monitoring (AAIM) which uses information from additional on-board sensors (e.g. barometric altimeter, clock and inertial navigation system INS)

This study only addresses RAIM techniques.

RAIM algorithm design mainly consists in two distinct parts. First, of course we have to detect (or detect and exclude) faulty measurements (monitoring) but we also have to predict our ability to protect the user considering satellite geometry and an assumed measurement error model.

As mentioned in part 2-5, the monitoring scheme generally consists of two functions: the fault detection and the fault exclusion. The goal of fault detection is to detect the presence of positioning failure. Upon detection, proper fault exclusion determines and excludes the source of the failure (without necessarily identifying the individual sources causing the problem) thereby allowing GNSS navigation to continue without interruption.

Most of the time, these functions are based on the comparison between a test statistic depending on the prediction error vector and a given threshold. It is a hypothesis test in which the test statistics computation is performed with the observable data. The decision threshold is set considering the statistical distribution of the test in the fault free case and a given false detection rate.

Concerning the performance prediction, as the position error remains unknown for the user, statistical tools have to be used to check requirements compliance (to predict the availability). This can be performed by predicting the smallest bias the algorithm is able to detect respecting the missed alert and false alert requirements (protection levels computation) or by predicting the probability of missed detection of dangerous biases.

This study focuses on three distinct classes of RAIM algorithms: the Least Square Residual (LSR) method, the Maximum Solution Separation (MSS) method and the constrained Generalized Likelihood Ratio (GLR) test method. Monitoring and performance prediction processes are detailed for these three algorithms.

Other promising techniques have been recently proposed such as NIORAIM method [Hwang and Brown, 2006] or the Multiple Hypothesis RAIM algorithm [Blanch et al., 2007] but are not studied here. It has been decided to focus on standard methods such as LSR and MSS and on a new one, the constrained GLR. This method seems very interesting because it is designed to detect only faults which lead to a positioning failure.

4-1-2 Least Squares Position Solution

The objective of this section is to detail least square user position estimation and the computation of measurement residual vector which is also called the prediction error vector. These computations constitute the starting point of every RAIM algorithms presented in this study.

The measurement model is generally expressed as:

$$Y(k) = h\big(X(k)\big) + E(k) \tag{4-1}$$

It can be seen that the measurements do not linearly depend on the true user position. This is why an iterative least squares estimation technique has to be implemented. This method uses the linearization of the measurement model around successive estimates of the receiver position.

Let us denote $\hat{X}_0(k)$ an initial estimate of $X(k)$. This initial estimate can be determined using past measurements or can be provided by other navigation means.

Denoting $X(k) = \hat{X}_0(k) + \Delta X(k)$, the measurement model can be rewritten as follows:

$$Y(k) = h\left(\hat{X}_0(k) + \Delta X(k)\right) + E(k) \tag{4-2}$$

This model is linearized around $\hat{X}_0(k)$:

$$Y(k) \cong h\left(\hat{X}_0(k)\right) + \frac{\partial h}{\partial X}\left(\hat{X}_0(k)\right) \times \Delta X(k) + E(k) \tag{4-3}$$

The first order derivative that appears in this last equation is an $N \times 4$ matrix that can be expressed as:

$$H = \frac{\partial h}{\partial X}\left(\hat{X}_0(k)\right) \tag{4-4}$$

$$H = \begin{bmatrix} \frac{\partial h^1}{\partial x}\left(\hat{X}_0(k)\right) & \frac{\partial h^1}{\partial y}\left(\hat{X}_0(k)\right) & \frac{\partial h^1}{\partial z}\left(\hat{X}_0(k)\right) & \frac{\partial h^1}{\partial b}\left(\hat{X}_0(k)\right) \\ \vdots & \vdots & \vdots & \vdots \\ \frac{\partial h^N}{\partial x}\left(\hat{X}_0(k)\right) & \frac{\partial h^N}{\partial y}\left(\hat{X}_0(k)\right) & \frac{\partial h^N}{\partial z}\left(\hat{X}_0(k)\right) & \frac{\partial h^N}{\partial b}\left(\hat{X}_0(k)\right) \end{bmatrix} \tag{4-5}$$

It can be shown that these derivatives can be expressed as:

$$\frac{\partial h^i}{\partial x}\left(\hat{X}_0(k)\right) = \frac{\hat{x}_0 - x^i(k)}{\sqrt{\left(\hat{x}_0 - x^i(k)\right)^2 + \left(\hat{y}_0 - y^i(k)\right)^2 + \left(\hat{z}_0 - z^i(k)\right)^2}} \tag{4-6}$$

$$\frac{\partial h^i}{\partial y}\left(\hat{X}_0(k)\right) = \frac{\hat{y}_0 - y^i(k)}{\sqrt{\left(\hat{x}_0 - x^i(k)\right)^2 + \left(\hat{y}_0 - y^i(k)\right)^2 + \left(\hat{z}_0 - z^i(k)\right)^2}} \tag{4-7}$$

$$\frac{\partial h^i}{\partial z}\left(\hat{X}_0(k)\right) = \frac{\hat{z}_0 - z^i(k)}{\sqrt{\left(\hat{x}_0 - x^i(k)\right)^2 + \left(\hat{y}_0 - y^i(k)\right)^2 + \left(\hat{z}_0 - z^i(k)\right)^2}} \tag{4-8}$$

$$\frac{\partial h^i}{\partial b}\left(\hat{X}_0(k)\right) = 1 \tag{4-9}$$

The linearized model can also be rewritten as:

$$Y(k) - h\left(\hat{X}_0(k)\right) = H \times \Delta X(k) + E(k)$$

Or

$$\Delta Y(k) = H \times \Delta X(k) + E(k) \tag{4-10}$$

Denoting $\Delta Y(k) = Y(k) - h\left(\hat{X}_0(k)\right)$, $\Delta Y(k)$ represents the deviation between the measurements made and the predicted noiseless measurements that the receiver would have made if its position and clock delay were $\hat{X}_0(k)$.

Considering this new linear model between $\Delta Y(k)$ and $\Delta X(k)$, a least squares estimate of $\Delta X(k)$ can be computed. This estimate is:

$$\Delta\hat{X}(k) = [H^t \mathrm{H}]^{-1} H^t \times \Delta Y(k) \tag{4-11}$$

Let us denote that if the measurement error covariance matrix is known, then the weighted least squares estimate is:

$$\Delta\hat{X}(k) = [H^t \Sigma^{-1} \mathrm{H}]^{-1} H^t \Sigma^{-1} \times \Delta Y(k) \tag{4-12}$$

where $\Sigma = \mathrm{cov}\big(E(k)\big)$.

This last estimator is the best linear unbiased estimator that is to say the one that reaches the Cramer-Rao lower bound [Söderström, 1989].

The quantity $\Delta\hat{X}(k)$ is an estimate of $\Delta X(k)$, which is defined as the deviation between the initial estimate $\hat{X}_0(k)$ and $X(k)$.

It is then possible to implement an iterative algorithm starting from an initial estimate $\hat{X}_0(k)$ and improving progressively this estimate through the comparison between the measurements and the predicted measurements for each estimated position. The iterative algorithm can be implemented to stop if $\Delta\hat{X}(k)$ is a vector that has a small norm.

The way the positioning error can be expressed as a function of the measurement error is detailed as follow (omitting the dependence on time):

$$\Delta\hat{X} = [H^t \Sigma^{-1} \mathrm{H}]^{-1} H^t \Sigma^{-1} \times \Delta Y$$

$$\Delta\hat{X} = [H^t \Sigma^{-1} \mathrm{H}]^{-1} H^t \Sigma^{-1} \times [H\,\Delta X + E]$$

then

$$\Delta\hat{X} = [H^t \Sigma^{-1} \mathrm{H}]^{-1} H^t \Sigma^{-1} H\,\Delta X + [H^t \Sigma^{-1} \mathrm{H}]^{-1} H^t \Sigma^{-1} E$$

As $[H^t \Sigma^{-1} \mathrm{H}]^{-1} H^t \Sigma^{-1} H = I_N$,

$$\Delta\hat{X} = \Delta X + [H^t \Sigma^{-1} \mathrm{H}]^{-1} H^t \Sigma^{-1} E$$

Then

$$\Delta X - \Delta\hat{X} = -[H^t \Sigma^{-1} \mathrm{H}]^{-1} H^t \Sigma^{-1} E \tag{4-13}$$

where $\Delta X - \Delta\hat{X} = \big(X - \hat{X}_0\big) - \big(\hat{X} - \hat{X}_0\big) = X - \hat{X}$ is the positioning error
E is the measurement error

The measurement residual represents the deviation between the measurements made and the predicted noiseless measurements that the receiver would have made if its position and clock delay were $\hat{X}$ and if there was no noise. It can be expressed such as:

$$\Delta Y = Y - h\big(\hat{X}\big)$$

$$\begin{aligned} \Delta Y &= h(X) + E(k) - h\big(\hat{X}\big) \\ &= h(X_0 + \Delta X) + E - h\big(X_0 + \Delta\hat{X}\big) \end{aligned}$$

By linearizing around X_0,

$$\Delta Y = H\Delta X - H\Delta\hat{X} + E = H\left(\Delta X - \Delta\hat{X}\right) + E$$

$$\Delta Y = -[H^t\Sigma^{-1}\mathrm{H}]^{-1}H^t\Sigma^{-1}E + E$$

Therefore,

$$\Delta Y = (I - H[H^t\Sigma^{-1}\mathrm{H}]^{-1}H^t\Sigma^{-1})E \tag{4-14}$$

which is the well-known relationship between the measurement residual and the measurement error.

At the end of the iterative process, $\hat{X}$ and $\hat{X}_0$ are very close and this why we can denote:

$$\Delta Y = Y - h\left(\hat{X}\right) = Y - h\left(\hat{X}_0\right) \tag{4-15}$$

It can be noticed that there is a linear relationship between the measurement residual and the measurement error which is very interesting for RAIM algorithms.

4-1-3 Pseudorange bias that leads to a positioning failure

The integrity monitoring requires that the navigation system detects the presence of an unacceptably large position error for a given mode of flight, and if possible, isolates and removes the source of unacceptably large position error from the navigation solution, thereby allowing navigation to return to normal performance without an interruption in service.

Therefore, only faults that lead to a positioning failure (horizontal or vertical) need to be detected.

The goal of this subsection is to identify pseudorange biases that lead to a positioning failure, that is say to compute for each available pseudorange, the smallest bias on this pseudorange that will lead to a positioning failure. These smallest biases correspond to the worst case detection/exclusion situation, they can be used to design RAIM algorithm and/or to estimate their statistical properties.

This concept has been introduced in [Nikiforov, 2005] as an input parameter of the constrained GLR test.

A pseudorange error γ is considered as a horizontal positioning failure if its impact violates the integrity risk, that is to say if:

$$\begin{gathered}\left(1 - P_f\right)P_0\left(\left\|X_H - \hat{X}_H\right\| > HAL\right) \\ +P_f P_\gamma\left(\left\|X_H - \hat{X}_H\right\| > HAL\right) > P_{Int}\end{gathered} \tag{4-16}$$

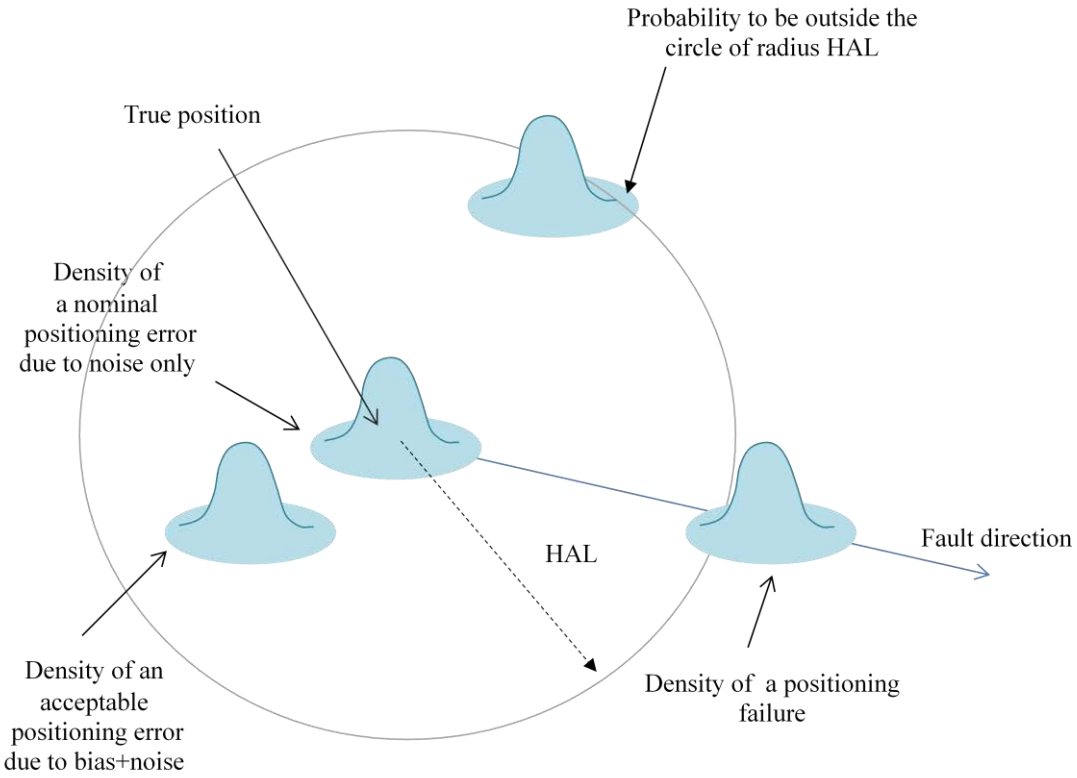

Figure 13 - Horizontal positioning failure

As it is depicted on the previous figure, each individual satellite fault (additional pseudorange bias) produces a fault direction in the horizontal plane [Nikiforov, 2005]. The main question is: how far from the true position the ellipse's centre can be moved along the corresponding fault direction in order to consider that this bias lead to a positioning failure?

That will depend on the mutual orientation of this "ellipse of uncertainty" and the fault direction. The computation, which has to be done for each pseudorange, is detailed in appendix A.

A pseudorange error γ is considered as a vertical positioning failure if its impact violates the integrity risk such as:

$$\begin{aligned}&(1-P_f)P_0\left(\left|X_V-\hat{X}_V\right|>VAL\right)\\&+P_fP_\gamma\left(\left|X_V-\hat{X}_V\right|>VAL\right)>P_{Int}\end{aligned} \tag{4-17}$$

where P_f is the probability of failure of one satellite
P_0 corresponds to the fault free case
P_γ corresponds to the faulty case

This case, which is simpler than the horizontal one, is illustrated on the following figure and the computation for each pseudorange of the smallest additional bias that will lead to a positioning failure has been particularly investigated during this PhD and is detailed in appendix A.

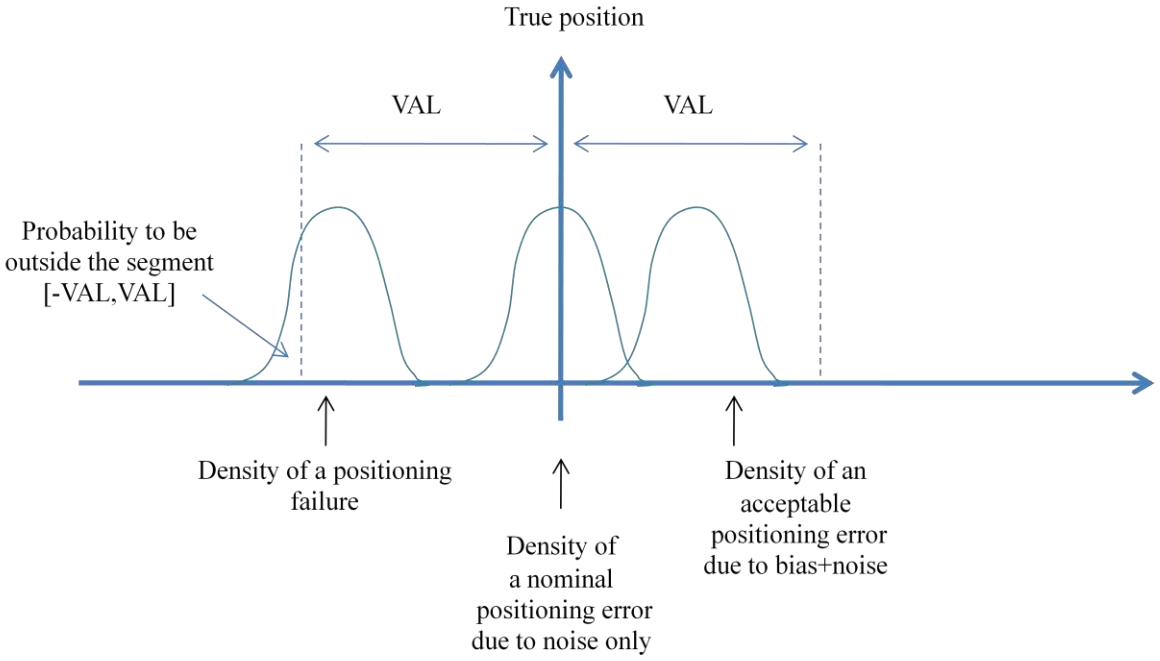

Figure 14 - Vertical positioning failure

These critical biases values are to be computed for a given user position at a given moment by (for a given sample):

- Computing the probability to exceed the alert limit in the fault free case
  $P_0\left(\left\|X_H - \hat{X}_H\right\| > HAL\right)$ and $P_0\left(\left|X_V - \hat{X}_V\right| > VAL\right)$

- For each available pseudorange measurement, computing the smallest additional bias b_i that leads to a probability $P_{b_i}\left(\left\|X_H - \hat{X}_H\right\| > HAL\right)$ or $P_{b_i}\left(\left|X_V - \hat{X}_V\right| > VAL\right)$ such as:

$$\begin{aligned}&\left(1 - P_f\right)P_0\left(\left\|X_H - \hat{X}_H\right\| > HAL\right)\\&+P_f P_{b_i}\left(\left\|X_H - \hat{X}_H\right\| > HAL\right) = P_{Int}\end{aligned}$$

$$\begin{aligned}&\left(1 - P_f\right)P_0\left(\left|X_V - \hat{X}_V\right| > VAL\right)\\&+P_f P_{b_i}\left(\left|X_V - \hat{X}_V\right| > VAL\right) = P_{Int}\end{aligned}$$

The computations of the probabilities P_0 and P_{b_i} do not depend on any detection algorithm. But it can be seen that they depend on the failure probability of occurrence.

4-2 Least Square Residual Method

The classical LSR RAIM method is based on the comparison between a test statistic depending on the prediction error vector and a given threshold

4-2-1 Implemented detection function

Let's consider the measurement residual ΔY (also called the prediction error vector) which can be expressed thanks to a linear relationship the measurement error vector *E*, its covariance matrix Σ and the observation matrix H:

$$\Delta Y = (I - H[H^t \mathrm{H}]^{-1} H^t) E \tag{4-18}$$

or for the weighted least square solution:

$$\Delta Y = (I - H[H^t \Sigma^{-1} \mathrm{H}]^{-1} H^t \Sigma^{-1}) E \tag{4-19}$$

Those statistics are observable whereas the positioning error of the least square solution is not. A scalar measurement is then defined such as:

$$SSE = \Delta Y^t . \Delta Y = \|\Delta Y\|^2 \tag{4-20}$$

or

$$WSSE = \Delta Y^t \Sigma^{-1} \Delta Y \tag{4-21}$$

Let's denote

$$s^2 = \frac{SSE}{\sigma^2} \tag{4-22}$$

or

$$s^2 = WSSE \tag{4-23}$$

In both cases, s^2 represents the sum of the squares of the range residual errors normalized by the standard deviation of the measurement errors.

The LSR RAIM test is defined by [Parkinson and Axelrad, 1988]:

$$T = \sqrt{\frac{SSE}{N-4}} \tag{4-24}$$

and the weighted LSR RAIM test is defined by [Walter and Enge, 1995]:

$$T = \sqrt{WSSE} \tag{4-25}$$

In both cases, the detection threshold is obtained by considering the test statistic in the fault free case

If the measurement error E is noise only such as:

$$E(k) = \begin{bmatrix} n^1(k) \\ \vdots \\ n^j(k) \\ \vdots \\ n^N(k) \end{bmatrix} \text{ with } n^i \sim N(0, \sigma_i^2) \text{ or } n^i \sim N(0, \sigma^2) \tag{4-26}$$

Therefore, s^2 is chi-squared distributed with N-4 degrees of freedom, $s^2 \sim \chi^2_{N-4}$, that is to say:

$$\exists \xi_i \, , s^2 = \xi_1^2 + \cdots + \xi_{N-4}^2 \; iid, \xi_i \sim N(0,1) \tag{4-27}$$

The probability of false alarm is used to determine the normalised detection threshold a_{Pfa} such as:

$$P\left(s^2 > a_{Pfa}\right) = P_{fa} \tag{4-28}$$

$$P_{fa} = \int_{a_{Pfa}}^{\infty} f_{\chi^2_{N-4}(x)} \, \mathrm{d}x \tag{4-29}$$

where

$$f_{\chi^2_{\lambda,N-4}}(x) = \frac{e^{-x/2} x^{\frac{(N-4)}{2}-1}}{2^{(N-4)/2}\Gamma\left(\frac{N-4}{2}\right)} \tag{4-30}$$

Thus, a fault is detected if the chi-squared variable is abnormally large above the assumed noise level.

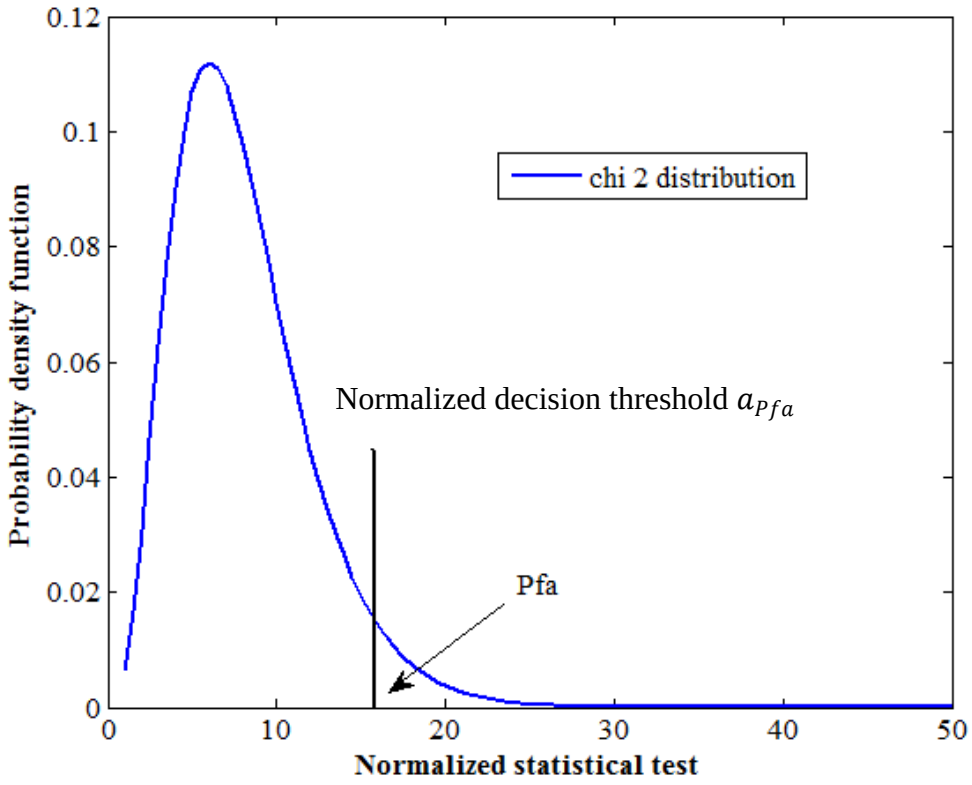

Figure 15 - Fault free LSR statistical test distribution

Finally, the threshold that it is compared to our criteria is for the LSR RAIM:

$$h = \sqrt{\frac{a_{Pfa}\,\sigma^2}{(N-4)}} \tag{4-31}$$

and for the weighted LSR method:

$$h = \sqrt{a_{Pfa}} \tag{4-32}$$

The LSR test δ is given by the following equation:

$$\delta = \begin{cases} \mathcal{H}_0 \text{ if } T \leq h \\ \mathcal{H}_1 \text{ if } T > h \end{cases} \tag{4-33}$$

4-2-2 Protection levels computation

The protection levels derive from the smallest bias the algorithm is able to detect satisfying the false alarm and the missed detection requirement.

Let‘s consider that the measurement error E is noise and a bias b on one satellite *j* such as*:*

$$E(k) = \begin{bmatrix} n^1(k) \\ \vdots \\ n^j(k) \\ \vdots \\ n^N(k) \end{bmatrix} + \begin{bmatrix} 0 \\ \vdots \\ b \\ \vdots \\ 0 \end{bmatrix} \tag{4-34}$$

In this case, s^2 is chi-squared distributed with N-4 degrees of freedom and non-centrality parameter λ such as $s^2 \sim \chi^2_{\lambda,N-4}$. This means that s^2 can be written like this:

$$\exists \xi_i\,, s^2 = \xi_1^2 + \cdots + \xi_{N-4}^2 \;\; iid, \xi_i \sim N(\mu_i, 1) \tag{4-35}$$

$$\lambda = \sum_{i=1}^{N-4} \mu_i^2 \tag{4-36}$$

The non central chi-square probability density function is given by:

$$f_{\chi^2_{\lambda,N-4}}(x) = \frac{e^{-(x+\lambda)/2} x^{\frac{(N-4)}{2}-1}}{2^{(N-4)/2}} \sum_{j=0}^{\infty} \frac{x^j \;\lambda^j}{\Gamma\left(\frac{N-4}{2}+j\right).2^{2j}.j!} \tag{4-37}$$

The non centrality parameter λ is computed in order to satisfy the Pmd requirement such as:

$$P_{md} = \int_0^{a_{Pfa}} f_{\chi^2_{\lambda,N-4}(x)}\,\mathrm{d}x \tag{4-38}$$

The obtained non centrality parameter λ is the smallest that can be detected by the test. It does not depend of any pseudorange.

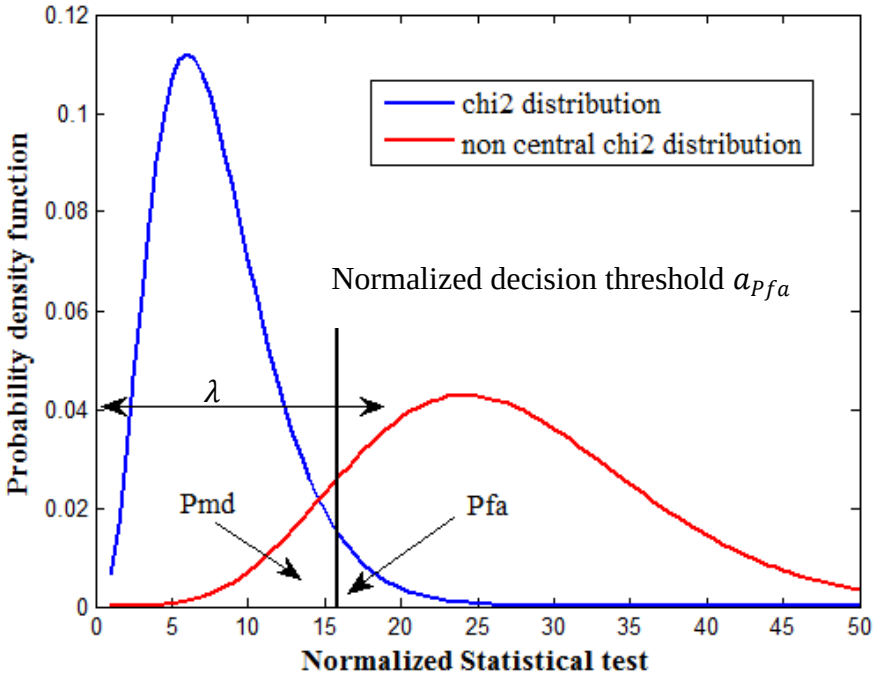

Figure 16 - Fault free and faulty LSR statistical test distribution

The relation between the smallest detectable bias on the pseudorange j and the test statistic is simplified as:

$$\sigma^2\lambda = b\left(1 - B_{j,j}\right)b = \left(1 - B_{j,j}\right)b^2 \tag{4-39}$$

where $B = H[H^t\Sigma^{-1}\mathrm{H}]^{-1}H^t\Sigma^{-1}$

λ is the smallest detectable non-centrality parameter previously obtained

The smallest detectable measurement bias b on satellite j can be then expressed as:

$$b_j = \sigma\sqrt{\frac{\lambda}{1 - B_{j,j}}} \tag{4-40}$$

The relationship between the position error and the measurement error is:

$$X(k) - \hat{X}(k) = -A \times E(k) \tag{4-41}$$

with $A = [H^t\Sigma^{-1}\mathrm{H}]^{-1}H^t\Sigma^{-1}$

Therefore the impact of the bias b_j in position domain is obtained by:

$$\Delta X = X(k) - \hat{X}(k) = A \times \begin{bmatrix} 0 \\ \vdots \\ b_j \\ \vdots \\ 0 \end{bmatrix} = \begin{bmatrix} \cdots & A_{N,j} & \cdots \\ \cdots & A_{E,j} & \cdots \\ \cdots & A_{V,j} & \cdots \\ \cdots & A_{T,j} & \cdots \end{bmatrix} \times \begin{bmatrix} 0 \\ \vdots \\ b_j \\ \vdots \\ 0 \end{bmatrix}$$

Then,

$$\Delta X_H = \sqrt{\Delta X_N{}^2 + \Delta X_\mathrm{E}{}^2} = \sqrt{A_{N,j}{}^2 + A_{E,j}{}^2} \times b_j$$

$$\Delta X_{\mathrm{V}} = A_{V,j} \times b_j$$

Denoting,

$$p_{bias} = \sigma \times \sqrt{\lambda} \tag{4-42}$$

$$\Delta X_{\mathrm{H}} = \frac{\sqrt{{A_{N,j}}^2 + {A_{E,j}}^2}}{\sqrt{1 - B_{j,j}}} \times p_{\mathrm{bias}}$$

$$\Delta X_{\mathrm{V}} = \frac{\left|\mathrm{A_{V,j}}\right|}{\sqrt{1 - B_{j,j}}} \times \mathrm{p_{bias}}$$

Denoting,

$$VSLOPE_j = \frac{A_{V,j}}{\sqrt{1 - B_{j,j}}}, HSLOPE_j = \frac{\sqrt{{A_{N,j}}^2 + {A_{E,j}}^2}}{\sqrt{1 - B_{j,j}}} \tag{4-43}$$

The protection levels are computed referring to the worst satellite:

$$HSLOPE_{max} = \max_j\left(HSLOPE_j\right) \tag{4-44}$$

$$VSLOPE_{max} = \max_j\left(VSLOPE_j\right) \tag{4-45}$$

And

$$HPL = HSLOPE_{max} \times p_{bias} \tag{4-46}$$

$$VPL = VSLOPE_{max} \times p_{bias} \tag{4-47}$$

A proposed LSR RAIM method that takes into account nominal biases on pseudorange measurement is detailed in appendix B.

4-3 Maximum Solution Separation Method

4-3-1 Introduction

The maximum solution separation method is based on the observed separation between the position estimate generated by the full-set filter (using all the satellite measurements) and that generated by each one of the subset filters (each using all but one of the satellite measurements). Its principle is described in [Brown and McBurney, 1988].

The separation d_i between each pair of the estimates (the full filter estimate and each sub-filter estimate) forms a test statistic and each test statistic is compared to its respective detection threshold D_i which is determined to meet the maximum allowable rate requirement.

The full LSR position estimate is:

$$\Delta\hat{X}(k) = [H^t\Sigma^{-1}\mathrm{H}]^{-1}H^t\Sigma^{-1} \times \Delta\mathrm{Y(k)} \qquad (4\text{-}48)$$

with $\Sigma = cov(E)$

Let's denote this full solution $\Delta\hat{X}_0$ and for $i \in [1, N]$ the corresponding sub solution is denoted $\Delta\hat{X}_i$.

For $i \in [1, N]$, the discriminator d_i is defined as:

$$d_i(k) = \hat{X}_0(k) - \hat{X}_i(k) = \Delta\hat{X}_0 - \Delta\hat{X}_i \qquad (4\text{-}49)$$

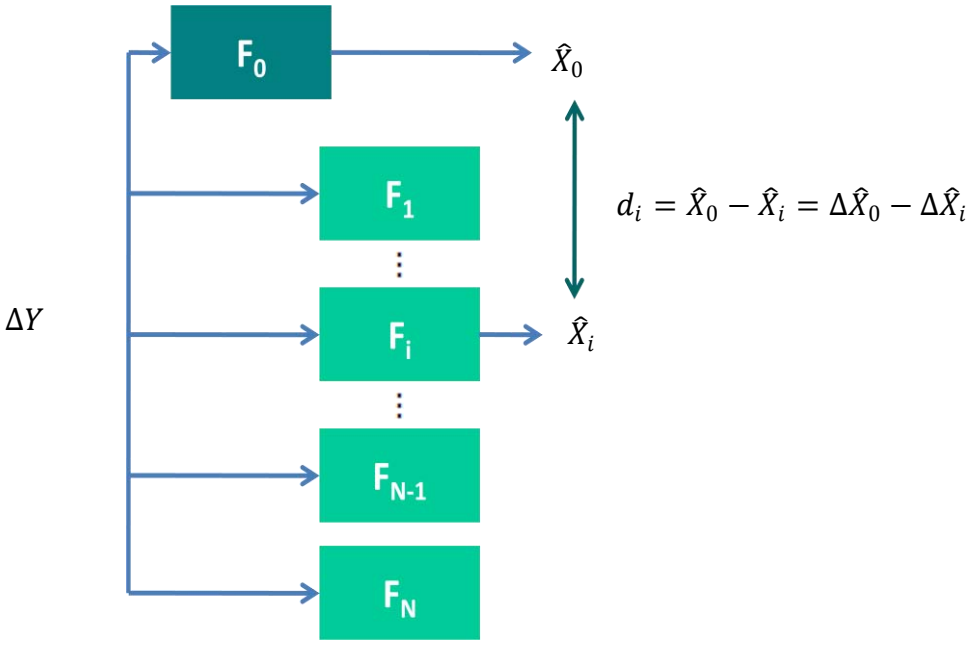

Figure 17 - Solution Separation method principle

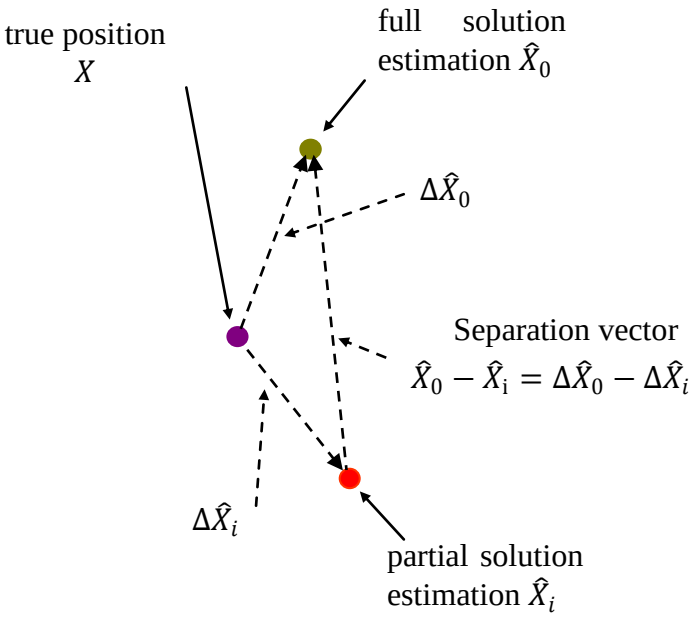

Figure 18 - Full and partial solutions

4-3-2 Detection function

Let $X(k)$ be the true user position at the instant k.
Let $\hat{X}_0(k)$ be the full filter LSR user position estimation at the instant k.

As detailed in 4-1-2, the relationship between the position error and the measurement error can be expressed such as:

$$\Delta X(k) - \hat{X}_0(k) = X(k) - \hat{X}_0(k) = -[H^t\Sigma^{-1}H]^{-1}H^t\Sigma^{-1} \times E(k)$$

that is to say,

$$X(k) - \hat{X}_0(k) = -A_0 \times E(k) \qquad (4\text{-}50)$$

with $A_0 = [H^t\Sigma^{-1}\mathrm{H}]^{-1}H^t\Sigma^{-1}$

For $i\epsilon[1,N]$, let $\hat{X}_i(k)$ be the LSR user position estimation at the instant k do not considering the pseudo range obtained from the satellite i.

The solution separation discriminators are 4×1 vectors linearly depending of the error measurement such as:

$$d_i(k) = \hat{X}_0(k) - \hat{X}_i(k) = (A_i - A_0) \times E(k) \qquad (4\text{-}51)$$

Their covariance matrix is given by

$$dP_i(k) = (A_i - A_0)\Sigma(A_i - A_0)^t \qquad (4\text{-}52)$$

Thus the method provides N criteria which are the separation d_i and their horizontal and vertical component ($d_{i,\mathrm{H}}$ and $d_{i,V}$) have to be compared with their respective thresholds D_i and V_i. The detection test is given by the following equation:

$$\delta = \begin{cases} \mathcal{H}_0 \text{ if } \forall i \in [1,N], \left|d_{i,\mathrm{H}}\right| \leq D_i \text{ and } \left|d_{i,V}\right| \leq V_i \\ \mathcal{H}_k \text{ if } \exists k \in [1,N], \left|d_{k,\mathrm{H}}\right| > D_k \text{ or } \left|d_{k,V}\right| > V_k \end{cases} \quad (4\text{-}53)$$

where for $i \in [1,N]$, D_i and V_i are thresholds whose computation is detailed in the next sections.

For $i \in [1,N]$, thresholds have to cope with the corresponding false alert rate. To set them let us consider the statistic behaviour of the criteria in the fault free case. Thus, we have:

$$E(k) = \begin{bmatrix} n^1(k) \\ \vdots \\ n^i(k) \\ \vdots \\ n^N(k) \end{bmatrix} \quad (4\text{-}54)$$

with for $i \in [1,N]$, $n^i \sim N(0,\sigma_i^2)$

$$\mathrm{cov}(E) = \Sigma$$

The horizontal and the vertical criteria components, $d_{i,H}$ and $d_{i,V}$ for $i \in [1,N]$, are going to be considered separately. They are directly expressed in the local coordinate frame because of the expression of the observation matrices H_0 and H_i.

4-3-2-1 Computation of the horizontal thresholds

$d_{i,H}$ is a bi-dimensional random variable following a Gaussian distribution in the fault-free case such as $d_{i,H} \sim N\left(\begin{bmatrix}0\\0\end{bmatrix}, dP_{i,H}\right)$ and the general expression of the probability density function of the variable $d_{i,H}$ is given by:

$$f_{d_{i,H}}(X) = \frac{1}{2\pi\sqrt{det\left(\mathrm{d}P_{i,H}\right)}} \exp\left(-\frac{1}{2}\mathrm{X}^{\mathrm{t}}.\mathrm{d}{P_{i,H}}^{-1}.\mathrm{X}\right) \quad (4\text{-}55)$$

where $dP_{i,H} = dP_i(1{:}\,2,1{:}\,2)$ and $dP_i = (A - A_i)\Sigma(A - A_i)^t$

Since $dP_{i,H}$ is not diagonal, the components of $d_{i,H}$ are not mutually independent and the separations on the North and East axes are correlated. But as $dP_{i,H}$ is a positive definite matrix, it is diagonalizable and its eigenvalues are all positive. In particular we can find an orthonormal basis $\mathcal{B}_i = \left(\vec{e}_{1,i}, \vec{e}_{2,i}\right)$ that is composed of eigenvectors $\vec{e}_{1,i}$, $\vec{e}_{2,i}$ corresponding with the eigenvalues $\lambda_{1,i}$ and $\lambda_{2,i}$ of $dP_{i,H}$ and we have:

$$\mathrm{d}P_{i,H} = \mathrm{P}_{\perp,\mathrm{i}}.\Delta_{\mathrm{i}}.{\mathrm{P}_{\perp,\mathrm{i}}}^{\mathrm{t}} \quad (4\text{-}56)$$

where,

$\Delta_{\mathrm{i}} = \mathrm{diag}\left(\lambda_{1,i}, \lambda_{2,i}\right)$ is the diagonal matrix whose elements are the eigenvalues of $\mathrm{d}P_{i,H}$

$\mathrm{P}_{\perp,\mathrm{i}}$ is the projection matrix whose columns are the eigenvectors $\vec{e}_{1,i}$, $\vec{e}_{2,i}$.

In particular $\mathrm{P}_{\perp,\mathrm{i}}$ is orthogonal: ${\mathrm{P}_{\perp,\mathrm{i}}}^{-1} = {\mathrm{P}_{\perp,\mathrm{i}}}^{\mathrm{t}}$.

Let $d_{i,\perp}$ be the projection of $d_{i,H}$ in the orthonormal basis $\mathcal{B}_i = \left(\vec{e}_{1,i}, \vec{e}_{2,i}\right)$ such as:

$$d_{i,\perp} = \mathrm{P}_{\perp,\mathrm{i}}{}^{\mathrm{t}} d_{i,H} \tag{4-57}$$

$d_{i,\perp}$ is a 2-dimensional Gaussian vector whose covariance matrix is the diagonal matrix Δ_i $d_{i,\perp} \sim N\left(\begin{bmatrix}0\\0\end{bmatrix}, \Delta_\mathrm{i}\right)$. In particular, the components of $d_{i,\perp}$ are mutually independent and the general expression of the probability density function of variable $d_{i,\perp}$ is given by:

$$f_{d_{i,\perp}}(X) = \frac{1}{2\pi\sqrt{\lambda_{1,i}\,\lambda_{2,i}}} \exp\left(-\frac{1}{2}\mathrm{X}^{\mathrm{t}}.\Delta_\mathrm{i}{}^{-1}.\mathrm{X}\right) \tag{4-58}$$

Let λ_i be the dominant eigenvalue and $\lambda_i{}'$ the other eigenvalue. For simplification, without loss of generality, we will assume that $\lambda_i = \lambda_{1,i}$ and $\lambda_i^{'} = \lambda_{2,i}$.

The set of points $\mathcal{E}_{a,i} = \left\{X \in \mathbb{R}^2 : \mathrm{X}^{\mathrm{t}}.\Delta_\mathrm{i}{}^{-1}.\mathrm{X} = a^2\right\}$ is an ellipse whose semi-major axis is oriented along $\vec{e}_{1,i}$ and whose semi-minor axis is oriented along $\vec{e}_{2,i}$. This ellipse defines an equipotential curve of the probability density function:

$$f_{d_{i,\perp}}\left(X \in \mathcal{E}_{a,i}\right) = \frac{1}{2\pi\sqrt{\lambda_{1,i}\,\lambda_{2,i}}} \mathrm{e}^{-\frac{a^2}{2}}$$

The probability that the point corresponding to $d_{i,\perp}$ belongs to the region $D_{a,i}$ delimited by $\mathcal{E}_{a,i}$ is:

$$P\left(d_{i,\perp} \in D_{a,i}\right) = \iint_{D_{a,i}} f_{d_{i,\perp}}(X)\mathrm{d}X$$

The analytical expression of this ellipse is in the coordinate frame $\left(O, \vec{e}_{1,i}, \vec{e}_{2,i}\right)$:

$$\frac{X_1^2}{\lambda_{1,i}} + \frac{X_2^2}{\lambda_{2,i}} = a^2$$

O is the centre of this ellipse, it is at full-solution position. The length of the semi-major axis is $a\sqrt{\lambda_{1,i}}$ and the length of the semi-minor axis is $a\sqrt{\lambda_{2,i}}$.

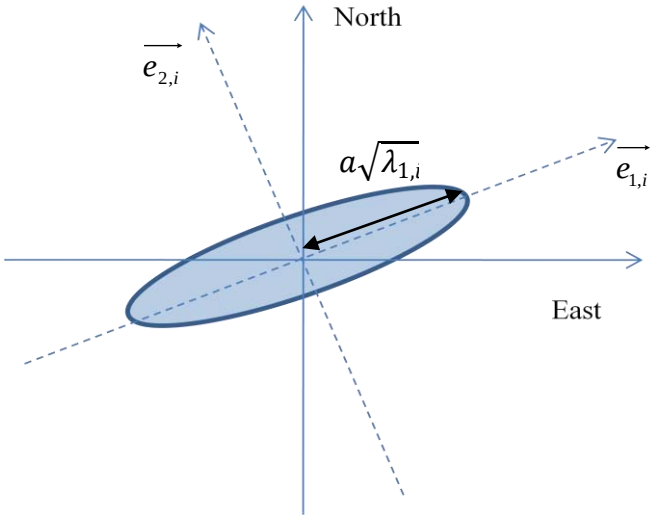

Figure 19 - Fault free ellipse

The partial horizontal threshold could have been obtained using:

$$P\left[\left\|d_{i,H}\right\| \leq a\right] = 1 - p$$

or

$$P\left[\left\|d_{i,H}\right\|^2 \leq a^2\right] = 1 - p$$

where $p \in [0,1]$ corresponds to the allocated P_{fa}

Or it would have better to work with a normalized relationship:

$$\mathrm{P}\left({d_{i,\perp}}^{\mathrm{t}}.{\Delta_{\mathrm{i}}}^{-1}.d_{i,\perp} \leq b^2\right) = 1 - p$$
$$P\left(\frac{{d_{i,\perp}}^2(1)}{\lambda_{1,i}} + \frac{{d_{i,\perp}}^2(2)}{\lambda_{2,i}}\right) = 1 - p$$

But in fact $\left|d_{i,\perp}(1)\right|$ is set as an approximation of $\left\|d_{i,\perp}\right\| = \left\|d_{i,H}\right\|$ and for $i \in [1,N]$:

$$\left\|d_{i,H}\right\| \cong \left|d_{i,\perp}(1)\right| \tag{4-59}$$

Considering both sides of the distribution and the fact that any of the N tests may cause a false alarm with the same probability, for $i \in [1,N]$, the threshold D_i is calculated as:

$$\frac{P_{fa}}{N} = P\left(\left|d_{i,\perp}(1)\right| \geq D_i\right)$$

$$\frac{P_{fa}}{N} = P\left(\left|\frac{d_{i,\perp}(1)}{\sqrt{\lambda_i}}\right| \geq \frac{D_i}{\sqrt{\lambda_i}}\right)$$

with

$$\frac{d_{i,\perp}(1)}{\sqrt{\lambda_i}} \sim N(0,1) \tag{4-60}$$

Therefore, for $i \in [1,N]$, as in [Brenner, 1996],

$$D_i = \sqrt{\lambda_i}\, Q^{-1}\left(\frac{P_{fa}}{2N}\right) \tag{4-61}$$

where

$Q(x) = \frac{1}{\sqrt{2\pi}} \int_x^{\infty} e^{\frac{-t^2}{2}} dt$

λ_i is the largest eingenvalue of the covariance matrix $dP_{i,H} = dP_i(1{:}2, 1{:}2)$

4-3-2-2 Computation of the vertical thresholds

$d_{i,V}$ is a random variable following a Gaussian distribution in the fault-free case such as:

$$d_{i,V} \sim N\left(0, {\sigma_{V,i}}^2\right) \tag{4-62}$$

where ${\sigma_{V,i}}^2 = dP_i(3,3)$

Thus, for the vertical part of the detection, for $i \in [1, N]$ the threshold V_i are obtained such as:

$$\frac{P_{fa}}{N} = P\left(\left|d_{i,\mathrm{V}}\right| \geq V_i\right)$$

$$\frac{P_{fa}}{N} = \frac{1}{\sqrt{2\pi}\sigma_{V,i}}\left[\int_{-\infty}^{-V_i} \exp\left(\frac{-t^2}{2{\sigma_{V,i}}^2}\right) \mathrm{d}t + \int_{V_i}^{+\infty} \exp\left(\frac{-t^2}{2{\sigma_{V,i}}^2}\right) dt\right]$$

$$\frac{P_{fa}}{2N} = \frac{1}{\sqrt{2\pi}\sigma_{V,i}} \int_{V_i}^{+\infty} \exp\left(\frac{-t^2}{2{\sigma_{V,i}}^2}\right) dt$$

$$\frac{P_{fa}}{2N} = \frac{1}{\sqrt{2\pi}} \int_{V_i/\sigma_{V,i}}^{\infty} e^{\frac{-u^2}{2}} du$$

Therefore, for $i \in [1, N]$,

$$V_i = \sigma_{V,i}\, Q^{-1}\left(\frac{P_{fa}}{2N}\right) \tag{4-63}$$

where

$Q(x) = \frac{1}{\sqrt{2\pi}} \int_x^{\infty} e^{\frac{-t^2}{2}} dt$

4-3-2-3 Conclusion

Finally, the test for detecting one range failure is given by the following equation:

$$\delta = \begin{cases} \mathcal{H}_0 \text{ if } \forall i \in [1, N], \left|d_{i,\perp}(1)\right| \leq D_i \text{ and } \left|d_{i,V}\right| \leq V_i \\ \mathcal{H}_k \text{ if } \exists k \in [1, N], \left|d_{k,\perp}(1)\right| > D_k \text{ or } \left|d_{k,V}\right| > V_k \end{cases}$$

with for $i \in [1, N]$,

$$V_i = \sigma_{V,i}\, Q^{-1}\left(\frac{P_{fa}}{2N}\right) \text{ and } D_i = \sqrt{\lambda_i}\, Q^{-1}\left(\frac{P_{fa}}{2N}\right)$$

4-3-3 Protection levels computation

The objective in this section is to detail the MSS protection level computation. As the position error remains unknown for the user, statistic bounds have to be used to check requirements compliance. Several approaches are presented:

The first one is an existing method whose consists in finding a bound of the horizontal error consistent with the required probability of missed detection and the required probability of false alarm (section 4-3-3-1).

The second class of approach which has been proposed during this PhD consists in predicting the smallest bias on each pseudorange that will be detected by the algorithm with the required allocated probability of missed detection. Then this bias will be projected in the position domain and will give the protection level (section 4-3-3-2).

4-3-3-1 Existing horizontal protection level computation

Our goal is to compute a statistical bound called horizontal protection level that will be such as:

$$\mathrm{P}\left(\left\|X-\hat{X}_0\right\|_H \leq \mathrm{HPL}\ /\exists \text{ a non detected bias on a pseudorange}\right) = P_{md}$$

For $i \in [1, N]$, let's assume that there is a bias b on the pseudorange i and that it is not detected by the corresponding criteria. That means that $\left\|\hat{X}_i-\hat{X}_0\right\|_H \leq D_i$.

As $X-\hat{X}_0 = X-\hat{X}_i+\hat{X}_i-\hat{X}_0$,

$$\left\|X-\hat{X}_0\right\|_H \leq \left\|X-\hat{X}_i\right\|_H + \left\|\hat{X}_i-\hat{X}_0\right\|_H \tag{4-71}$$

Thus,

$$\left\|X-\hat{X}_0\right\|_H \leq \left\|X-\hat{X}_i\right\|_H + D_i \tag{4-72}$$

The method consists now in over bounding the term $\left\|X-\hat{X}_i\right\|_H$.

Since the faulty measurement has been removed from $\hat{X}_i$ computation, the vector $X-\hat{X}_i$ corresponds to a fault free case situation.

So let's consider the distribution of this vector $\Delta\hat{X}_i = X-\hat{X}_i$ is the position error resulting from the sub solution that does not take into account the i^{th} pseudo range.

$$\Delta\hat{X}_i = -A_i \times E \tag{4-73}$$

The behaviour of its horizontal component, denoted $\Delta X_{i,H}$, is studied here.

$\Delta X_{i,H}$ is a bi-dimensional random variable following a Gaussian distribution such as $\Delta X_{i,H} \sim N\left(\begin{bmatrix}0\\0\end{bmatrix}, C_{i,H}\right)$

Since $C_{i,H}$ is not diagonal, the components of $\Delta X_{i,H}$ are not mutually independent and the separations on the North and East axes are correlated. But as $C_{i,H}$ is a positive definite matrix, it is diagonalizable and its eigenvalues are all positive. In particular we can find an orthonormal basis $\beta_i = (\vec{u}_{1,i}, \vec{u}_{2,i})$ that is composed of eigenvectors $\vec{u}_{1,i}$ and $\vec{u}_{2,i}$ corresponding with the eigenvalues $\mu_{1,i}$ and $\mu_{2,i}$ of $C_{i,H}$ and we have:

$$C_{i,H} = \Pi_{\perp,\mathrm{i}} \,.\, \mathrm{M_i} \,.\, {\Pi_{\perp,\mathrm{i}}}^{\mathrm{t}} \tag{4-75}$$

where,

$\mathrm{M_i} = \mathrm{diag}(\mu_{1,i}, \mu_{2,i})$is the diagonal matrix whose elements are the eigenvalues of $C_{i,H}$

$\Pi_{\perp,\mathrm{i}}$ is the projection matrix whose columns are the eigenvectors $\vec{u}_{1,i}$ and $\vec{u}_{2,i}$In particular $\Pi_{\perp,\mathrm{i}}$ is orthogonal ${\Pi_{\perp,\mathrm{i}}}^{-1} = {\Pi_{\perp,\mathrm{i}}}^{\mathrm{t}}$.

Let $\Delta X_{i,\perp}$ be the projection of $\Delta X_{i,H}$ in the orthonormal basis $\beta_i = (\vec{u}_{1,i}, \vec{u}_{2,i})$ such as:

$$\Delta X_{i,\perp} = {\Pi_{\perp,\mathrm{i}}}^{\mathrm{t}} \Delta X_{i,H} \tag{4-76}$$

$\Delta X_{i,\perp}$ is a 2-dimensional Gaussian vector whose covariance matrix is the diagonal matrix $\mathrm{M_i}$, $\Delta X_{i,\perp} \sim N\left(\begin{bmatrix}0\\0\end{bmatrix}, \mathrm{M_i}\right)$ or $\Delta X_{i,\perp} \sim N\left(\begin{bmatrix}0\\0\end{bmatrix}, \begin{bmatrix}\mu_{1,i} & 0\\ 0 & \mu_{2,i}\end{bmatrix}\right)$.

In particular, the components of $\Delta X_{i,\perp}$ are mutually independent and $\|\Delta X_{i,\perp}\| = \|\Delta X_{i,H}\|$

Let's denote

$$s_i^2 = {\Delta X_{i,\perp}}^{\mathrm{t}} \,.\, {\mathrm{M_i}}^{-1} \,.\, \Delta X_{i,\perp} \tag{4-77}$$

that is to say,

$$s_i^2 = \frac{\Delta X_{i,\perp}(1)^2}{{\mu_{1,i}}^2} + \frac{\Delta X_{i,\perp}(2)^2}{{\mu_{2,i}}^2} \tag{4-78}$$

s_i^2 is chi-squared distributed with 2 degrees of freedom, ${s_i}^2 \sim \chi_2^2$, and we can easily find δ such as:

$$P(s_i^2 \le \delta) = 1 - P_{md} \tag{4-79}$$

$$1 - P_{md} = \int_{-\infty}^{\delta} f_{\chi_2^2(x)} \,\mathrm{d}x$$

Let's denote

$$\delta = F_{\chi_2^2}^{-1}(1 - P_{md}) \tag{4-80}$$

Our goal is to bound $\|\Delta X_{i,\perp}\| = \|\Delta X_{i,H}\| = \sqrt{\Delta X_{i,\perp}(1)^2 + \Delta X_{i,\perp}(2)^2}$.

Assuming that $\mu_{1,i} = \max(\mu_{1,i}, \mu_{2,i})$, we have

$$\sqrt{\Delta X_{i,\perp}(1)^2 + \Delta X_{i,\perp}(2)^2} \le \sqrt{\Delta X_{i,\perp}(1)^2 + \frac{\mu_{1,i}}{\mu_{2,i}} \Delta X_{i,\perp}(2)^2} \le \sqrt{\mu_{1,i}} \sqrt{\frac{\Delta X_{i,\perp}(1)^2}{\mu_{1,i}} + \frac{\Delta X_{i,\perp}(2)^2}{\mu_{2,i}}}$$

Then,

$$\|\Delta X_{i,\perp}\| \le \sqrt{\mu_{1,i} \,.\, s_i^2}$$

As

$$P(s_i^2 \leq \delta) = 1 - P_{md}$$

$$P\left(\sqrt{\mu_{1,i}\,.\,s_i^2} \leq \sqrt{\mu_{1,i}\,.\delta}\right) = 1 - P_{md}$$

Let's denote

$$\delta_i = \sqrt{\mu_{1,i}\,.\delta} \tag{4-81}$$

$$P\left(\left\|\Delta X_{i,\perp}\right\| \leq \delta_i\right) \geq 1 - P_{md}$$

Therefore,

$$P\left(\begin{matrix}\left\|X - \hat{X}_0\right\| \leq \delta_i + D_i / \exists \text{ non detected} \\ \text{bias on the i}^{\text{th}}\text{pseudorange}\end{matrix}\right) \geq 1 - P_{md}$$

And a class of horizontal protection levels can be defined as proposed in [Escher, 2003]:

$$HPL = \max_{i\epsilon[1,N]}(\delta_i + D_i) \tag{4-82}$$

where $D_i = \sqrt{\lambda_i}\, Q^{-1}\left(\frac{P_{fa}}{2N}\right)$

$$Q(x) = \frac{1}{\sqrt{2\pi}}\int_x^{\infty} e^{\frac{-t^2}{2}} dt$$

λ_i is the largest eingenvalue of the covariance matrix $dP_{i,H}$

$\delta_i = \sqrt{\mu_{1,i}}\,.\sqrt{\delta}$

$\mu_{1,i}$ is the largest eingenvalue of the covariance matrix $C_{i,H}$

It is demonstrated in appendix C that δ is equal to $-2\ln(P_{md})$

In [Vanderwerf, 2001], the proposed value corresponding to our δ_i is:

$$a_i = \sqrt{\mu_{1,i}}\,.\,Q^{-1}(P_{md}) \tag{4-83}$$

This approach leads to smaller values and this is why we keep the theoretical expression:

$$\delta_i = \sqrt{\mu_{1,i}}\,.\sqrt{F_{\chi_2^2}^{-1}(1 - P_{md})} = \sqrt{\mu_{1,i}}\,.\sqrt{-2\ln(P_{md})} \tag{4-84}$$

This horizontal protection level computation is illustrated on the following figure. The decomposition $\left\|X - \hat{X}_0\right\|_H \leq \left\|X - \hat{X}_i\right\|_H + \left\|\hat{X}_i - \hat{X}_0\right\|_H$ is represented in red. The inequality $\left\|\hat{X}_i - \hat{X}_0\right\|_H \leq D_i$ is represented by the green circle; the inequality $\left\|\Delta\hat{X}_i\right\|_H \leq \delta_i$ is represented by the blue ellipse. The final error over bounding corresponding to the protection level is represented by the red circle.

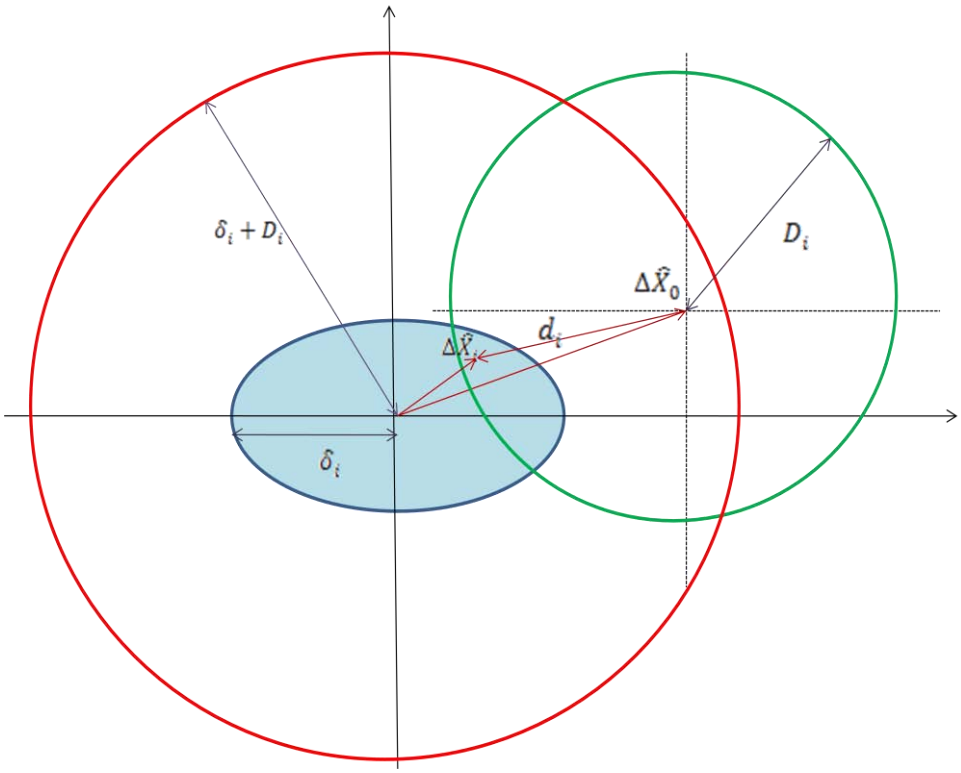

Figure 20 - Existing protection level computation illustration

Nevertheless, some situation can be less favorable as it is illustrated on the following figure. This is why some new methods for horizontal protection level computation are proposed in the next section.

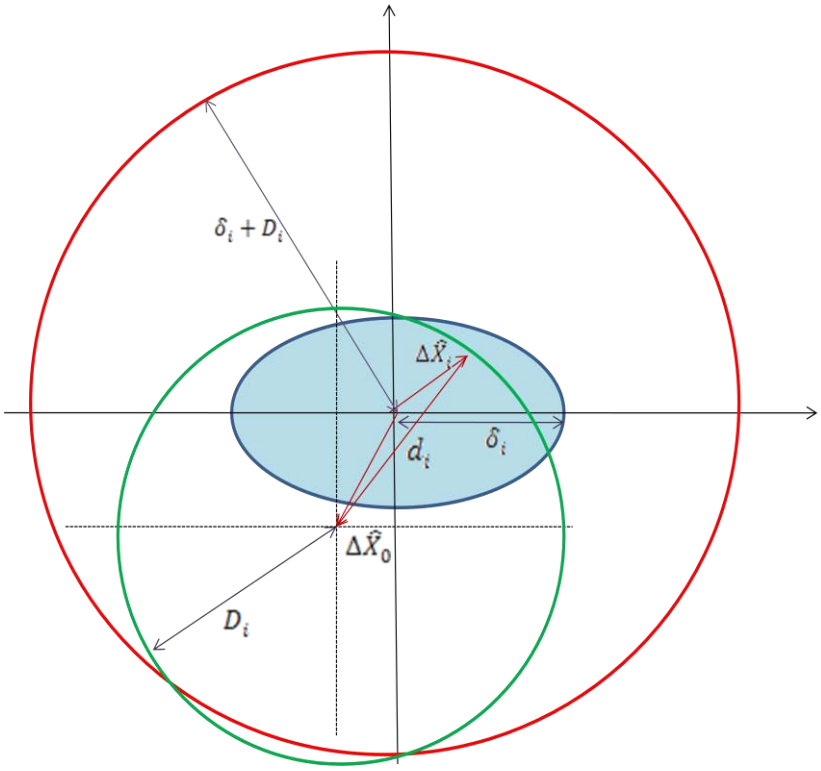

Figure 21 - Existing protection level computation illustration (other configuration)

4-3-3-2 Proposed horizontal protection level computation

Another method to compute protection levels has been proposed during this PhD and is detailed in his section. It consists in predicting the smallest bias on each pseudorange that will be detected by the algorithm with the required allocated probability of missed detection and to project this bias in the position domain to obtain the protection level.

The objective of this method is to avoid the following operation:

$$\left\|X - \hat{X}_0\right\|_H \leq \left\|X - \hat{X}_i\right\|_H + \left\|\hat{X}_i - \hat{X}_0\right\|_H$$

when the positioning error is over bound.

4-3-3-2-1 Faulty case horizontal criteria density function

For $i \in [1, N]$, let's assume that there is a bias b on the pseudorange i. The impact on the corresponding criteria d_i is such as:

$$d_i(k) = \hat{X}(k) - \hat{X}_i(k) = (A_i - A) \times E(k) \tag{4-85}$$

with

$$E(k) = \begin{bmatrix} n^1(k) \\ \vdots \\ n^i(k) \\ \vdots \\ n^N(k) \end{bmatrix} + \begin{bmatrix} 0 \\ \vdots \\ b \\ \vdots \\ 0 \end{bmatrix} \tag{4-86}$$

As in the fault free case, d_i is projected in the local reference frame and we first focus on its horizontal component $d_{i,H}$.

In this case, $d_{i,H}$ is a two dimensions vector which follows a Gaussian bi-dimensional law with a mean $b_{i,H}$ corresponding to the projection of b in the horizontal plane and with a covariance matrix $dP_{i,H}$:

$$b_i = (A_i - A)\begin{bmatrix} 0 \\ \vdots \\ b \\ \vdots \\ 0 \end{bmatrix} \text{ and } b_{i,H} = b_i(1:2) \tag{4-87}$$

Its density function is:

$$f_{d_{i,H}}(X) = \frac{1}{2\pi\sqrt{det\left(\mathrm{d}P_{i,H}\right)}} \exp\left(-\frac{1}{2}\left(\mathrm{X} - b_{i,H}\right)^{\mathrm{t}}.\mathrm{d}{P_{i,H}}^{-1}.\left(\mathrm{X} - b_{i,H}\right)\right) \tag{4-88}$$

where X is expressed in the North East local frame such as $X = \begin{bmatrix} x_N \\ x_E \end{bmatrix}$

As in the fault free case $dP_{i,H}$ is a positive definite matrix, it is diagonalizable and its eigenvalues $\lambda_{1,i}$ and $\lambda_{2,i}$ are all positive such as:

$$\mathrm{d}P_{i,H} = \mathrm{P}_{\perp,\mathrm{i}}.\Delta_{\mathrm{i}}.\mathrm{P}_{\perp,\mathrm{i}}{}^{\mathrm{t}} \tag{4-89}$$

where

$\Delta_{\mathrm{i}} = \mathrm{diag}(\lambda_{1,i}\ ,\ \lambda_{2,i})$ is the diagonal matrix whose elements are the eigenvalues of $\mathrm{d}P_{i,H}$

$\mathrm{P}_{\perp,\mathrm{i}}$ is the projection matrix whose columns are the eigenvectors $\vec{e}_{1,i}$, $\vec{e}_{2,i}$. In particular $\mathrm{P}_{\perp,\mathrm{i}}$ is orthogonal: $\mathrm{P}_{\perp,\mathrm{i}}{}^{-1} = \mathrm{P}_{\perp,\mathrm{i}}{}^{\mathrm{t}}$

Then, $\det(\mathrm{d}P_{i,H}) = \lambda_{1,i}\ \lambda_{2,i}$ and $\mathrm{d}P_{i,H}{}^{-1} = \mathrm{P}_{\perp,\mathrm{i}}.\Delta_{\mathrm{i}}{}^{-1}.\mathrm{P}_{\perp,\mathrm{i}}{}^{\mathrm{t}}$

$$\begin{aligned}(\mathrm{X} - b_{i,H})^{\mathrm{t}}.\mathrm{d}P_{i,H}{}^{-1}.(\mathrm{X} - b_{i,H}) &= (\mathrm{X} - b_{i,H})^{\mathrm{t}}.\mathrm{P}_{\perp,\mathrm{i}}.\Delta_{\mathrm{i}}{}^{-1}.\mathrm{P}_{\perp,\mathrm{i}}{}^{\mathrm{t}}.(\mathrm{X} - b_{i,H}) \\ &= \left[\mathrm{P}_{\perp,\mathrm{i}}{}^{\mathrm{t}}(\mathrm{X} - b_{i,H})\right]^{\mathrm{t}}.\Delta_{\mathrm{i}}{}^{-1}.\left[\mathrm{P}_{\perp,\mathrm{i}}{}^{\mathrm{t}}.(\mathrm{X} - b_{i,H})\right]\end{aligned}$$

Denoting $X_{\perp} = \mathrm{P}_{\perp,\mathrm{i}}{}^{\mathrm{t}}.X$ and $\Omega = \mathrm{P}_{\perp,\mathrm{i}}{}^{\mathrm{t}}.b_{i,H}$, $X_{\perp}$ is the vector X expressed in the new local frame and Ω is the vector $b_{i,H}$ in the new local frame.

$$f_{d_{i,\perp},b}(X) = \frac{1}{2\pi\sqrt{\lambda_{1,i}\ \lambda_{2,i}}}\exp\left(-\frac{1}{2}\left(\frac{(\mathrm{x}_{\perp} - \Omega_1)^2}{\lambda_{1,\mathrm{i}}} + \frac{(\mathrm{y}_{\perp} - \Omega_2)^2}{\lambda_{2,\mathrm{i}}}\right)\right) \tag{4-90}$$

As it has been done it the fault free case, $|d_{i,\perp}(1)|$ is set as an approximation of $\|d_{i,H}\|$ and for $i \in [1, N]$,

$$d_{i,H} \cong d_{i,\perp}(1)$$

And we have:

$$d_{i,\perp}(1) \sim N(\Omega_{i,1}, \lambda_{1,\mathrm{i}}) \tag{4-91}$$

$$f_{d_{i,\perp},b}(x) = \frac{1}{2\pi\sqrt{\lambda_{1,i}}}\exp\left(-\frac{1}{2}\frac{(\mathrm{x}_{\perp} - \Omega_1)^2}{\lambda_{1,\mathrm{i}}}\right) \tag{4-92}$$

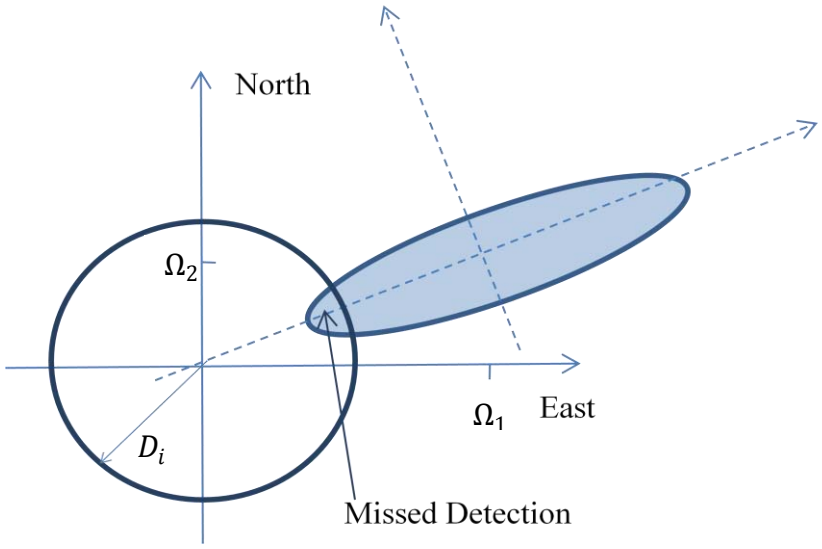

Figure 22 - Faulty situation

4-3-3-2-2 Bounding the horizontal positioning error

Let's consider two probabilities p_0 and p_1 such as $p_0 \in [0,1]$ and $p_0 \in [0,1]$

For $i \in [1, N]$, we can find the bias $b_i$on the pseudorange i that will be detected with the probability $1 - p_1$ by the corresponding criteria.

This bias can be obtained thanks to an iterative process. For the successive values of b_i, we compute $\Omega_{i,1}$ such as :

$$\begin{bmatrix} \Omega_{\mathrm{i},1} \\ \Omega_{\mathrm{i},2} \\ \Omega_{\mathrm{i},3} \end{bmatrix} = P_{i,\perp}^{t} \times n_{local}^{t} \times (A - A_i) \times E \tag{4-93}$$

with $A = [H^t \Sigma^{-1} \mathrm{H}]^{-1} H^t \Sigma^{-1}$, $E = [0 \quad \ldots \quad 0 \quad b_i \quad 0 \quad \ldots \quad 0]^{\mathrm{t}}$

and we compute:

$$p = \int_{-D_i}^{D_i} \frac{1}{2\pi\sqrt{\lambda_i}} e^{-\frac{1}{2}\left(\frac{x-\Omega_{i,1}}{\sqrt{\lambda_i}}\right)^2} dx \tag{4-94}$$

At the end of the process, we have the amplitude of the bias $b_i$on the pseudorange such as:

$$P\left(\left|d_{i,H}\right| \leq D_i / b_i\right) = p_1 \tag{4-95}$$

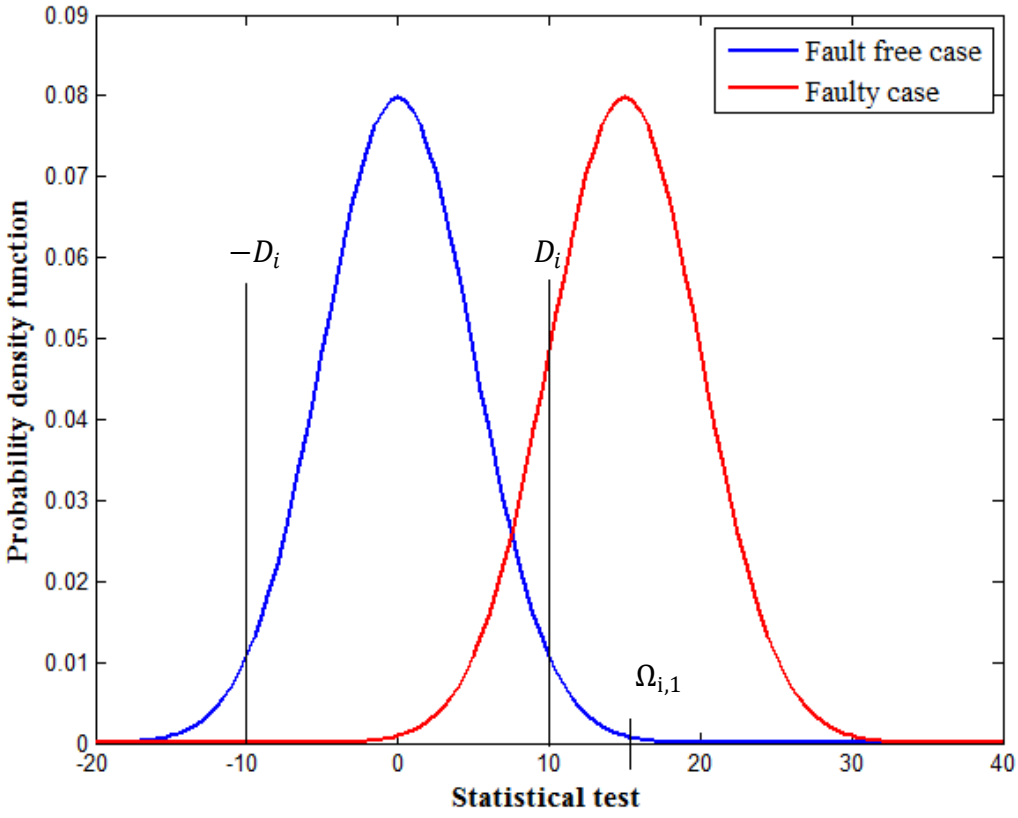

Figure 23 - Fault free and faulty statistical test distribution

On the other hand, we can look at the impact of a bias of amplitude b_i on the pseudorange i on the full filter position estimation and find a bound $\delta_{0,i}$ such as:

$$P\left(\left\|X-\hat{X}_0\right\|_H \leq \delta_{0,i}/\exists \text{ a bias of size } b_i \text{ on the } \mathrm{i^{th}} \text{ pseudorange}\right) = p_0 \qquad (4\text{-}96)$$

The method is described in appendix C.

Therefore, for every $i \in [1, N]$

$$P\left(\left\|X-\hat{X}_0\right\|_H \leq \delta_{0,\mathrm{i}}/\exists\ b_i\right) \times P\left(\left|d_{i,H}\right| \leq D_i/b_i\right) = p_0 p_1 \qquad (4\text{-}97)$$

And a class of horizontal protection levels can be proposed such as:

$$HPL = \max_{i\epsilon[1,N]}\left(\delta_{0,\mathrm{i}}\right) \qquad (4\text{-}98)$$

The setting of p_0 and p_1, such as $p_0 p_1 = P_{md}$, constitutes a tuning parameter of our protection level computation.

4-3-3-3 Vertical protection level computation

As for the horizontal case, vertical protection level can be computed as follow.

In the faulty case, $d_{i,V}$ is a one dimension vector which follows a Gaussian law with a mean $b_{i,V} = b_i(3)$ corresponding to the projection of b on the vertical local axe and with a variance ${\sigma_{V,i}}^2 = dP_i(3,3)$.

Its density function is:

$$f_{d_{i,V}}(x) = \frac{1}{\sqrt{2\pi}\sigma_{V,i}} \exp\left(-\frac{\left(\mathrm{x}-b_{i,v}\right)^2}{2{\sigma_{V,i}}^2}\right) \qquad (4\text{-}99)$$

For $i \in [1, N]$, let's assume that there is a bias b on the pseudorange i and that it is not detected by the corresponding criteria. That means that:

$$\left|d_{i,V}\right| = \left|\hat{X}_{V,i} - \hat{X}_{V,0}\right| \leq V_i \qquad (4\text{-}100)$$

As $X - \hat{X}_0 = X - \hat{X}_i + \hat{X}_i - \hat{X}_0$,

$$\left\|X-\hat{X}_0\right\|_{\mathrm{V}} \leq \left\|X-\hat{X}_i\right\|_{\mathrm{V}} + \left\|\hat{X}_i-\hat{X}_0\right\|_V \qquad (4\text{-}101)$$

Denoting $X_V = X(3)$

$$\left\|X-\hat{X}_0\right\|_{\mathrm{V}} \leq \left|X_V-\hat{X}_{V,i}\right| + \left|\hat{X}_{V,i}-\hat{X}_{V,0}\right|$$

Finally,

$$\left\|X-\hat{X}_0\right\|_{\mathrm{V}} \leq \left|X_V-\hat{X}_{V,i}\right| + V_i \qquad (4\text{-}102)$$

Since the faulty measurement has been removed from $\hat{X}_i$ computation, the vector $X - \hat{X}_i$ corresponds to a fault free case situation.

The behaviour of its horizontal component, denoted $\Delta X_{i,V} \left| = X_V - \hat{X}_{V,i} \right|$, is studied here.

$\Delta X_{i,V}$ is a random variable following a Gaussian distribution such as $\Delta X_{i,V} \sim N\left(0, {C_{i,V}}^2\right)$ and its probability density function is given by:

$$f_{\Delta X_{i,V}}(x) = \frac{1}{\sqrt{2\pi} C_{i,V}} \exp\left(-\frac{1}{2}\left(\frac{x}{C_{i,V}}\right)^2\right) \tag{4-103}$$

Thus $\left|X_V - \hat{X}_{V,i}\right|$ can be easily bounded. A bound γ_i is obtained such as

$$1 - P_{md} = \frac{1}{\sqrt{2\pi} C_{i,V}} \int_{-\gamma_i}^{\gamma_i} \exp\left(-\frac{1}{2}\left(\frac{t}{C_{i,V}}\right)^2\right) dt \tag{4-104}$$

A class of vertical protection levels can be defined as:

$$VPL = \max_{i \epsilon [1,N]} (\gamma_i + V_i) \tag{4-105}$$

This is a first method that derives from the existing HPL computation. Another method can be proposed.

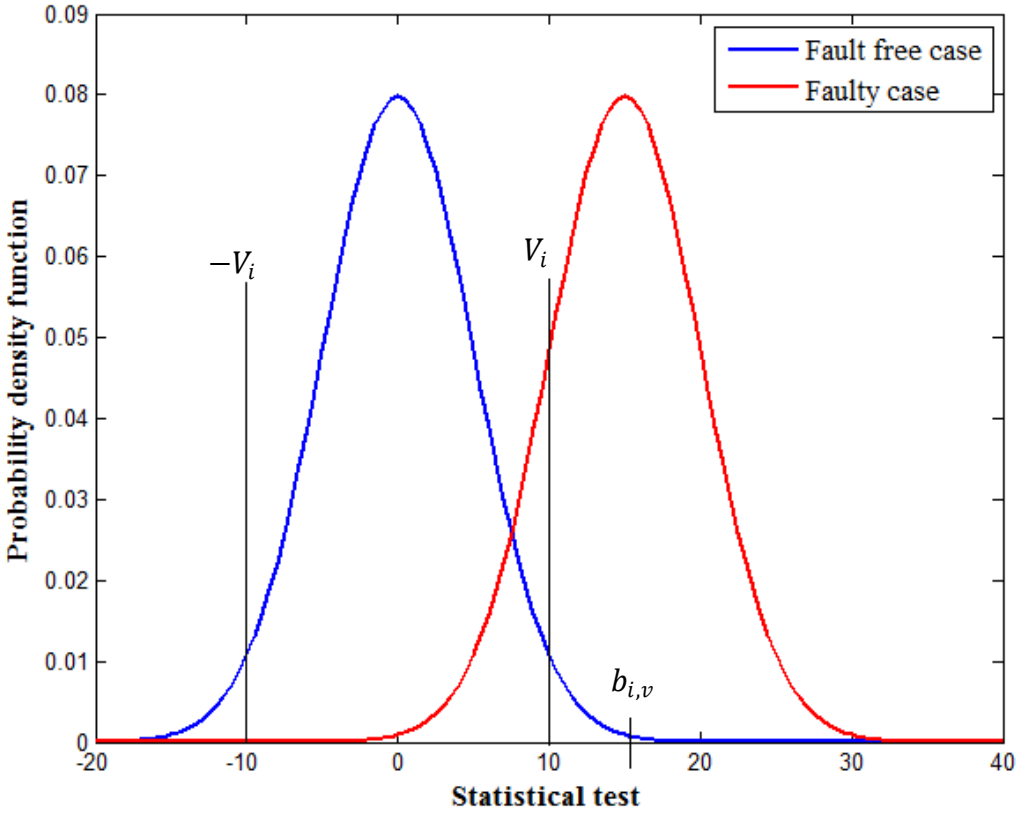

Figure 24 - Fault free and faulty statistical vertical test distribution

As explained in section 4-3-3-1, for the faulty case, $d_{i,V}$ is a one dimension vector which follows a Gaussian law with a mean $b_{i,V} = b_i(3)$ corresponding to the projection of b on the vertical local axe and with a variance ${\sigma_{i,V}}^2 = dP_i(3,3)$.

Its density function is:

$$f_{d_{i,V}}(x) = \frac{1}{\sqrt{2\pi}\sigma_{i,V}} \exp\left(-\frac{\left(x - b_{i,v}\right)^2}{2{\sigma_{i,V}}^2}\right) \tag{4-106}$$

The bias b on the pseudorange i that can be detect with the probability $1 - p_1$ can be easily computed by solving the equation:

$$p_1 = \int_{-V_i}^{V_i} \frac{1}{\sqrt{2\pi}\sigma_{i,V}} e^{-\frac{1}{2}\frac{\left(x-b_{i,v}\right)^2}{{\sigma_{i,V}}^2}} dx \tag{4-107}$$

Then, we can over bound the vertical positioning error in presence of such biases as it has been proposed for the horizontal case. It consists in finding a bound $\gamma_{0,i}$ such as:

$$P\left(\left\|X - \hat{X}_0\right\|_V \leq \gamma_{0,i} / \exists \text{ a bias of size } b_i \text{ on the } \text{i}^{\text{th}} \text{pseudorange}\right) = p_0 \tag{4-108}$$

The method is described in appendix C.

Therefore, for every $i \in [1, N]$

$$P\left(\left\|X - \hat{X}_0\right\|_H \leq \gamma_{0,\text{i}} / \exists\ b_i\right) \times P\left(\left|d_{i,V}\right| \leq V_i / b_i\right) = p_0 p_1 \tag{4-109}$$

And a class of vertical protection levels can be proposed such as:

$$VPL = \max_{i \epsilon [1,N]}\left(\gamma_{0,\text{i}}\right) \tag{4-110}$$

The setting of p_0 and p_1, such as $p_0 p_1 = P_{md}$, constitutes a tuning parameter of our protection level computation.

4-3-4 Conclusion

The maximum solution separation method which is based on the observed separation between the position estimate generated by the full-set filter (using all the satellite measurements) and that generated by each one of the subset filters (each using all but one of the satellite measurements), has been described.

The test for detecting one range failure is based on the comparison of N horizontal sub criteria and N vertical sub criteria with their respective thresholds which are compliant with the required false alert probability.

The classical way of computing protection level has been described and a proposed method has been introduced. They are based on the same detection function but can lead to different availabilities.

4-4 Constrained Generalized Likelihood Ratio Test

The use of constrained generalized likelihood ration test as a RAIM algorithm has been proposed in [Nikiforov, 2005]. This algorithm is designed to detect only faults which lead to a positioning failure. It is supposed to be stable against insignificant additional pseudorange biases with bounded impacts on the aircraft position and simultaneously more sensitive with respect to the dangerous biases producing positioning failures.

4-4-1 Parity vector

As detailed in chapter 3, the navigation equation gives us $Y(k) = h\big(X(k)\big) + E(k)$.

In this part of the study, the measurement error E is supposed to be noise only such as:

$$E(k) = \begin{bmatrix} n^1(k) \\ \vdots \\ n^j(k) \\ \vdots \\ n^N(k) \end{bmatrix} \text{ with } n^i \sim N(0, \sigma_i^2) \tag{4-111}$$

or it can be noise and a bias b on one satellite *l* such as*:*

$$E(k) = \begin{bmatrix} n^1(k) \\ \vdots \\ n^l(k) \\ \vdots \\ n^N(k) \end{bmatrix} + \begin{bmatrix} 0 \\ \vdots \\ b \\ \vdots \\ 0 \end{bmatrix} \tag{4-112}$$

E can be denoted such as:

$$E = \xi + B \tag{4-113}$$

where $\xi \sim N(0, \Sigma)$ and $\Sigma = \begin{bmatrix} \sigma_1^2 & & 0 \\ & \ddots & \\ 0 & & \sigma_N^2 \end{bmatrix}$

The navigation equation linearization leads to:

$$\Delta Y = H\Delta X + E \tag{4-114}$$

Let's consider the matrix $\Sigma^{-1/2} = \begin{bmatrix} 1/\sigma_1 & & \\ & \ddots & \\ & & 1/\sigma_N \end{bmatrix}$:

The previous equation becomes:

$$\Delta Y_{\text{norm}} = \Sigma^{-1/2}\Delta Y = \Sigma^{-1/2}H\Delta X + \Sigma^{-1/2}E = H_{\text{norm}}\,\Delta X + E_{\text{norm}} \tag{4-115}$$

Now the goal is to obtain a statistic which is independent from ΔX.

As mentioned in [Sturza, 1988], for a given $N \times 4$ measurement matrix H_{norm} with rank 4, it is possible to find an $(N-4) \times N$ matrix W such as:

$$W H_{\text{norm}} = 0 \tag{4-116}$$

This matrix W satisfies the following conditions:

$$\text{rank}(W) = N - 4 \tag{4-117}$$

$$W W^t = I_{N-4} \tag{4-118}$$

The $(N-4) \times 1$ parity vector Z is then defined by:

$$Z = W \Delta Y_{\text{norm}} \tag{4-119}$$

Since W satisfies the following condition $W H_{\text{norm}} = 0$, transformation by W removes the interference of the parameter ΔX such as:

$$Z = W \Delta Y_{\text{norm}} = \text{W} E_{\text{norm}}$$

Let's denote

$$P = W^t W \tag{4-120}$$

P is an $N \times N$ matrix with rank $N-4$ and is idempotent:

$$P^2 = P \tag{4-121}$$

The P matrix can be directly calculated from H_{norm} such as [Sturza, 1988]:

$$P = I - H_{\text{norm}} \left[{H_{\text{norm}}}^t \text{H}_{\text{norm}} \right]^{-1} H^t \tag{4-122}$$

or

$$P = \left(I - \Sigma^{-1/2} H [H^t \Sigma^{-1} \text{H}]^{-1} H^t \Sigma^{-1/2} \right) \tag{4-123}$$

The matrix $W = \begin{bmatrix} w_1 \\ \vdots \\ w_{N-4} \end{bmatrix}$ is composed of the eigenvectors w_1, ..., w_{N-4} of the P matrix [Nikiforov, 2005].

4-4-2 Snapshot Constrained Generalized Likelihood Ratio Test

The statistical test will be applied on this parity vector Z. The corresponding detection/exclusion algorithm is designed assuming that only a single failure can occur at the same time. Therefore, in the faulty case, if for example there is an additional bias on the measurement l, the parity vector Z will be expressed as follow:

$$Z = W \xi_{norm} + W B_{\text{l,norm}} \tag{4-124}$$

where for $l \in [1,N]$, $B_{\text{l,norm}} = \begin{bmatrix} 0 \\ \vdots \\ 0 \\ v_l/\sigma_l \\ 0 \\ \vdots \\ 0 \end{bmatrix}$ and $\xi_{\text{norm}} \sim N(0, I_n)$

The test will have to choose between different hypothesis:

$$\text{- } \mathcal{H}_0 = \bigcup_{i=1}^{N} \mathcal{H}_{i,0} \tag{4-125}$$

$$\text{where } \mathcal{H}_{i,0} = \left\{ Z \sim N\left(WB_{\text{i,norm}}, I_{N-4}\right), |v_i| \leq a_i \right\}, \text{ for } i \in [1,N] \tag{4-126}$$

$$\text{- } \mathcal{H}_l = \left\{ Z \sim N\left(WB_{\text{l,norm}}, I_{N-4}\right), |v_l| \geq b_l \right\}, \text{ for } l \in [1,N] \tag{4-127}$$

where the parameters $0 \leq a_i \leq b_i$, $i \in [1,N]$ define the selectivity of the test with respect to each pseudo range bias v_i such as for $i \in [1,N]$:

- b_i is the smallest bias on the channel i that leads to a positioning failure
- a_i the smallest bias that have to be consider or the largest bias that can be considered as nominal

The constrained GLR test principle is illustrated by the following equation:

$$\begin{cases} \mathcal{H}_0 & \text{if } \max\limits_{l \in [1,N]} \dfrac{f_l(Z)}{f_0(Z)} \leq T \\ \mathcal{H}_l & \text{if } \arg\max\limits_{l \in [1,N]} \dfrac{f_l(Z)}{f_0(Z)} \geq T \end{cases} \tag{4-128}$$

where a decision variable is constructed and tested against a threshold T.

To have a geometric interpretation of the decision rule, the former equation is re-written this way:

$$\delta = \begin{cases} \mathcal{H}_0 \text{ if } \max\limits_{l \in [1,N]} \left[\min\limits_{i \in [1,N]} \left(\min\limits_{|v_i| \leq a_i} \left\| Z - W_i \dfrac{v_i}{\sigma_i} \right\|^2 \right) - \min\limits_{|v_l| \geq b_l} \left\| Z - W_l \dfrac{v_l}{\sigma_l} \right\|^2 \right] \leq h \\ \mathcal{H}_l \text{ if } \operatorname{argmax}\limits_{l \in [1,N]} \left[\min\limits_{i \in [1,N]} \left(\min\limits_{|v_i| \leq a_i} \left\| Z - W_i \dfrac{v_i}{\sigma_i} \right\|^2 \right) - \min\limits_{|v_l| \geq b_l} \left\| Z - W_l \dfrac{v_l}{\sigma_l} \right\|^2 \right] > h \end{cases} \tag{4-129}$$

where:

- $d\left(Z, \mathcal{H}_{i,0}\right) = \min\limits_{|v_i| \leq a_i} \left\| Z - W_i \frac{v_i}{\sigma_i} \right\|^2$ is the distance from the observation Z to the partial null hypothesis $\mathcal{H}_{i,0}$
- $d(Z, \mathcal{H}_0) = \min_{i \in [1,N]} \left(\min\limits_{|v_i| \leq a_i} \left\| Z - W_i \frac{v_i}{\sigma_i} \right\|^2 \right) = \min\limits_{i \in [1,N]} d\left(Z, \mathcal{H}_{i,0}\right)$ is the distance from Z to $\mathcal{H}_0$
- $d(Z, \mathcal{H}_l) = \min\limits_{|v_l| \geq b_l} \left\| Z - W_l \frac{v_l}{\sigma_l} \right\|^2$, for $l \in [1,N]$ are the distance from Z to each alternatives hypothesis $\mathcal{H}_l$

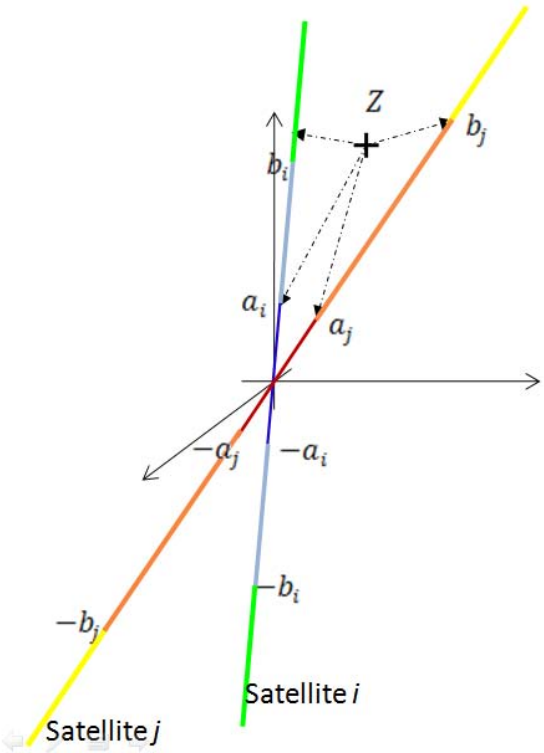

Figure 25 - Geometric interpretation of the decision rule

In order to choose between the alternatives $\mathcal{H}_l$ for $l \in [1, N]$ and the null hypothesis $\mathcal{H}_0$, the differences $d(Z, \mathcal{H}_0) - d(Z, \mathcal{H}_l)$ are computed and the index that maximizes them is observed.

This is why two functions are defined for $i \in [1, N]$:

- $S_0(\Delta Y, i) = \min_{|v_i| \le a_i} \left\| Z - W_i \frac{v_i}{\sigma_i} \right\|^2$ which represents the probability that there is no fault or no significant fault on the pseudo range *i*.

- $S_1(\Delta Y, i) = \min_{|v_i| \ge b_i} \left\| Z - W_l \frac{v_i}{\sigma_i} \right\|^2$ which represents the probability that there is a bias on the channel *i* that will lead to a positioning failure.

$$\left\| Z - W_i \frac{v_i}{\sigma_i} \right\|^2 = \|Z\|^2 - 2\frac{v_i}{\sigma_i} {W_i}^t Z + \|W_i\|^2 \frac{{v_i}^2}{{\sigma_i}^2}$$

The function $g_i(x) = x^2 \frac{\|W_i\|^2}{{\sigma_i}^2} - 2x \frac{{W_i}^t Z}{\sigma_i} + \|Z\|^2$ reaches its minimum for:

$$\hat{v}_i = \frac{\sigma_i {W_i}^t Z}{\|W_i\|^2} \tag{4-130}$$

Therefore, if $|\hat{v}_i| \le a_i, S_0(\Delta Y, i) = \min_{|v_i| \le a_i} \left\| Z - W_i \frac{v_i}{\sigma_i} \right\|^2 = g_i(\hat{v}_i)$ (4-131)

and if $|\hat{v}_i| > a_i, S_0(\Delta Y, i) = \min_{|v_i| \le a_i} \left\| Z - W_i \frac{v_i}{\sigma_i} \right\|^2 = g_i(a_i)$ (4-132)

$$S_0(\Delta Y, i) = \begin{cases} \hat{v}_i{}^2 \dfrac{\|W_i\|^2}{\sigma_i{}^2} - 2\hat{v}_i \dfrac{W_i{}^t Z}{\sigma_i} + \|Z\|^2 \text{ if } |\hat{v}_i| \le a_i \\ a_i{}^2 \dfrac{\|W_i\|^2}{\sigma_i{}^2} - 2a_i \dfrac{W_i{}^t Z}{\sigma_i} + \|Z\|^2 \text{ if } |\hat{v}_i| > a_i \end{cases}$$

Finally,

$$S_0(\Delta Y, i) = \begin{cases} \|Z\|^2 - \dfrac{\left(W_i{}^t Z\right)^2}{\|W_i\|^2} & \text{if } |\hat{v}_i| \le a_i \\ \|Z\|^2 - 2a_i \dfrac{W_i{}^t Z}{\sigma_i} + a_i{}^2 \dfrac{\|W_i\|^2}{\sigma_i{}^2} & \text{if } |\hat{v}_i| > a_i \end{cases}$$

As $W^t W = P_{norm}$,

$$\|W_i\|^2 = p_{ii}$$

and as $W^t Z = PE_{\text{norm}} = \Delta Y_{\text{norm}}$,

$$W_i{}^t Z = \Delta Y_{\text{norm}}(i) = \frac{\Delta Y_i}{\sigma_i}$$

Using the least square residual vector to represent these values, for $i \in [1, N]$:

$$S_0(\Delta Y, i) = \begin{cases} \|Z\|^2 - \dfrac{\Delta Y_i{}^2}{\sigma_i{}^2 p_{ii}} & \text{if } |\hat{v}_i| \le a_i \\ \|Z\|^2 - 2a_i \dfrac{|\Delta Y_i|}{\sigma_i{}^2} + a_i{}^2 \dfrac{p_{ii}}{\sigma_i{}^2} & \text{if } |\hat{v}_i| > a_i \end{cases} \tag{4-133}$$

Similarly, if $|\hat{v}_l| \ge b_l$, $S_1(\Delta Y, l) = \min_{|v_l| \ge b_l} \left\| Z - W_l \frac{v_l}{\sigma_l} \right\|^2 = g_l(\hat{v}_l)$

and if $|\hat{v}_l| < b_l$, $S_1(\Delta Y, l) = \min_{|v_l| \ge b_l} \left\| Z - W_l \frac{v_l}{\sigma_l} \right\|^2 = g_l(b_l)$

$$S_1(\Delta Y, l) = \begin{cases} \|Z\|^2 - \dfrac{\Delta Y_l{}^2}{\sigma_l{}^2 p_{ll}} & \text{if } |\hat{v}_l| \ge b_l \\ \|Z\|^2 - 2b_l \dfrac{|\Delta Y_l|}{\sigma_l{}^2} + b_l{}^2 \dfrac{p_{ll}}{\sigma_l{}^2} & \text{if } |\hat{v}_l| < b_l \end{cases} \tag{4-134}$$

where for $i \in [1, N]$, $\hat{v}_i = \frac{\sigma_i W_i{}^t Z}{\|W_i\|^2} = \frac{\Delta Y_i}{p_{ii}}$

The detection/exclusion function is based on the decision rule given by equation:

$$\delta = \begin{cases} \mathcal{H}_0 & \text{if } \max_{l \in [1,N]} \left[\min_{i \in [1,N]} S_0(\Delta Y, i) - S_1(\Delta Y, l) \right] \le h \\ \mathcal{H}_l & \text{if } \operatorname{argmax}_{l \in [1,N]} \left[\min_{i \in [1,N]} S_0(\Delta Y, i) - S_1(\Delta Y, l) \right] > h \end{cases} \tag{4-135}$$

This algorithm needs several parameters to be implemented and used as a RAIM algorithm:

- the threshold h that will be compare to the statistic test and that need to be compliant with the required probability of false alert

- the vector a of size $N \times 1$ representing the smallest bias to detect on each pseudo range
- the vector b of size $N \times 1$ representing the largest nominal bias on each pseudo range

The Snapshot Constrained GLR test is given by [Nikiforov, 2005]:

$$T = \max_{l\in[1,N]} \left[\min_{i\in[1,N]} S_0\,(\Delta Y, i) - S_1(\Delta Y, l) \right] \tag{4-136}$$

where S_0 refers to the fault free situation such as:

$$S_0(\Delta Y, i) = \begin{cases} -\dfrac{{\Delta Y_i}^2}{{\sigma_i}^2 p_{ii}} & \text{if } |\hat{v}_i| \le a_i \\ -2a_i \dfrac{|\Delta Y_i|}{{\sigma_i}^2} + {a_i}^2 \dfrac{p_{ii}}{{\sigma_i}^2} & \text{if } |\hat{v}_i| > a_i \end{cases} \tag{4-137}$$

and S_1 refers to the faulty situation such as:

$$S_1(\Delta Y, l) = \begin{cases} -\dfrac{{\Delta Y_l}^2}{{\sigma_l}^2 p_{ll}} & \text{if } |\hat{v}_l| \ge b_l \\ -2b_l \dfrac{|\Delta Y_l|}{{\sigma_l}^2} + {b_l}^2 \dfrac{p_{ll}}{{\sigma_l}^2} & \text{if } |\hat{v}_l| < b_l \end{cases} \tag{4-138}$$

where for $i\epsilon[1,n]$:

ΔY_{i} is the ith component of the LS residual such as:

$$\Delta Y = (I - H[H^t \Sigma^{-1} \mathrm{H}]^{-1} H^t \Sigma^{-1}) E \tag{4-139}$$

$$\Delta Y = PE \tag{4-140}$$

E is the measurement error vector
b_i is the smallest bias ont he pseudorange i that leads to a positioning failure
a_i is the smallest error that have to be considered
σ_i is the variance of the error E_i
$p_{ii} = P(i,i)$ and $P = (I - H[H^t \Sigma^{-1} \mathrm{H}]^{-1} H^t \Sigma^{-1})$

$$\hat{v}_i = \frac{\sigma_i {W_i}^t Z}{\|W_i\|^2} = \frac{\Delta Y_i}{p_{ii}}$$

It can be seen that $\|Z\|^2$ has been removed from the equation since it disappears with the subtraction of S_0 and S_1.

This test has to be compared to a threshold h which has to be set in order to satisfy the false alarm probability. Its computation has been investigated during this Ph.D.

We are going to first study the case where $\forall i\epsilon[1,n]$, a_i=0.

4-4-2-1 Snapshot Constrained GLR test implementation: without considering nominal biases

In this case $S_0(\Delta Y, i) = 0$ and our test becomes:

$$T = \max_{l\in[1,N]}[-S_1(\Delta Y, l)] \tag{4-141}$$

4-4-2-1-1 Setting the threshold that satisfies the Pfa

It is first necessary to define a false alarm situation. There is a false alarm when there is no dangerous error on each available pseudo range and the test exceeds the threshold.

The first part of the test process for a given situation consists in comparing for $l\epsilon[1,n]$, $\hat{v}_l = \frac{\Delta Y_l}{p_{ll}}$ with the corresponding critical bias b_l .

Let's define for $l\epsilon[1,n]$, $f_l(\Delta Y) = -S_1(\Delta Y, l)$. The function f_l is such as:

for $l\epsilon[1,n]$, for $x \epsilon \mathbb{R}$,

$$f_l(x) = \begin{cases} \dfrac{x^2}{{\sigma_l}^2 p_{ll}} & \text{if } |x| \geq b_l|p_{ll}| \\ 2b_l\dfrac{|x|}{{\sigma_l}^2} - {b_l}^2\dfrac{p_{ll}}{{\sigma_l}^2} & \text{if } |x| < b_l|p_{ll}| \end{cases} \tag{4-142}$$

The test can be thus written such as:

$$T = \max_{l\in[1,N]}[f_l(\Delta Y_l)] \tag{4-143}$$

where for $l\,\epsilon[1,N]$, ΔY_l is a Gaussian random variable
b_l, σ_l, p_{ll} are known

For every positive number h,

$$P(T \geq h) = P\left(\max_{i\in[1,N]}[f_i(\Delta Y)] \geq h\right) \leq \sum_{i=1}^{N} P(f_i(\Delta Y) \geq h) \tag{4-144}$$

Our goal is to find the threshold h_0 such as:

$$\sum_{i=1}^{N} P(f_i(\Delta Y) \geq h_0) = P_{fa} \tag{4-145}$$

This threshold will satisfy:

$$P(T \geq h_0) \leq P_{fa} \tag{4-146}$$

First let us consider the statistical behavior of $f_i(\Delta Y)$ for $i\,\epsilon[1,N]$. A false alarm situation addresses the fault free case such as:

$$\forall i \epsilon [1,n], E(i) \sim N(0,\sigma_i)$$

We have

$$cov(E) = \begin{bmatrix} \sigma_1^2 & & 0 \\ & \ddots & \\ 0 & & \sigma_n^2 \end{bmatrix}$$

As $\Delta Y = PE$, denoting $C = cov(\Delta Y)$,

$$C = P cov(E) P^t$$

and for $i \epsilon [1,n]$, $\Delta Y(i) \sim N(0, C_{ii})$ with C_{ii} such as:

$$C_{ii} = \sum_{k=1}^{N} p_{ik}\, \sigma_{kk}\, p_{ki} \qquad (4\text{-}147)$$

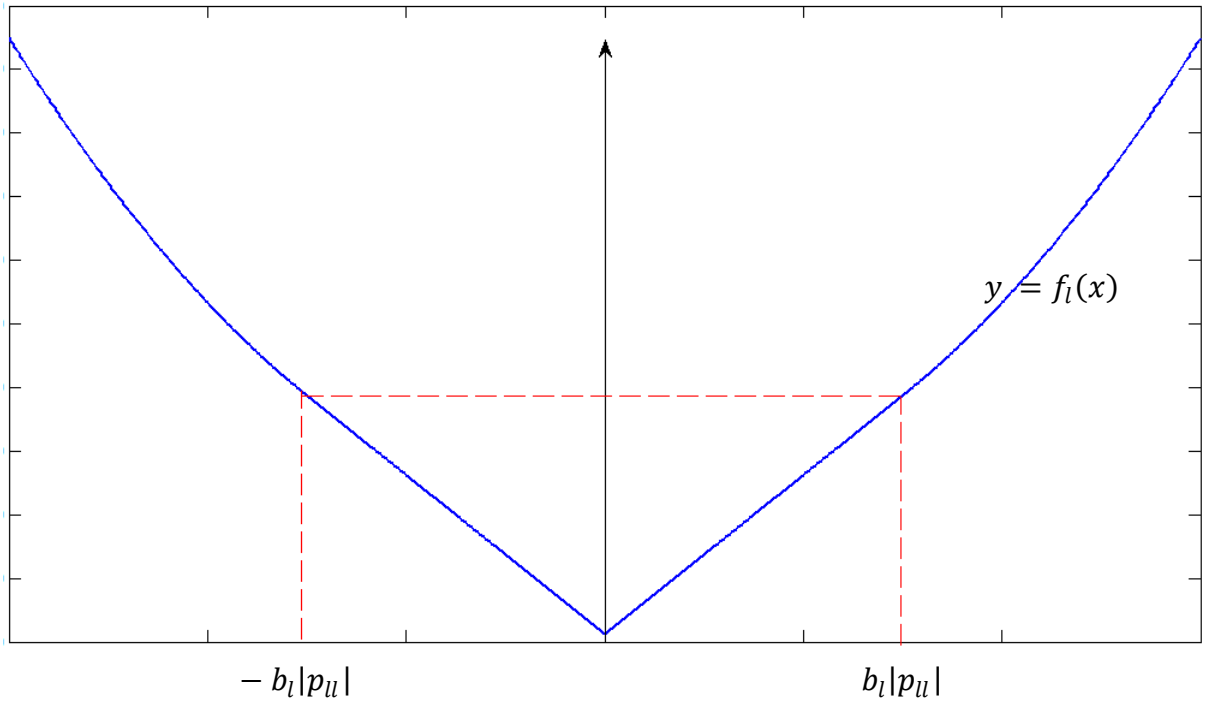

Figure 26 - Function $f_l(\Delta Y)$

The function f_i is even and it is increasing for $x \geq 0$. Therefore, for every positive number h we can define $x_{h,i}$ such as:

- $x_{h,i} \geq 0$
- $f_i(x_{h,i}) = h$

For $i \epsilon [1,n]$,

$$P(f_i(\Delta Y) \geq h) = \frac{1}{\sqrt{2\pi C_{ii}}} \left(\int_{-\infty}^{-x_{h,i}} exp\left(-\frac{1}{2}\frac{x^2}{C_{ii}}\right) dx + \int_{x_{h,i}}^{\infty} exp\left(-\frac{1}{2}\frac{x^2}{C_{ii}}\right) dx \right)$$

$$P(f_i(\Delta Y) \geq h) = \frac{2}{\sqrt{2\pi C_{ii}}} \left(\int_{x_{h,i}}^{\infty} exp\left(-\frac{1}{2}\frac{x^2}{C_{ii}}\right) dx \right) \quad (4\text{-}148)$$

Our goal is to find the threshold h_0 such as:

$$\sum_{i=1}^{N} P(f_i(\Delta Y) \geq h_0) = P_{fa}$$

or such as

$$\sum_{i=1}^{N} \frac{2}{\sqrt{2\pi C_{ii}}} \left(\int_{x_{h0,i}}^{\infty} exp\left(-\frac{1}{2}\frac{x^2}{C_{ii}}\right) dx \right) = P_{fa} \quad (4\text{-}149)$$

This threshold h_0 is easily computed numerically and satisfies the required probability of false alarm P_{fa}.

4-4-2-1-2 Predicting the probability of missed detection

One major aspect of RAIM design is that we have to predict the algorithm ability to protect the user for the intended operation considering satellite geometry and an assumed level of noise. As the position error remains unknown for the user, statistic tools have to be used to check requirements compliance and to predict the availability. A first method consists in computing the smallest bias the algorithm is able to detect respecting the missed alert and false alert requirements, in projecting it on the worst satellite, in deducing the smallest position error for which this algorithm guaranties to protect the user respecting the requirements. These levels will be then compared to their corresponding alert limit. This is the principle of LSR method. A second method has been developed during this Ph.D. for the constrained GLR method. It consists in computing for a given geometry and an assumed level of noise the smallest bias on each pseudorange that will lead to a positioning failure, then in predicting the probability of missed detection of these biases, and finally comparing it to the required Pmd. The objective of this section is to present the Pmd prediction.

There is a missed detection situation when the test T is smaller than the threshold h_0 and when there is an error. This bias or this error has to be dangerous, that is to say larger that the corresponding critical bias, and remained undetected to be considered as a missed detection.

Referring to the concept of smallest biases that lead to a positioning failure mentioned in section 4-2, errors that have to be detected, and thus errors that have to be considered in probability of missed detection computation, are such that:

$$\exists k \in [1, N] \text{ such as } E(k) > b_k \text{ or } E(k) = b + \xi_k \text{ with } b \geq b_k$$

Considering that this error on the pseudo range is present (or has a known probability of occurrence), only conditional probabilities will be mentioned in this section:

Let's assume that $\exists k \in [1, N]$ such as $E(k) = b_k + \xi_k$ where b_k is the single critical bias corresponding to the pseudorange *k*. The probability that the snapshot constrained GLR test do not detect this bias is first evaluated.

As $T = \max_{l\in[1,N]}[-S_1(\Delta Y, l)]$,

$$P(T \geq h_0) = P\left(\max_{l\in[1,N]}[-S_1(\Delta Y, l)] \geq h_0\right)$$

And for every $i \in [1, N]$,

$$P(T \geq h_0) = P\left(\max_{l\in[1,N]}[-S_1(\Delta Y, l)] \geq h_0\right) \geq P([-S_1(\Delta Y, i)] \geq h_0) \tag{4-150}$$

Or using the functions f_i for $i \in [1, N]$, such as:

$$f_i(x) = \begin{cases} \dfrac{x^2}{{\sigma_i}^2 p_{ii}} & \text{if } |x| \geq b_i|p_{ii}| \\ 2b_i\dfrac{|x|}{{\sigma_i}^2} - {b_i}^2\dfrac{p_{ii}}{{\sigma_i}^2} & \text{if } |x| < b_i|p_{ii}| \end{cases}$$

for every $i \in [1, N]$,

$$P(T \geq h_0) \geq P(f_i(\Delta Y) \geq h_0) \tag{4-151}$$

and particularly for the faulty measurement k,

$$P(T \geq h_0) \geq P(f_k(\Delta Y) \geq h_0) \tag{4-152}$$

We are in a faulty situation such as:

$\forall i \epsilon [1, n], i \neq k$, $E(i) \sim N(0, \sigma_i)$
$E(k) \sim N(b_k, \sigma_k)$

As $\Delta Y = PE$, ΔY_k is a Gaussian variable such as:

$$\Delta Y_k \sim N(m_k, C_{kk})$$

with
$C_{kk} = \sum_{j=1}^{N} p_{kj}\,\sigma_{jj}\,p_{jk}$ (as in the fault free case)

$$m_k = b_k p_{kk}$$

Therefore,

$$P(f_k(\Delta Y) \geq h_0) = \frac{1}{\sqrt{2\pi C_{kk}}}\left[\int_{-\infty}^{-x_{h_0,k}} \exp\left(-\frac{(u-m_k)^2}{2C_{kk}}\right)\mathrm{d}u + \int_{x_{h_0,k}}^{+\infty} \exp\left(-\frac{(u-m_k)^2}{2C_{kk}}\right)\right]$$

Finally,

$$P(T \geq h_0) \geq \frac{1}{\sqrt{2\pi C_{kk}}}\left[\int_{-\infty}^{-x_{h_0,k}} \exp\left(-\frac{(u-m_k)^2}{2C_{kk}}\right)\mathrm{d}u + \int_{x_{h_0,k}}^{+\infty} \exp\left(-\frac{(u-m_k)^2}{2C_{kk}}\right)\right]$$

As $P_{md} = 1 - P(T \geq h_0)$,

$$P_{md} \leq 1 - \frac{1}{\sqrt{2\pi C_{kk}}}\left[\int_{-\infty}^{-x_{h_0,k}} \exp\left(-\frac{(u-m_k)^2}{2C_{kk}}\right)\mathrm{d}u + \int_{x_{h_0,k}}^{+\infty} \exp\left(-\frac{(u-m_k)^2}{2C_{kk}}\right)\mathrm{d}u\right]$$

$$P_{md} \leq \int_{-x_{h_0,k}}^{x_{h_0,k}} \frac{1}{\sqrt{2\pi C_{kk}}} \exp\left(-\frac{(u-m_k)^2}{2C_{kk}}\right)\mathrm{d}u \tag{4-153}$$

Let's denote

$$P_{md}(b_k,k) = \int_{-x_{h_0,k}}^{x_{h_0,k}} \frac{1}{\sqrt{2\pi C_{kk}}} \exp\left(-\frac{(u-m_k)^2}{2C_{kk}}\right)\mathrm{d}u \tag{4-154}$$

Therefore, for each available measurement the probability $P_{md}(b_k,k)$ will be computed where b_k is the smallest single bias on the pseudorange k that leads to a positioning failure.

The final guaranteed P_{md} could correspond to the worst case that is to say to:

$$\max_{k\in[1,N]} P_{md}(b_k,k) \tag{4-155}$$

4-4-2-2 Snapshot Constrained GLR test implementation: considering nominal biases

In this case $S_0(\Delta Y,i) \neq 0$ and the test cannot be systematically simplified and we have:

$$T = \max_{l\in[1,N]}\left[\min_{i\in[1,N]} S_0(\Delta Y,i) - S_1(\Delta Y,l)\right] \tag{4-156}$$

where S_0 refers to the fault free situation such as:

$$S_0(\Delta Y,i) = \begin{cases} -\dfrac{{\Delta Y_i}^2}{{\sigma_i}^2 p_{ii}} & \text{if } |\hat{v}_i| \leq a_i \\ -2a_i\dfrac{|\Delta Y_i|}{{\sigma_i}^2} + {a_i}^2\dfrac{p_{ii}}{{\sigma_i}^2} & \text{if } |\hat{v}_i| > a_i \end{cases} \tag{4-157}$$

and S_1 refers to the faulty situation such as:

$$S_1(\Delta Y,l) = \begin{cases} -\dfrac{{\Delta Y_l}^2}{{\sigma_l}^2 p_{ll}} & \text{if } |\hat{v}_l| \geq b_l \\ -2b_l\dfrac{|\Delta Y_l|}{{\sigma_l}^2} + {b_l}^2\dfrac{p_{ll}}{{\sigma_l}^2} & \text{if } |\hat{v}_l| < b_l \end{cases} \tag{4-158}$$

For the same threshold h_0, the probability of false alarm will be smaller if the test takes into account the existence of nominal bias in the fault free case. This is why, for a conservative approach, it is still possible to consider the former threshold. Nevertheless a more precise threshold that satisfies the Pfa needs to be computed numerically as well as the predicted probability of missed detection.

4-4-3 Sequential Constrained Generalized Likelihood Ratio Test

A sequential RAIM algorithm based on the Constrained GLR test can also be implemented.

In this case, the pseudo range correlation is directly integrated in the constrained GLR algorithm through an AR model and the last m observations $Z_1, \dots, Z_m$ are considered.

The test is given by the following equation:

$$T = \begin{cases} \mathcal{H}_0 \text{ if } \max\limits_{l\in[1,N]} \dfrac{f_l(Z_1,\dots,Z_m)}{f_0(Z_1,\dots,Z_m)} \le h \\ \mathcal{H}_l \text{ if } \arg\max\limits_{l\in[1,N]} \dfrac{f_l(Z_1,\dots,Z_m)}{f_0(Z_1,\dots,Z_m)} \ge h \end{cases} \tag{4-159}$$

Thus a sequential pseudorange measurement error model is taken into account, as presented in section 3-4-3. The additional measurement error E can be denoted such as:

$$E = \xi + B \tag{4-160}$$

The additive pseudo range noise ξ is represented by the following first autoregressive model:

$$\xi_{k+1} = \xi_k + \sqrt{1-a^2}\zeta_k \tag{4-161}$$

with for $k \in \mathbb{N}$, $\zeta_k \sim N(0,\Sigma)$ and $\xi_1 \sim N(0,\Sigma)$

$$\Sigma = \begin{bmatrix} \sigma_1^2 & \cdots & 0 \\ \vdots & \ddots & \vdots \\ 0 & \cdots & \sigma_N^2 \end{bmatrix}$$

Here again, the algorithm is designed assuming that only a single failure can occur at the same time. Therefore, in the faulty case, only one additional bias (step profile) on one measurement is taking into account. More complex failure profiles are addressed in section 4-4-4.

Thanks to the matrix $N = \Sigma^{-1/2} = \begin{bmatrix} 1/\sigma_1 & & \\ & \ddots & \\ & & 1/\sigma_N \end{bmatrix}$, the pseudo range error measurement is normalized $NE = E_{\text{norm}}$ as well as its auto correlated noise component: $\xi_{\text{norm}} = N\xi$:

$$\xi_{k+1,\text{norm}} = \xi_{k,\text{norm}} + \sqrt{1-a^2}w_{k,\text{norm}} \tag{4-162}$$

with $w_{k,\text{norm}} \sim N(0, I_n)$, $\xi_{1,\text{norm}} \sim N(0, I_n)$

The successive parity vector are built. In the faulty case, if for example there is an additional bias on the measurement l, the parity vector Z_k will be expressed as follow:

$$Z_k = W\xi_{k,\text{norm}} + WB_{l,\text{norm}}$$

where for $l \in [1, N]$, $B_{\text{l,norm}} = \begin{bmatrix} 0 \\ \vdots \\ 0 \\ v_l/\sigma_l \\ 0 \\ \vdots \\ 0 \end{bmatrix}$

In order to have a geometric interpretation of the decision rule,

- $Z_1 \sim N(WB_{\text{norm}}, \mathrm{I}_{n-4})$ is compared with $W_i \frac{v_i}{\sigma_i}$, for $i\epsilon[1, n]$
- for $k \geq 2$ the random variable $\frac{1}{\sqrt{1-a^2}}[Z_k - aZ_{k-1}]$ is compared with $\frac{(1-a)}{\sqrt{1-a^2}} W_i \frac{v_i}{\sigma_i}$, for $i\epsilon[1, n]$.

Thus considering the m last observations, the following expression has to be minimised:

$$\left\| Z_1 - W_i \frac{v_i}{\sigma_i} \right\|^2 + \frac{1}{1-a^2} \sum_{\mathrm{k}=2}^{\mathrm{m}} \left\| Z_k - aZ_{k-1} - (1-a) W_i \frac{v_i}{\sigma_i} \right\|^2$$

with respect to v_i.

Here again two functions are defined for $i \in [1, N]$:

- $S_0(\Delta Y, i) = \min_{|v_i| \leq a_i} \left\| Z_1 - W_i \frac{v_i}{\sigma_i} \right\|^2 + \frac{1}{1-a^2} \sum_{\mathrm{k}=2}^{\mathrm{m}} \left\| Z_k - aZ_{k-1} - (1-a) W_i \frac{v_i}{\sigma_i} \right\|^2$ which represents the probability that there is no fault or no significant fault on the pseudo range i.
- $S_1(\Delta Y, i) = \min_{|v_l| \geq b_l} \left\| Z_1 - W_l \frac{v_l}{\sigma_l} \right\|^2 + \frac{1}{1-a^2} \sum_{\mathrm{k}=2}^{\mathrm{m}} \left\| Z_k - aZ_{k-1} - (1-a) W_l \frac{v_l}{\sigma_l} \right\|^2$ which represents the probability that there is a bias on the channel l that will lead to a positioning failure.

Let us define the function:

$$g_i(x) = \|Z_1\|^2 + \frac{1}{1-a^2} \sum_{\mathrm{k}=2}^{\mathrm{m}} \|Z_k - aZ_{k-1}\|^2 - 2 \left[Z_1 + \frac{1-a}{1-a^2} \sum_{\mathrm{k}=2}^{\mathrm{m}} Z_k - aZ_{k-1} \right]^{\mathrm{t}} \frac{W_i}{\sigma_i} x + \left(1 + \frac{(1-a)^2}{1-a^2} (\mathrm{m}-1) \right) \frac{\|W_i\|^2}{{\sigma_i}^2} x^2$$

This function reaches its minimum for :

$$\widehat{v_i} = \frac{\sigma_i [Z_1 + (1-a) \sum_{\mathrm{k}=2}^{\mathrm{m}-1} Z_k + \mathrm{Z_m}]^{\mathrm{t}} W_i}{\|W_i\|^2 (2a + \mathrm{m}(1-a))} \qquad (4\text{-}163)$$

Therefore, if $|\hat{v}_i| \leq a_i$, $S_0(\Delta Y, i) = \min_{|v_i| \leq a_i} g_i(v_i) = g_i(\hat{v}_i)$

and if $|\hat{v}_i| > a_i$, $S_0(\Delta Y, i) = \min_{|v_i| \leq a_i} g_i(v_i) = g_i(a_i)$

Using the least square residual vector to represent these values, for $i \in [1, N]$:

$$S_0(\Delta Y, i) =$$
$$\begin{cases} -\dfrac{\left[\Delta Y_{i,1} + (1-a)\sum_{\mathrm{k}=2}^{\mathrm{m}-1}\Delta Y_{i,\mathrm{k}} + \Delta Y_{i,\mathrm{m}}\right]^2}{{\sigma_i}^2 p_{ii}\big(2a + \mathrm{m}(1-a)\big)(1+a)} & \text{if } |\hat{v}_i| \le a_i \\ -2a_i\dfrac{\left|\Delta Y_{i,1} + (1-a)\sum_{\mathrm{k}=2}^{\mathrm{m}-1}\Delta Y_{i,\mathrm{k}} + \Delta Y_{i,\mathrm{m}}\right|}{{\sigma_i}^2(1+a)} + {a_i}^2\dfrac{p_{ii}}{{\sigma_i}^2}\left(1 + \dfrac{(1-a)^2}{1-a^2}(\mathrm{m}-1)\right) & \text{if } |\hat{v}_i| > a_i \end{cases} \quad (4\text{-}164)$$

Similarly, if $|\hat{v}_l| \ge b_l$, $S_1(\Delta Y, l) = \min_{|v_l| \ge b_l} g_l(v_l) = g_l(\hat{v}_l)$

and if $|\hat{v}_l| < b_l$, $S_1(\Delta Y, l) = \min_{|v_l| \ge b_l} g_l(v_l) = g_l(b_l)$

$$S_1(\Delta Y, l) =$$
$$\begin{cases} -\dfrac{\left[\Delta Y_{l,1} + (1-a)\sum_{\mathrm{k}=2}^{\mathrm{m}-1}\Delta Y_{l,\mathrm{k}} + \Delta Y_{l,\mathrm{m}}\right]^2}{{\sigma_l}^2 p_{ll}\big(2a + \mathrm{m}(1-a)\big)(1+a)} & \text{if } |\hat{v}_l| \ge b_l \\ -2b_l\dfrac{\left|\Delta Y_{l,1} + (1-a)\sum_{\mathrm{k}=2}^{\mathrm{m}-1}\Delta Y_{l,\mathrm{k}} + \Delta Y_{l,\mathrm{m}}\right|}{{\sigma_l}^2} + {b_l}^2\dfrac{p_{ll}}{{\sigma_l}^2}\left(1 + \dfrac{(1-a)^2}{1-a^2}(\mathrm{m}-1)\right) & \text{if } |\hat{v}_l| < b_l \end{cases} \quad (4\text{-}165)$$

where for $i\epsilon[1,n]$

$$\hat{v_i} = \frac{\Delta Y_{i1} + (1-a)\sum_{\mathrm{k}=2}^{\mathrm{m}-1}\Delta Y_{ik} + \Delta Y_{im}}{p_{ii}\big(2a + \mathrm{m}(1-a)\big)}$$

Let's define the following function:

$$g(t,l) = \left[\min_{i\in[1,N]} S_0\left(\Delta Y_t, \dots, \Delta Y_{t-m+1}, i\right) - S_1(\Delta Y_t, \dots, \Delta Y_{t-m+1}, l)\right]^+ \quad (4\text{-}166)$$

The statistical test for this algorithm will be:

$$T(t) = \max_{l\in[1,N]}\left[g(t,l) - \max_{\substack{j\in[1,N]\\ j\neq l}} g(t,j)\right] \quad (4\text{-}167)$$

m is chosen such that the satellites in view at the epochs $t-m+1, \dots, t$ are the same and our technique comes down to work with a weighted mean of the last m observations:

$$\bar{\mathrm{Z}} = \frac{Z_1 + (1-a)\sum_{\mathrm{k}=2}^{\mathrm{m}-1} Z_k + \mathrm{Z_m}}{2a + \mathrm{m}(1-a)} \quad (4\text{-}168)$$

and its associated distances for $i = 1,\dots,n$:

- $d\big(\bar{Z}, \mathcal{H}_{i,0}\big) = \min_{|v_i|\le a_i}\left\|\bar{Z} - W_i\frac{v_i}{\sigma_i}\right\|^2$ is the distance from the observation Z to the partial null hypothesis $\mathcal{H}_{i,0}$
- $d(\bar{Z}, \mathcal{H}_0) = \min_{i\in[1,N]}\left(\min_{|v_i|\le a_i}\left\|\bar{Z} - W_i\frac{v_i}{\sigma_i}\right\|^2\right) = \min_{i\in[1,N]} d\big(\bar{Z}, \mathcal{H}_{i,0}\big)$ is the distance from $\bar{Z}$ to $\mathcal{H}_0$

- $d(\bar{Z}, \mathcal{H}_l) = \min_{|v_l| \geq b_l} \left\| \bar{Z} - W_l \frac{v_l}{\sigma_l} \right\|^2$, for $l \in [1, N]$ are the distance from $\bar{Z}$ to each alternatives hypothesis $\mathcal{H}_l$

A threshold that satisfies the Pfa as well as the predicted probability of missed detection are computed numerically.

4-4-4 Adaptation of the Sequential Constrained Generalized Likelihood Ratio Test to step + ramp failure detection

The objective here is to target more complex fault profiles that is to say, the case where faults depend on two parameters: the initial position (amplitude of the step) and the speed (rate of the slope).

For each pseudo range "error couples" will be denoted $(v_i, \dot{v}_i)$ with v_i and $\dot{v}_i$ constant.

The criterion will be designed in the same way as previously, that is to say comparing a weighted mean of parity vectors with several hypothetic increasing errors on different channels.

In order to have a geometric interpretation of the decision rule,

- $Z_1 \sim N(WB_{\text{norm}}, \mathrm{I}_{n-4})$ is compared with $W_i \frac{v_i}{\sigma_i}$, for $i \epsilon [1, n]$
- for $k \geq 2$ the random variable $\frac{1}{\sqrt{1-a^2}}[Z_k - aZ_{k-1}]$ is compared with $\frac{(1-a)}{\sqrt{1-a^2}_i} \frac{W_i}{\sigma_i}(v_i + (k-1)\dot{v}_i)$, for $i \epsilon [1, n]$

Thus considering the m last observations, the following expression has to be minimised:

$$\left\| Z_1 - W_i \frac{v_i}{\sigma_i} \right\|^2 + \frac{1}{1-a^2} \sum_{\mathrm{k}=2}^{\mathrm{m}} \left\| Z_k - aZ_{k-1} - \left[(1-a)v_i + \left((1-a)k + 2a - 1 \right) \dot{v}_i \right] \frac{W_i}{\sigma_i} \right\|^2 \tag{4-169}$$

with respect to v_i and $\dot{v}_i$

As for the previous constrained GLR implementation, two functions are defined for $i \in [1, N]$, $S_0(\Delta Y, i)$ representing the probability that there is no fault or no significant fault on the pseudo range *i* and $S_1(\Delta Y, i)$ representing the probability that there is a bias on the channel *i* that will lead to a positioning failure.

This technique is more complicated since a recursive function of two variables has to minimize under more complex constraints. Its implementation is detailed in appendix D.

4-5 Synthesis

Three distinct classes of RAIM have been addressed in this chapter.

The Least Square Residual method in which the sum of the squares of the pseudorange residuals plays the role of the basic observable has been first recalled.

The Maximum Solution Separation method has been discussed and an improved way of computing the associated protection level has been proposed. This MSS technique is based on the observation of the separation between the position estimate generated by a full-set filter (using all the satellite measurements) and that generated by each one of the subset filters (each using all but one of the satellite measurements). Nominal biases have not been taken into account in MSS RAIM design.

Finally, a new method based on the Generalized Likelihood Ratio test has been introduced and several implementations have been described. First a snapshot one that does not take into account nominal biases and for which an analytical threshold expression that satisfies a given probability of false alarm and a predictive probability of missed detection have been presented. A snapshot implementation that takes into account potential nominal has also been proposed. Finally, two sequential techniques have been described: one designed to detect step error and another one design to detect step plus ramp failure.

The way these different methods will be implemented in order to take into account both civil aviation requirement and threat model is detailed in the next chapter.

It is quite difficult to implement sequential methods and especially to obtain a representative evaluation of their worldwide availability performance. This is mainly due to the great number of various parameters and to simulation time. Detection performance has been evaluated through representative situations but no analytical method to predict availability has been developed. Therefore, it has been decided to not present simulation results relative to sequential methods in this document.

Chapître 5

Implementation des algorithmes RAIM

Le but de ce chapître est de présenter les hypothèses principales qui ont été faite afin d'évaluer les performances des algorithmes RAIM.

La section 5.1 décrit la grille utilisateur. Il s'agit d'une grille espacée de 5° en latitude et de 5° en longitude représentant un total de 2520 positions.

Certaines simulations impliquent la constellation GPS seule, d'autres la constellation Galileo seule et certaines considererent les deux systèmes. Afin d'avoir des geometries satellitaires representatives, les durées de simutlation doivent correspondre aux périodes orbitales des constellations considérées. Ces considérations sont adressées dans la section 5.2.

La section 5.3 traitent des mesures satellitaires disponibles, c'est-à-dire la manière dont elles sont obtenues et leur nombre moyen. L'obtention de la position des satellites de navigation et les angles de masquage choisis sont ainsi présentés.

Le nombre d'inconnues à considérer dans l'estimation de la position uitlisateur est adressé dans la section 5.4. En effet cette étude se base sur une combinaison de GPS et de Galileo au niveau des mesures de pseudodistance. Or même si le décalage d'horloge entre les systèmes Galileo et GPS sera diffusé dans le message de navigation, cette valeur pourrait être critique. C'est pourquoi il peut être utile de présenter ces résultats de simulations basées sur l'hypothèse selon laquelle l'utilisateur doit résoudre le décalage entre son horloge récepteur et le temps du système GPS ainsi que le décalage entre son horloge récepteur et le temps du système Galileo; la manière dont cela est réalisé est alors explicitée.

La détermination de la probabilité de fausse alarme maximale pour chaque opération est détaillée dans la section 5.5. Le raisonnement est en parti basé sur le temps de corrélation eds mesures.

Au même titre que la probabilité de fausse alerte, la probabilité de detection manquée constitue une entrée majeure des algorithmes RAIM. Ce paramètre découle du risque d'integrité mais depend également de la probabilité d'occurence des pannes satellite. Dans la mesure où ce calcul fait référence au modèle de menace, il doit être particulièrement détaillé. C'est l'objet de la section 5.6.

La section 5.7 décris la manière dont sera évaluée la disponibilité des fonctions de détection et d'exclusion des différents algorithmes implémentés.

Chapter 5

RAIM Implementation

The aim of this chapter is to present major assumptions that have been made for RAIM performance evaluation whose results are presented in chapter 6. In particular, some methods to obtain the inner probability values that RAIM algorithms need to use are detailed.

5-1 User grid

A worldwide evaluation of RAIM performance will be conducted and thus a user grid needs to be defined. It has been decided for this study to use a grid with a latitude step of 5° and a longitude step of 5°. This represents a total amount of 2520 user positions.

5-2 Simulation period

Some simulations will imply both Galileo and GPS satellites. In order to have representative satellite geometries, the simulation period has to correspond to both constellation orbital periods.

According to ESA, Galileo satellites will have orbit altitude of 23 222 kilometers resulting in a ground track repeat cycle of ten days during which each satellite has completed seventeen revolutions. Nevertheless, each Galileo satellite has an approximate orbit revolution period of 14 hours and 7 minutes which corresponds to five revolutions in three days.

The nominal orbital period of all vehicles in the GPS constellation is 12 sidereal hours that is to say that each GPS satellite has an orbital period of 11 hours and 58 minutes, at an altitude of 20 183 kilometers. Therefore, three days also approximately correspond to six GPS satellites periods.

This is why a simulation time of three days has been chosen for dual constellation whereas a simulation time of one day has been chosen for single constellation studies.

The frequency of the simulation test will depend on simulation time.

A first class of value will be evaluated every 4 minutes which correspond for three days simulation duration to 1080 values for each user point. Thus, that will provide an amount of 2 721 600 values for the 2520 points of the user grid.

A second class of value will be evaluated every minute which correspond for one day simulation duration to 1440 values for each user point. That will provide an amount of 3 628 800 values for the 2520 points the user grid.

5-3 Available satellite measurements

5-3-1 Satellites position computation

The future Galileo space segment will comprise 30 satellites in a Walker constellation with three orbital planes at 56° nominal inclination. Each plane will contain nine operational satellites, equally spaced, 40° apart, plus one spare satellite to replace any of the operational satellites in case of failures.

The nominal GPS system constellation has 24 satellites in six 55° orbital planes, with four satellites in each plane, with room for spares.

In practice GPS signal carries with it data from the satellite that the user receiver needs to solve its position, its velocity. Because of many perturbations to the ideal purely elliptical Kepler orbit such as lunar, solar gravitational attraction, solar flux…, the GPS orbit is modeled as a modified elliptical orbit with correction terms to account for these perturbations. These ephemeris parameters are changed periodically to give a best fit to the actual satellite orbit. By demodulating and extracting the navigation data, the user can calculate the satellite position as a function of time. Ephemeris parameters and elements of ephemeris model equations are given in [Spilker, 1996].

Another type of data is transmitted through GPS signal providing a truncated and reduced precision set of the ephemeris parameters: the almanac data, which are much less accurate than the detailed ephemeris data. However the almanac data are valid for longer period of time and do not require frequent update. The almanac parameters are given in [Spilker, 1996]. The algorithm for computing the satellite position from this set of parameters is the same as ephemeris one. The only difference is that where the almanac does not include a parameter, this parameter is set to zero.

Almanac data which are usually used for satellite selection and as aids to acquisition, will be used for satellite position computation in simulations. To be more precise, a 27 satellites Galileo constellation [Eurocae, 2006] and an optimized 24 satellites GPS constellation [RTCA, 2006] will be considered for these simulations and the satellite position computation will be made thanks to corresponding almanac data.

5-3-2 Mask Angles

As indicated in the Galileo Integrity Concept [ESA, 2005], the user elevation angle above which SISA is guaranteed is 10°. Even if this study does not concern Galileo ground integrity channel, this SISA value has been consider for UERE provision. This is why a 10° degree mask will be used for Galileo satellite visibility computation.

As specified in [GPS SPS, 2001], GPS performance are given for a receiver which tracks all satellites in view above a 5° mask angle. This is why a 5° degree mask will be used for GPS satellite visibility computation.

5-3-3 Average number of visible satellites

Those assumptions lead to a given set of visible satellites. Actually a greater number of GPS satellites can be expected in future and therefore, the following results are quite conservative.

It can be seen on the following figure that, considering the GPS and Galileo constellations described above, an average number of 17 satellites will be available.

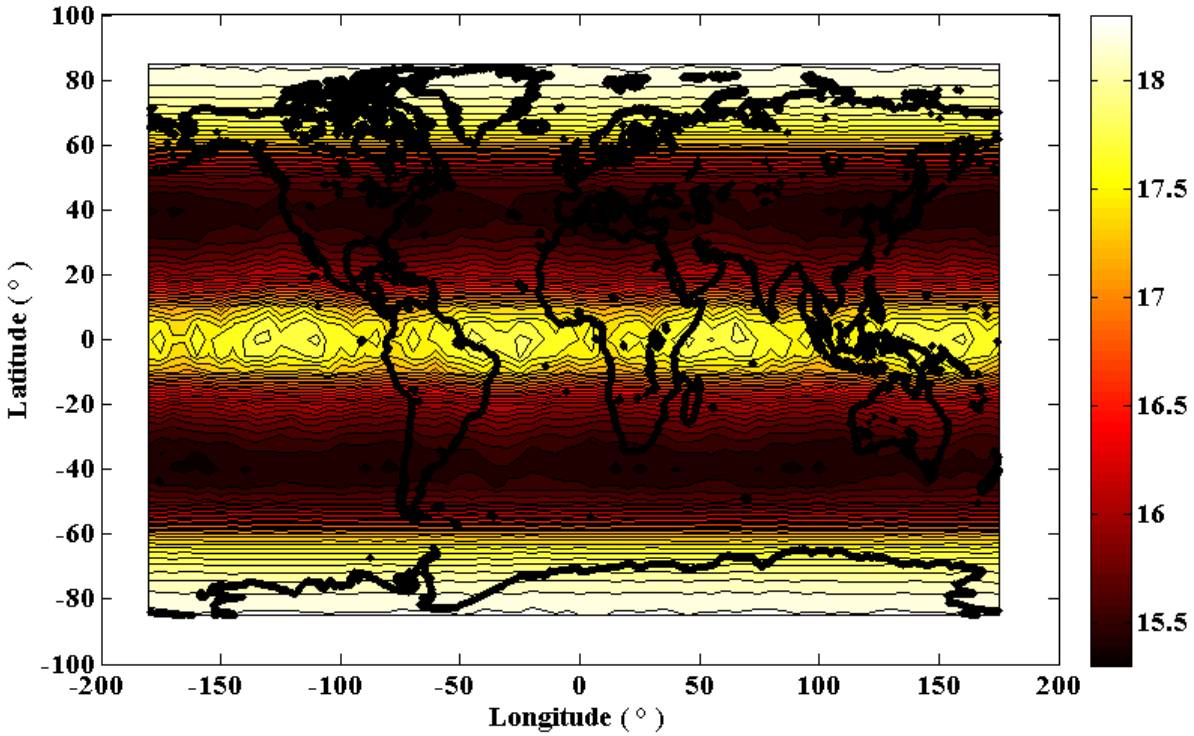

Figure 27 - Average number visible satellites over 3 days considering 24 sat GPS and 27 sat Galileo constellations

The same computation has been conducted only considering 24 satellite GPS constellation, then only considering 27 Galileo constellation (with a 5° masking angle and 10° masking angle).

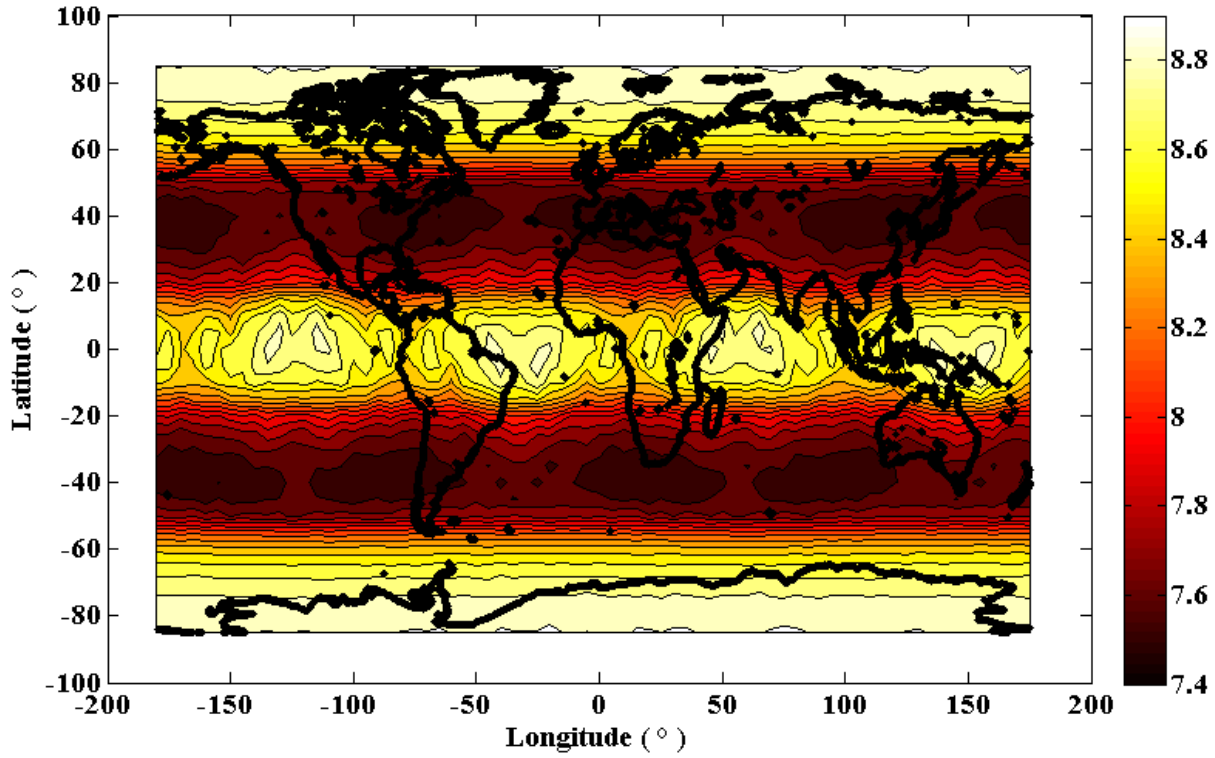

Figure 28 - Average number of satellites over 3 days considering 24 satellites GPS constellation

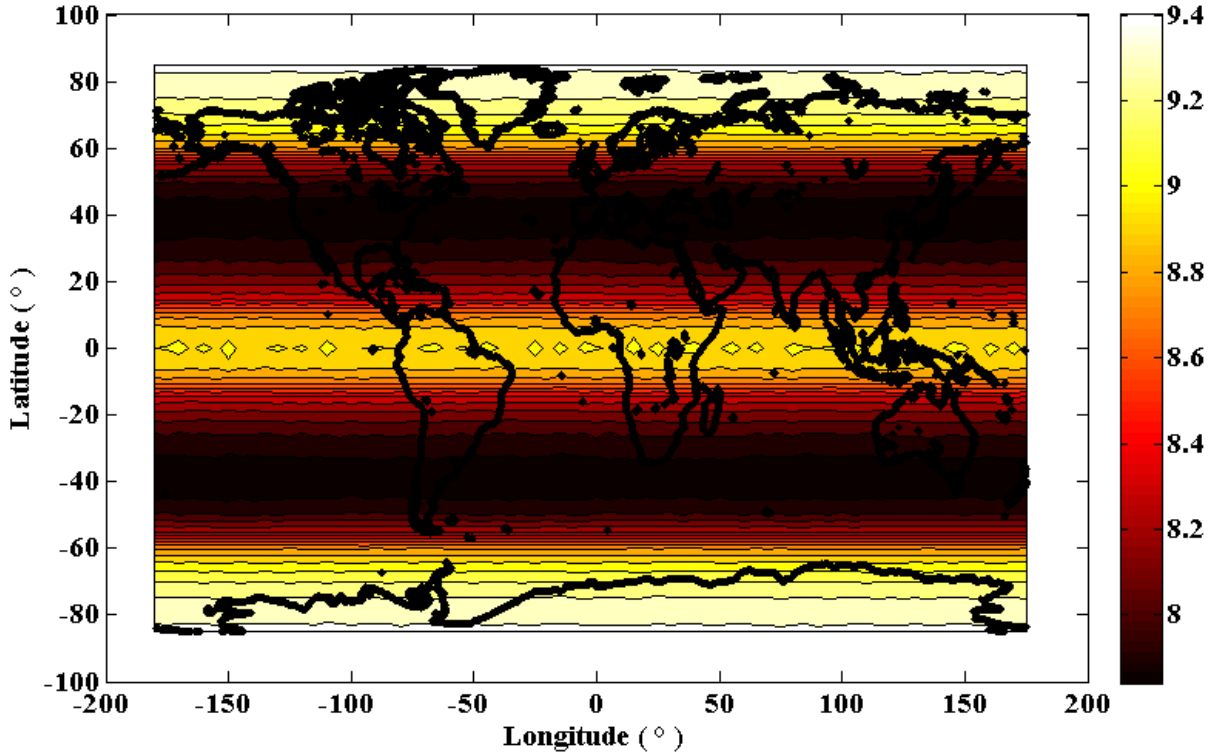

Figure 29 - Average number of satellites over 3 days considering 27 satellites Galileo constellation (mask angle 10°)

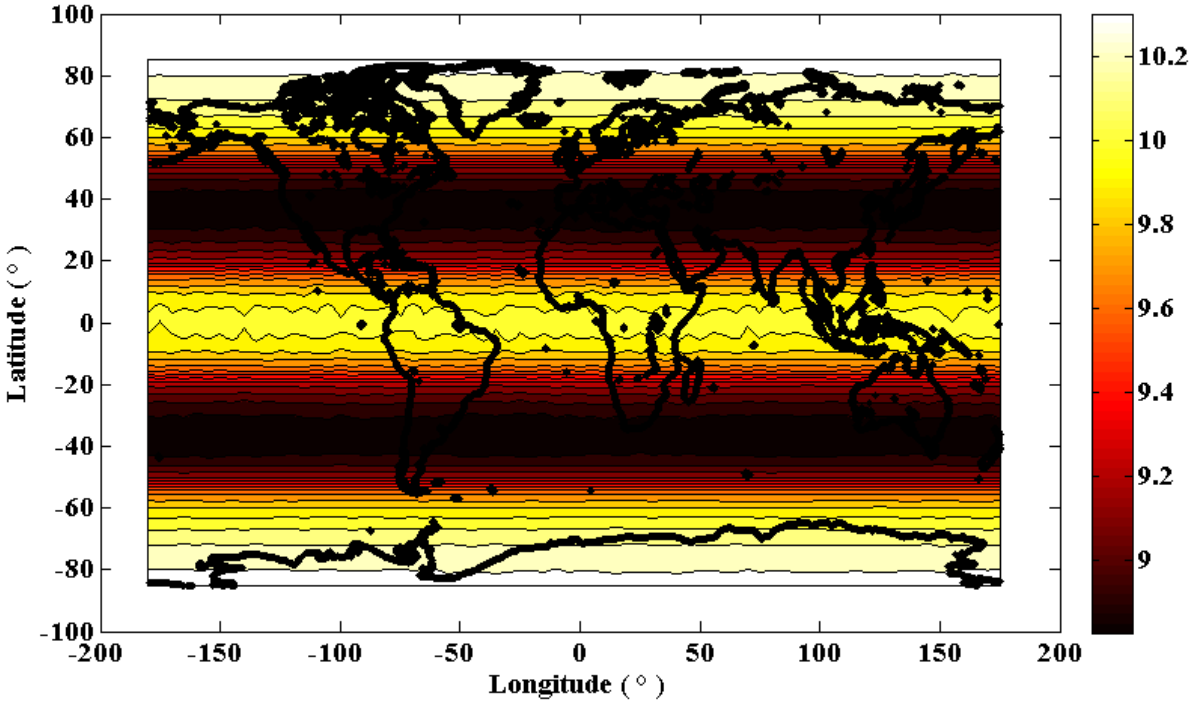

Figure 30 - Average number of satellites over 3 days considering 27 satellites Galileo constellation (mask angle 5°)

5-4 Number of unknowns for position solution estimation

This study has focused on combining GPS and Galileo at the pseudorange level. Even if United States and European Union have agreed to provide the GPS to Galileo Time Offset GGTO through each system's navigation signals, the determination of this offset is thought not to be part of a safety-critical chain [Hahn and Powers, 2005]. This is why it is useful to provide some simulation results based on the assumption that the user solves for the offset between the GNSS receiver clock and GPS system time, and between the GNSS receiver clock and Galileo system time.

This operation consists in adding an additional column to the observation matrix such that the first time column contains ones in row corresponding to GPS satellites and zeros in Galileo rows and vice versa for the second time column.

$$H = \begin{bmatrix} \vdots & \vdots & \vdots & 1 & 0 \\ \cos(E_i)\cos(A_i) & \cos(E_i)\sin(A_i) & \sin(E_i) & \vdots & \vdots \\ \vdots & \vdots & \vdots & 1 & 0 \\ \vdots & \vdots & \vdots & 0 & 1 \\ \cos(E_j)\cos(A_j) & \cos(E_j)\sin(A_j) & \sin(E_j) & \vdots & \vdots \\ \vdots & \vdots & \vdots & 0 & 1 \end{bmatrix} \quad (5\text{-}1)$$

This fifth unknown variable is thus taken into account in the navigation solution computation. Indeed, the following user position vector has to be estimated:

$$X(k) = [\, x(k)\ y(k)\ z(k)\ b_{GPS}(k)\ b_{\text{Galileo}}\,(k)\,] \quad (5\text{-}2)$$

where

$x(k)$, $y(k)$, $z(k)$ are the three user coordinates in the WGS84 reference frame
$b_{GPS}(k)$ is the time offset between the GNSS receiver clock and GPS system time
$b_{\text{Galileo}}(k)$ is the time offset between the GNSS receiver clock and Galileo system time

This fifth unknown variable is also taken into account in some RAIM equations by means of the observation matrix and more particularly for the LSR RAIM, by considering that the sum of the squares of the pseudorange residuals is chi-squared distributed with N-5 degrees of freedom, instead of N-4.

5-5 Probability of false alert

5-5-1 Requirements analysis

Concerning Non Precision Approaches, DO 229C [RTCA, 2001] states a Maximum Allowable False Alert rate for En-route to NPA of 10^{-5}per hour. It is said that assuming a correlation time of 120 seconds, leads to a Maximum Allowable False Alert rate of 3.33×10^{-7}per test. This value of 3.33×10^{-7}per test is straightly given in DO229D [RTCA, 2006] without explanation.

Concerning Approaches with Vertical Guidance, DO 229C states a Maximum Allowable False Alert rate for APV of 2×10^{-5}per approach, one approach duration being 150 s. It is said that assuming a correlation time of 75 seconds leads to a Max Allowable False Alert rate of 10^{-5}per test. DO229D now gives 1.6×10^{-5}per test without explanation. It can be seen that this last value corresponds to an assumed correlation time of two minutes.

In fact, a correlation time of two minutes allows to consider two minutes independent sample intervals and to realize 30 independent tests within the time of one hour or 1.25 independent tests within the time of 150 s. Under this assumption, the NPA requirement of 10^{-5}per hour becomes 3.33×10^{-7}per test (30 independent tests per hour and global false alarm allocation divided by 30 for each test).

In fact, the correlation time is a major issue here. In the past, for GPS, Selective Availability SA was the most likely cause of false alerts and its effects were assumed to have a correlation time of two minutes. Without SA, in single frequency operations, the ionosphere has become the largest error source. But as we assume dual frequency operation in an ionosphere free combination, the residual ionospheric error will be zero in our study.

According to [Van Dyke, 2000], two correlation time values can be considered.

First, it can be considered that an ionospheric error large enough to cause an alert should be considered as a true alert. Under this assumption, the ionosphere contribution to the correlation time is not considered anymore for false alarm discussion and the correlation time is then driven by the receiver noise. The smoothing time constant of the receiver noise is assumed to be of the order of two minutes.

The second philosophy is that the correlation time is approximately one hour, based on the average length of time satellites are visible to the user [Kovach et al, 1995]. This would lead to consider only one independent sample per hour. For example for NPA operations, it would allow to set RAIM decision threshold based on a false alert probability of 10^{-5}per sample

rather than the false alert probability of 10^{-5}/(30 samples per hour)/hour, that is to say 3.33×10^{-7} per sample. This would improve RAIM availability but this proposition has not been adopted by RTCA SC 159.

5-5-2 Conclusion

For this study, a correlation time of two minutes will be considered. As it is the maximum allowable false alert rate per sample that constitutes an input for RAIM algorithms threshold computation, the following values will be used:

Operations	Maximum Allowable False Alert rate	Maximum Allowable False Alert rate (per sample)
En-route to Non precision approach	10^{-5}per hour [RTCA, 2001]	3.33×10^{-7} per test [RTCA, 2001], [RTCA, 2006]
Approach with Vertical Guidance	2×10^{-5}per approach [RTCA, 2001]	1.6×10^{-5}per test [RTCA, 2006]
LPV 200	2×10^{-5}per approach	1.6×10^{-5}per test

Table 11 - Maximum allowable false alert rate

For simplification reasons, it has been decided to adopt the same false alert probability model for LPV200 and APV simulation. It can be mentioned that [Lee and McLaughlin, 2007] suggested to derive this requirement from the ICAO continuity risk requirement, setting the allowable false alert probability per sample to 4×10^{-6}.

5-6 Probability of missed detection

As recalled in section 2-5-2, a missed detection is defined to occur when a positioning failure is not detected. Positioning failures that are not annunciated as an alert within the time to alert are defined to be missed alert; they can be due to missed detection or to wrong exclusion [RTCA, 2006]. Missed alert and missed detection events will be merged for the rest of the study.

As the probability of false alarm, the targeted probability of missed detection constitutes a major input of RAIM algorithm. This parameter derives from the integrity risk but also depends on the probability of satellite failure. Thus it refers to the threat model and particularly needs to be detailed.

5-6-1 Existing results

Some requirements are given for En-route, terminal and LNAV operations in [RTCA, 2006]. It is specified that the probability of missed alert shall be less than or equal to 0.001 for every geometry and every navigation mode, regardless of which satellite is causing the positioning failure. If this requirement is not met for a given geometry, the detection function is defined to be unavailable for that geometry.

This requirement comes from the corresponding integrity risk and the probability of satellite failure. Indeed, for these phases of flight the required integrity risk is 1×10^{-7}/h (see section 2-4-1) and the only feared events used to be the major service failure (see section 3-3-1-1) because of the wide acceptance regions.

According to the GPS signal specification [GPS SPS, 2001], 3 major failures are allowed per year and per constellation approximately which corresponds for a constellation of 24 satellites to an individual major satellite failure such as:

$$p \cong 1.43 \times 10^{-5}/h \tag{5-4}$$

Let's us denote p the individual major satellite failure probability and N the number of satellite in view from the user, then the probability of having k simultaneous failures among N satellites in view is:

$$P_{\text{major satellite failure ,N,k}} = C_N^k p^k (1-p)^{N-k} \tag{5-3}$$

If an average of 8 GPS satellites are in view, the global probability of having a major satellite failure is:

$$P_{\text{major satellite failure}} = 8p(1-p)^7 \cong 1.14 \times 10^{-4}/h \tag{5-5}$$

Usually, this probability is approximated by:

$$P_{\text{major satellite failure}} \cong 10^{-4}/h$$

And the probability of missed detection is the result of:

$$P_{md} = \frac{P_{int}}{P_{\text{major satellite failure}}} = \frac{10^{-7}/h}{10^{-4}/h} = 10^{-3} \quad (5\text{-}6)$$

This result is only valid for En-route to NPA operations, only assuming single satellite failure from major service failure category and only considering GPS constellation.

[RTCA, 2006] states that there is not missed alert probability requirement for APV operations.

5-6-2 Dual constellation consideration

5-6-2-1 Smallest single bias that leads to a positioning failure

To correctly address this issue, it is first necessary to know the minimal amplitude of a single pseudorange failure that leads to an unacceptable positioning error for the intended operation and thus the minimal bias amplitude that needs to be detected by RAIM algorithms.

The computation of the critical bias is presented in section 4-1-3 and is detailed in appendix A. It does not depend on any detection algorithm. But the amplitude of the smallest dangerous single bias on a pseudorange will depend on the failure probability of occurrence. Indeed, the lower a failure occurrence rate is, the higher its amplitude can be.

The two following figures represent the average and minimal values of smallest biases that lead to a positioning failure for APVI and LPV 200 requirements. The objective of this preliminary study is to evaluate the amplitude of every critical bias as a function of their occurrence rate.

These values have been computed for different satellite failure probabilities of occurrence and are represented as a function of the integrity risk-probability of satellite failure occurrence ratio. A 24-satellite GPS constellation and a 27-satellite Galileo constellation have been considered over a 3 days period. The user grid described in section 5.1 has been used. The nominal error has been generated using the smoothed iono free UERE described in section 3.2.1 with an URA of 0.85 m.

We compute for each pseudorange the smallest bias that leads to a horizontal positioning failure and the smallest bias that leads to a vertical positioning failure. For each pseudorange, the minimum of these two biases is the smallest bias that leads to a positioning failure. In most of the cases, this smallest bias leads to a vertical positioning failure.

It can be seen that in both cases (APVI and LPV 200 operations) and for a large scale of probability of occurrence, the amplitude of smallest critical biases belongs to the major service failure category. As defined in 3-3-1-1, a major service failure refers to a situation during which a healthy GPS satellite's ranging signal error exceeds the larger of 30 m and 4.42 times the URA.

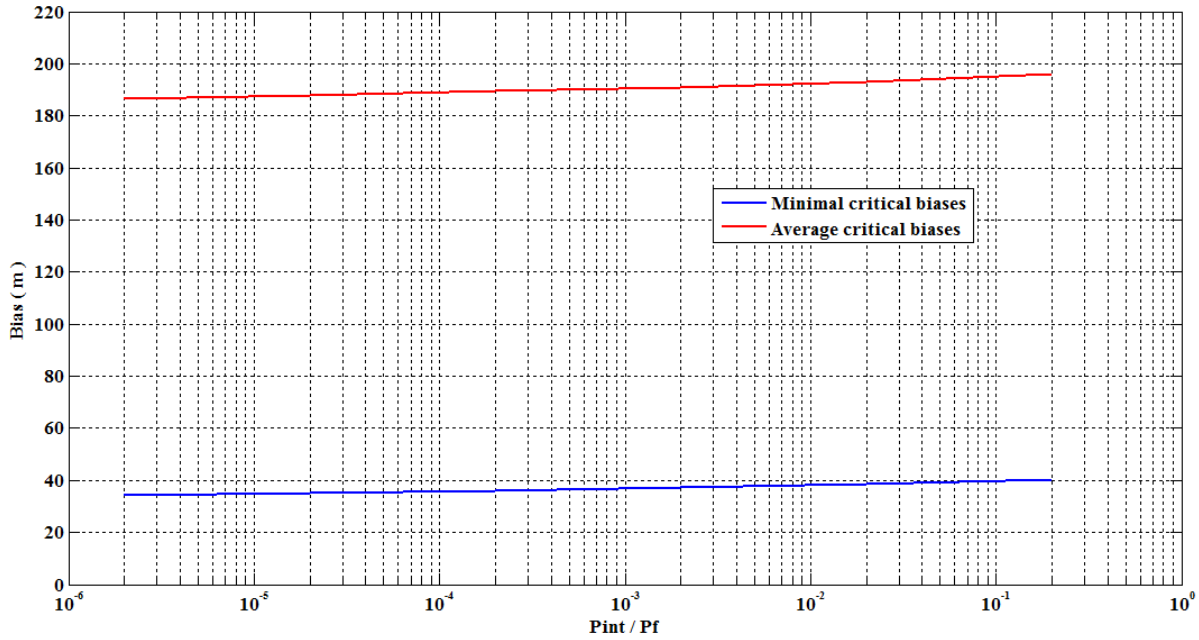

Figure 31 - Smallest bias that leads to a positioning failure - APVI operations – dual constellation (GPS + Galileo)

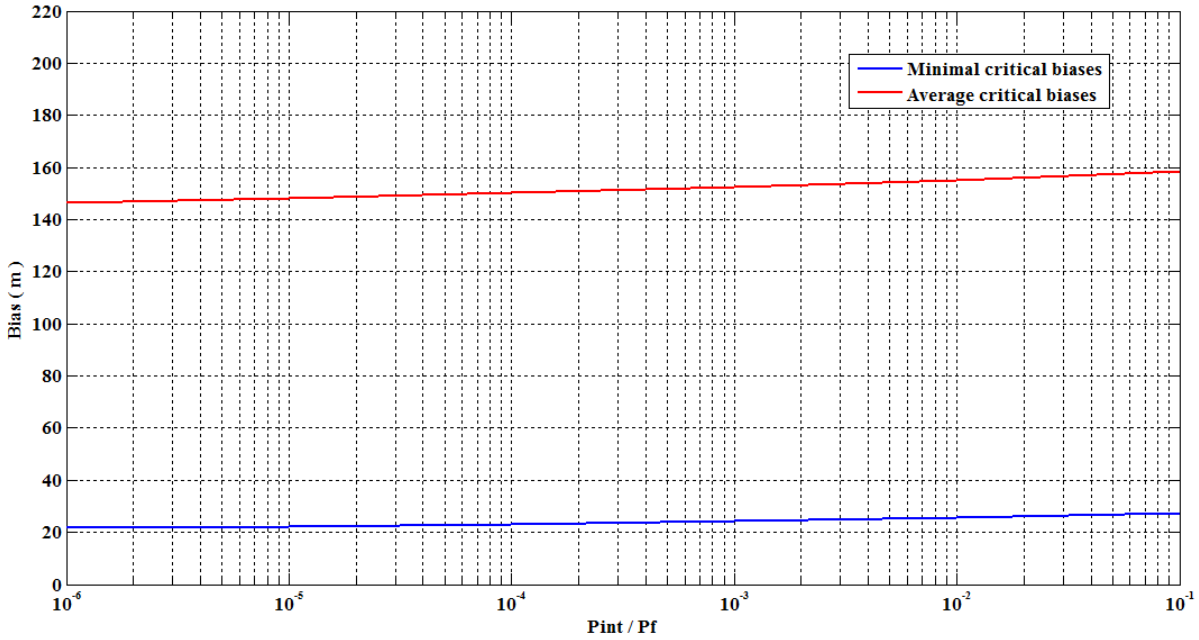

Figure 32 - Smallest bias that leads to a positioning failure - LPV200 operations – dual constellation (GPS + Galileo)

It can be noticed that there is very minimal sensitivity of the smallest bias to the probability of occurrence. An explanation of this phenomenon can be given.

The method consists in projecting biases on a pseudorange in the position domain. For simplification reasons, we can focus on the vertical case. The smallest bias that will lead to a vertical positioning is such as:

$$(1 - P_f)P_0(|X_V - \hat{X}_V| > VAL)$$
$$+P_f P_{b_i}(|X_V - \hat{X}_V| > VAL) = P_{Int}$$

This expression can be simplified because positioning failure due to fault free condition are very rare: $P_0(|X_V - \hat{X}_V| > VAL) \cong 0$

Therefore the smallest bias b_i on the pseudorange i that will lead to a vertical positioning is such as:

$$P_{b_i}(|X_V - \hat{X}_V| > VAL) = \frac{P_{Int}}{P_f}$$

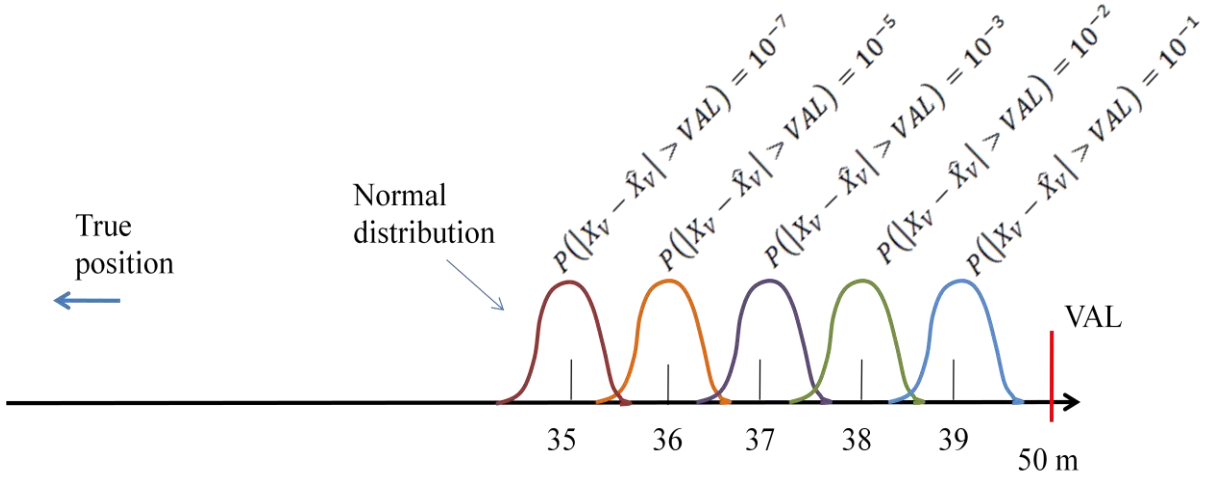

Figure 33 - Positioning failure

It can be seen that there is a factor 10^4 between the orange and the blue distributions but only 3 meters between their mean that represents only 10% of the global error. There is not much difference between the mean of the distribution that lead to $P_{b_i}(|X_V - \hat{X}_V| > VAL) = 10^{-5}$ and the one that leads to $P_{b_i}(|X_V - \hat{X}_V| > VAL) = 10^{-1}$

Therefore, there is not much difference between the biases that lead to these two distributions only 3 meters in the position domain and 10 - 15 meters in the range domain. This is due to the small UERE standard deviation compared to the alert limit.

5-6-2-2 Associated probability of missed detection computation

Thus, for single failure study, only Major Service Failure events are considered as failures that have to be detected by RAIM. Although they could participate to misleading information, faulty measurements due to local effects such as CW interference or ionosphere disturbance are not taken into account in required Pmd computation as their rate of occurrence cannot be quantified. This assumption leads to the following process.

Let's us denote p the individual major satellite failure probability and N the number of satellite in view, then the probability of having k simultaneous failures among N satellites is:

$$P_{\text{major satellite failure ,N,k}} = C_N^k p^k (1-p)^{N-k} \quad (5\text{-}7)$$

As previously detailed, for GPS current constellation, three major failures per year lead to

$$p \cong 1.43 \times 10^{-5}/h \quad (5\text{-}8)$$

It is assumed that a future GPS or Galileo satellite will have the same probability of failure than a current GPS satellite, even if better performance could be expected from GPS III constellation.

For a dual constellation, if 17 satellites are in view, the probability of one satellite failure becomes:

$$P_{\text{major satellite failure ,17,1}} = 2.43 \times 10^{-4}/h \quad (5\text{-}9)$$

Only considering the single failure case, the probability of missed detection P_{md} shall be lower than the integrity risk requirement divided by the probability of failure of one satellite among the all satellites in view.

$$P_{md} = \frac{P_{int}}{P_{\text{major satellite failure ,N,1}}} \quad (5\text{-}10)$$

Thus, for En-route to Non precision approach, considering only major service failure such as $P_{\text{major satellite failure ,17,1}} = 2.43 \times 10^{-4}/h$, the obtained probability of missed detection is:

$$P_{md} = 4.13 \times 10^{-4} \quad (5\text{-}11)$$

As the integrity risk is specified for an approach duration for APV and LPV operation, one method to obtain the probability of one satellite failure per approach could have been to divide the hourly rate by 24 (as $24 \times 150 = 3600$).

But in the determination of the probability of encountering a major failure, the outage duration time is a major parameter.

The GPS specified time to remove the faulty satellite when a major service failure has occurred is 6 hours and actual performance is typically one hour.

[Lee and McLaughlin, 2007] suggested that a failure duration can be of 45 minutes, even if shorter delays can be expected from GPS III and Galileo system. [Walter, 2008] indicate that the GPS III specification is still 6 hours and that it may be lowered but likely not below 1 hour.

A failure duration of one hour can lead to convert this integrity failure rate for one satellite $p \cong 1.43 \times 10^{-5}$ per hour in $p \cong 1.43 \times 10^{-5}$ per approach for example. As if an approach duration was artificially set to one hour, because a failure that had occurred one hour before could still have an impact.

For this study, it will be considered that a failure duration is one hour which leads to convert this integrity failure rate for one satellite $p \cong 1.43 \times 10^{-5}/h$ in $p \cong 1.43 \times 10^{-5}$ per approach and thus:

$$P_{\text{major satellite failure},17,1} = 2.43 \times 10^{-4}/\text{approach} \quad (5\text{-}12)$$

For APV operations, if $P_{int} = 2 \times 10^{-7}$ per approach:

$$P_{md} = \frac{2 \times 10^{-7}}{2.43 \times 10^{-4}} = 8.23 \times 10^{-4} \quad (5\text{-}13)$$

If it is finally decided to set the LPV 200 integrity risk requirement to 1×10^{-7} per approach, the corresponding probability of missed detection will be:

$$P_{md} = \frac{1 \times 10^{-7}}{2.43 \times 10^{-4}} = 4.12 \times 10^{-4} \quad (5\text{-}14)$$

5-6-2-3 Multiple failures consideration

This situation cannot be considered in the same way. Single failure assumption allowed us to compute for every pseudo range the smallest additional bias that will lead the global solution estimation to be outside the required containment region.

It is still possible for multiple failures case to add simultaneously several biases on different pseudorange and observe the consequence on the position error. But even in the dual failure case, it is not possible to determine for a given pseudorange couple, the two most critical associated biases. It is thus quite difficult to fully address this problem.

Fortunately, multiple failures are very rare. For instance GEA has adopted a rate of common mode faults causing multiple satellite integrity failures equal to 1.3×10^{-8}/approaches and a rate of two or more independent faults of about 0.45×10^{-8}/approaches, representing a total of 1.75×10^{-8}/approaches for multiple faults [Lee and McLaughlin, 2007]

It is thus possible not to try to detect these multiple failures and therefore to set the probability of detecting an integrity failure cause by multiple faults to zero (corresponding P_{md} equal to one) such as:

$$P_{int} = P_{\text{satellite failure},N,1} \times P_{md} + P_{\text{multiple satellite failures},N} \quad (5\text{-}15)$$

Therefore, the multiple failure case is derived from the single failure case by allocating a smaller integrity risk.

$$P_{md} = \frac{P_{int} - P_{\text{multiple satellite failures},N}}{P_{\text{major satellite failure},N,1}} \quad (5\text{-}16)$$

The probability of occurrence of multiple faults can be decomposed as:

- the common mode fault probability of occurrence assumed to be equal to 1.3×10^{-8}/approaches
- the probability of occurrence of two or more independent faults.

If 17 satellites are in view, with $p \cong 1.43 \times 10^{-5}$ per approach, we have for the more independent faults:

$P_{\text{major satellite failure},17,2} = C_{17}^{2} p^{2}(1-p)^{15} = 2.78 \times 10^{-8}$ per approach

$P_{\text{major satellite failure},17,3} = C_{17}^{3} p^{3}(1-p)^{14} = 1.99 \times 10^{-12}$ per approach which is negligible

Therefore, the probability of occurrence of multiple faults will be set as:

$$P_{\text{multiple satellite failures},17} = 4.08 \times 10^{-8} \text{ per approach}$$

For APV operations, if $P_{int} = 2 \times 10^{-7}$ per approach:

$$P_{md} = \frac{1.59 \times 10^{-7}}{2.43 \times 10^{-4}} = 6.56 \times 10^{-4} \quad (5\text{-}17)$$

For LPV 200, if $P_{int} = 1 \times 10^{-7}$ per approach, the corresponding probability of missed detection will be:

$$P_{md} = \frac{0.59 \times 10^{-7}}{2.43 \times 10^{-4}} = 2.43 \times 10^{-4} \quad (5\text{-}18)$$

5-6-2-4 Conclusion

Dual constellation	APV	LPV 200
Single failure case	$P_{md} = 8.23 \times 10^{-4}$	$P_{md} = 4.12 \times 10^{-4}$
Multiple failures case (single failure detection)	$P_{md} = 6.56 \times 10^{-4}$	$P_{md} = 2.43 \times 10^{-4}$

Table 12 - Required probabilities of missed detection

5-6-3 Single constellation consideration

The same computation has to be done when only constellation (GPS or Galileo) is considered. Indeed, the reduction in the number of available measurement can increase the impact a of single satellite bias on the global positioning error. If smallest biases that lead to a positioning failure do not systematically belong to the major service failure, other failure occurrence rate have to be considered in the required probability of missed detection computation.

5-6-3-1 Smallest single bias that leads to a positioning failure

Considering only one constellation (GPS or Galileo), the average amplitude of the smallest single critical bias falls to approximately 70 meters. For some unfavorable satellites - user geometries, a bias with an amplitude of 10 meters on the worst satellite pseudorange measurement can lead to a positioning failure for LPV200 operations. This is represented on the following figure.

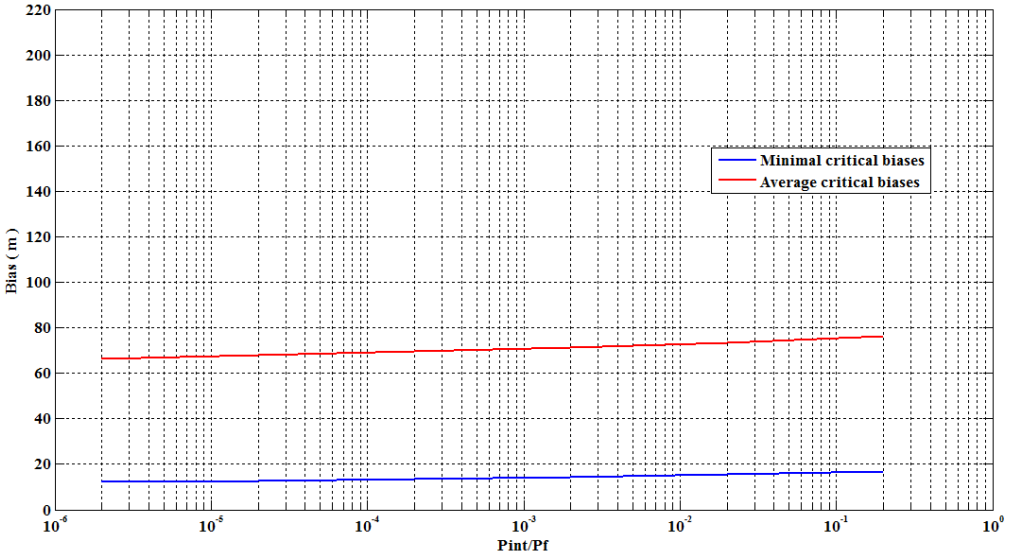

Figure 34 - Smallest bias that leads to a positioning failure - LPV200 operations - single constellation (GPS)

Nevertheless, this amplitude does exceed 4.42 times the expected URA, which is assumed to equal to 0.85 m in this study.

If one critical satellite was out, this amplitude might become much smaller (down to 5 meters).

5-6-3-2 Associated probability of missed detection computation

We can therefore consider that a 10 meter failure belongs to the major service failure category. Therefore, for single constellation RAIM performance evaluation, only Major Service Failure events are considered as failures that have to be detected, as it has been done for dual constellation.

For a single constellation, if 8 satellites are in view, the probability of one satellite failure uses to be:

$$P_{\text{major satellite failure },8,1} = 10^{-4}/h \qquad (5\text{-}19)$$

But as previously detailed in section 5-6-1, the assumption of 3 major service leads to consider $p \cong 1.43 \times 10^{-5}/h$ as an individual satellite failure rate and we get:

$$P_{\text{major satellite failure },8,1} = 1.14 \times 10^{-4}/h$$

As it has been previously detailed for dual constellation consideration, considering that a failure duration can be one hour, we get $p \cong 1.43 \times 10^{-5}/\text{approach}$ and:

$$P_{\text{major satellite failure },8,1} = 1.14 \times 10^{-4}/\text{approach} \qquad (5\text{-}20)$$

Only considering the single failure case, the probability of missed detection is given by:

$$P_{md} = \frac{P_{int}}{P_{\text{major satellite failure ,8,1}}} \quad (5\text{-}10)$$

For APV operations, if $P_{int} = 2 \times 10^{-7}$ per approach:

$$P_{md} = \frac{2 \times 10^{-7}}{1.14 \times 10^{-4}} = 1.70 \times 10^{-3} \quad (5\text{-}13)$$

If it is finally decided to set the LPV 200 integrity risk requirement to 1×10^{-7} per approach, the corresponding probability of missed detection will be:

$$P_{md} = \frac{1 \times 10^{-7}}{1.14 \times 10^{-4}} = 8.74 \times 10^{-4} \quad (5\text{-}14)$$

5-6-3-3 Multiple failures consideration

The probability of occurrence of multiple faults can be decomposed as:

- the common mode fault probability of occurrence assumed to be equal to 1.3×10^{-8}/approaches

- the probability of occurrence of two or more independent faults. If 8 satellites are in view with $p \cong 1.43 \times 10^{-5}$ per approach:

$P_{\text{major satell ite failure ,8,2}} = C_8^2 p^2 (1-p)^6 = 5.72 \times 10^{-9}$ per approach
$P_{\text{major satellite failure ,8,3}} = C_8^3 p^3 (1-p)^5 = 1.64 \times 10^{-13}$ per approach which is negligible

Therefore assuming that 8 satellites are in view, the probability of occurrence of multiple faults will be set as 1.9×10^{-8} per approach

As for dual constellation, the multiple failure case is derived from the single failure case by allocating a smaller integrity risk.

$$P_{md} = \frac{P_{int} - P_{\text{multiple satellite failures ,N}}}{P_{\text{major satellite failure ,N,1}}} \quad (5\text{-}16)$$

For APV operations, if $P_{int} = 2 \times 10^{-7}$ per approach:

$$P_{md} = \frac{1.81 \times 10^{-7}}{1.14 \times 10^{-4}} = 1.60 \times 10^{-3} \quad (5\text{-}21)$$

For LPV 200, if $P_{int} = 1 \times 10^{-7}$ per approach, the corresponding probability of missed detection will be:

$$P_{md} = \frac{0.81 \times 10^{-7}}{1.14 \times 10^{-4}} = 7.10 \times 10^{-4} \quad (5\text{-}22)$$

Or we could consider that this type of fault does not really belong to major service failure category. But, as it has been seen in section 3-3-1-2, the rate of occurrence of small satellite failure is more difficult to evaluate. For example, the failure rate of a step error larger than 3.6 meters could be taken into account. It is assumed to be less than 10^{-4} per hour per satellite in

GPS integrity related assumptions listed in [Van Dyke et al., 2003]. This consideration would allow us to be more conservative.

The same process could be then conducted leading to an individual satellite failure rate of 10^{-4} per approach instead of the rate of 1.43×10^{-5} per approach previously used.

Then, the probability of occurrence of multiple faults could be decomposed as:

- the common mode fault probability of occurrence assumed to be equal to 1.3×10^{-8}/approaches
- the probability of occurrence of two or more independent faults. If 8 satellites are in view with $p \cong 1 \times 10^{-4}$ per approach:

$P_{\text{major satellite failure ,8,2}} = C_8^2 p^2 (1-p)^6 = 2.80 \times 10^{-7}$ per approach
$P_{\text{major satellite failure ,8,3}} = C_8^3 p^3 (1-p)^5 = 5.60 \times 10^{-11}$ per approach which is negligible

Therefore assuming that 8 satellites are in view, the probability of occurrence of multiple faults will be set to 2.93×10^{-7} per approach.

This probability of occurrence is larger than APV integrity risk requirement. Under this assumption, the multiple failure missed detection probability cannot be set to 1 anymore (as it has been done in section 5-6-2-3). Indeed, multiple failures are not rare enough and it is not possible anymore to choose to not detect them.

5-6-3-4 Conclusion

For this study, it will be considered that the probability of dangerous failure is $p \cong 1.43 \times 10^{-5}/h$ (major service failure category) even when only on constellation is considered (GPS or Galileo). Indeed, every bias that leads to a positioning failure exceeds 4.42 times the URA. The same assumption is made in [Lee and McLaughlin, 2007] where only future GPS constellation is considered.

Single constellation (8 satellites in view)	APV	LPV 200
Single failure case	$P_{md} = 1.7 \times 10^{-3}$	$P_{md} = 8.74 \times 10^{-4}$
Multiple failures case (single failure detection)	$P_{md} = 1.60 \times 10^{-3}$	$P_{md} = 7.10 \times 10^{-4}$

Table 13 - Required probabilities of missed detection

5-7 Fault detection, identification and exclusion availability

As mentioned in section 2-5, fault detection and exclusion consists of two distinct parts:

- The fault detection part detects the presence of an unacceptably large position for a given mode of flight.
- Upon the detection, the fault exclusion follows and excludes the source of the unacceptably large position error, thereby allowing navigation to return to normal performance without an interruption of service.

Integrity monitoring algorithms generally involve these two functions. Their definitions are further used in chapter 6 where simulations results are presented.

5-7-1 Fault detection

The detection function is defined to be available when the constellation of satellites provides a geometry for which the missed alert and false alert requirement can be met on all satellites being used for the applicable alert limit and time to alert. When the constellation is inadequate to meet these requirements, the fault detection is defined to be unavailable [RTCA, 2006].

[RTCA, 2006] defines the availability of detection for a specific location, time, constellation and horizontal alert limit as:

$$\text{Detection Availability}(X, t, \text{constellation}, HAL) = \prod_{i=1}^{N} D(i) \qquad (5\text{-}23)$$

where N is the number of satellite being used by the equipment

$D(i) = 1$ if Pr(detection given error in ith satellite causing positioning error equal to HAL) ≥ the detection requirement and Pr(false alert) ≤ false alert requirement

$D(i) = 0$ otherwise

This definition can be extended to approaches with vertical guidance operations such as:

$$\text{Detection Availability}(X, t, \text{constellation}, HAL, VAL) = \prod_{i=1}^{N} D(i) \qquad (5\text{-}24)$$

where N is the number of satellite being used by the equipment

$D(i) = 1$ if Pr(detection given error in i^{th} satellite causing an horizontal positioning error equal to HAL or a vertical positioning error equal to VAL) ≥ the detection requirement and Pr(false alert) ≤ false alert requirement

$D(i) = 0$ otherwise

In practice, for a given phase of flight the availability of the FD functions is determined by comparing the computed protection levels with the corresponding alert limit requirement such as:

$HPL(X, t, \text{constellation}) \leq HAL$ and $VPL(X, t, \text{constellation}) \leq VAL$: available (5-25)

$$HPL(X,t,\text{constellation}) > HAL \text{ or } VPL(X,t,\text{constellation}) > VAL\text{: unavailable} \quad (5\text{-}26)$$

LSR and MSS fault detection availability are computed this way. It is not the case of the GLR RAIM where the predicted probability of missed detection is computed to obtain the algorithm availability.

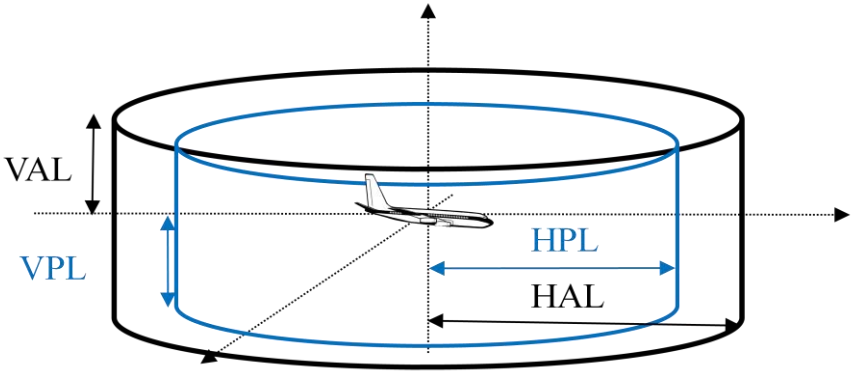

Figure 35 - Fault Detection function availability illustration for phases of flight with vertical guidance [Escher, 2003]

5-7-2 Fault exclusion

Similarly the exclusion function is defined to be available when the constellation of satellites provides a geometry for which the FDE algorithm can meet the failed exclusion requirement and prevent the indication of a positioning failure or a loss of integrity monitoring function.

As for the detection function, the horizontal and vertical exclusion level may be computed in order to check the exclusion function availability. These levels serve as decision levels for the whole fault and exclusion algorithm availability.

The Horizontal Exclusion Level (HEL) is the radius of a circle in the horizontal plan, with its center being at the true position, that describes the horizontal region where the missed alert and failed exclusion requirement are met for the chosen set of satellites when autonomous fault detection and exclusion is used.

The Vertical Exclusion Level (VEL) can be defined as the half the length of a segment on the vertical axis with its center being at the true position, that describes the region where the missed alert and failed exclusion requirement are met for the chosen set of satellites when autonomous fault detection and exclusion is used.

Availability of the FDE functions can be determined by comparing the computed exclusion levels with the corresponding alert limit requirement such as:

$$HEL(X,t,\text{constellation}) \leq HAL \text{ and } VEL(X,t,\text{constellation}) \leq VAL\text{: available} \quad (5\text{-}27)$$

$$HEL(X,t,\text{constellation}) > HAL \text{ or } VEL(X,t,\text{constellation}) > VAL\text{: unavailable} \quad (5\text{-}28)$$

In this study, LSR RAIM exclusion function availability will be obtained by computing detection function availability assuming one satellite has failed.

The failed satellite is chosen to have the largest effect on availability. Our criterion to choose the most important satellite (the one with the best geometry) is the vertical slope:

$$\text{Failed satellite} = \arg\min_i \left(VSLOPE_j\right) = \arg\min_i \left(\frac{A_{V,j}}{\sqrt{1 - B_{j,j}}}\right) \qquad (5\text{-}29)$$

where $B = H[H^t \Sigma^{-1} \mathrm{H}]^{-1} H^t \Sigma^{-1}$

$$A = [H^t \Sigma^{-1} \mathrm{H}]^{-1} H^t \Sigma^{-1} = \begin{bmatrix} \cdots & A_{N,j} & \cdots \\ \cdots & A_{E,j} & \cdots \\ \cdots & A_{V,j} & \cdots \\ \cdots & A_{T,j} & \cdots \end{bmatrix}:$$

5-7-3 Fault identification

A Fault Detection and Identification function is implemented for the GLR RAIM.

Indeed this test does not only raise an alert when a failure has been detected: the faulty measurement is also identified within the same operation. In fact, FDI function availability is evaluated through the predicted Pmd computation.

Chapître 6

Analyse des performances RAIM

L'objectif de ce chapître est de présenter les résultats de simulations qui ont été conduits afin d'évaluer la capacité des algorithmes RAIM à fournir le contrôle d'integrité pour les approches à guidage vertical.

La section 6-1 présente les resultats d'études preliminaires. Ainsi la section 6.1.1 constitue une illustration du comportement des differents tests étudiés face à diverses amplitudes d'erreurs. L'effet des interferences sur les mesures de pseudodistance est étudié dans la section 6.1.2.

Les performances de l'algorithme des moindres carrés sont adressées dans la section 6.2. Les résultats présentés concernent les approches à guidage vertical de type APV I et LPV200 et considère la constellation GPS seule, la constellation Galileo seule puis les deux constellations.

La section 6.3 traite des performances de la méthode de séparation des solutions alors que la section 6.4 adresse celles de l'algorithme RAIM basée sur le test du rapport de vraisemblance généralisé.

La section 6.5 constitue une synthèse de ces résultats. Toutes les hypothèses de simulations y sont rappelées et les performances de chacun des algorithmes étudiés y sont rassemblées sous forme de tableau.

Chapter 6

RAIM Performance Analysis

6-1 Preliminary studies
6-2 LSR RAIM Performance
6-3 MSS RAIM Performance
6-4 GLR RAIM Performance
6-5 Synthesis

The objective of this chapter is to present results of the simulations that have been conducted to evaluate RAIM ability to provide integrity monitoring for vertically guided approaches. Some preliminary studies are first presented in order to illustrate the different implemented tests reactions to several amplitudes of error and also to address the interferences issue.

This evaluation consists in predicting RAIM algorithm performance and to compare it to the corresponding requirements that is to say in predicting protection levels compared to alert limit or in predicting the probability of missed detection of critical failures. This is performed without injecting any failure. This chapter also includes limited tests to illustrate the detection capability.

6-1 Preliminary studies

6-1-1 Tests performance illustration

Three classes of RAIM test have been presented in chapter 4: the Least Square Residual, the Maximum Solution Separation and the Generalized Likelihood Ratio methods. It has been seen that their detection thresholds are designed to cope with the required false alert rate. To set them, criteria statistics is considered under fault free case assumption.

An issue would be: do RAIM algorithms have to detect biases that are above the assumed level of noise but that do not lead to a positioning failure? Indeed, as detailed in section 5-6-2-1, average critical biases that lead to a positioning failure are around 150 meters for LPV 200 and 180 meters for APV1. Section 3-2-2 proposes to include in the pseudorange measurement fault free case model some nominal biases with an amplitude of up to 2 meters. Thus, a large gap remains between nominal biases and dangerous biases.

For instance, if a RAIM algorithm detects a bias on a given pseudorange that corresponds to 50 % of the smallest critical bias:

- it is not a false alarm from classical RAIM design point of view since this failure really departs from the assumed level of noise

- it could be considered as a false alarm since this bias does not correspond to a positioning failure
- this bias reflects a satellite bad health , it may be a good thing to detect it before it may become really dangerous

On that subject, it may be interesting to detect a ramp failure that would become dangerous in a few seconds as suggested in section 4-4-4.

The question of detecting errors that do not lead to a positioning failure remains open. Nevertheless, it could be interesting to evaluate the reactions of the different algorithms that have been studied in this thesis.

Simulations presented in this section 6-1-1 have been conducted for a given user position, at a given moment. The objective of these simulations is only to provide an illustration of the different implemented tests reactions to several amplitudes of error and the number of selected cases is not sufficient to draw conclusions relative to civil aviation requirements.

A bias with various possible amplitudes has been injected on the worst pseudorange. In fact, the smallest additional single bias on this pseudorange that leads to a positioning failure has been computed for LPV 200 requirement (see section 4-1-3) and the injected biases amplitude is expressed as a percentage of this critical bias amplitude. Thus, pseudorange error measurement has been modeled as some noise plus a bias on this worst pseudorange *l* such as*:*

$$E = \begin{bmatrix} n^1 \\ \vdots \\ n^l \\ \vdots \\ n^N \end{bmatrix} + \alpha \begin{bmatrix} 0 \\ \vdots \\ b_l \\ \vdots \\ 0 \end{bmatrix} = \begin{bmatrix} n^1 \\ \vdots \\ n^l \\ \vdots \\ n^N \end{bmatrix} + \alpha B \qquad (6\text{-}1)$$

where $n^i \sim N(0, \sigma_i^2)$

$\sigma_1^2, \dots, \sigma_N^2$ are nominal error variances corresponding to UERE computation described in section 3-2-1 ($URA = 0.85\ m$)

$\alpha = \{0, 0.1, 0.5, 1\}$

b_l smallest additional single bias on pseudorange l that leads to a positioning failure

Figure 36 shows the impact of these biases on the positioning error for 1000 noise realizations.

It can be seen that in the case $\alpha = 1$ (in black) the chosen satellite primarily affects the vertical position error and not the horizontal. It can also be noticed that in this case, 1 in 1000 position fixes is above the VAL which approximately corresponds to the ratio $P_{int}/P_{\text{satellite failure}}$. This illustration confirms that this amplitude of bias on this pseudorange would lead to a positioning failure with a probability equal to the integrity risk.

The following figure also illustrates that a bias on the chosen pseudorange that corresponds to the half of the smallest critical bias could lead to non negligible error in the positioning domain (in green).

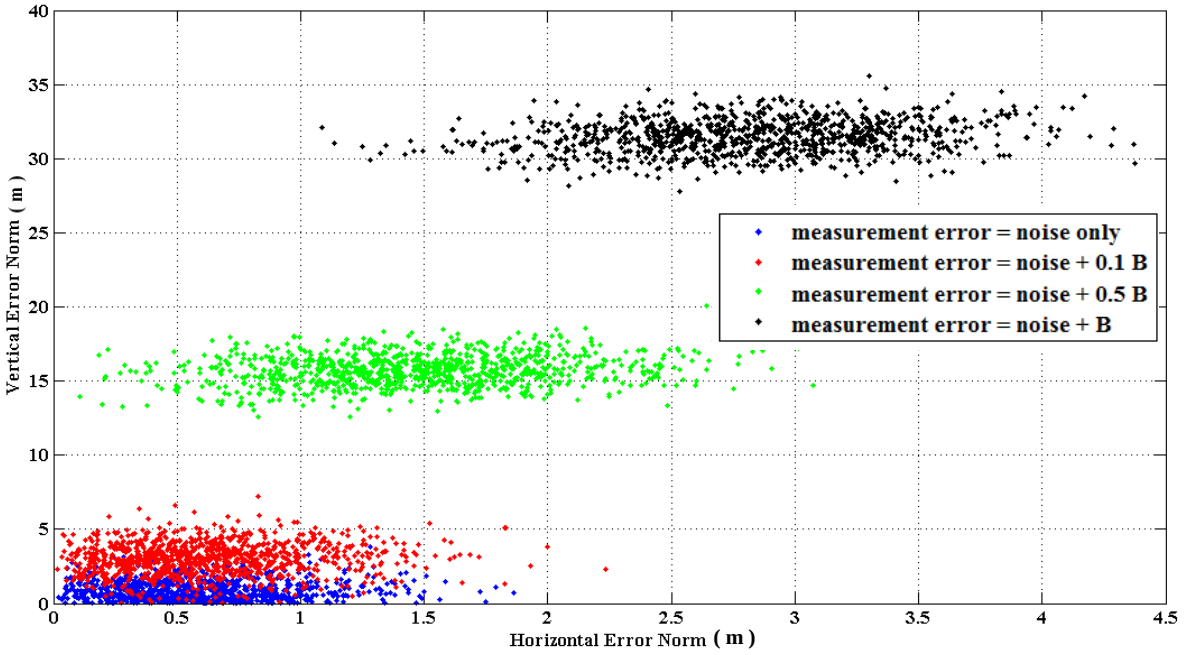

Figure 36 - Positioning error when injecting a bias with various possible amplitudes on the worst satellite pseudorange measurement, 1000 noise realizations in each of the four cases

Three RAIM algorithms' reactions to these errors are represented on the following figures: LSR ones (fig. 37), MSS ones (fig. 38) and snapshot constrained GLR ones (fig. 39). The objective of these figures is only to provide a rough illustration of what happens. They do not intend to be exhaustive. Concerning MSS RAIM method, only the vertical sub - test corresponding to the faulty pseudorange is represented.

As illustrated on the following figures, for fault free case simulations, detection threshold is systematically above the criteria (in blue) for the three considered algorithms.

Whereas, GLR and LSR tests seem to never detect the presence of the additional bias $0{,}1 \times B$ (in red), the MSS vertical criteria corresponding to the faulty measurement detects this type of failure approximately half of the time. It shows the great sensitivity of the MSS test.

As GLR test is explicitly designed to detect single pseudorange failure larger than corresponding critical bias, it systematically does not detect the presence of the additional bias $0{,}1 \times B$ (in red) and most of the time, it does not detect additional bias $0{,}5 \times B$(in green). Thus, GLR test presents some interesting properties, since, strictly speaking, those failures are not dangerous. Moreover, this method also offers the possibility to take into account some nominal biases in its fault free case model. Thus it has great potential for protecting the user from false alarm situations.

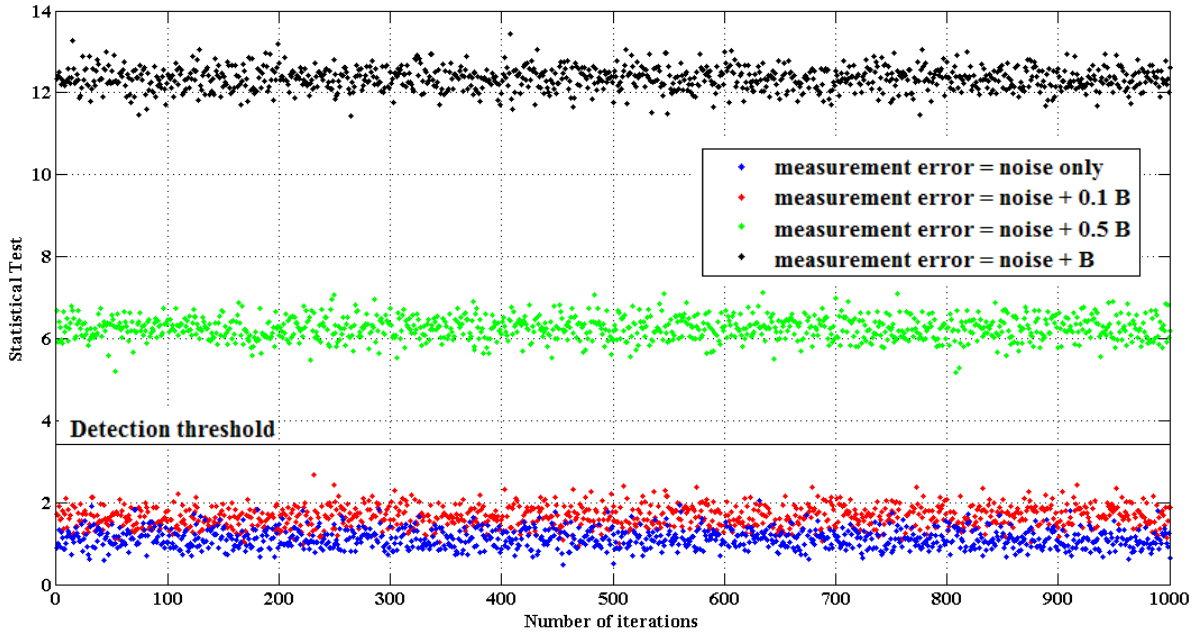

Figure 37 - LSR test performance for LPV 200 requirements when injecting a bias with various possible amplitudes on the worst satellite pseudorange measurement (1000 noise realizations in each of the four cases)

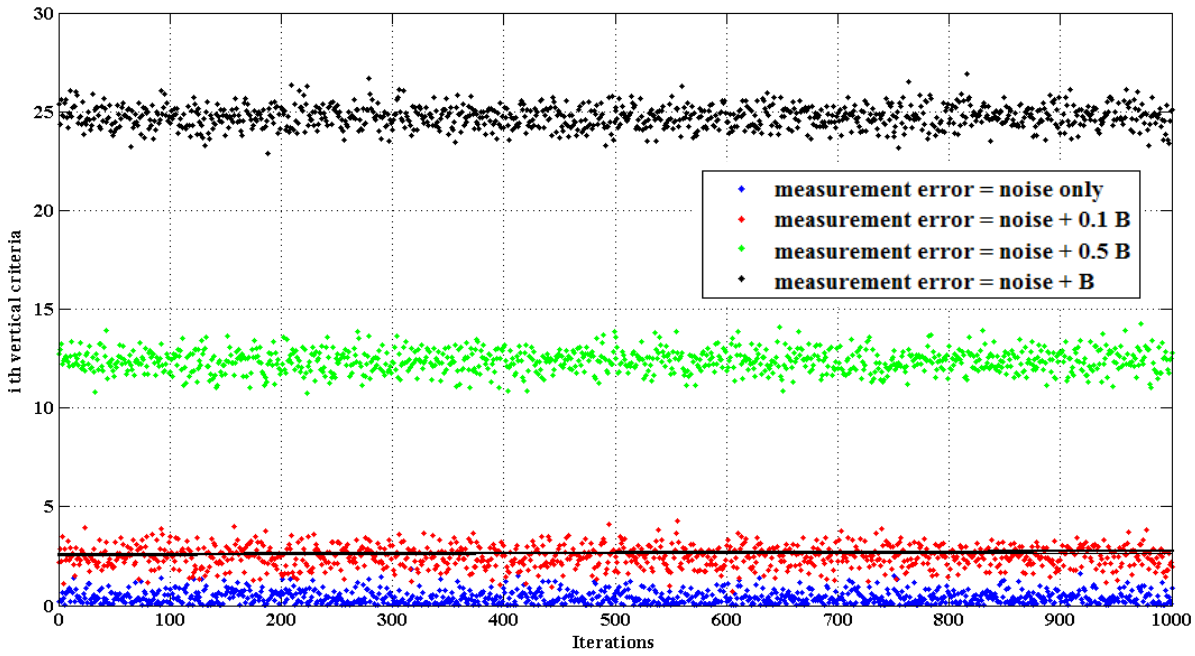

Figure 38 - MSS vertical sub - test performance for LPV 200 requirements when injecting a bias with various possible amplitudes on the worst satellite pseudorange measurement (1000 noise realizations in each of the four cases)

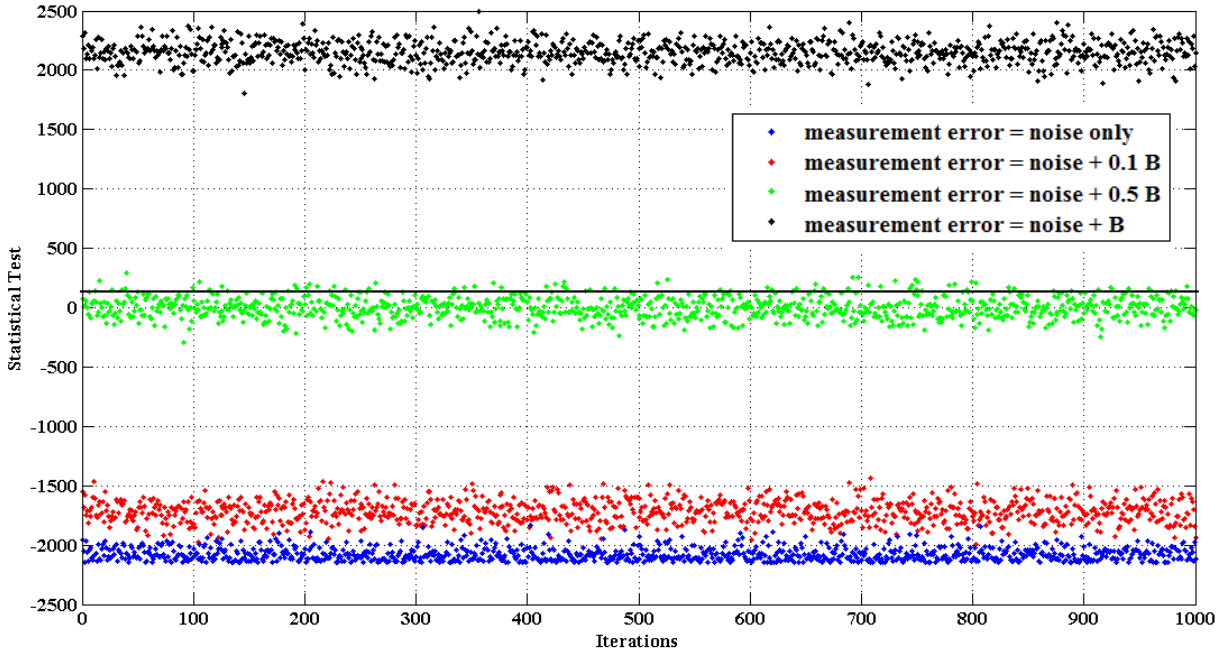

Figure 39 - GLR test performance for LPV 200 requirements when injecting a bias with various possible amplitudes on the worst satellite pseudorange measurement (1000 noise realizations in each of the four cases)

6-1-2 Interference effects

A complete model of pseudo range measurements that includes interference effects has been proposed in chapter 3. But as mentioned in chapter 5, faulty measurements due to local effects such as CW interference have a rate of occurrence that it is not clearly quantified.

RAIM algorithms are usually designed to detect biases that are mainly due to satellite clock failure, not to detect pseudorange error variance jumps, which are the main effect of interference. Fortunately, an interference will not easily lead to an integrity failure. For instance, a CW interference centered in the GNSS frequency band will significantly increase the variance of only a few pseudorange measurement errors. But globally, the average pseudorange measurement error variance will not change a lot and the impact on the positioning error will be limited.

This is illustrated on the following figures. For a given user position and for 1440 different satellites geometries, the error variance of each available pseudorange measurement have been computed assuming:

- a nominal level of noise ($URA = 0.5\ m$) as in section 3-2-1-6
- a nominal level of noise plus a CW on the worst Galileo spectrum line($f_J = 839\ kHz$) with a power of $-156.5\ dBW$ (corresponding to GPS interference mask), as in section 3-3-2-2-2
- a nominal level of noise plus a CW on the worst Galileo spectrum line with a power of $-136.5\ dBW$ (20 dB above this interference mask), as in section 3-3-2-2-2

PRN with a code tracking error envelope value superior to the loss of lock threshold (set to 40 meters) have been removed from the computation. The maximum, minimum and mean values of the 1440 available sets of UERE standard deviation have been represented.

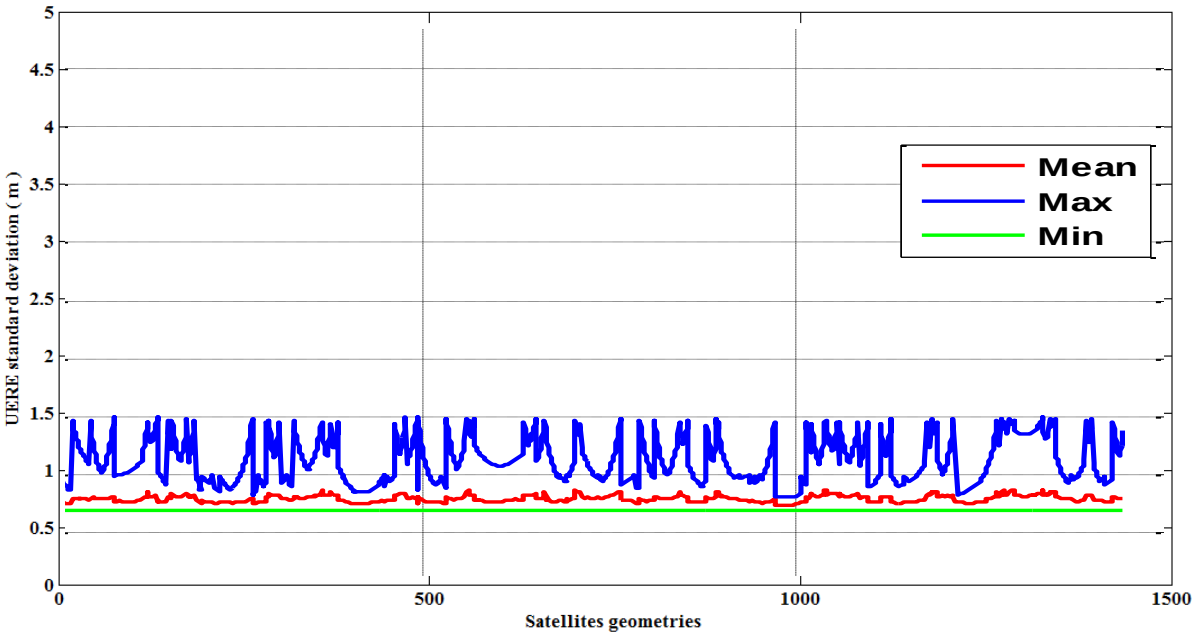

Figure 40 - UERE standard deviation in presence of nominal noise only

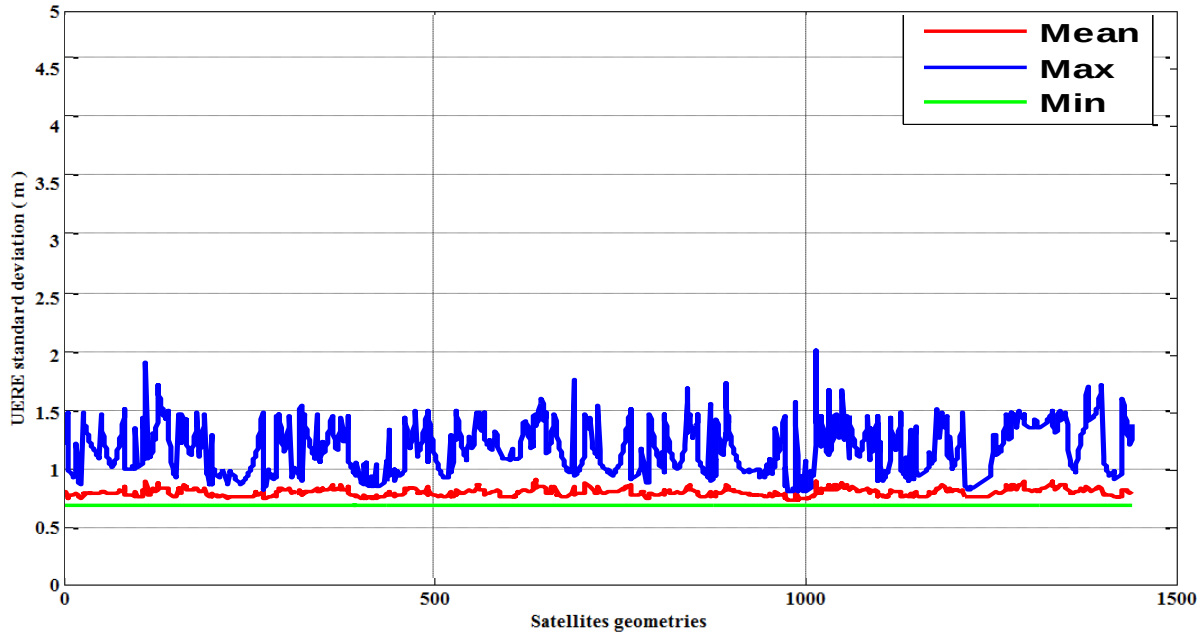

Figure 41 - UERE standard deviation in presence of nominal noise + a CW interference on the worst Galileo spectrum line, power -156.5 dBW

It can be noticed that the presence of a CW within the interference mask has no significant impact on UERE standard deviation (figure 41) comparing to the reference simulation (figure 40). This is due to the fact that worst case C/N_0 have been taken into account for the nominal noise computation (see section 3-2-1-1-2).

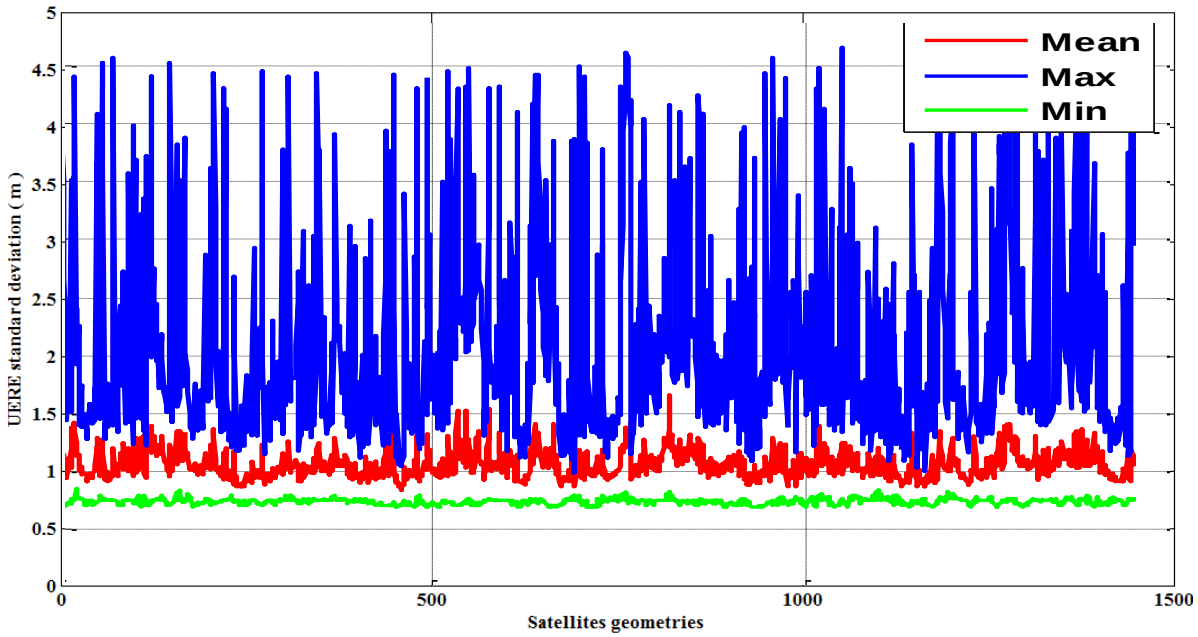

Figure 42 - UERE standard deviation in presence of nominal noise + a CW interference on the worst Galileo spectrum line, power -136.5 dBW

Even for a powerful CW, the UERE standard deviation of the most affected pseudorange measurement does not exceed 5 meters (figure 42). The real issue for integrity monitoring is that, in presence of powerful interference, biases that lead to a positioning failure could be smaller and thus can be more difficult to detect. Therefore, RAIM performance to detect satellite failures could be degraded in presence of interference. Nevertheless, even if its rate of occurrence cannot be precisely quantified, this type of situation is very rare since it supposes simultaneous occurrence of an interference and a satellite failure.

This is why in this study it is considered that interference is equivalent to an increased receiver noise. This effect has been systematically modelled in the fault free case as a drop of the equivalent C/N_0 down to tracking threshold for all satellites.

6-1-3 RAIM performance analysis simulation parameters

RAIM performance evaluation has been conducted thanks to Matlab simulations. Major assumptions that have been made for this evaluation have been previously detailed in chapter 5. Some simulations parameters will remain the same for all simulations that will be presented in this chapter. They are recalled in the following table:

One major aspect is that RAIM algorithms availability has been evaluated only by predicting protection levels or by predicting critical biases probability of missed detection (we haven't try to detect any failure).

Performance evaluation		
User grid, user speed	As in section 5-2 (2520 points), no velocity	
Period and frequency of the test	As in section 5-2	
Specification interpretation: probability of false alarm, probability of missed detection	As in sections 5-5 and 5-6	
Expected performance bounds	APVI	LPV200
HAL/VAL	40 m/ 50 m	40 m/ 35 m
Pmd	As in section 5-6: multiple failure case	
Pfa	1.6×10^{-5} per sample	
Internal RAIM parameters:		
Mask angles	5 ° for GPS and 10° for Galileo	
Number of considered reference frames	One WGS84	
Signals used	L1/L5 for GPS E1/E5b for Galileo	
Standard deviation as a function of the elevation angle	As in section 3-2-1-6 ($URA = 0.85\ m$)	
Receiver smoothing time	100 seconds	
Threat model	As in section 5-6-3	

Table 14 - Simulations parameters

6-2 LSR RAIM Performance

The Least Square Residual method in which the sum of the squares of the pseudorange residuals plays the role of the basic observable has been presented in section 4-2.

The goal of this section is to evaluate LSR algorithm ability to provide integrity monitoring during approaches with vertical guidance operations.

Performance evaluation		
Type of RAIM algorithm	LSR	
Criterion used for availability computation	HPL and VPL HEL and VEL	
Type of implemented function: fault detection, fault detection and identification or fault detection and exclusion	FD and FDE	
Expected performance bounds	APV 1	LPV 200
Internal RAIM parameters:		
Satellite Constellation	GPS + Galileo, GPS, Galileo	
Number of unknowns for position solution estimation	4 and 5	
Consideration of nominal biases	No	

Table 15 - LSR simulations parameters

6-2-1 LSR RAIM performance evaluation considering dual constellation (GPS + Galileo)

Both horizontal and vertical protection levels have been computed for our user grid considering GPS and Galileo constellation. For both APV1 and LPV 200 inputs, the obtained protection level values are very much lower than the corresponding alert limit.

This leads to a LSR detection function availability of 100 % for each point of our user grid for both APV1 and LPV 200 operations.

The same evaluation has been conducted for the corresponding exclusion function and the obtained exclusion level values are very much lower than the corresponding alert limit, leading to a LSR detection / exclusion function availability of 100% for each point of the user grid.

As an illustration of great LSR RAIM performance, the average HPL, VPL, HEL and VEL values for each point of our user grid are represented on the following figures for LPV200 operations.

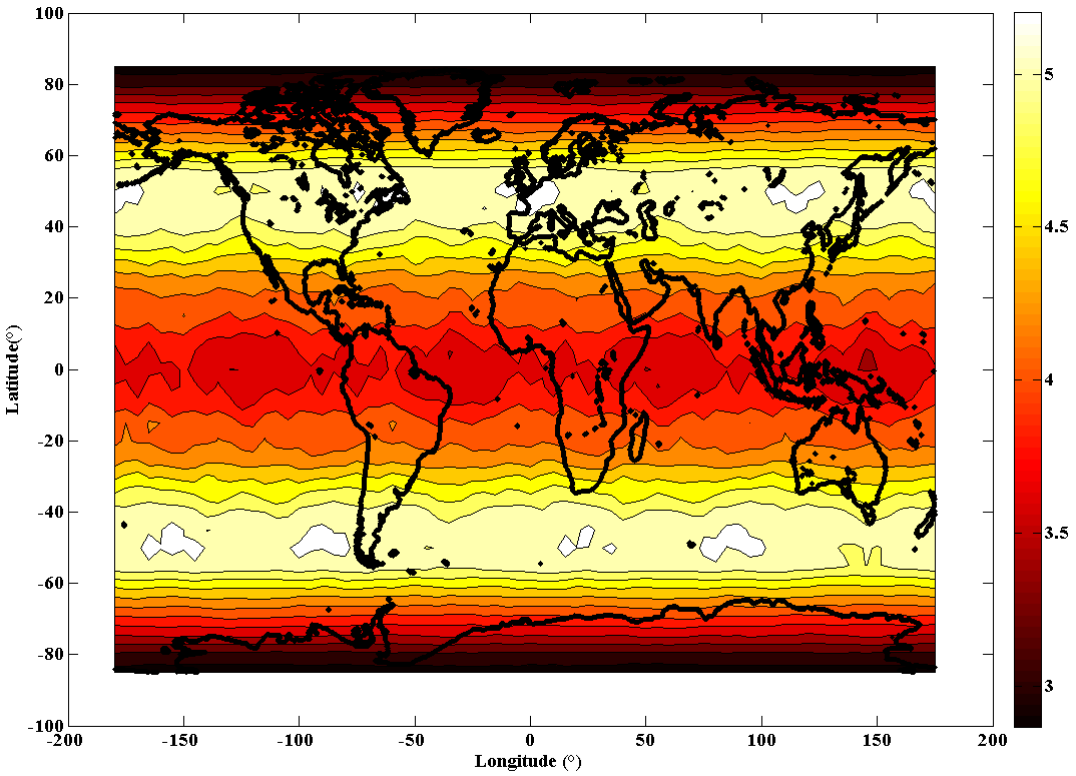

Figure 43 - LSR RAIM – LPV200 operations considering 24 sat GPS constellation + 27 sat Galileo constellation and dual frequency measurements, assuming multiple failures (detecting only single failure): average HPL (in meters) over 3 days simulation

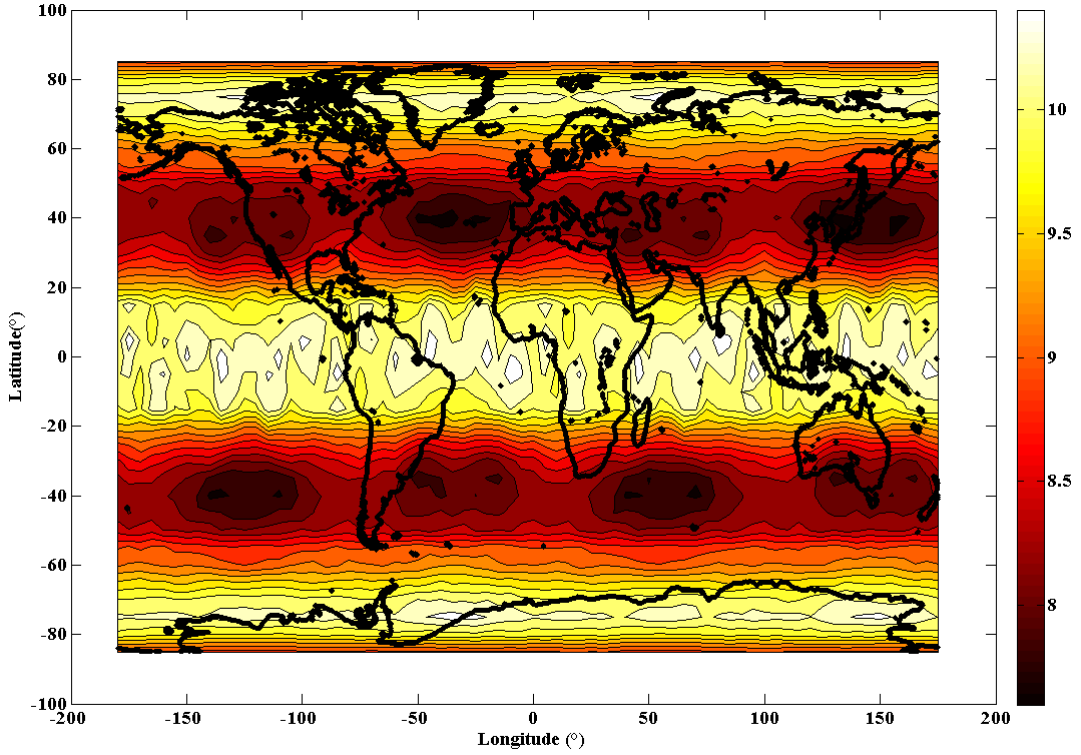

Figure 44 - LSR RAIM – LPV200 operations considering 24 sat GPS constellation + 27 sat Galileo constellation and dual frequency measurements, assuming multiple failures (detecting only single failure): average VPL (in meters) over 3 days simulation

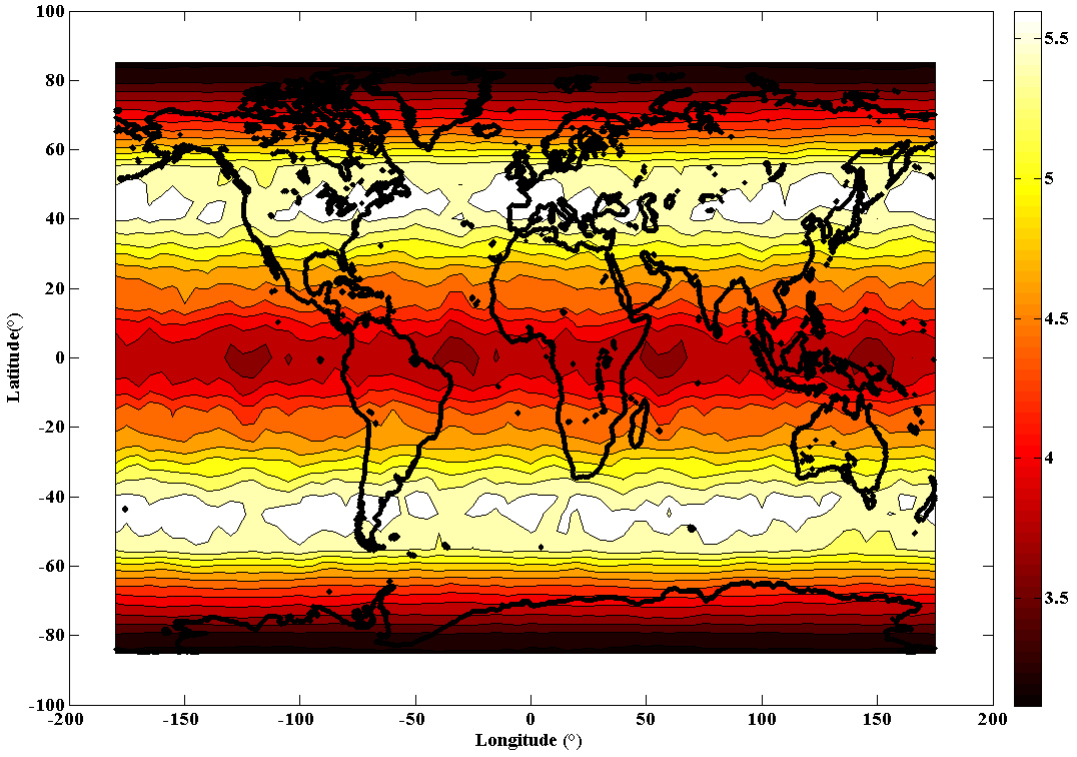

Figure 45 - LSR RAIM – LPV200 operations considering 24 sat GPS constellation + 27 sat Galileo constellation and dual frequency measurements, assuming multiple failures (detecting only single failure): average HEL (in meters) over 3 days simulation

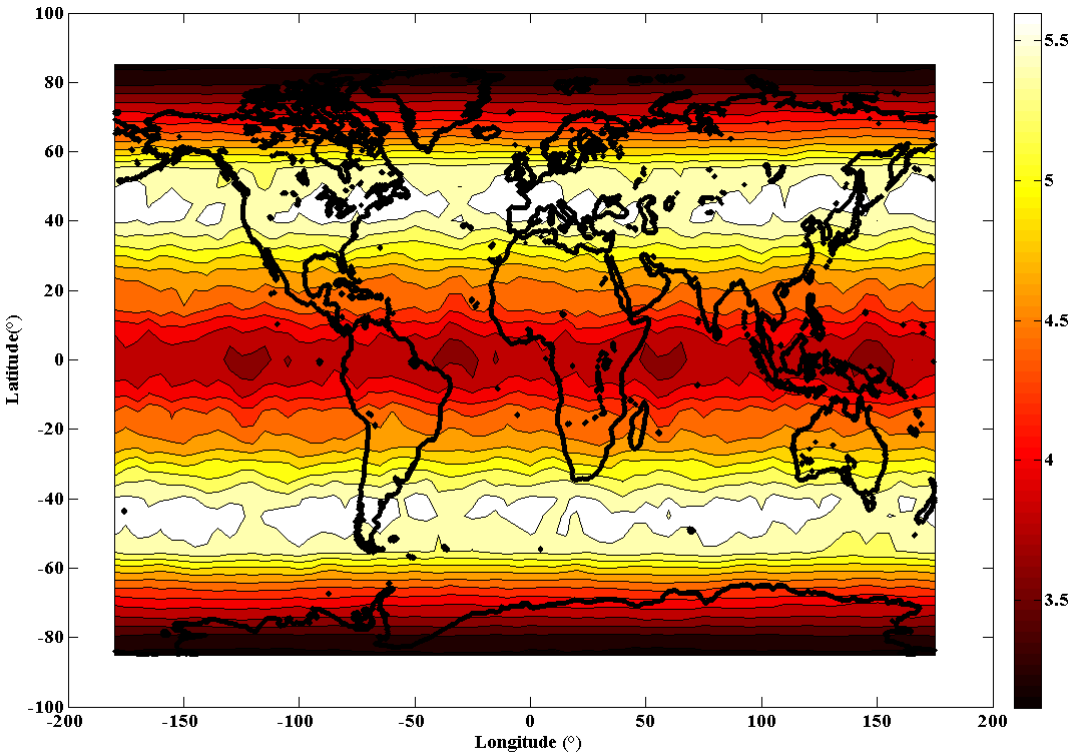

Figure 46 - LSR RAIM – LPV200 operations considering 24 sat GPS constellation + 27 sat Galileo constellation and dual frequency measurements, assuming multiple failures (detecting only single failure): average VEL (in meters) over 3 days simulation

As it has been seen in chapter 3, RAIM performance improvement is due to two main factors:

- augmentation in the number of measurement
- reduction of the nominal pseudorange measurement error due to the use of iono-free measurements, an improved tracking accuracy, a better clock and ephemeris information.

This is why it could be interesting to also evaluate RAIM ability to provide integrity monitoring in approaches with vertical guidance operations considering only one constellation.

6-2-2 LSR RAIM performance evaluation considering only GPS constellation

Results presented in this section are quite pessimistic since a 24-satellites constellation has been considered.

Thus, both horizontal and vertical protection levels have been computed for each point of the user grid considering only GPS constellation and LSR RAIM detection function mean availability is represented on figure 47 for APV1 operations and on figure 48 for LPV200 ones.

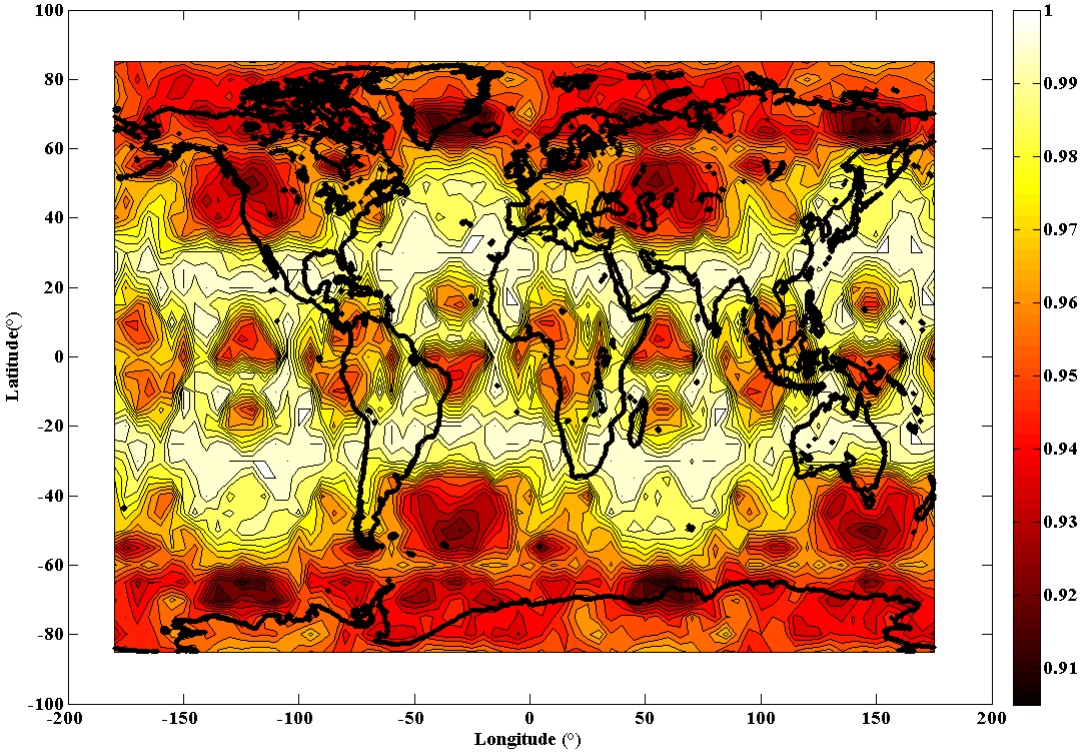

Figure 47 - LSR RAIM – Detection function mean availability for APV1 operations over 1 day simulation considering 24 sat GPS constellation and dual frequency measurements, assuming multiple failures (detecting only single failure)

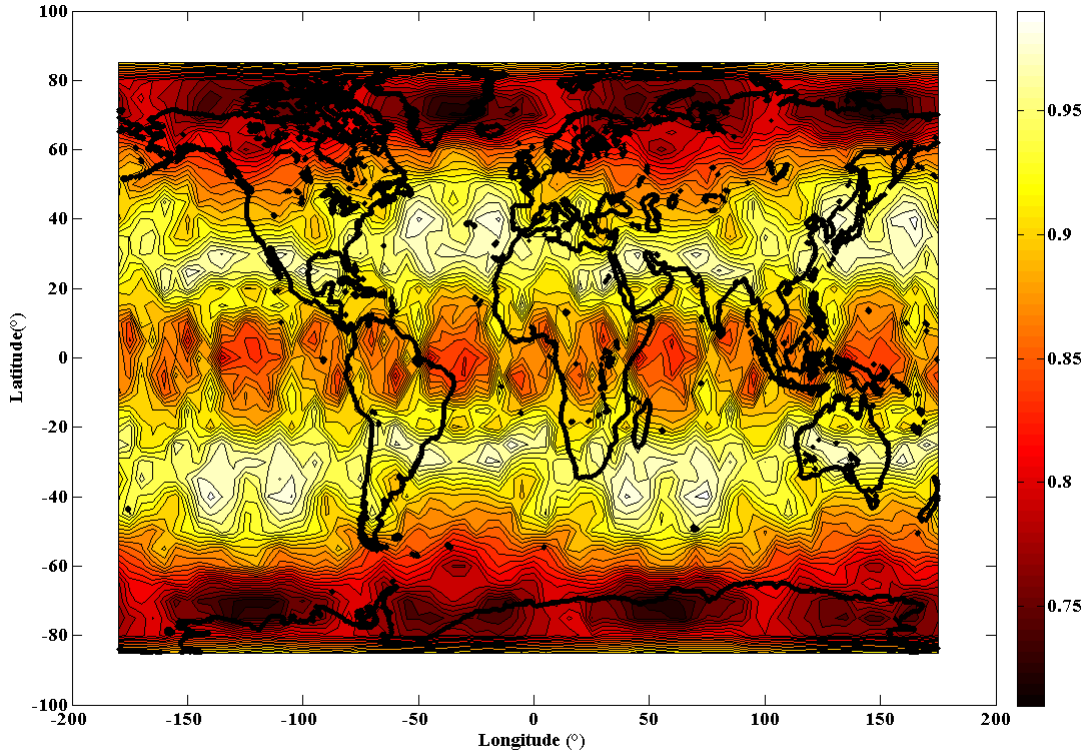

Figure 48 - LSR RAIM – Detection function mean availability for LPV 200 operations over 1 day simulation considering 24 sat GPS constellation and dual frequency measurements, assuming multiple failures (detecting only single failure)

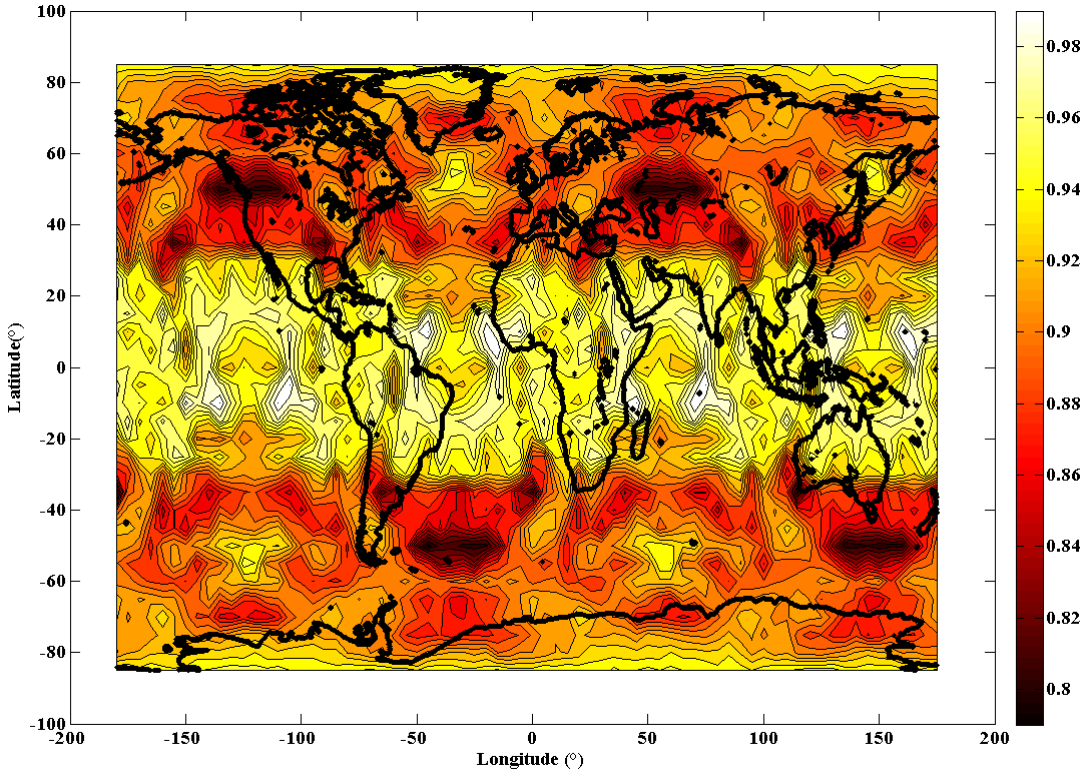

Figure 49 - LSR RAIM - Exclusion function mean availability for APV1 operations over 1 day simulation considering 24 sat GPS constellation and dual frequency measurements, assuming multiple failures (detecting only single failure)

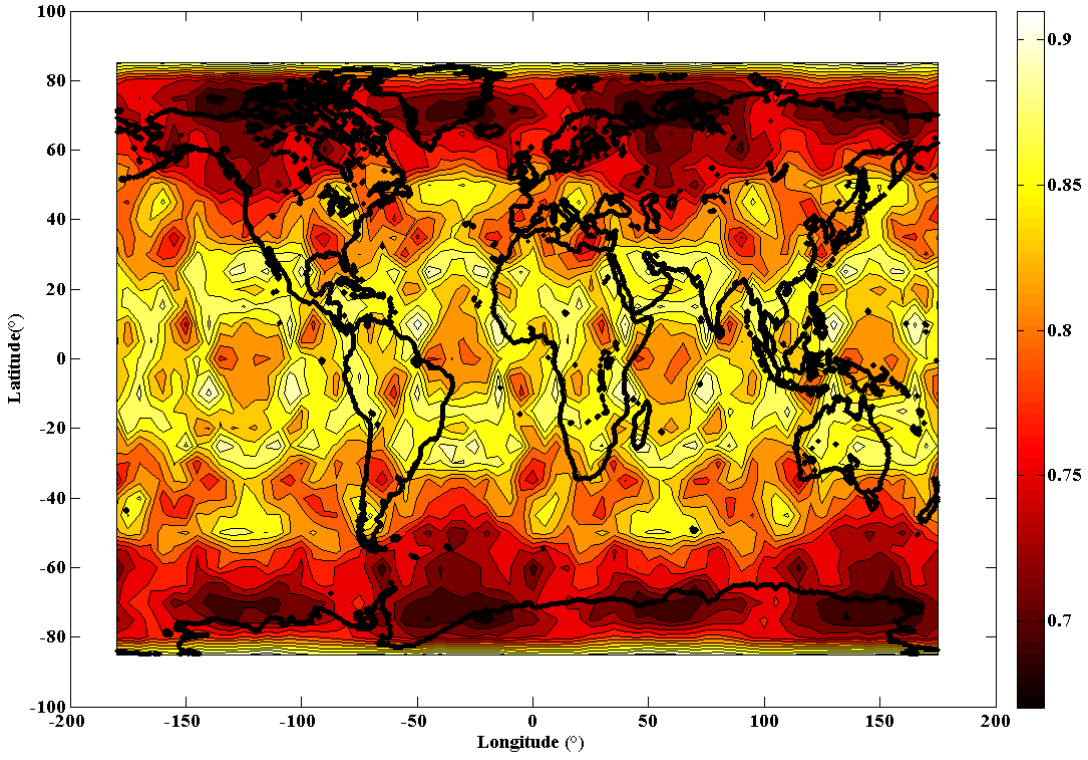

Figure 50 - ExclusionLPV200 operations over 1 day simulation considering 24 sat GPS constellation and dual frequency measurements, assuming multiple failures (detecting only single failure)

6-2-3 LSR RAIM performance evaluation considering only Galileo constellation

The same study has been conducted only considering 27 satellite Galileo constellation. An availability of 100% has been obtained for APV 1 operation for each point of the user grid for LSR RAIM detection function. LSR RAIM detection function mean availability is represented on the following figure for LPV200 operation.

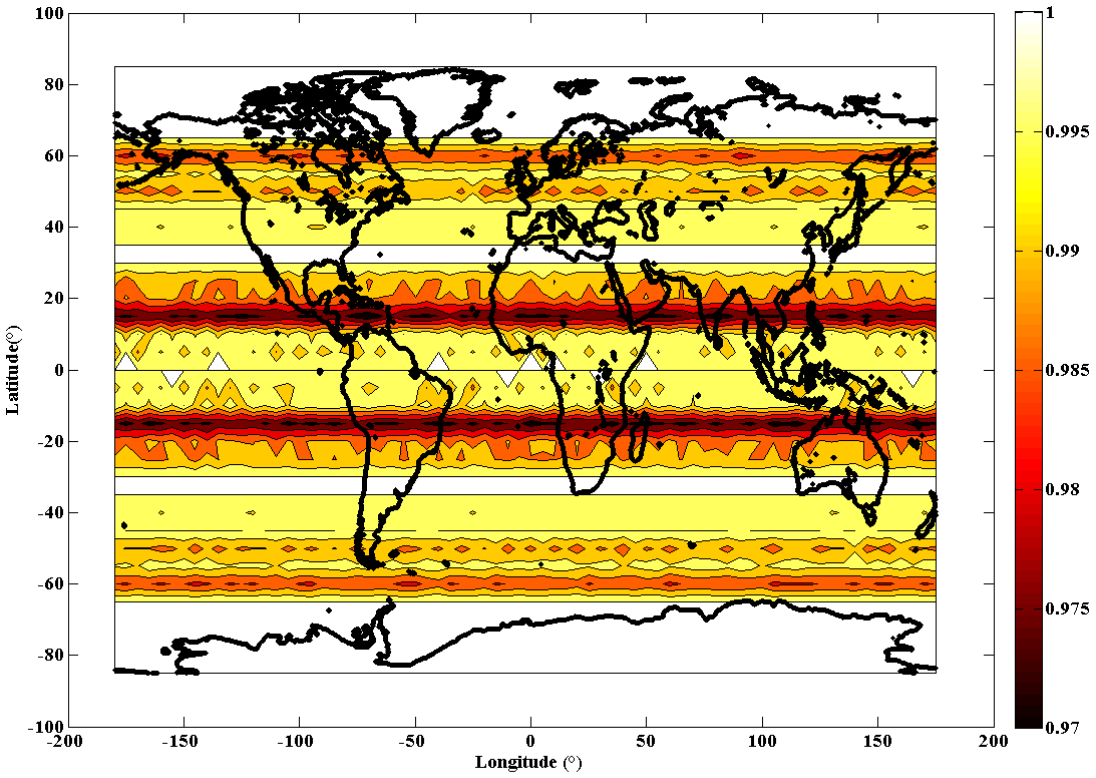

Figure 51 - LSR RAIM – Detection function mean availability for LPV200 operations over 1 day simulation considering 27 sat Galileo constellation and dual frequency measurements, assuming multiple failures (detecting only single failure)

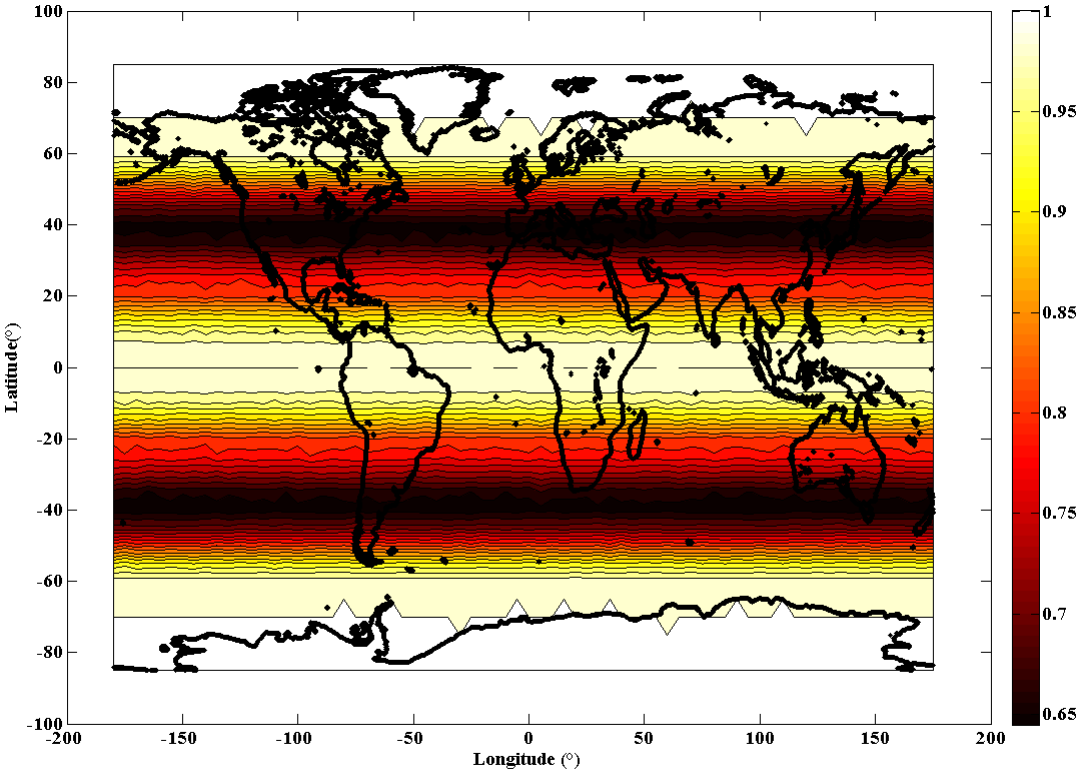

Figure 52 - LSR RAIM – Exclusion function mean availability for APV1 operations over 1 day simulation considering 27 sat Galileo constellation and dual frequency measurements, assuming multiple failures (detecting only single failure)

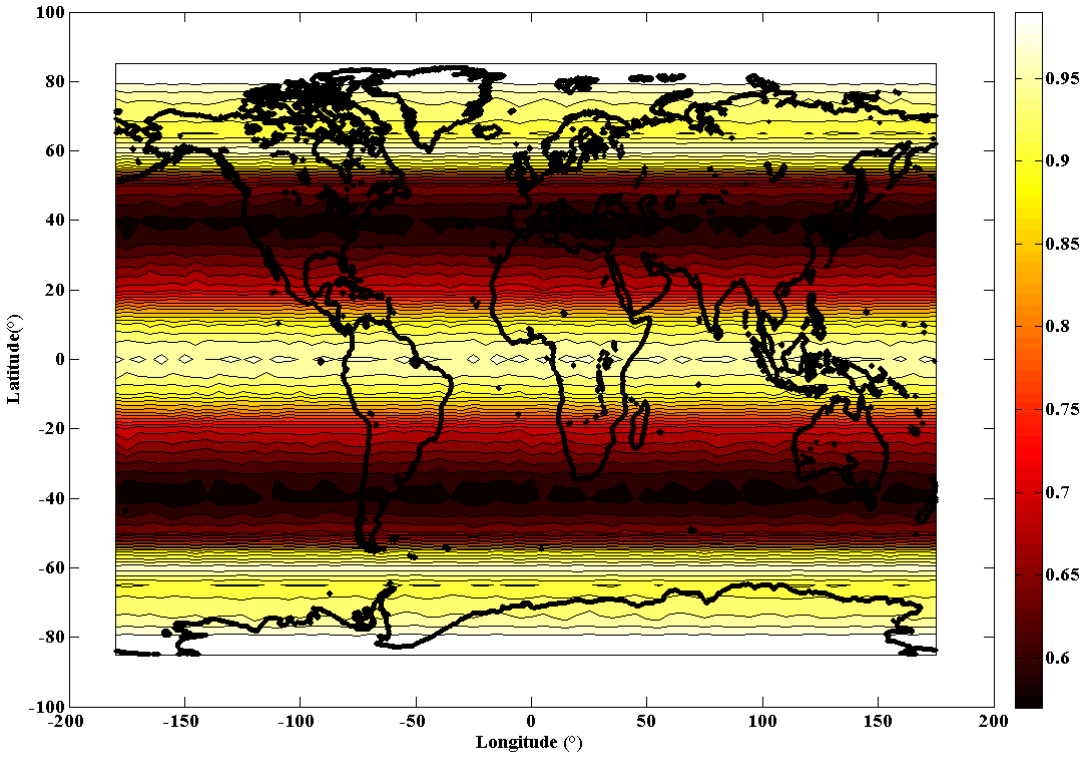

Figure 53 - LSR RAIM – Exclusion function mean availability LPV200 operations over 1 day simulation considering 27 sat Galileo constellation and dual frequency measurements, assuming multiple failures (detecting only single failure)

6-3 MSS RAIM Performance

This Maximum Separation Solution technique is based on the observation of the separation between the position estimate generated by a full-set filter (using all the satellite measurements) and that generated by each one of the subset filters (each using all but one of the satellite measurements).

As detailed in section 4-3, some protection levels computation improvements have been proposed for MSS RAIM. This is why performance is evaluated here computing two types of protections levels (classical ones and proposed ones).

Performance evaluation		
Type of RAIM algorithm	MSS	
Criterion used for availability computation	HPL and VPL	
Type of implemented function: fault detection, fault detection and identification or fault detection and exclusion	FDI	
Expected performance bounds	APV 1	LPV 200
Internal RAIM parameters:		
Satellite Constellation	GPS + Galileo, GPS, Galileo	
Number of unknowns for position solution	4 and 5	
Consideration of nominal biases.	No	

Table 16 - MSS simulations parameters

6-3-1 MSS RAIM performance evaluation considering dual constellation (GPS + Galileo)

As it has been done for LSR RAIM, both horizontal and vertical MSS protection levels have been computed for the user grid considering GPS and Galileo constellation. For both APV1 and LPV 200 inputs, the obtained protection values are very much lower than the corresponding alert limit. This leads to an availability of 100% for each point of our user grid for both APVI and LPV 200 operations.

As an illustration the average HPL and VPL values for each point of the user grid are represented on the following figures for LPV200 operations. It can be seen that the proposed method to compute protection levels leads to smaller values, as expected. This indicates that our proposed method to compute protection levels would lead to better RAIM availabilities in more stringent situations.

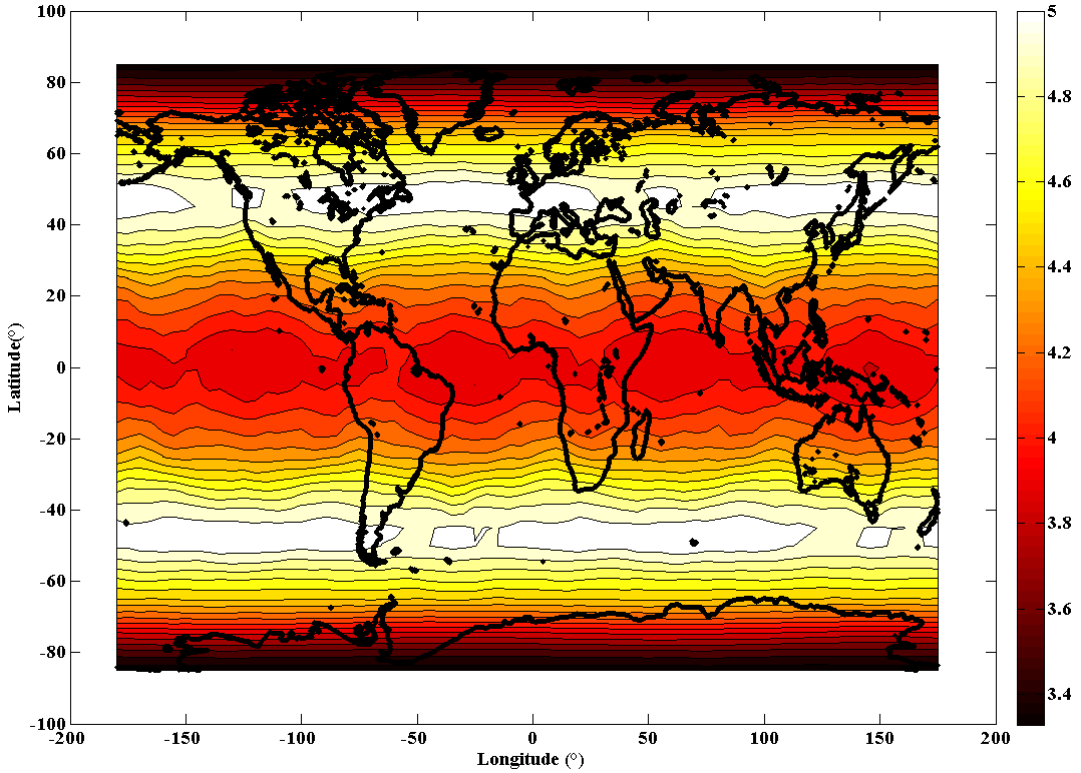

Figure 54 - MSS RAIM – LPV200 operations considering 24 sat GPS const. + 27 sat Galileo const. and dual frequency measurements, assuming multiple failures (detecting only single failure): average HPL (in meters) over 3 days simulation (class.method)

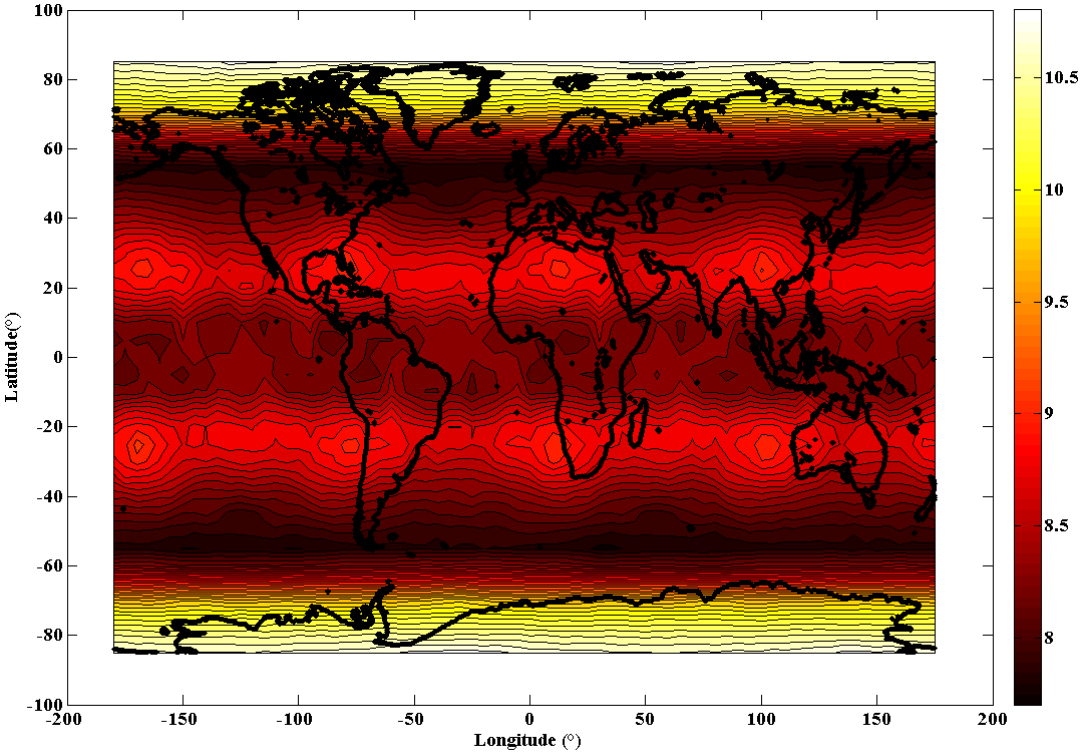

Figure 55 - MSS RAIM - LPVI operations considering 24 sat GPS const. + 27 sat Galileo const. and dual frequency measurements, assuming multiple failures (detecting only single failure): average VPL (in meters) over 3 days simulation (class.method)

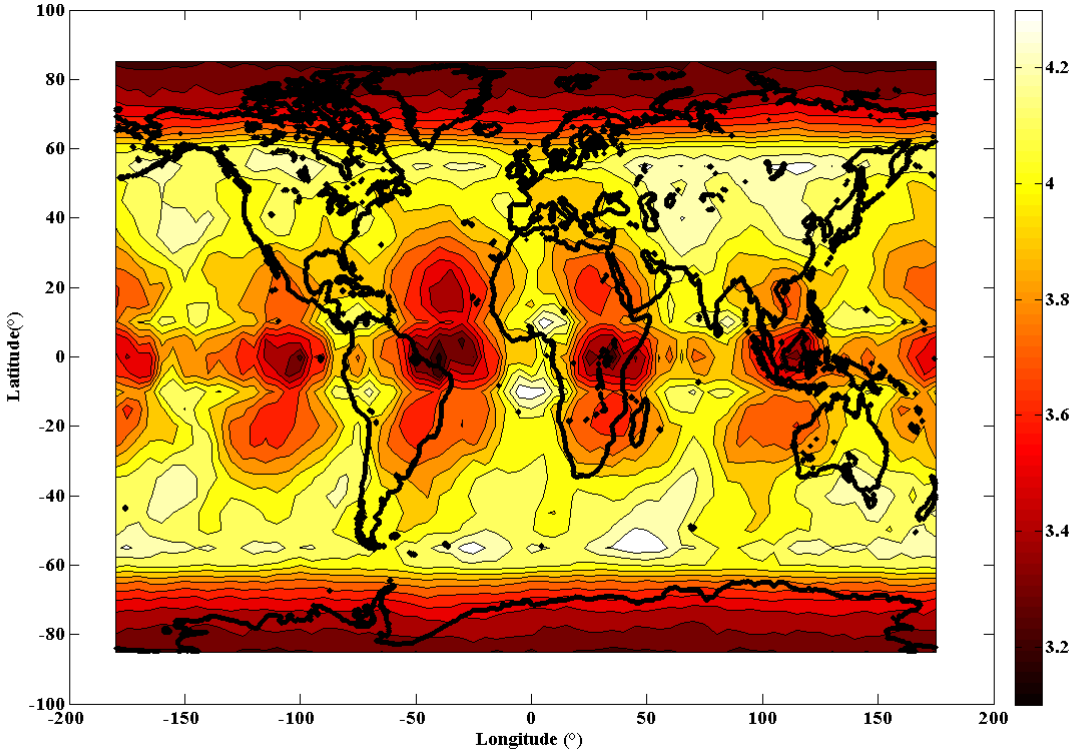

Figure 56 - MSS RAIM - APVI operations considering 24 sat GPS const. + 27 sat Galileo const. and dual frequency measurements, assuming multiple failures (detecting only single failure): average HPL (in meters) over 3 days simulation(prop.method)

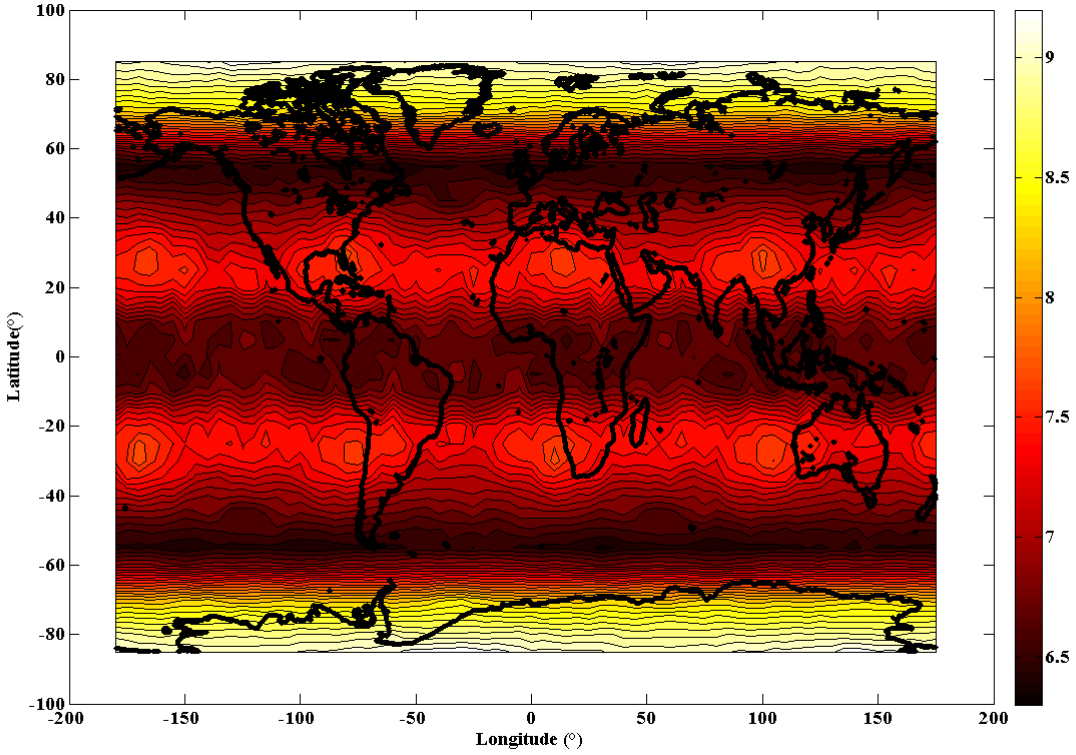

Figure 57 - MSS RAIM - APVI operations considering 24 sat GPS const. + 27 sat Galileo const. and dual frequency measurements, assuming multiple failures (detecting only single failure): average VPL (in meters) over 3 days simulation (prop.method)

6-3-2 MSS RAIM performance evaluation considering only GPS constellation

As it has been done for LSR RAIM simulations, MSS performance has been also evaluated only considering 24 satellites GPS constellation.

Obtained results show that MSS RAIM has globally a better availability than LSR RAIM. It is to be noticed that classical method and proposed one provide approximately the same availability for APVI operations. The proposed method to compute protection levels leads to better MSS RAIM availability for more stringent operations such as LPV200.

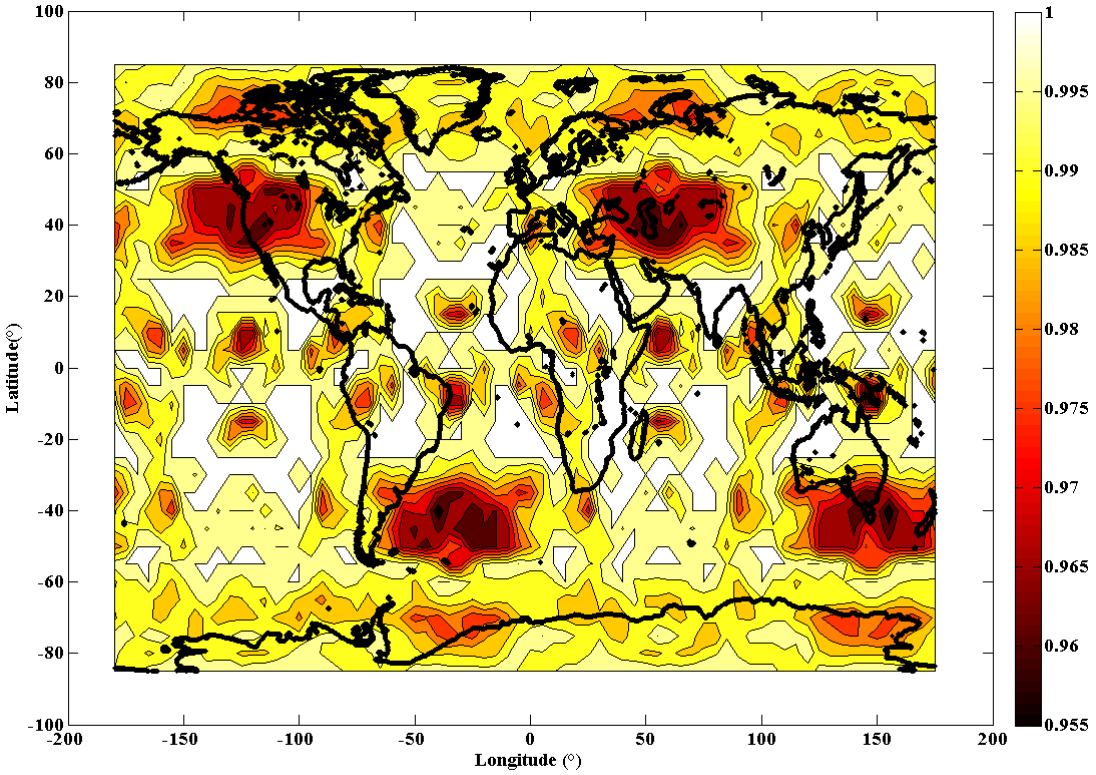

Figure 58 - MSS RAIM - Mean availability for APV1 operations over 1 day simulation considering 24 sat GPS constellation and dual frequency measurements, assuming multiple failures (detecting only single failure) (classical method)

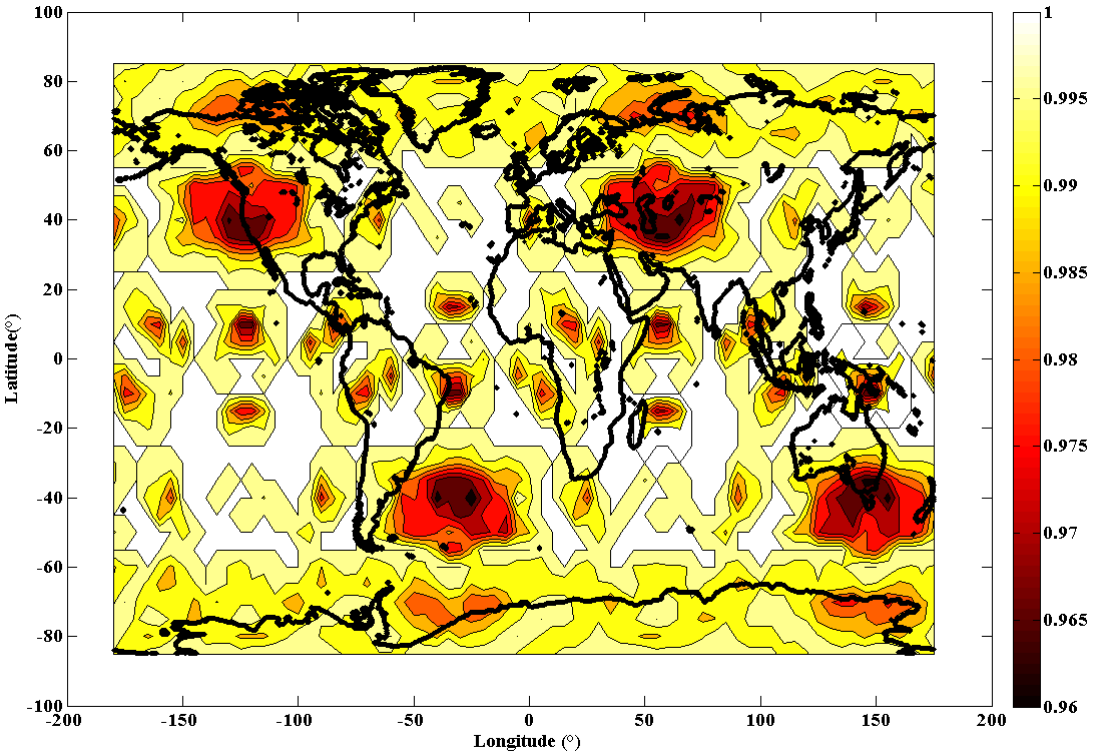

Figure 59 - MSS RAIM - Mean availability for APV1 operations over 1 day simulation considering 24 sat GPS constellation and dual frequency measurements, assuming multiple failures (detecting only single failure) (proposed method)

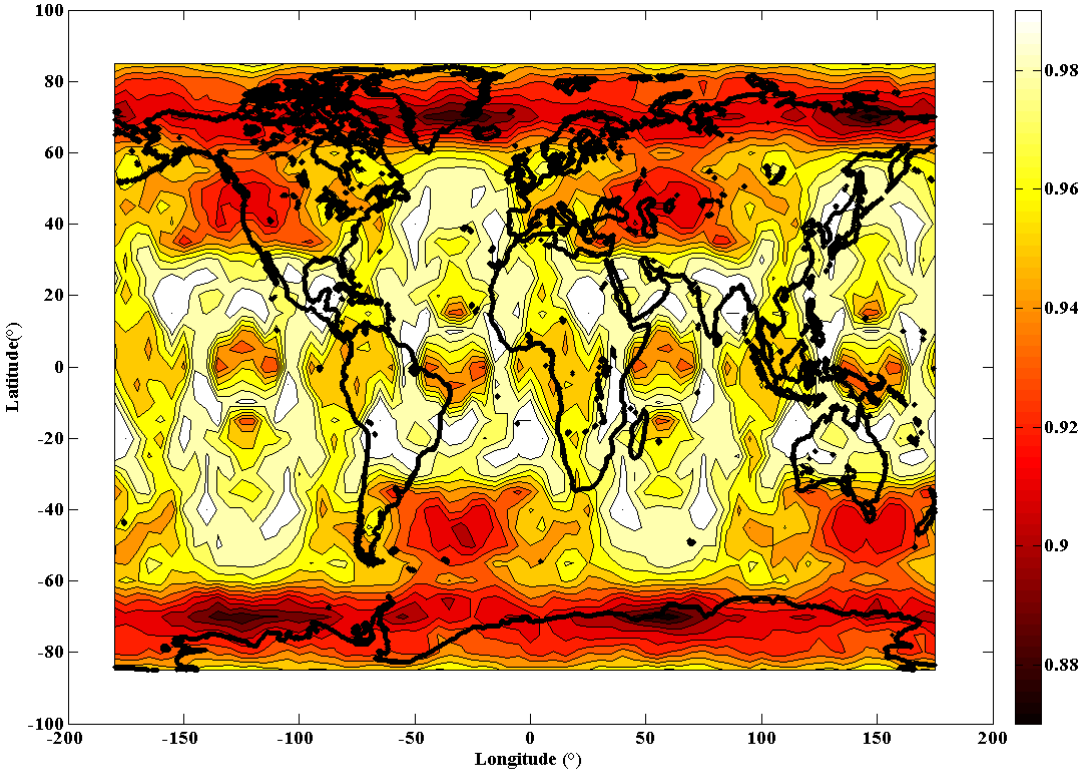

Figure 60 - MSS RAIM - Mean availability for LPV200 operations over 1 day simulation considering 24 sat GPS constellation and dual frequency measurements, assuming multiple failures (detecting only single failure) (classical method)

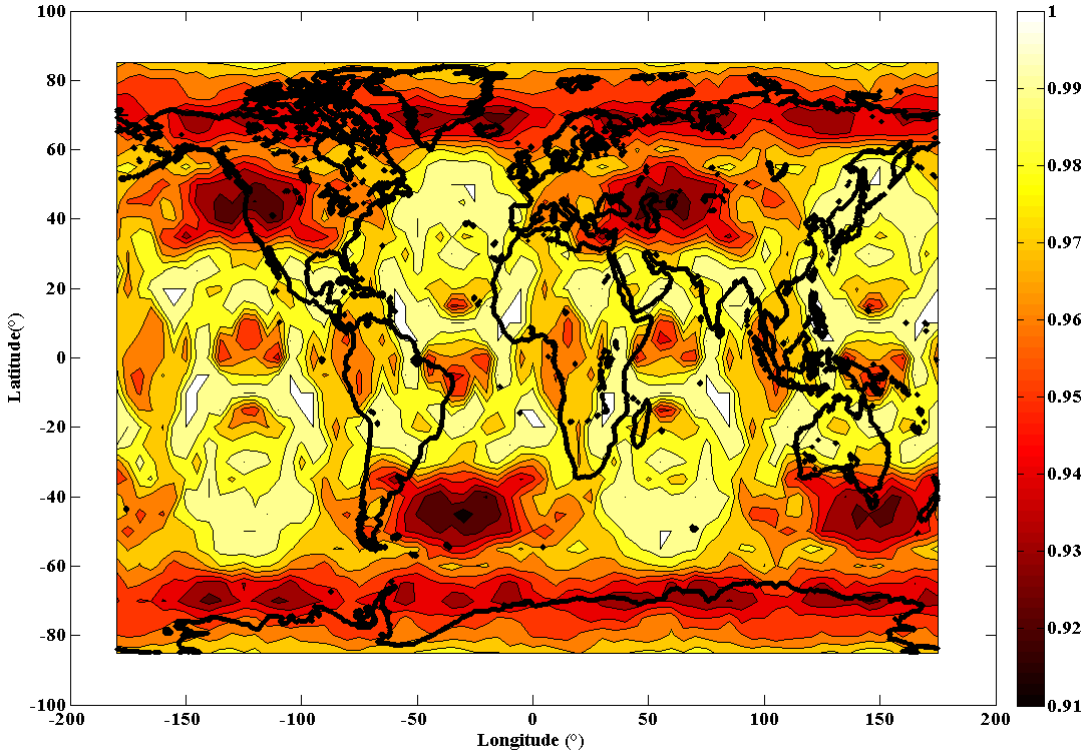

Figure 61 - MSS RAIM - Mean availability for LPV200 operations over 1 day simulation considering 24 sat GPS constellation and dual frequency measurements, assuming multiple failures (detecting only single failure) (proposed method)

6-3-3 MSS RAIM performance evaluation considering only Galileo constellation

The same study has been conducted only considering 27 satellite Galileo constellation and an availability of 100% has been obtained for APV 1 and LPV 200 operations for each point of the user grid.

6-4 GLR RAIM Performance

Previous studies have shown that the sequential constrained GLR based RAIM has no serious advantage over the snapshot one to detect stepwise fault [Nikiforov, 2005]. This is mainly due to the large pseudorange measurements correlation time. Moreover, sequential constrained GLR RAIM performance cannot be predicted easily. Monte Carlo simulations are necessary to evaluate the algorithm ability to detect dangerous biases and thus to protect the user. Future implementation problems are not solved for the moment.

This is why only snapshot constrained GLR RAIM performance evaluation will be presented in this section.

Performance evaluation		
Type of RAIM algorithm	Snapshot constrained GLR	
Criterion used for availability computation	Predicted probability of missed detection	
Type of implemented function: fault detection, fault detection and identification or fault detection and exclusion	FDI	
Expected performance bounds	APV 1	LPV 200
Internal RAIM parameters:		
Satellite Constellation	GPS + Galileo, GPS, Galileo	
Number of unknowns for position solution	4 and 5	
Consideration of nominal biases	No	

Table 17 - GLR simulations parameters

6-4-1 Snapshot constrained GLR RAIM performance evaluation considering dual constellation (GPS + Galileo)

Snapshot constrained GLR performance can't be evaluated the same way as LSR and MSS algorithms since protection levels computation has not been proposed. Nevertheless, the probability of missed detection can be predicted.

Thus APV1 and LPV 200 simulations have been performed considering GPS and Galileo constellation showing an availability of 100% for each point of the user grid for both operations. Indeed the obtained probabilities of missed detection were very much lower than the required one for each point of the user grid.

6-4-2 Snapshot constrained GLR RAIM performance evaluation considering GPS constellation only

As it has been done for other RAIM algorithms, GLR performance has been also evaluated considering 24 satellites GPS constellation only. The obtained average availabilities for APV1 and LPV 200 operations are represented on the following figures.

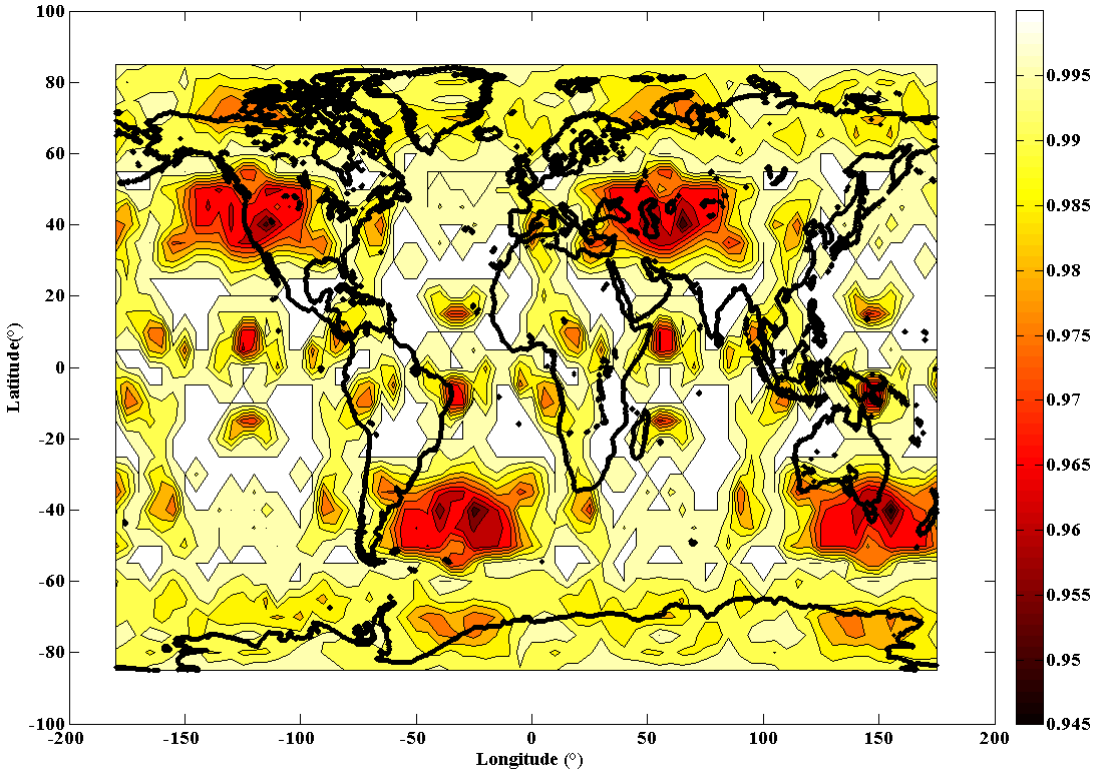

Figure 62 - GLR RAIM - Mean availability for APV1 operations over 1 day simulation considering 24 sat GPS constellation and dual frequency measurements, assuming multiple failures (detecting only single failure)

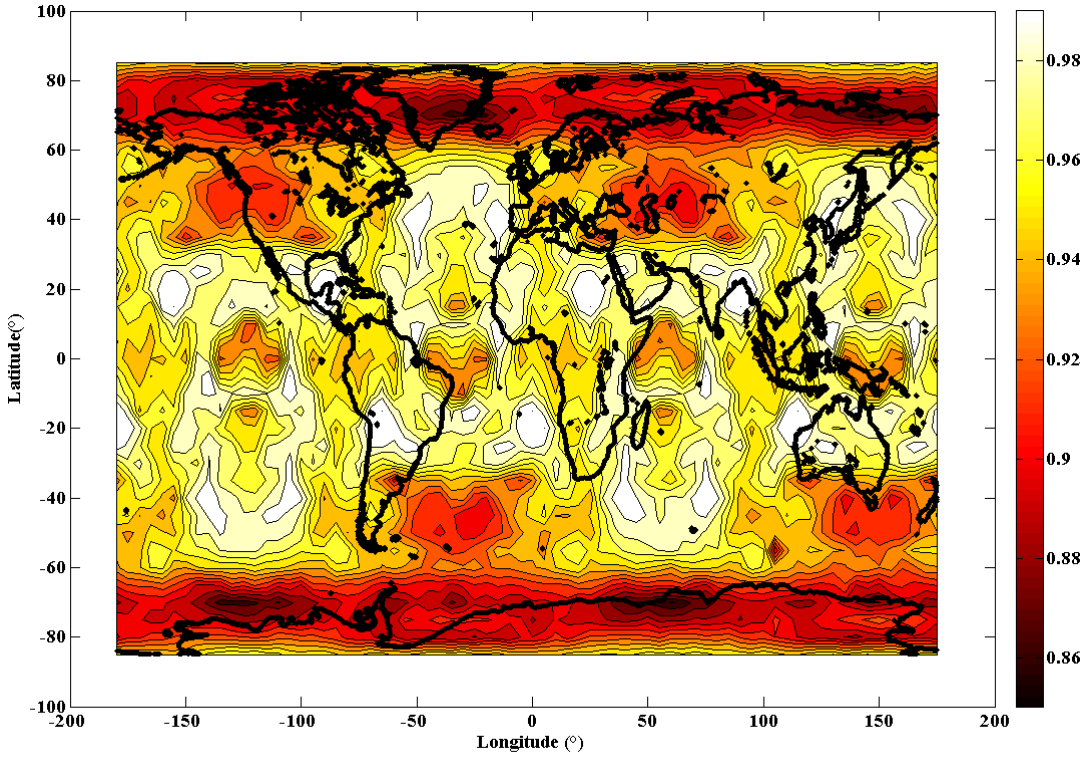

Figure 63 - GLR RAIM - Mean availability for LPV200 operations over 1 day simulation considering 24 sat GPS constellation and dual frequency measurements, assuming multiple failures (detecting only single failure)

6-4-3 Snapshot constrained GLR RAIM performance evaluation considering Galileo constellation only

The same study has been conducted only considering 27 satellite Galileo constellation.

An availability of 100% has been obtained for APV 1 operations for each point of the user grid

Mean availabilities obtained for LPV 200 operations are represented below.

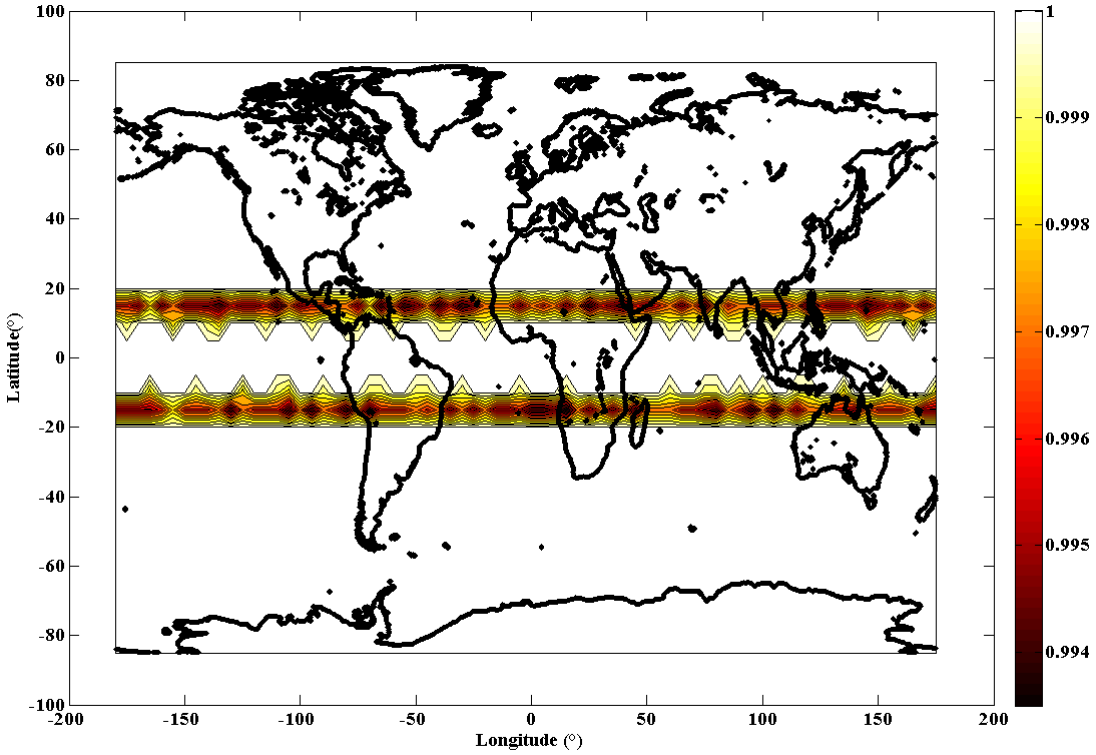

Figure 64 - GLR RAIM - Mean availability for LPV200 operations over 1 day simulation considering 27 sat Galileo constellation and dual frequency measurements, assuming multiple failures (detecting only single failure)

6-5 Synthesis

The objective of the first part of this chapter was to illustrate the performance of different RAIM algorithms when injecting a bias with various possible amplitudes. The great robustness of the GLR test toward errors that do not lead to a positioning failure is to be noticed.

An illustration of the effect of CW interference on the accuracy of pseudorange measurement has also been given, and their effect on the performance of RAIM has been discussed. It has been seen that a CW interference centered in the GNSS frequency band has a limited impact on the positioning error. In fact, a single interference will not easily lead to an integrity failure. The real issue for integrity monitoring is that, in presence of powerful interference

(more than 20 dB above the mask), biases that lead to a positioning failure can be smaller and thus can be more difficult to detect. In this situation, which is very rare since it suppose simultaneous occurrence of a powerful interference and a satellite failure, RAIM performance to detect dangerous biases could be degraded.

Then, numerous Matlab simulations have been conducted to evaluate RAIM ability to provide integrity monitoring during approaches with vertical guidance operations.

Main assumptions that have been made for these evaluations are detailed and explained in chapter 5 and are listed below:

- A user grid with a latitude step and a longitude step of 5° representing a total amount of 2520 positions has been considered (see section 5-1).
- Values have been evaluated every 4 minutes over 3 days simulations for dual constellation simulations and every minute over 1 day simulation for single constellation simulations (see section 5-2).
- A 10° mask angle has been used for Galileo satellites and a 5° mask angle has been used for GPS ones (see section 5-3-2).
- A 24 satellites GPS constellation and a 27 Galileo satellite have been considered (see section 5-3-1).
- Signals used were L1/L5 for GPS and E1/E5b for Galileo (see section 3-2-1).
- Multiple failures have been into account by allocating a smaller integrity risk to the required probability of missed detection computation (see section 5-6).
- Detection function availability has been obtained by comparing computed protection levels with alert limit requirement for LSR and MSS RAIM. For GLR algorithm, it has been obtained by comparing predicted probability of missed detection with required one (see 5-7-1).
- Detection/Exclusion function availability have been obtained by computing detection function availability assuming that the most important satellite has failed (see section 5-7-2)
- Nominal biases have not been taken into account (see section 6-1-3)
- For dual constellation simulations, four and five unknowns have been taken into account in the navigation solution and in RAIM equations (see section 5-4)

Main simulation results obtained in this chapter are summarized in the following tables.

4 unknowns	LSR	MSS		GLR
		Proposed method	Classical method	
APV I	100 %	100 %	100 %	100 %
LPV200	100 %	100 %	100 %	100 %

Table 18 - FD RAIM mean availability worldwide over 3 days simulations considering 24 sat GPS + 27 sat Galileo constellations (4 unknowns) and dual frequency measurements, assuming multiple failures (detecting only single failure)

5 unknowns	LSR	MSS		GLR
		Proposed method	Classical method	
APV I	100 %	100 %	100 %	100 %
LPV200	100 %	100 %	100 %	100 %

Table 19 - FD RAIM mean availability worldwide over 3 days simulations considering 24 sat GPS + 27 sat Galileo constellations (5 unknowns) and dual frequency measurements, assuming multiple failures (detecting only single failure)

	LSR	MSS		GLR
		Proposed method	Classical method	
APV I	96.67 %	99.44 %	99.22 %	99.21 %
LPV200	87.87 %	97.05 %	95.53 %	94.75 %

Table 20 - FD RAIM mean availability worldwide over 1 day simulations considering 24 sat GPS constellation and dual frequency measurements, assuming multiple failures (detecting only single failure)

	LSR	MSS		GLR
		Proposed method	Classical method	
APV I	100 %	100 %	100 %	100 %
LPV200	99.52 %	100 %	100 %	99.98 %

Table 21 - FD RAIM mean availability worldwide over 1 day simulations considering 27 sat Galileo constellation and dual frequency measurements, assuming multiple failures (detecting only single failure)

	Dual Constellation *4 unknowns*	Dual Constellation *5 unknowns*	24 sat GPS constellation	27 sat Galileo constellation
APV I	100 %	100 %	91.76 %	88.25 %
LPV200	100 %	100 %	80.91 %	81.43 %

Table 22 - LSR FDE RAIM mean availability worldwide over 3 days simulations considering 24 sat GPS + 27 sat Galileo constellations and dual frequency measurements, assuming multiple failures (detecting only single failure)

It can be seen that considering 5 unknowns instead of 4, in position estimation and in RAIM algorithm design, do not degrade dual constellation GPS/Galileo RAIM availability. This is due to the great number of available measurements.

The main result is that considering both GPS and Galileo constellations, with dual frequency measurements, assuming multiple failures (detecting only single failure), the three studied RAIM techniques can provide integrity monitoring for both APV I and LPV200 (VAL=35m) operations.

Single constellation performance is not as good as the one obtained for dual constellation, especially when only a 24-satellite constellation is considered. In particular, LSR failure detection/exclusion function mean availability seems to be not sufficient to consider 24-sat GPS + RAIM or 27-sat Galileo + RAIM as a sole means of navigation for approaches with vertical guidance operations.

A 10 meter Vertical Alert Limit could be proposed for LPV200 operations. Considering such a stringent requirement, it would not be possible to only consider major service failure events in our threat model. Therefore, we cannot just compare the obtained LPV 200 VPL values with a 10 meter VAL to predict RAIM availability. Setting LPV200 VAL to 10 meters would cause more important change in RAIM design. This is why this study does not address LPV200 (VAL=10 m) RAIM performance evaluation.

Chapître 7

Conclusions et travaux futurs

Ce chapître présente les conclusions des études des chapitres précédents et suggére quelques perspectives pour de futures études.

Un modèle complet de mesure de pseudodistance, incluant les effets des interferences et les pannes satellitaires a été proposé. Le calcul de la variance de l'erreur de pseudo distance au niveau utilisateur a été développé et la contribution du bruit récepteur particulièrement détaillée. On a pu ainsi constater que l'amélioration de la qualité des mesures (bi fréquences, signaux de positionnement améliorés…) a fait diminuer de manière significative la variance de l'erreur de mesure au niveau utilisateur (UERE). Un écart type d'environ 1 mètre a en effet été obtenu. Dans la mesure où l'UERE est un paramètre préponderant en ce qui concerne la qualité du positionnement et les performances du controle d'intégrité, une grande disponibilité pouvait être attendue pour les approches à guidage vertical. Le modèle avec panne a considéré les pannes satellitaires ainsi que les phénomenes d'interference. En particulier, l'effet des interférences large bande et CW a été étudié.

Le concept de plus petit biais sur une mesure de pseudodistance conduisant à une erreur de position a été développé. Il est basé sur le fait que le contrôle d'intégrité exige que le système de navigation détecte la présence d'erreurdont la taille est inacceptable pour la phasede vol envisagée. Par conséquent, seules les fautes conduisant à une erreur de position (horizontale ou verticale) supérieure à la limite d'alerte correspondant ont besoin d'être détectée.

Trois types d'algorithme RAIM ont été étudiés dans cette thèse. La méthode des moindres carrés où la sommes des carrés des résidus des pseudodistances constitue le test statistique. La méthode de séparation des solutions basée sur la comparaison de l'estimée de position obtenue en utilisant toutes les mesure satellitaires disponibles (filtre principal) et celles générées par chacun des sous filtres utilisant toute les mesures à l'exception d'une seule a été présentée et une nouvelle methode de calcul des niveaux de protection est proposée. Une nouvelle méthode basée sur le test du rapport de vraisemblance généralisée et plus particulièrement sur le test du rapport de vraisemblance généralisée contraint a été développée. Plusieurs de ses implémentations ont été présentées. Tout d'abord une méthode snapshot ne prenant pas en compte les biais nominaux mais pour laquelle l'expression analytique d'un seuil satisfaisant le taux de fausse alerte requis et une prédiction de la probabilité de détection manquée sont proposées.Une implémentation prenant en compte les biais nominaux ainsi que deux implémentations séquentielles (dont une adaptation pour la détection de pannes de type échelon plus rampe) ont également été présentées.

La manière dont les exigences aviation civile et le modèle d'erreur sont interprétés afin de constituer les paramètres d'entrée des algorithmes RAIM a été discutée. Une revue détaillée des hypothèses qui ont été faite afin d'évaluer les performances des algorithmes RAIM a

également été effectuée. La manière dont les probabilités de fausse alarme et de detection manquée requises sont calculées a particulièrement été détaillée.

Il a été montré que dans le cas d'une panne unique en considérant les constellations GPS et Galileo l'amplitude des biais sur les mesures de pseudodistance conduisant à une erreur de positionnement appartient systèmatiquement à la catégorie « major service failure » que ce soit pour l'APV I ou LPV200. Ainsi même si les phasesde vol visées sont caractérisées par de plus petits niveaux d'alerte (horizontaux ou verticaux) comparés aux approches de non précision, cet effet est compensé par le grand nombre de mesures de pseudodistance disponibles. Cela a pour effet de sérieusement diminuer l'impact de la panne d'un satellite sur l'erreur globale de position. Ainsi seule les « major service failures » ont été prises en compte dans le cas d'une panne unique.

Le cas de pannes multiples a été également été traité dans cette thèse. Il a été décidé de tirer parti de la rareté de ces pannes multiples. Il est en effet possible de ne pas chercher à les détecter en fixant la probabilité de détecter une perte d'intégrité due à une panne multiple à zero (P_{md} correspondante égale à un). Cela entraine des probabilités de détection manquée pour les pannes uniques plus faibles mais permet l'utilisation des differents algorihtmes conçus pour la détection de pannes uniques.

Les disponibilités des algorithmes RAIM basés sur les méthodes LSR, MSS et GLR ont été calculées pour les approches de type APVI et LPV200 en considérant les mesures GPS L1/L5 et Galileo E1/E5b.

Une disponibilité de 100 % a été obtenue pour les trois algorithmes, en considerant à la fois GPS et Galileo, des mesures bi frequences, prenant en compte les pannes multiples (detectant que les pannes uniques), pour les approches APV I et LPV200 (VAL=35m). Pour les RAIM LSR et MSS, tous les xPL calculés étaient inférieurs aux niveaux d'alerte correspondants pour tous les points de la grille utilisateur et à chaque époque. La probabilité de detection manquée prédite du GLR contraint était systematiquement inférieure à la probabilité de detection manquée requise. La disponibilité de la fonction de detection/exclusion de pannes du RAIM LSR a également été evalué à 100 % pour chaque point de la grille utilisateur.

Etant donné que la manière dont les mesures de pseudodistance GPS et Galileo vont être combinées dans les récepteurs aviation civile n'est pas définie, la capacité du RAIM à assurer le contrôle d'integrité pour les approches à guidage vertical en ne considerant qu'une seule constellation a également été étudiée.

Les résultats obtenus sont particulierement pessimistes pour GPS, puisquee une constellation comprenant seulement 24 satellites a été considérée pour les simulations alors que plus de satellites peuvent être envisagés pour la future constellation GPS. On a ainsi vu qu'en considerant une constellation de 24 satellites GPS, le RAIM ne pouvait pas assurer le contrôle d'integrité pour les approches à guidage vertical avec une disponibilité suffisante. Même si des résultats prometteurs ont été obtenus pour la disponibilité de la fonction de détection en considérant une constellation de 27 satellites Galileo, une disponibilité de 88.2 % pour l'APVI et de 81.4 % pour la LPV200 de la fonction de détection/exclusion du RAIM LSR ce qui n'est pas suffisant pour avoir Galileo + RAIM comme moyen principal de navigation.

Il faut rappeler que tous ces résultats ont été obtenus en supposant des mesures de pseudodistance de bonne qualité.

Quelques pistes peuvent être évoquées concernant de futurs travaux.

La détection des pannes multiples peut être adressée d'une autre manière que celle proposée dans cette thèse, c'est à dire en essayant de les détecter. A cet effet, les algorithmes Maximum Solution Separation RAIM, DT-RAIM [Zhang et al., 2008], RANCO [Schroth et al., 2008] semblent être des méthodes très prometteuses mais des études complémentaires restent nécessaires. En particulier, le calcul des paramètres internes au RAIM conçus pour les pannes multiples, satifaisant à la fois les exigences aviation civiles et le modèle d'erreur, et celui des niveaux de protection constitue une étape majeure.

L'amélioration majeure est l'utilisation de measures bi fréquences qui permet de supprimer l'erreur ionosphèrique de mesure de pseudo distance mais d'autre améliorations telle qu'une meilleure horloge et des informations s d'éphémerides plus précises constiitue des hypothèses s importante de ces travaux de thèse. Ainsi bien que les outils de simulation utilisés ont été conçus pour être le plus proche possible des fututres conditions réelles, il serait intéressant de tester les differents algorithmes proposés sur des mesures de pseudodistances dérivées de données réelles.

La satisfaction du critère de précision n'a été vérifiée. Par exemple, les opérations de type LPV 200 exige que 95% de la valeur absolue de l'erreur verticale de position soit inférieure à 4 mètres .Cela constitue une condition supplémentaire qu'il faudra vérifier.

On a pu voir que l'idée d'utiliser à la fois les mesures de pseudodistances GPS et Galileo est très interessante du point de vue de la disponibilité du RAIM. Cependant des considerations stratégiques ou politique pourraient favoriser l'usage d'un seul système de navigation. Dans ce cas, des simulations impliquant différentes tailles de constellation sont nécesaires pour traiter pleinement la question de la disponibilité du RAIM.

Alors que le guidage vertical semble possible sans aide externe en considérant deux constellations, il pourrait être intéressant d'étudier la combinaison des mesures bi fréquences GNSS avec celles d'autres capteurs dans le cas ou l'on ne considérerait qu'une seule constellation.

Ainsi des études complémentaires sont nécessaires pour définitivement conclure quant à l'utilisation du RAIM pour les approaches à guidage vertical mais ces premiers résultats semblent prometteurs.

Chapter 7

Conclusions and future work

This chapter presents the conclusions from the results obtained in the previous chapters and draws some perspectives for future work.

7-1 Conclusions

A complete model of pseudo range measurements, including interference effects and satellites failures, has been proposed. The fault free case as well as the faulty case have been addressed in this pseudorange error model study. The User Equivalent Range Error variance computation has been investigated and the receiver noise contribution has been particularly detailed. It has been seen that the improvement in the quality of measurements (dual frequency measurements, better clock and ephemeris information, better ranging signals) has significantly decreased the UERE variance. Considering that UERE is the major parameter of position estimation and autonomous integrity monitoring performance, great RAIM availability could be expected from an UERE standard deviation of approximately one meter. The faulty case study addresses satellite failure as well as interference phenomenon. In particular, wide band and CW interference effects on pseudorange measurement have been investigated.

The concept of smallest bias on a single pseudorange measurement that leads to a positioning failure has been developed. It is based on the fact that integrity monitoring requires that the navigation system detects the presence of an unacceptably large position error for a given mode of flight. Therefore, only faults that lead to a positioning failure (horizontal or vertical) need to be detected. The constrained Generalized Likelihood Ratio test design is based on this fact.

Three distinct classes of RAIM have been addressed in this study. The Least Square Residual method in which the sum of the squares of the pseudorange residuals plays the role of the basic observable has been first recalled. The Maximum Solution Separation method, which is based on the observation of the separation between the position estimate generated by a full-set filter (using all the satellite measurements) and the one generated by each one of the subset filters (each using all but one of the satellite measurements), has been discussed and an improved way of computing the associated protection level has been proposed. Finally, a new method based on the Generalized Likelihood Ratio test has been developed and several implementations have been described. First a snapshot one that does not take into account nominal biases and for which an analytical threshold expression that satisfies a given probability of false alarm and a predictive probability of missed detection have been presented. A snapshot implementation that takes into account potential nominal biases has

also been proposed. Finally, two sequential techniques have been described: one designed to detect step error and another one design to detect step plus ramp failure.

The way RAIM technique can be implemented in order to take into account both civil aviation requirement and threat model has been then addressed. Thus a complete review of the assumptions that are made in RAIM simulations has been detailed in this thesis. The way the required probability of false alarm and the required probability of missed detection can be set has been particularly investigated.

It has been demonstrated that, for the single failure case using GPS + Galileo constellations, the amplitude of pseudo range additional biases that lead to a positioning failure systematically belongs to the major service failure category for both APV I and LPV 200 operations. Therefore even if the targeted phases of flight are characterized by smaller horizontal and vertical tolerable position errors compared to NPA, this effect is mitigated by the great number of available measurements that reduces the impact a of single satellite bias on the global positioning error. Thus only Major Service Failures are taken into account for single failure case consideration.

Nevertheless, multiple failure case has been addressed in this thesis. It has been decided to benefit from the fact that multiple failures are very rare. It is thus possible not to try to detect these multiple failures and therefore to set the probability of detecting an integrity failure caused by multiple faults to zero (corresponding P_{md} equal to one). This operation leads to more stringent required probability of missed detection for single failure but allows the use of various detection algorithms that have been designed assuming only one pseudorange failure at the same time.

An issue has been raised concerning the response that is to be expected from RAIM detection function in presence of a bias larger than nominal biases but smaller than its corresponding critical biases.

Least Squared Residual, Maximum Solution Separation and constrained Generalized Likelihood Ratio RAIM availabilities have been computed for APVI and LPV200 approaches using both GPS L1/L5 and Galileo E1/E5b pseudorange measurements.

An availability of 100 % has been obtained for the three algorithms, considering both GPS and Galileo constellations, dual frequency measurements, assuming multiple failures (detecting only single failure), for both APV I and LPV200 (VAL=35m) operations. For the LSR RAIM and the Solution Separation RAIM, all computed xPL were below the corresponding xAL for every point of the user grid and for each epoch. Constrained GLR predicted probability of missed detection was systematically below the required probability of missed detection. The availability of the LSR Failure Detection/Exclusion function has been also evaluated at 100 % for each point of the user grid.

As the way future GPS and Galileo pseudorange measurement are going to be combined in civil aviation receivers is not defined yet, RAIM capability to provide integrity monitoring for approaches with vertical guidance considering only one constellation has been also addressed.

The obtained results were particularly pessimistic for GPS, since a 24 satellites constellation has been taken into account for simulations whereas more satellites could be expected for the future GPS constellation. It has been seen that considering a 24 satellite GPS constellation,

RAIM can't provide integrity monitoring for approach with vertical guidance with a sufficient availability. Even if some promising results has been obtain for fault detection function availability considering 27 satellite Galileo constellation, LSR RAIM FDE availabilities of 88.2 % for APVI and 81.4 % for LPV200 have been obtained which is not sufficient to have Galileo + RAIM as a sole means of navigation.

It is to be noticed that all those results have been obtained assuming high pseudorange measurements quality and in particular a high signal in space accuracy, that is to say a very good URA.

7-2 Perspectives for future work

The detection of multiple failures could be addressed in a different way by trying to detect them. For this purpose, Maximum Solution Separation RAIM, DT-RAIM [Zhang et al., 2008], RANCO [Schroth et al., 2008] algorithms seem to be promising methods but complete studies need to be conducted. In particular, the computation of internal RAIM parameters designed for multiple failures detection, coping with both civil aviation requirements and threat model, and the associated protection level prediction would constitute a major step.

Even if major improvement is due to the use of dual frequency measurements that allow removing ionosphere error from pseudorange measurements, other improvements such as better clock and ephemeris information constitute some major assumptions of this work and need to be achieved by satellite navigation systems. Although simulation tools used in this thesis were designed to be as close as possible to actual conditions, it would be valuable to test the various proposed algorithms on pseudo range error measurements derived from real data.

A key assumption of this thesis is that if a satellite does not have a major service failure, it follows a nominal distribution. Unfortunately historical off-line monitoring of GPS satellites has not focused on errors smaller than 30 m and the true probability that the satellite errors not well-described by nominal distribution is not currently known [Walter,2008]. This probability would be the relevant input for every integrity monitoring algorithm. This is why a service history against this future high signal in space accuracy is needed.

It has been seen that the idea of using both GPS and Galileo pseudorange measurements is very attractive from RAIM availability point of view. Yet, some strategic or political considerations could favor the use of only one navigation system. In this case, simulations implying different sizes of constellation are needed to fully address the question of RAIM availability.

Whereas vertical guidance seems achievable without any external augmentation considering dual constellation, it could be interesting to investigate the combination of dual frequency GNSS with other sensors for single constellation considerations.

Thus, further studies are needed to definitively conclude on the use of RAIM for approaches with vertical guidance even if these results seem promising.

References

[Akrour et al, 2005] Akrour B., R. Santerre, A. Geiger, "Calibrating Antenna Phase Centers A Tale of Two Methods", GPS World, February 2005.

[Anastasia, 2008] Anastasia ProjectWeb Site http://www.anastasia-fp6.org

[Bastide, 2001] Bastide F., "Equivalent C/N_0 degradation in presence of interference", 2001.

[Betz and Kolodziejski, 2000], Betz J.,and K. Kolodziejski, "Extended Theory of Early-Late Code-Tracking for a Band limited GPS Receiver", Journal of the Institute of Navigation, Vol. 47, N°3, Fall 2000

[Betz, 2000], Betz J., "Effect of Narrowband Interference on GPS Code Tracking Accuracy", ION NTM 2000.

[Blanch et al., 2007] Blanch J., A. Ene, T. Walter, P. Enge, "An Optimized Multiple Hypothesis RAIM Algorithm for Vertical Guidance", ION GNSS 2007, September 2007

[Booth,2000] Booth J., T. Murphy, B. Clark, F. Liu, "Validation of the Airframe Multipath Error Allocation for Local Area Differential GPS", ION Annual Meeting 2000

[Brenner, 1990] Brenner M. (1990), "Implementation of a RAIM Monitor in a GPS Receiver and an Integrated GPS/IRS", ION 1990

[Brenner, 1996] Brenner M. (1996), "Integrated GPS/inertial detection availability", Journal of The Institute of Navigation, Vol. 43, No. 2, Summer 1996

[Brown and Chin, 1997] Brown R. G., G. Y. Chin, "GPS RAIM: calculation of threshold and protection radius using chi-square methods – a geometric approach", Global Positioning System: Institute of Navigation, vol. V, pp. 155–179, 1998

[Brown and McBurney, 1988] Brown R. G., P. McBurney, "Self-Contained GPS Integrity Check Using Maximum Solution Separation", Navigation: Journal of the Institute of navigation, Vol. 35, No. 1, Spring 1988

[Cabler and DeCleene, 2002] Cabler H., B. DeCleene (2002), "LPV: New, Improved WAAS Instrument Approach", ION GPS 2002, September 2002

[Chibout, 2005] Chibout B., "Ionospheric effects and corrections", ENAC internal report

[CICTT, 2006] Commercial Aviation Safety Team/ International Civil Aviation Organization, Common Taxonomy Team, "Phase of flight definitions and usage notes", February 2006.

[Corrigan et al., 1999] Corrigan T. M., J. F. Hartranft, L. J. Levy, K. E. Parker, J. E. Pritchett, A. J. Pue, S. Pullen, T. Thompson, "GPS Risk Assessment Study", Final Report, The Johns Hopkins University, Applied Physics Laboratory, January 1999

[DeCleene,2002] DeCleene B. (2002), "Defining Pseudorange Integrity", ION GPS 2000

[DeCleene,2007] DeCleene B. (2007), "Proposed Revision to GNSS Performance Requirements for Precision Approach", Navigation Systems Panel (NSP) Working Groups 1 and 2 Meeting, March 5-17 2007

[ESA, 2005] European Space Agency, "Galileo Integrity Concept", Technical Note, July 2005

[Escher, 2003] Escher A. C., "Study of the contribution of GNSS/INS hybridization to GNSS integrity monitoring for civil aviation applications ", Ph.D. thesis, Institut National Polytechnique de Toulouse, December 2003

[Eurocae, 2006] EUROCAE WG 62, "Interim Minimum Operational Performance Specification for Airborne Galileo Satellite Receiver Equipment", White paper, may 2006.

[Fernow, 2005] Fernow J.P., "WAAS Integrity Risks: Fault Tree, Threats and Assertions", June 2005

[FIT] RNAV Tutorial, Florida International University

[Fossard, 1983], Fossard A. J., "Représentation d'état des systèmes linéaires", Ecole Nationale Supérieure de l'Aéronautique et de l'Espace, Département Automatique, 1983

[GEAS, 2008].GNSS Evolutionary Architecture Study,Phase 1-Panel Report, February 2008

[GPS, 1995] Global Positioning System Standard Positioning Service Signal Specification, Second Edition, June 1995

[GPS SPS, 2001] Global Positioning System Standard Positioning Service Performance Standard, Department of Defense, United States of America, October 2001

[GSA, 2008] European GNSS Supervisory Authority Web Site http://www.gsa.europa.eu/

[Hahn and Powers, 2005] Hahn J. H., E. D. Powers, "Implementation of the GPS to Galileo time offset (GGTO)", IEEE Frequency Control Symposium and Exposition, August 2005

[Have, 2003] Have D., "Reference set of parameters for RAIM availability simulations" Working paper Sofréavia, 8-9 April, Madrid Spain, 2003.

[Hegarty, 1996] Hegarty C., "Analytical Derivation of Maximum Tolerable In-Band Interference Level for Aviation Applications of GNSS", 1996.

[Hwang and Brown, 2006] Hwang P.Y., R.G. Brown, "RAIM FDE Revisited: A New Breakthrough in RAIM Availability Performance with NIORAIM", Journal of the Institute of Navigation, Vol. 53, N°1, Spring 2006

[ICAO, 1991] International Civil Aviation Organization, ICAO News Release, PIO 11/91 and 12/91, August and September 1991

[ICAO, 1999] International Civil Aviation Organization, Manual on Required Navigation Performance (RNP), Doc 9613, Second Edition 1999

[ICAO, 2001] International Civil Aviation Organization, International Standards and Recommended Practices, Annex 6 to Convention on International Civil aviation, Operation of aircraft, Eight edition, July 2001

[ICAO, 2005] International Civil Aviation Organization, International Standards and Recommended Practices, Annex 2 to Convention on International Civil aviation, Rules of the Air, Tenth edition, July 2005

[ICAO, 2006] International Civil Aviation Organization, International Standards and Recommended Practices, Annex 10 to Convention on International Civil aviation, Volume I, Radio Navigation Aids, Sixth edition, July 2006

[ICAO, 2008] International Civil Aviation Organization Web Site, http://www.icao.int/

[Julien, 2005] Julien O., "Design of Galileo L1F tracking loops", Ph.D. thesis, University of Calgary, Department of Geomatics Engineering, 2005.

[Julien et al., 2007] Julien O., C. Macabiau, J.L. Issler, L. Ries, "Performance of CBOC Tracking in Presence of Interference", GNSS Signal 2007, April 2007

[Kolodziejski and Betz, 1999], Kolodziejski K., J. Betz, "Effect of Non-White Gaussian Interference on GPS Code Tracking Accuracy", Mitre Report, 1999.

[Kovach et al, 1995], Kovach K., H. Maquet, D. Davis," PPS, RAIM Algorithm and their performance", Journal of the Institute of Navigation, Vol. 42, N°3, Fall 1995.

[Lee, 2004] Lee Y. C., "Performance of Receiver Autonomous Integrity Monitoring (RAIM) in the Presence of Simultaneous Multiple Satellite Faults", ION Annual Meeting 2004

[Lee et al., 2005] Lee Y. C., R. Braff, J.P. Fernow, D. Hashemi, M. P. McLaughlin, D. O'Laughlin "GPS and Galileo with RAIM or WAAS for Vertically Guided Approaches", ION GNSS 2005

[Lee and McLaughlin, 2007] Lee Y. C., M. P. McLaughlin, "Feasibility Analysis of RAIM to Provide LPV-200 Approaches with Future GPS", ION GNSS 2007, September 2007

[Liu, 1998] Liu F., "Airborne Multipath Analysis", Presentation given to RTCA SC-159 WG-4, December 1998

[Macabiau, 1997]. Macabiau C., "Analysis of the Feasibility of Using GPS Carrier Phase Ambiguity Resolution Techniques for Precision Approaches", Ph.D. thesis, Institut National Polytechnique de Toulouse, September 1997

[Macabiau and Julien, 2006] Macabiau C., O. Julien, “What are the major differences between Galileo and GPS current and forthcoming frequencies?”, GNSS Solutions column, Inside GNSS, Vol. 1, Number 3, 2006.

[Macabiau et al., 2006] Macabiau C., L. Moriella, M. Raimondi, C. Dupouy, A. Steingass, A. Lehner, “GNSS Airborne Multipath Errors Distribution Using the High Resolution Aeronautical Channel Model and Comparison to SARPs Error Curve”, ION NTM 2006, January.

[Macabiau, 2007] Macabiau, C., “GNSS Integrity Course”, GNSS Solutions Tutorials ION GNSS 2007

[Martineau and Macabiau, 2008] Martineau A., C. Macabiau, (2008), “Computation of the smallest bias that leads to a positioning failure”, ENAC internal report

[Martineau et al., 2007] Martineau A., C. Macabiau, O. Julien (2007), “Model of Pseudorange Measurement Error due to Interference”, ENAC internal report.

[Météo France, 2008], Météo france Web Site, http://www.meteofrance.com

[Murphy and Booth, 2000] Murphy T., J. Booth: “GBAS SARPs Review and Validation of Airborne Multipath Requirements”, GNSSP WG B Toulouse, October 1999 WP43

[Murphy et al., 2007] Murphy T., P. Geren, T. Pankaskie, “GPS Antenna Group Delay Variation Induced Errors in a GNSS Based Precision Approach and Landing Systems” ION GNSS 2007, September

[Nikiforov and Roturier, 2005] Nikiforov I., B. Roturier “Advanced RAIM Algorithm: first result”, ION GNSS 2005, September

[Nikiforov, 2005] Nikiforov I., “Autonomous Integrity monitoring of the GNSS”, Convention STNA – Astrée Final report, October 2005

[OFCM, 2005], Office of the Federal Coordinator Meteorology, Federal Meteorological Handbook n°1, Surface Weather Observations and Reports, September 2005

[Parkinson and Axelrad, 1988] Parkinson B.W., P. Axelrad, “Autonomous GPS Integrity Monitoring Using the Pseudorange Residual”, Journal of the Institute of Navigation, Vol. 35, N°2, Summer 1988

[Rebeyrol and Macabiau, 2005] Rebeyrol E., C. Macabiau (2005) “BOC power spectrum densities”, ION NTM 2005, January.

[Roturier, 2004] Roturier B., “APV EGNOS procedures, an efficient and reliable answer to the need for vertical guidance for approaches”, Technical revue n°67, Service Technique de la Navigation Aérienne, November 2004

[RTCA, 2001] RTCA/ DO 229C, “Minimum Operational Performance Standards for Global Positioning Systems / Wide Area Augmentation System Airborne Equipment”, RTCA, Inc., Washington D.C., USA

[RTCA, 2003] RTCA/ DO 236B, “Minimum Aviation System Performance Standards: Required Navigation Performance for Area Navigation”, RTCA, Inc., Washington D.C., USA.

[RTCA, 2004] RTCA/ DO 245A, “Minimum Aviation System Performance Standards for Local Area Augmentation System (LAAS)”, RTCA, Inc., Washington D.C., USA.

[RTCA, 2006] RTCA/ DO 229D, “Minimum Operational Performance Standards for Global Positioning Systems / Wide Area Augmentation System Airborne Equipment”, RTCA, Inc., Washington D.C., USA.

[Söderström, 1989], Söderström T., P. Stoica, “System Identification”, Chapter 4 Linear Regression, Prentice Hall international Series in Systems and Control Engineering, 1989

[Schroth et al., 2008] Schroth G., M. Rippl, A. Ene, J. Blanch, B. Belabbas, T. Walter, P. Enge, M. Meurer, “Enhancements of the Range Consensus Algorithm (RANCO)”, ION GNSS 2008, September

[Spilker, 1996], Spilker J. J., “GPS Navigation Data”, Global Positioning System: Theory and Applications Volume I, Progress in Astronautics and Aeronautics, 1996

[Stephens and Thomas, 1995], Stephens S. A., J.B. Thomas, “Controlled-Root Formulation for Digital Phase-Locked Loops”, IEEE Transactions on Aerospace and Electronic Systems, Vol. 31, n°1, January 1995

[Sturza,1988] Sturza M. A., “Navigation System Integrity Monitoring Using Redundant Measurements”, Journal of the Institute of Navigation, Vol. 35, N°4, Winter 1988-89

[Vanderwerf, 2001] Vanderwerf K., “FDE Using Multiple Integrated GPS/Inertial Kalman Filters in the Presence of Temporally and Spatially Correlated Errors”, ION GPS 2001, September.

[Van Dyke, 2000] Van Dyke K., “The World After SA: Benefit to GPS Integrity”, Position Location and Navigation Symposium, IEEE 2000, March

[Van Dyke et al., 2003] Van Dyke K., K. Kovach, J. Lavrakas, J.P. Fernow, J. Carroll, J. Kraemer, N. Attallah, B. Baevitz, ”GPS Integrity Failure Modes and Effects analysis”, ION NTM 2003, January

[Walter and Enge, 1995] Walter T., P. Enge, “Weighted RAIM for Precision Approaches”, ION GPS 1995, September.

[Walter, 2008] Walter T., “Ph.D. Evaluation Report”, October 2008

[Walter et al., 2008] Walter T., J. Blanch, P. Enge, B. Pervan, L. Gratton, “Future Architecture to Provide Aviation Integrity”, ION NTM 2008, January.

[Zhang et al., 2008] Zhang M., J. Zhang, Y. Qin, “Multi-Constellation RAIM for Simultaneous Double-Fault Satellite Scenarios”, ION GNSS 2008, September

Appendix A

Critical bias computation

The aim of this section is to detail the computation for each pseudo range of the bias b_i that will lead to a horizontal positioning failure with a given probability.

A-1 First method

Let us consider the case where there is a bias on the pseudo range i,

The error in the position domain is:

$$\Delta X_{\text{WGS 84}} = \left[H^t \Sigma^{-1} \mathrm{H}\right]^{-1} H^t \Sigma^{-1} E$$

where

$$E \sim N(B, \Sigma)$$

$$\Sigma = \begin{bmatrix} \sigma_1^2 & \cdots & 0 \\ \vdots & \ddots & \vdots \\ 0 & \cdots & \sigma_N^2 \end{bmatrix}, B = \begin{bmatrix} 0 \\ \vdots \\ b_i \\ \vdots \\ 0 \end{bmatrix}$$

If the matrix H is expressed in the local geographic frame such as:

$$H = \begin{bmatrix} \cos E_1 \cos A_1 & \cos E_1 \sin A_1 & \sin E_1 & 1 \\ \vdots & \vdots & \vdots & \vdots \\ \cos E_N \cos A_N & \cos E_N \sin A_N & \sin E_N & 1 \end{bmatrix}$$

Then the positioning error is directly expressed in the local geographic frame

$$\Delta X_{\text{local}} = [H^t \Sigma^{-1} \mathrm{H}]^{-1} H^t \Sigma^{-1} E \qquad \text{(A-1)}$$

The covariance matrix C of the error is such as:

$$C = E\left[\Delta X_{\text{local}} . \Delta X_{\text{local}}{}^{\mathrm{t}}\right] = \left(\left[H^t \Sigma^{-1} \mathrm{H}\right]^{-1} H^t \Sigma^{-1}\right) \Sigma \left(\left[H^t \Sigma^{-1} \mathrm{H}\right]^{-1} H^t \Sigma^{-1}\right)^t$$

$$C = [H^t \Sigma^{-1} \mathrm{H}]^{-1} \qquad \text{(A-2)}$$

The horizontal positioning error is a two dimensions vector which follows a gaussian bi-dimensional law of mean $b_{i,H,\text{local}}$ the projection of b_i in the horizontal plane and of covariance matrix C_H, such as $C_H = C(1{:}2,1{:}2)$, $b_{i,\text{local}} = \left[H^t \Sigma^{-1} \mathrm{H}\right]^{-1} H^t \Sigma^{-1} \mathrm{B}$ and $b_{i,H,\text{local}} = b_{i,\text{local}}(1{:}2)$

Its density function is:

$$f_{\Delta X_{\mathrm{H,local}}}(X) = \frac{1}{2\pi\sqrt{det(C_H)}} \exp\left(-\frac{1}{2}\left(\mathrm{X} - b_{i,H,\mathrm{local}}\right)^{\mathrm{t}}.{C_H}^{-1}.\left(\mathrm{X} - b_{i,H,\mathrm{local}}\right)\right) \tag{A-3}$$

where X is expressed in the Nord East local frame such as $X = \begin{bmatrix} x_N \\ x_E \end{bmatrix}$

Since C_H is a covariance matrix, C_H is a positive definite matrix, it is diagonalizable and its eigenvalues are all positive. In particular we can find an orthonormal basis $B = \left(\vec{e}_1, \vec{e_2}\right)$ that is composed of eigenvectors $\vec{e}_{1,i}, \vec{e}_{2,i}$ corresponding to the eigenvalues λ_1 and λ_2 and such as:

$$C_H = \mathrm{P}_{\perp}.\Delta.{\mathrm{P}_{\perp}}^{\mathrm{t}} \tag{A-4}$$

where

$\Delta = \mathrm{diag}(\lambda_1\ ,\ \lambda_2)$ is the diagonal matrix whose elements are the eigenvalues of C_H

$\mathrm{P}_{\perp}$ is the projection matrix whose columns are the eigenvectors $\vec{e}_1\ ,\vec{e}_2$. In particular $\mathrm{P}_{\perp}$ is orthogonal: ${\mathrm{P}_{\perp}}^{-1} = {\mathrm{P}_{\perp}}^{\mathrm{t}}$

Then, $\det(C_H) = \lambda_1\,\lambda_2$ and ${C_H}^{-1} = \mathrm{P}_{\perp}.\Delta^{-1}.{\mathrm{P}_{\perp}}^{\mathrm{t}}$

$$\begin{aligned}\left(\mathrm{X} - b_{i,H,\mathrm{local}}\right)^{\mathrm{t}}.{C_H}^{-1}.\left(\mathrm{X} - b_{i,H,\mathrm{local}}\right) &= \left(\mathrm{X} - b_{i,H,\mathrm{local}}\right)^{\mathrm{t}}.\mathrm{P}_{\perp}.\Delta^{-1}.{\mathrm{P}_{\perp}}^{\mathrm{t}}.\left(\mathrm{X} - b_{i,H,\mathrm{local}}\right) \\ &= \left[{\mathrm{P}_{\perp}}^{\mathrm{t}}\left(\mathrm{X} - b_{i,H,\mathrm{local}}\right)\right]^{\mathrm{t}}.\Delta^{-1}.\left[{\mathrm{P}_{\perp}}^{\mathrm{t}}.\left(\mathrm{X} - b_{i,H,\mathrm{local}}\right)\right]\end{aligned}$$

Denoting $X_{\perp} = {\mathrm{P}_{\perp}}^{\mathrm{t}}.\mathrm{X}$ and $\Omega = {\mathrm{P}_{\perp}}^{\mathrm{t}}.b_{i,H,\mathrm{local}}$, $X_{\perp}$ is the vector X expressed in the new local frame and Ω is the vector $b_{i,H,\mathrm{local}}$ in the new local frame.

$$f_{\Delta X_{\mathrm{H,local}}\ ,\mathrm{b}}(X) = \frac{1}{2\pi\sqrt{\lambda_1\,\lambda_2}} \exp\left(-\frac{1}{2}\left(\frac{(\mathrm{x}_{\perp} - \Omega_1)^2}{\lambda_1} + \frac{(\mathrm{y}_{\perp} - \Omega_2)^2}{\lambda_2}\right)\right) \tag{A-5}$$

The probability that a couple (x, y) be such that $x^2 + y^2 \leq HAL^2$ is the probability that ${x_{\perp}}^2 + {y_{\perp}}^2 \leq HAL^2$and considering the distribution of the horizontal positioning error, this probability is:

$$P\left(\Delta X_{\mathrm{H,local}}\ \in \mathrm{D}\right) = \iint_D \frac{1}{2\pi\sqrt{\lambda_1\,\lambda_2}} \exp\left(-\frac{1}{2}\left(\frac{(x_{\perp} - \Omega_1)^2}{\lambda_1} + \frac{(y_{\perp} - \Omega_2)^2}{\lambda_2}\right)\right) \mathrm{d}x\ \mathrm{d}y$$

denoting D the domain such as ${x_{\perp}}^2 + {y_{\perp}}^2 \leq HAL^2$.

Let's make a change of coordinates such as we could have:

$$\frac{(x_{\perp} - \Omega_1)^2}{\lambda_1} + \frac{(y_{\perp} - \Omega_2)^2}{\lambda_2} = \mathrm{r}^2$$

$(x_{\perp}, y_{\perp})$ re-written this way:

$$\begin{cases} x_\perp = \Omega_1 + \mathrm{r}\cos\theta\sqrt{\lambda_1} \\ y_\perp = \Omega_2 + \mathrm{r}\sin\theta\sqrt{\lambda_2} \end{cases}$$

The equation ${x_\perp}^2 + {y_\perp}^2 = HAL^2$ that defines the boundaries of the integration domain becomes:

$$\begin{gathered} {x_\perp}^2 + {y_\perp}^2 = \left(\Omega_1 + \mathrm{r}\cos\theta\sqrt{\lambda_1}\right)^2 + \left(\Omega_2 + \mathrm{r}\sin\theta\sqrt{\lambda_2}\right)^2 \\ = {\Omega_1}^2 + \mathrm{r}^2\lambda_1\cos^2\theta + 2\Omega_1\mathrm{r}\sqrt{\lambda_1}\cos\theta + {\Omega_2}^2 + \mathrm{r}^2\lambda_2\sin^2\theta + 2\Omega_2\mathrm{r}\sqrt{\lambda_2}\sin\theta = HAL^2 \end{gathered}$$

$$\mathrm{r}^2(\lambda_1\cos^2\theta + \lambda_2\sin^2\theta) + r\left(2\Omega_1\sqrt{\lambda_1}\cos\theta + 2\Omega_2\sqrt{\lambda_2}\sin\theta\right) + \left({\Omega_1}^2 + {\Omega_2}^2 - HAL^2\right) = 0$$

Finally, denoting $a(\theta) = (\lambda_1\cos^2\theta + \lambda_2\sin^2\theta)$
$b(\theta) = \left(2\Omega_1\sqrt{\lambda_1}\cos\theta + 2\Omega_2\sqrt{\lambda_2}\sin\theta\right)$
$c(\theta) = \left({\Omega_1}^2 + {\Omega_2}^2 - HAL^2\right)$

Solving this equation, two roots $r_1(\theta)$ and $r_2(\theta)$ for $\theta\epsilon[0,\pi]$ are obtained such as:

$\begin{cases} x_\perp = \Omega_1 + r_1(\theta)\cos\theta\sqrt{\lambda_1} \\ y_\perp = \Omega_2 + r_1(\theta)\sin\theta\sqrt{\lambda_2} \end{cases}, \theta\epsilon[0,\pi]$ and $\begin{cases} x_\perp = \Omega_1 + r_2(\theta)\cos\theta\sqrt{\lambda_1} \\ y_\perp = \Omega_2 + r_2(\theta)\sin\theta\sqrt{\lambda_2} \end{cases}, \theta\epsilon[0,\pi]$
define the boundaries of the integration domain.

The jacobian of this transformation is computed to make the change of coordinates $J = |r|\sqrt{\lambda_1\lambda_2}$, and:

$$P\left(\Delta X_{\mathrm{H,local}} \in \mathrm{D}\right) = \iint_{D'} \frac{|r|}{2\pi}\exp\left(-{r^2}/{2}\right)\mathrm{d}r\mathrm{d}\theta$$

where the new domain D' is defined by $\begin{cases} \left(r - r_1(\theta)\right)\left(r - r_2(\theta)\right) \le 0 \\ \theta\epsilon[0,\pi] \end{cases}$.

Considering properties of second order polynomials:

$$P\left(\Delta X_{\mathrm{H,local}} \in \mathrm{D}\right) = \frac{1}{2\pi}\int_{\theta=0}^{\theta=\pi}\int_{\mathrm{r}=r_1(\theta)}^{\mathrm{r}=r_2(\theta)} |\mathrm{r}|\exp\left(-{r^2}/{2}\right)\mathrm{d}r\mathrm{d}\theta$$

Assuming for example that $r_1(\theta) \le 0 \le r_2(\theta)$,

$$P\left(\Delta X_{\mathrm{H,loca\,l}} \in \mathrm{D}\right) = \frac{1}{2\pi}\int_{\theta=0}^{\theta=\pi}\left[-\int_{\mathrm{r}=r_1(\theta)}^{\mathrm{r}=0}\mathrm{r}\exp\left(-{r^2}/{2}\right)\mathrm{d}r + \int_{\mathrm{r}=0}^{\mathrm{r}=r_2(\theta)}\mathrm{r}\exp\left(-{r^2}/{2}\right)\mathrm{d}r\right]\mathrm{d}\theta$$

$$P\left(\Delta X_{\mathrm{H,local}} \in \mathrm{D}\right) = 1 - \frac{1}{2\pi}\int_{\theta=0}^{\theta=\pi}\left[\exp\left(-{r_2(\theta)^2}/{2}\right) + \exp\left(-{r_1(\theta)^2}/{2}\right)\right]\mathrm{d}\theta$$

This last integral is computed numerically.

Thus the probability that the point(x, y) representing the horizontal position error is out of the circle of radius HAL is:

$$P\left(\Delta X_{\mathrm{H,local}} \notin \mathrm{D}\right) = \frac{1}{2\pi} \int_{\theta=0}^{\theta=\pi} \left[\exp\left(-r_2(\theta)^2/2\right) + \exp\left(-r_1(\theta)^2/2\right)\right] \mathrm{d}\theta \tag{A-6}$$

A-2 Second method

The error in the position domain is:

$$\Delta X_{\mathrm{WGS\ 84}} = \left[H^t \Sigma^{-1} \mathrm{H}\right]^{-1} H^t \Sigma^{-1} E$$

where

$$E \sim N(B, \Sigma)$$

$$\Sigma = \begin{bmatrix} \sigma_1^2 & \cdots & 0 \\ \vdots & \ddots & \vdots \\ 0 & \cdots & \sigma_N^2 \end{bmatrix}, B = \begin{bmatrix} 0 \\ \vdots \\ b_i \\ \vdots \\ 0 \end{bmatrix}$$

If the matrix H is expressed in the local geographic frame such as:

$$H = \begin{bmatrix} \cos E_1 \cos A_1 & \cos E_1 \sin A_1 & \sin E_1 & 1 \\ \vdots & \vdots & \vdots & \vdots \\ \cos E_N \cos A_N & \cos E_N \sin A_N & \sin E_N & 1 \end{bmatrix}$$

Then the positioning error is directly expressed in the local geographic frame

$$\Delta X_{\mathrm{local}} = \left[H^t \Sigma^{-1} \mathrm{H}\right]^{-1} H^t \Sigma^{-1} E$$

The covariance matrix C of the error is such as:

$$C = E\left[\Delta X_{\mathrm{local}} \,.\, \Delta X_{\mathrm{local}}{}^{\mathrm{t}}\right] = \left(\left[H^t \Sigma^{-1} \mathrm{H}\right]^{-1} H^t \Sigma^{-1}\right) \Sigma \left(\left[H^t \Sigma^{-1} \mathrm{H}\right]^{-1} H^t \Sigma^{-1}\right)^t$$

$$C = \left[H^t \Sigma^{-1} \mathrm{H}\right]^{-1}$$

The horizontal positioning error is a two dimensions vector which follows a gaussian bi-dimensional law of mean $b_{i,H,\mathrm{local}}$ the projection of b_i in the horizontal plane and of covariance matrix C_H, such as $C_H = C(1{:}2,1{:}2)$, $b_{i,\mathrm{local}} = \left[H^t \Sigma^{-1} \mathrm{H}\right]^{-1} H^t \Sigma^{-1} \mathrm{B}$ and $b_{i,H,\mathrm{local}} = b_{i,\mathrm{local}}(1{:}2)$

This method rather considers that $E = \xi + B$ where $\xi \sim N(0, \Sigma)$.

So the horizontal positioning error is such $\Delta X_H = \varepsilon_H + b_{local\ ,H}$

such as $\varepsilon_H = \varepsilon(1:2)$ with $\varepsilon = [H^t\Sigma^{-1}\mathrm{H}]^{-1}H^t\Sigma^{-1}\xi$ and $\varepsilon_H = N\left(\begin{bmatrix}0\\0\end{bmatrix}, C_H\right)$

We have $\|\Delta X_H\|^2 = \Delta X_H{}^{\mathrm{t}}\Delta X_H = \left(\varepsilon_H + b_{local,H}\right)^t\left(\varepsilon_H + b_{local,H}\right)$

We denote the matrix S such as $C_H = SS$ as the matrix C_H the matrix S and $S^{-1}$are symmetric.

$$\begin{aligned}\|\Delta X_H\|^2 &= \left(\varepsilon_H + b_{local,H}\right)^t\left(\varepsilon_H + b_{local,H}\right)\\ &= \left(\varepsilon_H + b_{local,H}\right)^t S^{-1}S\ SS^{-1}\left(\varepsilon_H + b_{local,H}\right)\\ &= \left(\varepsilon_H + b_{local,H}\right)^t S^{-1}C_H\ S^{-1}\left(\varepsilon_H + b_{local,H}\right)\end{aligned}$$

$$\|\Delta X_H\|^2 = \left(S^{-1}\varepsilon_H + S^{-1}b_{local,H}\right)^t C_H\ \left(S^{-1}\varepsilon_H + S^{-1}b_{local,H}\right) \tag{A-7}$$

with $S^{-1}\varepsilon_H = N\left(\begin{bmatrix}0\\0\end{bmatrix}, I_2\right)$

Since C_H is a covariance matrix, C_H is a positive definite matrix, it is diagonalizable and its eigenvalues are all positive. In particular we can find an orthonormal basis $B = \left(\vec{e}_1, \overrightarrow{e_2}\right)$ that is composed of eigenvectors $\vec{e}_{1,i}, \vec{e}_{2,i}$ corresponding to the eigenvalues λ_1 and λ_2 and such as:

$$C_H = \mathrm{P}_\perp.\Delta.\mathrm{P}_\perp{}^{\mathrm{t}}$$

where

$\Delta = \mathrm{diag}(\lambda_1\ ,\ \lambda_2)$is the diagonal matrix whose elements are the eigenvalues of C_H

$\mathrm{P}_\perp$ is the projection matrix whose columns are the eigenvectors $\vec{e}_1\ ,\ \vec{e}_2$. In particular $\mathrm{P}_\perp$ is orthogonal: $\mathrm{P}_\perp{}^{-1} = \mathrm{P}_\perp{}^{\mathrm{t}}$

Then, $\det(C_H) = \lambda_1\,\lambda_2$ and $C_H{}^{-1} = \mathrm{P}_\perp.\Delta^{-1}.\mathrm{P}_\perp{}^{\mathrm{t}}$

And we obtain

$$\|\Delta X_H\|^2 = \left(S^{-1}\varepsilon_H + S^{-1}b_{local,H}\right)^t P_\perp\,\Delta\,P_\perp{}^t\left(S^{-1}\varepsilon_H + S^{-1}b_{local,H}\right)$$
$$\|\Delta X_H\|^2 = \left(P_\perp{}^tS^{-1}\varepsilon_H + P_\perp{}^tS^{-1}b_{local,H}\right)^t\Delta\left(P_\perp{}^tS^{-1}\varepsilon_H + P_\perp{}^tS^{-1}b_{local,H}\right)$$

So we have

$$\begin{aligned}&\mathrm{P}(\|\Delta X_H\|^2 \le \mathrm{HAL}^2)\\ &= P\left(\left(P_\perp{}^tS^{-1}\varepsilon_H + P_\perp{}^tS^{-1}b_{local,H}\right)^t\Delta\left(P_\perp{}^tS^{-1}\varepsilon_H + P_\perp{}^tS^{-1}b_{local,H}\right) \le \mathrm{HAL}^2\right)\end{aligned}$$

Let us denote $\Omega_{\mathrm{norm}} = P_\perp{}^tS^{-1}b_{local,H}$ and $\varepsilon_{\perp,norm} = P_\perp{}^tS^{-1}\varepsilon_H$

$$\mathrm{P}(\|\Delta X_H\|^2 \le \mathrm{HAL}^2) = P\left(\left(\varepsilon_{\perp,norm} + \Omega_{\mathrm{norm}}\right)^t\Delta\left(\varepsilon_{\perp,norm} + \Omega_{\mathrm{norm}}\right) \le HAL^2\right) \tag{A-8}$$

where $\varepsilon_{\perp,norm} \sim N\left(\begin{bmatrix}0\\0\end{bmatrix}, I_2\right)$, Ω_{norm} and Δ are determinist.

Then $\mathrm{P}(\|\Delta X_H\|^2 \leq \mathrm{HAL}^2) = \iint_{(\varepsilon_{\perp,norm} + \Omega_{\mathrm{norm}})^t \Delta (\varepsilon_{\perp,norm} + \Omega_{\mathrm{norm}}) \leq HAL^2} \mathrm{f}_{\varepsilon_{\perp,norm}}(\mathrm{s})\mathrm{ds}$

$\varepsilon_{\perp,norm} = \begin{bmatrix} \varepsilon_{\perp,norm}(1) \\ \varepsilon_{\perp,norm}(2) \end{bmatrix}$ such as $\varepsilon_{\perp,norm}(1)$ and $\varepsilon_{\perp,norm}(2)$are independent.

Therefore for $(u,v)\epsilon\mathbb{R}^2$, $\mathrm{f}_{\varepsilon_{\perp,norm}}(\mathrm{u},\mathrm{v}) = \mathrm{f}_{\varepsilon_{\perp,norm}(1)}(\mathrm{u}) \times \mathrm{f}_{\varepsilon_{\perp,norm}(2)}(\mathrm{v})$

$$\mathrm{P}(\|\Delta X_H\|^2 \leq \mathrm{HAL}^2) = \iint_{(W+\Omega_{\mathrm{norm}})^t \Delta (W+\Omega_{\mathrm{norm}}) \leq HAL^2} \mathrm{f}_{\varepsilon_{\perp,norm}(1)}(\mathrm{u}) \times \mathrm{f}_{\varepsilon_{\perp,norm}(2)}(\mathrm{v})\mathrm{du}\,\mathrm{dv}$$

$$= \iint_{(W+\Omega_{\mathrm{norm}})^t \Delta (W+\Omega_{\mathrm{norm}}) \leq HAL^2} \frac{1}{\sqrt{2\pi}} \mathrm{e}^{-\frac{\mathrm{u}^2}{2}} \times \frac{1}{\sqrt{2\pi}} \mathrm{e}^{-\frac{\mathrm{v}^2}{2}} \mathrm{du}\,\mathrm{dv}$$

$$\mathrm{P}(\|\Delta X_H\|^2 \leq \mathrm{HAL}^2) = \iint_{(W+\Omega_{\mathrm{norm}})^t \Delta (W+\Omega_{\mathrm{norm}}) \leq HAL^2} \frac{1}{2\pi} \mathrm{e}^{-\frac{\|\mathrm{W}\|^2}{2}} \mathrm{dW} \tag{A-9}$$

with $W = \begin{bmatrix} u \\ v \end{bmatrix}$

Let us make a change of coordinate such as $\begin{cases} u = \rho\cos\theta \\ v = \rho\sin\theta \end{cases}$.

The Jacobian of the transformation is $J = |\rho|$

The integration domain will be defined as$\{(\theta,\rho) \in \mathbb{R}^2, 0 \leq \theta \leq 2\pi, 0 \leq \rho \leq r(\theta)\}$

$$\mathrm{P}(\|\Delta X_H\|^2 \leq \mathrm{HAL}^2) = \frac{1}{2\pi} \int_{\theta=0}^{\theta=2\pi} \int_{\rho=0}^{\rho=\mathrm{r}(\theta)} \rho \mathrm{e}^{-\rho^2/2} \mathrm{d}\rho\,\mathrm{d}\theta = \frac{1}{2\pi} \int_{\theta=0}^{\theta=2\pi} \left[-\mathrm{e}^{-\rho^2/2}\right]_{\rho=0}^{\rho=\mathrm{r}(\theta)} \mathrm{d}\theta$$

$$(\|\Delta X_H\|^2 \leq \mathrm{HAL}^2) = \frac{1}{2\pi} \int_{\theta=0}^{\theta=2\pi} \left[1 - -\mathrm{e}^{-\mathrm{r}(\theta)^2/2}\right] \mathrm{d}\theta$$

$$\mathrm{P}(\|\Delta X_H\|^2 \leq \mathrm{HAL}^2) = \frac{1}{2\pi} \int_{\theta=0}^{\theta=\pi} \left[1 - \mathrm{e}^{-\frac{\mathrm{r}_1(\theta)^2}{2}}\right] \mathrm{d}\theta + \frac{1}{2\pi} \int_{\theta=0}^{\theta=\pi} \left[1 - \mathrm{e}^{-\mathrm{r}_2(\theta)^2/2}\right] \mathrm{d}\theta$$

$$\mathrm{P}(\|\Delta X_H\|^2 \leq \mathrm{HAL}^2) = 1 - \frac{1}{2\pi} \int_{\theta=0}^{\theta=\pi} \left[\mathrm{e}^{-\frac{\mathrm{r}_1(\theta)^2}{2}} + \mathrm{e}^{-\frac{\mathrm{r}_1(\theta)^2}{2}}\right] \mathrm{d}\theta$$

$$\mathrm{P}(\|\Delta X_H\|^2 \geq \mathrm{HAL}^2) = \frac{1}{2\pi} \int_{\theta=0}^{\theta=\pi} \left[\mathrm{e}^{-\frac{\mathrm{r}_1(\theta)^2}{2}} + \mathrm{e}^{-\frac{\mathrm{r}_1(\theta)^2}{2}}\right] \mathrm{d}\theta \tag{A-10}$$

And this integral is computed numerically

$r_1(\theta)$ and $r_2(\theta)$ are obtained thanks to the equation $(W + \Omega_{\text{norm}})^t \Delta (W + \Omega_{\text{norm}}) = HAL^2$ that defines the boundaries of the integration domain:

$$\lambda_1 \left(u + \Omega_{\text{norm},1}\right)^2 + \lambda_2 \left(v + \Omega_{\text{norm},2}\right)^2 = HAL^2$$
$$\lambda_1 \left(\rho \cos\theta + \Omega_{\text{norm},1}\right)^2 + \lambda_2 \left(\rho \sin\theta + \Omega_{\text{norm},2}\right)^2 = HAL^2$$

$$\rho^2 (\lambda_1 \cos^2\theta + \lambda_2 \sin^2\theta) + \rho\left(2\lambda_1 \cos\theta\ \Omega_{\text{norm},1} + 2\lambda_2 \sin\theta\ \Omega_{\text{norm},2}\right) + \left(\lambda_1\ {\Omega_{\text{norm},1}}^2 + \lambda_2\ {\Omega_{\text{norm},2}}^2 - HAL^2\right) = 0$$

Finally, denoting
$$a(\theta) = \lambda_1 \cos^2\theta + \lambda_2 \sin^2\theta,$$
$$b(\theta) = 2\lambda_1 \cos\theta\ \Omega_{\text{norm},1} + 2\lambda_2 \sin\theta\ \Omega_{\text{norm},2}$$
$$c(\theta) = \lambda_1\ {\Omega_{\text{norm},1}}^2 + \lambda_2\ {\Omega_{\text{norm},2}}^2 - HAL^2$$

We have

$$r_1(\theta) = \frac{-b(\theta) - \sqrt{b(\theta)^2 - 4a(\theta)c(\theta)}}{2a(\theta)} \qquad \text{(A-11)}$$

and

$$r_2(\theta) = \frac{-b(\theta) + \sqrt{b(\theta)^2 - 4a(\theta)c(\theta)}}{2a(\theta)} \qquad \text{(A-12)}$$

Appendix B

Least square Residual Method: Adaptation to nominal biases

The objective of this appendix is to present the inclusion of nominal biases in the classical LSR method.

As in section 4-2, the detection threshold is obtained by considering the test statistic in the fault free case

As nominal biases are taken into account, the measurement error E is not noise only anymore but it is such as:

$$E(k) = \begin{bmatrix} n^1(k) \\ \vdots \\ n^j(k) \\ \vdots \\ n^N(k) \end{bmatrix} + \begin{bmatrix} a_1 \\ \vdots \\ a_j \\ \vdots \\ a_N \end{bmatrix} \text{ with } n^i \sim N(0, \sigma_i^2) \quad \text{(B-1)}$$

As in section 4-2, let's denote:

$$s^2 = \frac{SSE}{\sigma^2} \quad \text{(B-2)}$$

or

$$s^2 = WSSE \quad \text{(B-3)}$$

In both cases, s^2 represents the sum of the squares of the range residual errors normalized by the standard deviation of the measurement errors.

If we take into account nominal biases, s^2 is chi-squared distributed with N-4 degrees of freedom and non-centrality parameter $\lambda(a)$ such as $s^2 \sim \chi^2_{\lambda(a),N-4}$. This means that s^2 can be written like this:

$$\exists \xi_i \, , s^2 = \xi_1^2 + \cdots + \xi_{N-4}^2 \; iid, \xi_i \sim N(\mu_i(a), 1) \quad \text{(B-4)}$$

$$\lambda(a) = \sum_{i=1}^{N-4} \mu_i^2 \, (a) \quad \text{(B-5)}$$

The nominal bias model could be simplified such as:

$$a_1 = \cdots = a_j = \cdots = a_N$$

That is to say such as:

$$a = a_0 \begin{bmatrix} 1 \\ \vdots \\ 1 \\ \vdots \\ 1 \end{bmatrix} \tag{B-6}$$

But in this case all bias values have the same magnitude and sign which could mimic a clock offset and not affect the position error.

The nominal biases could also be assumed to line up with the user position matrix signs such as [Walter, 2008]:

$$a = a_0 \begin{bmatrix} \mathrm{sgn}(A_{V,1}) \\ \vdots \\ \mathrm{sgn}(A_{V,j}) \\ \vdots \\ \mathrm{sgn}(A_{V,N}) \end{bmatrix} \tag{B-7}$$

with $A = [H^t \Sigma^{-1} \mathrm{H}]^{-1} H^t \Sigma^{-1}$such as:

$$\Delta X = X(k) - \hat{X}(k) = A \times E(k) = \begin{bmatrix} \cdots & A_{N,j} & \cdots \\ \cdots & A_{E,j} & \cdots \\ \cdots & A_{V,j} & \cdots \\ \cdots & A_{T,j} & \cdots \end{bmatrix} \times E(k)$$

The non-centrality parameter $\lambda(a)$ is computed as follow.

As $SSE = E^t(I - H[H^t \Sigma^{-1} \mathrm{H}]^{-1} H^t \Sigma^{-1})E$, denoting $P = I - H[H^t \Sigma^{-1} \mathrm{H}]^{-1} H^t \Sigma^{-1}$and $a = a_0 \begin{bmatrix} \delta_1 \\ \vdots \\ \delta_j \\ \vdots \\ \delta_n \end{bmatrix}$ with for $i \epsilon [1, N]$, $\delta_j = \pm 1$,we obtain:

$$SSE = {a_0}^2 \left(\sum_{i=1}^{N} \sum_{j=1}^{N} \delta_i \delta_j P_{i,j} \right) \tag{B-8}$$

And the relation between the nominal bias on the every pseudorange and the test statistic can be simplified as:

$$\sigma^2 \lambda(a) = {a_0}^2 \left(\sum_{i=1}^{N} \sum_{j=1}^{N} \delta_i \delta_j P_{i,j} \right) \tag{B-9}$$

where $\sigma = \max_{i \in [1,N]} \sigma_i$

The probability of false alarm is used to determine the normalised detection threshold $h_{Pfa}(a)$ such as:

$$P\left(\frac{SSE}{\sigma^2} > h_{Pfa}(a) \right) = P_{fa} \tag{B-10}$$

$$P_{fa} = \int_{h_{Pfa}(a)}^{\infty} f_{\chi^2_{\lambda(a),N-4}(x)}\, dx \tag{B-11}$$

Finally, the threshold that it is compared to our criteria is:

$$T_h = \sqrt{\frac{h_{Pfa}(a)\sigma^2}{N-4}} \tag{B-12}$$

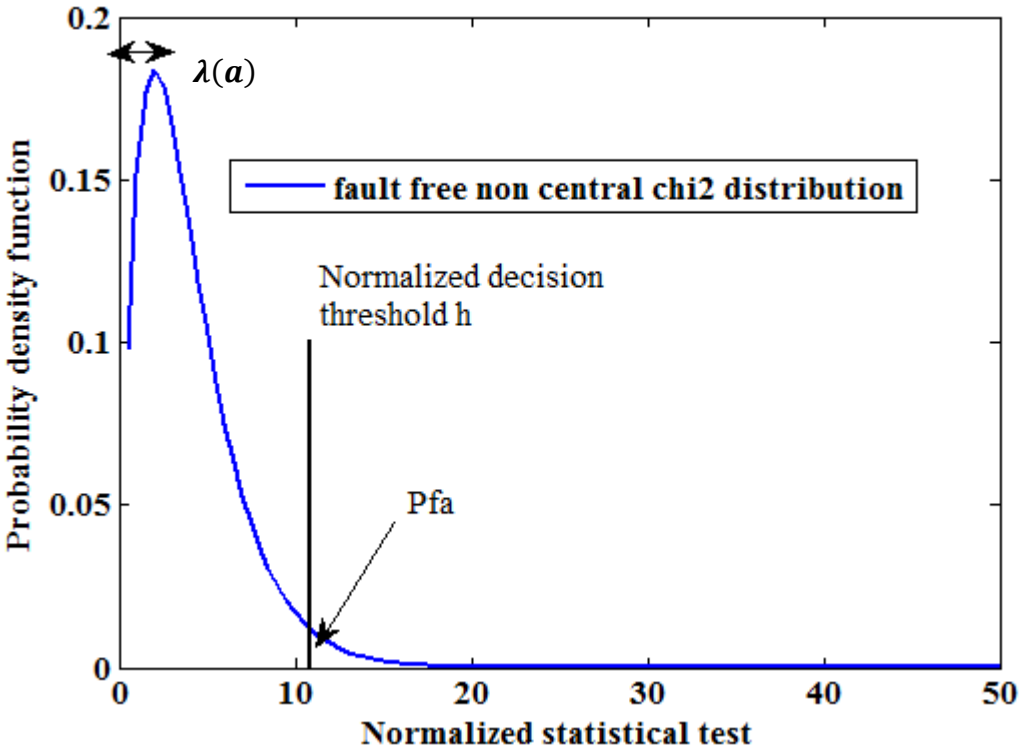

Figure 65 - Fault free LSR statistical test distribution

The protection levels derive from the smallest bias the algorithm is able to detect satisfying the false alarm and the missed detection requirement.

Let‘s consider that the measurement error E is noise and a bias b on one satellite *j* such as*:*

$$E(k) = \begin{bmatrix} n^1(k) \\ \vdots \\ n^j(k) \\ \vdots \\ n^N(k) \end{bmatrix} + a_0 \begin{bmatrix} \delta_1 \\ \vdots \\ \delta_j \\ \vdots \\ \delta_n \end{bmatrix} + \begin{bmatrix} 0 \\ \vdots \\ b \\ \vdots \\ 0 \end{bmatrix} \tag{B-13}$$

In this case, SSE is chi-squared distributed with N-4 degrees of freedom and non-centrality parameter $\lambda(a,b)$ such as SSE$\sim\chi^2_{\lambda(a,b),N-4}$.

The non centrality parameter $\lambda(a,b)$ is computed in order to satisfy the Pmd requirement such as:

$$P_{md} = \int_0^{h_{Pfa}(a)} f_{\chi^2_{\lambda(a,b),N-4}(x)}\,\mathrm{d}x \qquad \text{(B-14)}$$

The determination of $\lambda(a,b)$ is the same as the classic LSR without nominal biases one. The only difference is that the detection threshold $h_{Pfa}\,(a)$ is higher due to nominal biases.

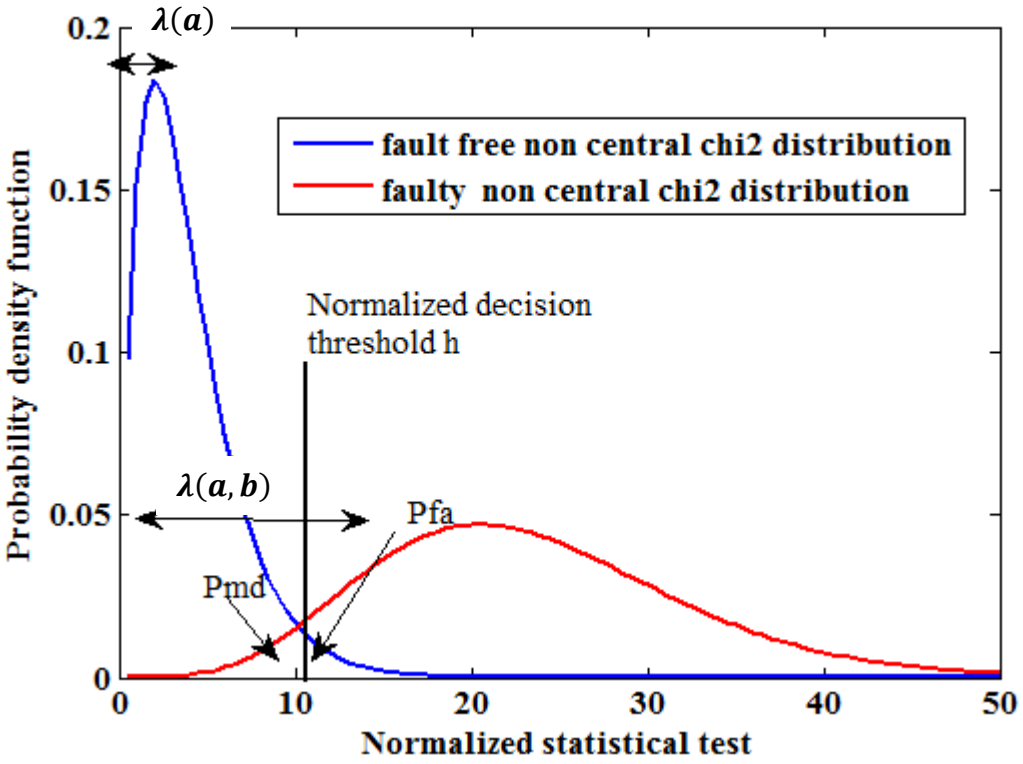

Figure 66 - Fault free and faulty LSR statistical test distribution

As in section 4-2-2, the relation between the smallest detectable bias on the pseudorange j and the test statistic is simplified.

$$\sigma^2\lambda(a,b) = (a_0 + b)P_{jj}\,(a_0 + b) = p_{jj}\,(a_0 + b)^2$$

or as

$$\sigma^2\lambda(a,b) = P_{jj}\,(a_0 - b)^2$$

depending on the sign of $\delta_j\,.\,b$

The smallest detectable measurement bias b on satellite j can be then expressed as:

$$b_j = \sigma\sqrt{\frac{\lambda(a,b)}{P_{jj}}} \pm a_0 \qquad \text{(B-15)}$$

depending on the sign of $\delta_j\,.\,b$

Considering the worst case (the one that will lead to the most conservative protection levels) we obtain:

$$b_j = \sigma \sqrt{\frac{\lambda(a,b)}{P_{jj}}} + a_0$$

As previously, the impact of the bias b_j in position domain is obtained by:

$$\Delta X = X(k) - \hat{X}(k) = \begin{bmatrix} \cdots & A_{N,j} & \cdots \\ \cdots & A_{E,j} & \cdots \\ \cdots & A_{D,j} & \cdots \\ \cdots & A_{T,j} & \cdots \end{bmatrix} \times \begin{bmatrix} 0 \\ \vdots \\ b_j \\ \vdots \\ 0 \end{bmatrix}$$

Then,

$$\Delta X_{\mathrm{H}} = \sqrt{{\Delta X_V}^2 + {\Delta X_{\mathrm{E}}}^2} = \sqrt{{A_{N,j}}^2 + {A_{E,j}}^2} \times \mathrm{b_j}$$

$$\Delta X_{\mathrm{V}} = A_{V,j} \times b_j$$

Denoting,

$$P_{jj} = 1 - B_{j,j} \tag{B-16}$$

where $B = H[H^t \Sigma^{-1} \mathrm{H}]^{-1} H^t \Sigma^{-1} = HA$

$$\Delta X_{\mathrm{H}} = \frac{\sqrt{{A_{N,j}}^2 + {A_{E,j}}^2}}{\sqrt{1 - \mathrm{B_{j,j}}}} \times \left(\sigma \sqrt{\lambda(a,b)} + \sqrt{1 - \mathrm{B_{j,j}}} a_0 \right)$$

$$\Delta X_{\mathrm{V}} = \frac{|A_{V,j}|}{\sqrt{1 - \mathrm{B_{j,j}}}} \times \left(\sigma \sqrt{\lambda(a,b)} + \sqrt{1 - \mathrm{B_{j,j}}} a_0 \right)$$

Denoting,

$$VSLOPE_j = \frac{|A_{V,j}|}{\sqrt{1 - B_{j,j}}} \, , HSLOPE_j = \frac{\sqrt{{A_{N,j}}^2 + {A_{E,j}}^2}}{\sqrt{1 - B_{j,j}}}$$

The protection levels are computed referring to the worst satellite:

$$HPL = \max_j \left(HSLOPE_j \times \left(\sigma \sqrt{\lambda(a,b)} + \sqrt{1 - \mathrm{B_{j,j}}} a_0 \right) \right) \tag{B-17}$$

$$VPL = \max_j \left(VSLOPE_j \times \left(\sigma \sqrt{\lambda(a,b)} + \sqrt{1 - \mathrm{B_{j,j}}} a_0 \right) \right) \tag{B-18}$$

Appendix C

Maximum Solution Separation Method

C-1 Existing protection level computation

The objective of this section is to detail the way the term $\left\|X-\hat{X}_i\right\|_H$ is over bound.

$\Delta X_{i,H}$ is a bi-dimensional random variable following a Gaussian distribution such as $\Delta X_{i,H} \sim N\left(\begin{bmatrix}0\\0\end{bmatrix}, C_{i,H}\right)$ and the general expression of the probability density function of the variable $\Delta X_{i,H}$ is given by:

$$f_{\Delta X_{i,H}}(X) = \frac{1}{2\pi\sqrt{det\left(C_{i,H}\right)}} \exp\left(-\frac{1}{2} \mathrm{X}^{\mathrm{t}} . {C_{i,H}}^{-1} . \mathrm{X}\right) \qquad \text{(C-1)}$$

Since $C_{i,H}$ is not diagonal, the components of $\Delta X_{i,H}$ are not mutually independent and the separations on the North and East axes are correlated. But as $C_{i,H}$ is a positive definite matrix, it is diagonalizable and its eigenvalues are all positive. In particular we can find an orthonormal basis $\beta_i = \left(\vec{u}_{1,i}, \vec{u}_{2,i}\right)$ that is composed of eigenvectors $\vec{u}_{1,i}$ and $\vec{u}_{2,i}$ corresponding with the eigenvalues $\mu_{1,i}$ and $\mu_{2,i}$ of $C_{i,H}$ and we have:

$$C_{i,H} = \Pi_{\perp,\mathrm{i}} . \mathrm{M_i} . {\Pi_{\perp,\mathrm{i}}}^{\mathrm{t}} \qquad \text{(C-2)}$$

where,

$\mathrm{M_i} = \mathrm{diag}\left(\mu_{1,i}, \mu_{2,i}\right)$is the diagonal matrix whose elements are the eigenvalues of $C_{i,H}$

$\Pi_{\perp,\mathrm{i}}$ is the projection matrix whose columns are the eigenvectors $\vec{u}_{1,i}$ and $\vec{u}_{2,i}$

In particular $\Pi_{\perp,\mathrm{i}}$ is orthogonal ${\Pi_{\perp,\mathrm{i}}}^{-1} = {\Pi_{\perp,\mathrm{i}}}^{\mathrm{t}}$.

Let $\Delta X_{i,\perp}$ be the projection of $\Delta X_{i,H}$ in the orthonormal basis $\beta_i = \left(\vec{u}_{1,i}, \vec{u}_{2,i}\right)$ such as:

$$\Delta X_{i,\perp} = {\Pi_{\perp,\mathrm{i}}}^{\mathrm{t}} \Delta X_{i,H} \qquad \text{(C-3)}$$

$\Delta X_{i,\perp}$ is a 2-dimensional Gaussian vector whose covariance matrix is the diagonal matrix $\mathrm{M_i}$, $\Delta X_{i,\perp} \sim N\left(\begin{bmatrix}0\\0\end{bmatrix}, \mathrm{M_i}\right)$. In particular, the components of $\Delta X_{i,\perp}$ are mutually independent and the general expression of the probability density function of variable $\Delta X_{i,\perp}$ is given by:

$$f_{\Delta X_{i,\perp}}(X) = \frac{1}{2\pi\sqrt{\mu_{1,i}\,\mu_{2,i}}} \exp\left(-\frac{1}{2} \mathrm{X}^{\mathrm{t}} . {\mathrm{M_i}}^{-1} . \mathrm{X}\right) \qquad \text{(C-4)}$$

Let's denote

$$s_i^2 = \Delta X_{i,\perp}{}^{\mathrm{t}}.\mathrm{M_i}^{-1}.\Delta X_{i,\perp}$$

s_i^2 is chi-squared distributed with 2 degrees of freedom, ${s_i}^2 \sim \chi_2^2$, and we can easily find δ_i such as:

$$P(s_i^2 > \delta_i) = P_{md} \tag{C-5}$$

$$P_{md} = \int_{\delta_i}^{\infty} f_{\chi_2^2(x)}\,\mathrm{d}x \tag{C-6}$$

The set of points $\mathcal{E}_{\alpha,i} = \{X \in \mathbb{R}^2 : X^{\mathrm{t}}.\mathrm{M_i}^{-1}.X = \alpha^2\}$ is an ellipse whose semi-major axis is oriented along $\vec{u}_{1,i}$ and whose semi-minor axis is oriented along $\vec{u}_{2,i}$. This ellipse defines an equipotential curve of the probability density function:

$$f_{\Delta X_{i,\perp}}(X \in \mathcal{E}_{\alpha,i}) = \frac{1}{2\pi\sqrt{\mu_{1,i}\,\mu_{2,i}}}\,\mathrm{e}^{-\frac{\alpha^2}{2}}$$

The probability that the point corresponding to $\Delta X_{i,\perp}$ belongs to the region $D_{\alpha,i}$ delimited by $\mathcal{E}_{\alpha,i}$ is:

$$P(\Delta X_{i,\perp} \in D_{\alpha,i}) = \iint_{D_{\alpha,i}} f_{\Delta X_{i,\perp}}(X)\mathrm{d}X$$

The analytical expression of this ellipse is in the coordinate frame $(O, \vec{u}_{1,i}, \vec{u}_{2,i})$:

$$\frac{X_1^2}{\mu_{1,i}} + \frac{X_2^2}{\mu_{2,i}} = \alpha^2$$

O is the centre of this ellipse, it is at full-solution position. The length of the semi-major axis is $\alpha\sqrt{\mu_{1,i}}$ and the length of the semi-minor axis is $\alpha\sqrt{\mu_{2,i}}$.

We want to find the ellipse that contains this vector with the probability $1-p$, that is to say find $D_{\alpha,i}$ such as:

$$\iint_{X\in D_{\alpha,i}} f_{\Delta X_{i,\perp}}(x_1,x_2)\,dx_1dx_2 = \frac{1}{2\pi\sqrt{\mu_1\mu_2}} \iint_{X\in D_{\alpha,i}} \exp\left(-\frac{1}{2}\left(\frac{x_1^2}{\mu_1}+\frac{x_2^2}{\mu_2}\right)\right)dx_1dx_2 = 1-p$$

Let us set $\begin{cases} u = {x_1}/{\sqrt{\mu_1}} \\ v = {x_2}/{\sqrt{\mu_2}} \end{cases}$, the elliptical region $D_{\alpha,i}$ becomes the disk R_α of radius α and we get:

$$P(\Delta X_{i,\perp} \in D_{\alpha,i}) = \frac{1}{2\pi}\iint_{R_\alpha} \exp\left(-\frac{1}{2}\|v\|^2\right)dv = 1-\exp\left(-\frac{\alpha^2}{2}\right)$$

The ellipse $\mathcal{E}_{\alpha,i}$ that contains the vector $\Delta X_{i,\perp}$ with the probability $1-p$ is such that

$$\alpha = \sqrt{-2\ln(p)}$$

For any vector X inside the ellipse $\mathcal{E}_{\alpha,i}$:

$$\frac{X_1^2}{\mu_{1,i}} + \frac{X_2^2}{\mu_{2,i}} \leq \alpha^2 \qquad \sqrt{\frac{X_1^2}{\mu_{1,i}} + \frac{X_2^2}{\mu_{2,i}}} \leq \alpha$$

Assuming that $\mu_{1,i} = \max(\mu_{1,i}, \mu_{2,i})$,

$$\sqrt{X_1^2 + \frac{\mu_{1,i}}{\mu_{2,i}} X_2^2} \leq \alpha\sqrt{\mu_{1,i}}$$

and

$$\|X\| = \sqrt{X_1^2 + X_2^2} \leq \sqrt{X_1^2 + \frac{\mu_{1,i}}{\mu_{2,i}} X_2^2} \leq \alpha\sqrt{\mu_{1,i}}$$

Therefore, $\|X\| \leq \alpha\sqrt{\mu_i}$ with μ_i the maximum eigenvalue of $C_{i,H}$.

If we choose $\alpha = \sqrt{-2\ln(p)}$, any vector X inside the corresponding ellipse is such as:

$$\|X\| \leq \sqrt{-2\ln(p)}\sqrt{\mu_i} \qquad \text{(C-7)}$$

C-2 Proposed protection level computation

The objective of this section is to study the impact of a bias of amplitude b_i on the pseudorange i on the full filter position estimation and find a bound $\delta_{0,i}$ such as:

$$P\left(\left\|X - \hat{X}_0\right\|_H \leq \delta_{0,i} / \exists \text{ a bias of size } b_i \text{ on the } \mathrm{i^{th}} \text{ pseudorange}\right) = p_0 \qquad \text{(C-8)}$$

The relationship between the full filter position error and the measurement error can be expressed such as:

$$\Delta X(k) - \hat{X}_0(k) = X(k) - \hat{X}_0(k) = -[H^t \Sigma^{-1} H]^{-1} H^t \Sigma^{-1} \times E(k)$$

that is to say,

$$X(k) - \hat{X}_0(k) = -A_0 \times E(k) \qquad \text{(C-9)}$$

with $A_0 = [H^t \Sigma^{-1} \mathrm{H}]^{-1} H^t \Sigma^{-1}$

In our case, we have

$$E \sim N(B, \Sigma)$$

$$\Sigma = \begin{bmatrix} \sigma_1^2 & \cdots & 0 \\ \vdots & \ddots & \vdots \\ 0 & \cdots & \sigma_N^2 \end{bmatrix}, B = \begin{bmatrix} 0 \\ \vdots \\ b_i \\ \vdots \\ 0 \end{bmatrix}$$

The behaviour of the horizontal component of the full filter position error, denoted $\Delta X_{0,H}$, is studied here.

The horizontal positioning error $\Delta X_{0,H}$ is a bi-dimensional random variable following a Gaussian distribution such as:

$$\Delta X_{0,H} \sim N\left(b_{i,H,\text{local}}, C_{0,H}\right)$$

where the mean vector $b_{i,H,\text{local}}$ is the projection of b_i in the horizontal plane such as:

$$b_{i,\text{local}} = \left[H^t \Sigma^{-1} \text{H}\right]^{-1} H^t \Sigma^{-1} \text{B}$$
$$b_{i,H,\text{local}} = b_{i,\text{local}}\,(1{:}\,2)$$

the covariance matrix $C_{0,H}$, such as $C_{0,H} = C_0(1{:}\,2,1{:}\,2)$ with $C_0 = \left[H^t \Sigma^{-1} \text{H}\right]^{-1}$

Let's denote the measurement error such as:

$$E = \xi + B \text{ where } \xi \sim N(0, \Sigma)$$

So the horizontal positioning error is such as:

$$\Delta X_{0,H} = \varepsilon_H + b_{i,H,\text{local}}$$

with $\varepsilon_H = \varepsilon(1{:}\,2)$ with $\varepsilon = [H^t \Sigma^{-1} \text{H}]^{-1} H^t \Sigma^{-1} \xi$ and $\varepsilon_H = N\left(\begin{bmatrix}0\\0\end{bmatrix}, C_{0,H}\right)$

We have $\left\|\Delta X_{0,H}\right\|^2 = \Delta X_{0,H}{}^{\text{t}} \Delta X_{0,H} = \left(\varepsilon_H + b_{i,H,\text{local}}\right)^t \left(\varepsilon_H + b_{i,H,\text{local}}\right)$

We denote the matrix S such as $C_{0,H} = SS$ as the matrix $C_{0,H}$ the matrix S and $S^{-1}$are symmetric.

$$\|\Delta X_H\|^2 = \left(\varepsilon_H + b_{local,H}\right)^t \left(\varepsilon_H + b_{local,H}\right)$$
$$= \left(\varepsilon_H + b_{local,H}\right)^t S^{-1} S \; S S^{-1} \left(\varepsilon_H + b_{local,H}\right)$$
$$= \left(\varepsilon_H + b_{local,H}\right)^t S^{-1} C_H \; S^{-1} \left(\varepsilon_H + b_{local,H}\right)$$

$$\|\Delta X_H\|^2 = \left(S^{-1}\varepsilon_H + S^{-1} b_{local,H}\right)^t C_H \; \left(S^{-1}\varepsilon_H + S^{-1} b_{local,H}\right)$$

with $S^{-1}\varepsilon_H = N\left(\begin{bmatrix}0\\0\end{bmatrix}, I_2\right)$

Since $C_{0,H}$ is not diagonal, the components of $\Delta X_{0,H}$ are not mutually independent and the separations on the North and East axes are correlated. But as $C_{0,H}$ is a positive definite matrix, it is diagonalizable and its eigenvalues are all positive. In particular we can find an orthonormal basis $\beta_0 = \left(\vec{u}_{1,0}, \vec{u}_{2,0}\right)$ that is composed of eigenvectors $\vec{u}_{1,0}$ and $\vec{u}_{2,0}$ corresponding with the eigenvalues $\mu_{1,0}$ and $\mu_{2,0}$ of $C_{0,H}$ and we have:

$$C_{0,H} = \Pi_{\perp,0} \,.\, \text{M}_0 \,.\, \Pi_{\perp,0}{}^{\text{t}} \qquad \text{(C-10)}$$

where,

$\text{M}_0 = \text{diag}\left(\mu_{1,0}, \mu_{2,0}\right)$ is the diagonal matrix whose elements are the eigenvalues of $C_{0,H}$

$\Pi_{\perp,0}$ is the projection matrix whose columns are the eigenvectors $\vec{u}_{1,0}$ and $\vec{u}_{2,0}$. In particular $\Pi_{\perp,0}$ is orthogonal $\Pi_{\perp,0}{}^{-1} = \Pi_{\perp,0}{}^{\text{t}}$.

Then, $\det(C_{0,H}) = \mu_{1,0}\mu_{2,0}$ and ${C_{0,H}}^{-1} = \Pi_{\perp,0} \,.\, {\mathrm{M}_0}^{-1} .\, {\Pi_{\perp,0}}^{\mathrm{t}}$

And we obtain

$$\left\|\Delta X_{0,H}\right\|^2 = \left(S^{-1}\varepsilon_H + S^{-1}b_{local\,,H}\right)^t P_\perp\, \Delta\, {P_\perp}^t \left(S^{-1}\varepsilon_H + S^{-1}b_{local\,,H}\right)$$
$$\left\|\Delta X_{0,H}\right\|^2 = \left({P_\perp}^t S^{-1}\varepsilon_H + {P_\perp}^t S^{-1}b_{local\,,H}\right)^t \Delta \left({P_\perp}^t S^{-1}\varepsilon_H + {P_\perp}^t S^{-1}b_{local\,,H}\right)$$

So we have

$$\mathrm{P}\left(\left\|\Delta X_{0,H}\right\|^2 \le {\delta_{0,i}}^2\right)$$
$$= P\left(\left({P_\perp}^t S^{-1}\varepsilon_H + {P_\perp}^t S^{-1}b_{local\,,H}\right)^t \Delta \left({P_\perp}^t S^{-1}\varepsilon_H + {P_\perp}^t S^{-1}b_{local\,,H}\right) \le {\delta_{0,i}}^2\right)$$

Let us denote $\Omega_{\mathrm{norm}} = {P_\perp}^t S^{-1}b_{local\,,H}$ and $\varepsilon_{\perp,norm} = {P_\perp}^t S^{-1}\varepsilon_H$

$$\mathrm{P}\left(\|\Delta X_H\|^2 \le {\delta_{0,i}}^2\right) = P\left(\left(\varepsilon_{\perp,norm} + \Omega_{\mathrm{norm}}\right)^t \Delta \left(\varepsilon_{\perp,norm} + \Omega_{\mathrm{norm}}\right) \le {\delta_{0,i}}^2\right)$$

where $\varepsilon_{\perp,norm} \sim N\left(\begin{bmatrix}0\\0\end{bmatrix}, I_2\right)$, Ω_{norm} and Δ are determinist.

Then $\mathrm{P}\left(\left\|\Delta X_{0,H}\right\|^2 \le {\delta_{0,i}}^2\right) = \iint_{\left(\varepsilon_{\perp,norm} + \Omega_{\mathrm{norm}}\right)^t \Delta \left(\varepsilon_{\perp,norm} + \Omega_{\mathrm{norm}}\right) \le HAL^2} \mathrm{f}_{\varepsilon_{\perp,norm}}(\mathrm{s})\mathrm{ds}$

$\varepsilon_{\perp,norm} = \begin{bmatrix}\varepsilon_{\perp,norm}(1)\\ \varepsilon_{\perp,norm}(2)\end{bmatrix}$ such as $\varepsilon_{\perp,norm}(1)$ and $\varepsilon_{\perp,norm}(2)$are independent.

Therefore for $(u,v)\epsilon\mathbb{R}^2$, $\mathrm{f}_{\varepsilon_{\perp,norm}}(\mathrm{u},\mathrm{v}) = \mathrm{f}_{\varepsilon_{\perp,norm}\,(1)}(\mathrm{u}) \times \mathrm{f}_{\varepsilon_{\perp,norm}\,(2)}(\mathrm{v})$

$$\mathrm{P}\left(\left\|\Delta X_{0,H}\right\|^2 \le {\delta_{0,i}}^2\right) = \iint_{(W+\Omega_{\mathrm{norm}})^t \Delta (W+\Omega_{\mathrm{norm}}) \le {\delta_{0,i}}^2} \mathrm{f}_{\varepsilon_{\perp,norm}\,(1)}(\mathrm{u}) \times \mathrm{f}_{\varepsilon_{\perp,norm}\,(2)}(\mathrm{v})\mathrm{du}\,\mathrm{dv}$$

$$= \iint_{(W+\Omega_{\mathrm{norm}})^t \Delta (W+\Omega_{\mathrm{norm}}) \le {\delta_{0,i}}^2} \frac{1}{\sqrt{2\pi}} \mathrm{e}^{-\frac{\mathrm{u}^2}{2}} \times \frac{1}{\sqrt{2\pi}} \mathrm{e}^{-\frac{\mathrm{v}^2}{2}} \mathrm{du}\,\mathrm{dv}$$

$$= \iint_{(W+\Omega_{\mathrm{norm}})^t \Delta (W+\Omega_{\mathrm{norm}}) \le {\delta_{0,i}}^2} \frac{1}{2\pi} \mathrm{e}^{-\frac{\|\mathrm{W}\|^2}{2}} \mathrm{dW}$$

with $W = \begin{bmatrix}u\\v\end{bmatrix}$

Let us make a change of coordinate such as $\begin{cases}u = \rho\cos\theta\\ v = \rho\sin\theta\end{cases}$.

The Jacobian of the transformation is $J = |\rho|$

The integration domain will be defined as$\{(\theta,\rho) \in \mathbb{R}^2, 0 \le \theta \le 2\pi, 0 \le \rho \le r(\theta)\}$

$$\mathrm{P}\left(\left\|\Delta X_{0,H}\right\|^2 \leq {\delta_{0,i}}^2\right) = \frac{1}{2\pi}\int_{\theta=0}^{\theta=2\pi}\int_{\rho=0}^{\rho=\mathrm{r}(\theta)} \rho \mathrm{e}^{-\rho^2/2}\mathrm{d}\rho\,\mathrm{d}\theta = \frac{1}{2\pi}\int_{\theta=0}^{\theta=2\pi}\left[-\mathrm{e}^{-\rho^2/2}\right]_{\rho=0}^{\rho=\mathrm{r}(\theta)}\mathrm{d}\theta$$

$$\left(\left\|\Delta X_{0,H}\right\|^2 \leq {\delta_{0,i}}^2\right) = \frac{1}{2\pi}\int_{\theta=0}^{\theta=2\pi}\left[1 - -\mathrm{e}^{-\mathrm{r}(\theta)^2/2}\right]\mathrm{d}\theta$$

$$\mathrm{P}\left(\left\|\Delta X_{0,H}\right\|^2 \leq {\delta_{0,i}}^2\right) = \frac{1}{2\pi}\int_{\theta=0}^{\theta=\pi}\left[1-\mathrm{e}^{-\frac{\mathrm{r}_1(\theta)^2}{2}}\right]\mathrm{d}\theta + \frac{1}{2\pi}\int_{\theta=0}^{\theta=\pi}\left[1-\mathrm{e}^{-\mathrm{r}_2(\theta)^2/2}\right]\mathrm{d}\theta$$

$$\mathrm{P}\left(\left\|\Delta X_{0,H}\right\|^2 \leq {\delta_{0,i}}^2\right) = 1 - \frac{1}{2\pi}\int_{\theta=0}^{\theta=\pi}\left[\mathrm{e}^{-\frac{\mathrm{r}_1(\theta)^2}{2}} + \mathrm{e}^{-\frac{\mathrm{r}_1(\theta)^2}{2}}\right]\mathrm{d}\theta$$

$$\mathrm{P}\left(\left\|\Delta X_{0,H}\right\|^2 \geq {\delta_{0,i}}^2\right) = \frac{1}{2\pi}\int_{\theta=0}^{\theta=\pi}\left[\mathrm{e}^{-\frac{\mathrm{r}_1(\theta)^2}{2}} + \mathrm{e}^{-\frac{\mathrm{r}_1(\theta)^2}{2}}\right]\mathrm{d}\theta$$

And this integral is computed numerically

$r_1(\theta)$ and $r_2(\theta)$ are obtained thanks to the equation $(W + \Omega_{\mathrm{norm}})^t \Delta (W + \Omega_{\mathrm{norm}}) = {\delta_{0,i}}^2$ that defines the boundaries of the integration domain:

$$\lambda_1\left(u + \Omega_{\mathrm{norm},1}\right)^2 + \lambda_2\left(v + \Omega_{\mathrm{norm},2}\right)^2 = {\delta_{0,i}}^2$$
$$\lambda_1\left(\rho\cos\theta + \Omega_{\mathrm{norm},1}\right)^2 + \lambda_2\left(\rho\sin\theta + \Omega_{\mathrm{norm},2}\right)^2 = {\delta_{0,i}}^2$$

$$\rho^2(\lambda_1\, cos^2\theta + \lambda_2\, sin^2\theta) + \rho\left(2\lambda_1\, cos\theta\, \Omega_{\mathrm{norm},1} + 2\lambda_2\, sin\theta\, \Omega_{\mathrm{norm},2}\right) + \left(\lambda_1\ {\Omega_{\mathrm{norm},1}}^2 + \lambda_2\ {\Omega_{\mathrm{norm},2}}^2 - {\delta_{0,i}}^2\right) = 0$$

Finally, denoting
$$a(\theta) = \lambda_1\, cos^2\theta + \lambda_2\, sin^2\theta,$$
$$b(\theta) = 2\lambda_1\, cos\theta\, \Omega_{\mathrm{norm},1} + 2\lambda_2\, sin\theta\, \Omega_{\mathrm{norm},2}$$
$$c(\theta) = \lambda_1\ {\Omega_{\mathrm{norm},1}}^2 + \lambda_2\ {\Omega_{\mathrm{norm},2}}^2 - {\delta_{0,i}}^2$$

and $r_1(\theta) = \frac{-b-\sqrt{b^2-4ac}}{2a}$ and $r_2(\theta) = \frac{-b+\sqrt{b^2-4ac}}{2a}$

Appendix D

Sequential Constrained Generalized Likelihood Ratio Test adapted to step + ramp failure detection

D-1 Introduction

As introduced in 4-4-4, the sequential constrained GLR adapted to step + ramp failure detection consists in considering the m last observations and minimizing under constrain the following expression:

$$\left\| Z_1 - W_i \frac{v_i}{\sigma_i} \right\|^2 + \frac{1}{1-a^2} \sum_{\mathrm{k}=2}^{\mathrm{m}} \left\| Z_k - aZ_{k-1} - \left[(1-a)v_i + \left((1-a)k + 2a - 1 \right) \dot{v}_i \right] \frac{W_i}{\sigma_i} \right\|^2 \tag{D-1}$$

with respect to v_i and $\dot{v}_i$, that represent the initial position (amplitude of the step) and the speed (rate of the slope) of the failure.

As formerly, the least square residual vector is used to represent these values, for $i \in [1, N]$ and after simplifications, the following function of two variables is finally obtained:

$$\begin{aligned} g(x,y) = & \left[1 + \frac{(1-a)^2}{1-a^2}(m-1) \right] \frac{p_{ii}}{{\sigma_i}^2} \, \mathrm{x}^2 - 2 \frac{1-a}{1-a^2} \frac{\alpha}{{\sigma_i}^2} x - \frac{2}{1-a^2} \frac{\beta}{{\sigma_i}^2} y \\ & + \frac{1}{1-a^2} \left[(1-a)^2 \left(\frac{m(m+1)(2m+1)}{6} - 1 \right) + (2a-1)^2 (m-1) \right. \\ & \left. + 2(1-a)(2a-1) \left(\frac{m(m+1)}{2} - 1 \right) \right] \frac{p_{ii}}{{\sigma_i}^2} \, y^2 \\ & + \frac{2}{1-a^2} \left[\begin{matrix} (1-a)^2 \left(\frac{m(m-1)}{2} - 1 \right) \\ + (1-a)(2a-1)(m-1) \end{matrix} \right] \frac{p_{ii}}{{\sigma_i}^2} xy \end{aligned}$$

This function of two variables not considers constant terms and uses two cumulative sums:

$$\alpha = \Delta Y_1 + (1-a) \sum_{\mathrm{k}=2}^{\mathrm{m}-1} \Delta Y_{\mathrm{k}} + \Delta Y_{\mathrm{m}} \tag{D-2}$$

$$\beta = -a\Delta Y_1 + (a^2 + 2a - 1) \sum_{\mathrm{k}=2}^{\mathrm{m}-1} (1-\mathrm{k}) \Delta Y_{\mathrm{k}} + [(1-a)m + 2a - 1] \Delta Y_{\mathrm{m}} \tag{D-3}$$

Here again two functions are defined for $i \in [1, N]$:

- $S_0(\Delta Y, i) = g(\hat{x}_i, \hat{y}_i)$ with $(\hat{x}_i, \hat{y}_i) = \arg\min\{g(x,y) : |x + ty| \leq a_i, x \in \mathbb{R}, y \in \mathbb{R}, t \in [0, \Delta t]$, which represents the probability that there is no fault or no significant fault on the pseudo range *i*.

- $S_1(\Delta Y, i) = g(\bar{x}_i, \bar{y}_i)$ with $(\bar{x}_i, \bar{y}_i) = \arg\min\{g(x,y) : |x + ty| > b_i, x \in \mathbb{R}, y \in \mathbb{R}, t \in [0, \Delta t]$, which represents the probability that there is a bias on the channel *i* that will lead to a positioning failure.

The method will be a little bit more complicated since a recursive function of two variables has to minimize under more complex constraints.

D-2 Simplification of the constraint criteria

Under the assumption $\dot{v}_i$ constant:

$$(\exists t \in]0, \Delta t], |v_i + t\dot{v}_i| \geq b_i) \& (|v_i| < b_i) \Rightarrow (|v_i + \Delta t\dot{v}_i| > b_i) \qquad \text{(D-4)}$$

A couple (a constant step v_i and a constant slope $\dot{v}_i$) will be considered as faulty if $|v_i + \Delta t\dot{v}_i| > b_i$ or if $|v_i| \geq b_i$ as shows the following figure:

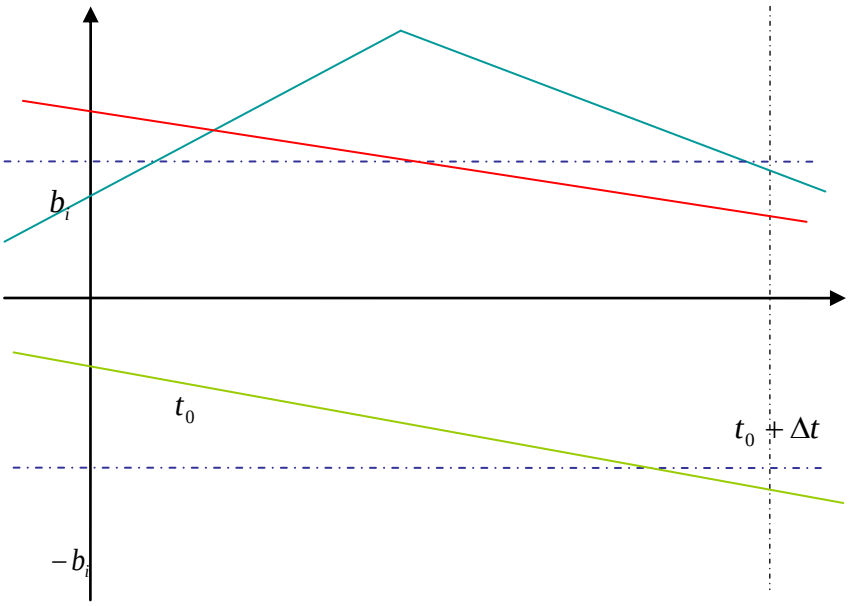

$|v_i| \geq b_i$, faulty
$|v_i + \Delta t\dot{v}_i| > b_i$, faulty
$(\exists t \in]0, \Delta t], |v_i + t\dot{v}_i| \geq b_i) \& (|v_i| < b_i) \& |v_i + \Delta t\dot{v}_i| < b_i$ but $\dot{v}_i$ is not a constant and this case is not taken into account

This is why,

$$\left((v_i, \dot{v}_i) : |v_i| < b_i, \exists t \in]0, \Delta t], |v_i + t\dot{v}_i| \geq b_i, \right) \Leftrightarrow \left((v_i, \dot{v}_i) : |v_i| < b_i, |v_i + \Delta t\dot{v}_i| \geq b_i\right) \qquad \text{(D-5)}$$

and the likelihood function has to be minimized on:

$$\begin{aligned}&\left((v_i,\dot{v}_i):|v_i|<b_i,\exists t\in[0,\Delta t],|v_i+t\dot{v}_i|\geq b_i,\right)\\&=\left((v_i,\dot{v}_i):|v_i|<b_i,|v_i+\Delta t\dot{v}_i|\geq b_i\right)+(|v_i|>b_i)\end{aligned}$$

Thus the likelihood function is first minimized under the constraint $(|v_i|>b_i)$ and then under the constraint $|v_i+\Delta t\dot{v}_i|>b_i$. The minimum of these two minimizations will be finally chosen. By this way $(v_i,\dot{v}_i)$ the most likely couple considering the m last observations and under the constraint $\exists t\in[0,\Delta t],|v_i+t\dot{v}_i|>b_i$, is obtained.

D-3 Computation of the GLR test

The minimum of the function g can be found by computing its gradient and finding its zeros. Effectively, numerical values of the polynomial coefficients are such that this function reaches a minimum and not a maximum.

$g(x,y)$is re written this way:

$$g(x,y)=ax^2+by^2+2cxy-2dx-2ey$$

then $\vec{\nabla}g(x,y)=\begin{bmatrix}\frac{\partial g}{\partial x}\\\frac{\partial g}{\partial y}\end{bmatrix}=\begin{bmatrix}-2d+2ax+2cy\\-2e+2by+2cx\end{bmatrix}$

which results in solving a simple linear system of two equations and two unknowns:

$$\left(\vec{\nabla}g(x,y)=0\right)\Leftrightarrow\begin{pmatrix}ax+cy=d\\by+cx=e\end{pmatrix}\Leftrightarrow\begin{pmatrix}x=\dfrac{ec-db}{c^2-ab}\\y=\dfrac{cd-ae}{c^2-ab}\end{pmatrix}$$

under the constraint $c^2-ab\neq 0$

Nevertheless, if the absolute minimum of this likelihood function is not in the constraint domain, we will carry out another way.

Minimizing $g(x,y)=ax^2+by^2+2cxy-2dx-2ey$ under the constraint $|x+\Delta ty|\geq b_i$ results, considering function g properties (monotonous, regular), in minimizing under the constraint $|x+\Delta ty|=b_i$ that is to say to consider the limits of the constraint domain. This is due to the fact that $g(x,y)$ forms a paraboloid.

$x+\Delta ty=b_i$ and $x+\Delta ty=-b_i$ are successively set, which results in considering the functions:

$$g(y)=a(b_i-\Delta t\,y)^2+by^2+2c(b_i-\Delta t\,y)y-2d(b_i-\Delta t\,y)-2ey$$

or

$$g(y)=a(-b_i-\Delta t\,y)^2+by^2+2c(-b_i-\Delta t\,y)y-2d(-b_i-\Delta t\,y)-2ey$$

Thus two « constrained » minimums are obtained:

$$y_1 = \frac{\Delta t\ a\ b_i - c b_i - \Delta t\ d + e}{a\ \Delta t^2 + b - \Delta t\ c}\ ,\quad x_1 = b_i - \Delta t\ y_1$$

$$y_2 = \frac{-\Delta t\ a\ b_i + c b_i - \Delta t\ d + e}{a\ \Delta t^2 + b - \Delta t\ c}\ ,\quad x_2 = b_i - \Delta t\ y_2$$

(D-6)

Likewise minimizing $g(x,y) = ax^2 + by^2 + 2cxy - 2dx - 2ey$ under the constraint $|x| \geq b_i$ results, considering function g properties (monotonous, regular), in minimizing under the constraint $x = |b_i|$, that is to say two cases: $x = b_i$ and $x = -b_i$.

If the memory has been reset (m=1) the likelihood function is $g(x,y) = ax^2 - 2dx$ and its absolute minimum $x = \frac{d}{a}$.

In the same way, if this absolute minimum does not respond to the constraints, the algorithm has to choose between the limits of the domain $x = -b_i$ or $x = b_i$ to find the "constrained" minimum.

A threshold that satisfies the Pfa as well as the predicted probability of missed detection are computed numerically.